Topology Optimization of Structures against Fatigue Life

A thesis submitted in fulfilment of the requirements for the degree of

Doctor of Philosophy

Khodamorad Nabaki

B.Sc., Yazd University, Iran

M.Sc., Azad University, Iran

School of Engineering

College of Science, Engineering and Health

RMIT University

July 2019

Declaration

I certify that except where due acknowledgement has been made, the work is that of the author alone; the work has not been submitted previously, in whole or in part, to qualify for any other academic award; the content of the thesis is the result of work which has been carried out since the official commencement date of the approved research program; any editorial work, paid or unpaid, carried out by a third party is acknowledged; and, ethics procedures and guidelines have been followed. I acknowledge the support I have received for my research through the provision of an Australian Government Research Training Program Scholarship.

Khodamorad Nabaki

July 2019

Acknowledgments

I would like to express my sincere thanks to all those who helped me to accomplish this research. Firstly, my sincere appreciation goes to my senior supervisor, Dr Jianhu Shen, for his valuable guidance and comments and his support throughout this study.

Secondly, I would like to express my special and warm gratitude to my second supervisor, Professor Xiaodong Huang, for all of his constructive comments, valuable suggestions, and support on my thesis.

Thirdly, the very special thanks go to my parents in Iran, who have always been a big part of my life and a constant source of selfless love.

Finally, my deepest love goes to my wife Armita Pashoutani, and my children Parsa and Homa Nabaki, who have accompanied me throughout my Ph.D. studies and through good times and bad times, patiently without complaints and this thesis is dedicated to them.

I would also like to warmly thank Dr Charlotte Forwood, and Ms Joan Forscutt for proofreading this thesis.

Additionally, I am very grateful for the financial research support of the Australian government and RMIT University.

Table of Contents

Publication list

Parts of this thesis have been presented in the following publications.

Journal papers

1. Nabaki, K, Shen, J & Huang, X 2019, 'Stress Minimization of Structures Based on Bidirectional Evolutionary Procedure', *Journal of Structural Engineering*, vol. 145, no. 2. DOI: 10.1061/(ASCE)ST.1943-541X.0002264

2. Nabaki, K, Shen, J & Huang, X 2019, 'Evolutionary topology optimization of continuum structures considering fatigue failure', *Materials & Design*, vol., p. 107586. DOI: 10.1016/j.matdes.2019.107586

Conference paper

3. NABAKI, K., SHEN, J., HUANG, X. Bi-directional evolutionary topology optimization based on critical fatigue constraint. *International Journal of Civil and Environmental Engineering*, Vol:12, No:2, 2018

List of the Figures

List of the Tables

Notations

$\boldsymbol{\rho}$	vector of filtered elements densities
$\boldsymbol{x}$	vector of design variables
x_j	design variables
w_j	weight factor
r_0	filter radius
r_j	distance between the design variables e and j
Ω_e	set of design variables which are located in a circle with the radius of r_0
$\boldsymbol{K}$	global stiffness matrix
$\boldsymbol{K_e}$	element stiffness matrix
$\boldsymbol{u}$	vector of displacement
$\boldsymbol{F}$	vector of the applied load
q	penalization factor
$\boldsymbol{D}$	constitutive matrix
$\boldsymbol{B}$	stress displacement matrix
$\rho_e(x)$	filtered design variables
$\eta_s(\rho_e(x))$	stress penalization factor
Ψ	aggregation function
n_c	number of sub-regions
n_e	number of elements
c	normalization factor
Ψ_{PN}	aggregation function based on p-norm
p	p-norm factor
σ^{I-1}_{max}	maximum local stress at the previous iteration
α^I	damped factor
c^{I-1}	normalization factor at the previous iteration
Ψ_{PN}^{I-1}	p-norm aggregation function at previous iteration

$\boldsymbol{U}$	displacement matrix
σ_{PN}	*p*-norm stress approximation
V_{req}	prescribed volume
$V(x)$	total volume
w_{ij}^{den}	linear weight factor
r_{sen}	sensitivity filter radius
h_e	element length
α_i	sensitivity numbers of the element *i*
n_{sc}	number of static stress constraint
n_{fc}	number of fatigue constraint
$\sigma_j^f(x)$	fatigue failure measurement of element *j*
$\overline{\sigma}^f$	fatigue constraint
$\sigma_j^s(x)$	static stress failure measurement of element *j*
$\overline{\sigma}^s$	static stress constraint
$\sigma^1{}_a$	the highest tensile principal stress of point *a*
Ω_j	set of fatigue evaluation point which belongs to the clusters *j*
n_l	number of the load cycles
N_l	number of cycles to failure
D	cumulative damage
$\tilde{\gamma}_e$	filtered density
σ_{TS}	tensile stress
σ_y	yield stress
σ_a	alternating stress
σ_m	mean stress
σ_{se}	stress amplitude with no mean stress
S_{ut}	tensile stress
S_y	yielding stress in tension

S_{yc}	yielding stress in comparison
S_e	endurance limit of the elements
D_e	is the accumulated damage in element e
C	mean compliance
r_{min}	filter radius of the BESO method
ER	evolutionary ratio
$\alpha_{i,k}$	sensitivity number of the current iteration
$\alpha_{i,k-1}$	sensitivity number of the previous iteration
V_{k+1}	target volume of the next iteration
V^*	volume constraint
α_{th}	threshold of the sensitivity number
λ	Lagrangian multiplier
u_j	displacement of element j
u_j^*	displacement constraint
u_j^{k+1}	estimated displacement of the next iteration
V_i	individual elements volume
x_i	binary design variables
σ^*	stress constraint
σ_G^{PN}	global modified p-norm function of von Mises stress
σ_i^{vm}	von Mises stress of elements
E^0	Young's modulus of the solid material
$\mathbf{K}_i^0$	elemental stiffness matrix of the solid elements
$\boldsymbol{\lambda}$	adjoint variable
G_s	gap function
σ'_f	fatigue strength coefficient
b	fatigue strength exponent
N_f	number of cycles to failure
σ_e	endurance limit of the material

σ_{ut}	ultimate tensile strength of the materials
λ^1, λ^2 and λ^3	eigenvalues of the stress tensor
$\mathbf{\Lambda}$	transformation vector
ϕ_i	eigenvector
$\sigma_{cfs}^{PN}(x)$	*p*-norm function of maximum tensile principal stress
σ_f^*	critical fatigue stress constraint
$f_{PN}(x)$	*p*-norm function of fatigue failure criteria
L_i^{GM}	modified Goodman fatigue failure criterion
$\mathbf{F}_{max}$	maximum force
$\mathbf{F}_{min}$	minimum force
σ_{max}	maximum stress
σ_{min}	minimum stress
$\sigma_{m_i}^{vonMises}$	von Mises mean stress
$\sigma_{a_i}^{vonMises}$	von Mises alternating stress
$(\sigma_i)_{Nf}$	critical fatigue stress for a prescribed number of cycles(N_f)
c_m	mean stress scaling factor
c_a	alternating stress scaling factor
L_i^{Gerber}	Gerber fatigue failure criterion

Note: Specific notations are defined by various subscripts or superscripts; see definitions in the text.

Abstract

Fatigue and stress are the most important criteria in engineering problems. Most of the failures of the structures and mechanical applications are due to fatigue and stress failures, therefore it is not sufficient to optimize the structures for the stiffness and other global responses such as frequencies, without considering stress and fatigue failure in the optimization process. This research investigated the fatigue and stress-based topology optimization in the framework of the bi-directional evolutionary structural optimization (BESO) method, where the goal is to find the optimal distribution of the materials by considering the stress and fatigue failure.

As the first part of this study, a stress-based BESO method has been developed, in which the sensitivity analysis is based on the stress, and the sensitivity numbers have been derived from the sensitivity analysis. To decrease the computational cost the global approach has been used to assemble all the local stresses in one function. To this, the modified *p*-norm method has been used to assemble all the local von Mises stress of the elements in a function. Three different problem formulations have been solved for the stress-based BESO method. In the first problem, the stiffness of the structure has been maximized, while volume and stress constraints have been satisfied. This is the original BESO method with an additional stress constraint. The second formulation deals with stress minimization of the structure with volume constraint, in which the *p*-norm stress has been minimized for prescribed volume constraint. The last problem formulation of the first part of this study is related to the volume minimization of the structure subject to stress constraint.

In the next stage of this study, the BESO method has been extended based on the critical fatigue stresses. First, the critical fatigue stress has been calculated according to the desired life cycle by fatigue analysis, and then this stress has been used as stress constraint in the topology optimization problem to achieve the optimal design. This means that the fatigue constraint has been changed to the stress constraint and used in the topology optimization process. Since the fatigue failure is related to the maximum principal stress, therefore in this part of the study, the sensitivity analysis is based on the principal stress, rather than the von Mises stress which has been considered in the first part. In this

part, the optimization problem is formulated to find the stiffest structure while the volume and the fatigue constraint have been satisfied.

The third and last part of this study is focused on the fatigue-based BESO method, in which the fatigue failure criteria have been considered directly in the sensitivity analysis, rather than applied as a stress constraint in the topology optimization problem. To calculate the fatigue failure criteria, the modified Goodman and Gerber theories have been used. To decrease the computational cost, we have used the global approach to assemble all the local fatigue failure criteria in one function by using the *p*-norm method. The optimization problem has been defined as maximizing the stiffness of a structure, with a volume constraint and a fatigue failure constrain to prevent fatigue within the prescribed life cycles. As before, this is the original BESO problem with an additional constraint in which the fatigue failure criterion is considered as an extra constraint. For the finite element analysis, the sensitivity number of the elements was calculated based on the results from the equivalent linear static analysis.

To show the validity of the stress and fatigue based BESO approaches several different numerical examples have been solved. To demonstrate the effectiveness of our proposed method, the original BESO problem in which the compliance was minimized, subject to volume constraint, was also solved and the results compared with the proposed methods.

Chapter 1

Introduction

1.1 Background

Although the structural optimization has been developed in recent years and different optimization methods have been proposed accordingly, the structural optimization method is still new, and its methods and approaches are being changed rapidly. Structural optimization is divided into three different categories: shape, size and topology optimization. Among these methods, topology optimization of the structures is the most applicable and effective way of the optimization method which has been considered in the engineering applications for decades, because it leads to the best optimal design, while compared economically with size and shape structural optimization. In the topology optimization approach, the aim of the optimization is to find the best material distribution of the structure to maximize its performance. It can be used as an effective tool to enhance the structural designs for engineering problems. Hence, topology optimization methods enable the designers to reach the proper structural layout for the structural performance requirements. This is achieved by seeking the optimal distribution of the material within the design domain while satisfying the specified design constraints.

Many topology optimization approaches including the Solid Isotropic Material Penalization (SIMP) (Bendsøe, MPa 1995), Evolutionary Structural Optimization (ESO) (Xie & Steven 1997) and Bi-directional ESO (BESO) (Hassani & Hinton 1999) have been proposed. The SIMP method, which is based on the continuous density of elements, was able to obtain the nearly black and white (0/1) optimal design by penalizing the intermediate densities. While, in the ESO method, elements with high stresses gradually removed from the ground structure. Huang and Xie (Huang, X & Xie, YM 2007, 2010) proposed a BESO method based on discrete densities of the element (solid or void) to search for the optimal design of structures, according to relative ranking of the derived sensitivity numbers of elements. However, the majority of the topology optimization methods were basically

focused on the stiffness maximization, with a volume constraint and other global responses, such as frequencies. In real life applications, stiffness optimization designs may not fully satisfy the engineering needs such as stress and fatigue failure. Therefore, it is important to consider stress and fatigue failure, which are the most important design criteria for engineering structures. They can be treated as constraints in topology optimization problems. Considering the local stress and fatigue failure directly in topology optimization has been a challenging major research area. Several fundamental difficulties should be overcome to apply the stress and fatigue failure as constraints in topology optimization process.

The first difficulty is related to the number of local constraints. Comparing the traditional topology optimization methods with two global responses, in which the compliance minimized with a volume constraint, the stress, and fatigue–based topology optimization includes large number of the local constraints, and since the local constraint applies on each point of the element in the design space, it is not possible to determine the region of the critical fatigue failure or stress. The gradient-based traditional topology optimization solves with the adjoint method effectively because the number of the constraints are less than the number of the design variables. However, solving the stress and fatigue-based topology optimization with a large number of local constraints is not possible with the adjoint method due to the expensive computational cost.

“Singularity “is the second difficulty which has arisen in the topology optimization problem with stress constraint. The singularity phenomenon was first introduced by (Sved & Ginos 1968), where the gradient-based optimization approach was not able to reach the proper optimal design of the tree-bar truss, as one of the truss members was removed during the optimization process to reach the optimal solution. However, the stress violation would happen by reducing the cross-sectional area of one member continuously.

The last difficulty of the stress and fatigue –based topology optimization, is the nonlinearity nature of the constraints, which lead to non-convergence of the optimization problem in some cases. Hence the algorithm should be robust enough to overcome the nonlinearity problem of the constraints.

Stress and fatigue constraints topology optimization problems are considered as one of the most difficult engineering problems, and the fatigue constraint topology optimization is a relatively new and rarely explored research area. Therefore, in this study, the novel stress and fatigue based BESO approaches have been proposed to reach the optimal design, while considering the fatigue and stress failure in the optimization process.

1.2 Aim and Scope

As stated earlier, fatigue and stress failure are the most important criteria for engineering applications, and nearly most of the mechanical components' failures are due to fatigue and stresses. In addition, topology optimization of the structure leads to designing the lightweight structures which can save material and energy resources significantly.

Nearly all the fatigue-based topology optimization methods were based on continuous densities of elements. So far there has been no report on considering the fatigue constraint in topology optimization, based on binary design variables (solid/void) as it is in the BESO method. Using continuous design variables such as SIMP resulted in an optimized design with various elemental densities, and intermediate elements were inevitable. Those intermediate elements constituted the "grey areas" of the optimized design which were hard to evaluate against fatigue. Therefore, it is worthwhile to explore an optimization process without the intermediate elements. BESO has the potential to provide explicit solid/void designs of structures, without intermediate elements, but has never been developed with fatigue constraint. In addition, stress constraint has rarely been used in terms of the BESO method. Recently, Xia et al. (2018) investigated the stress optimization problem using the BESO method to provide a solid/void optimized topology. Due to the complexity of the

stress-based topology optimization problems, Xia et al. (2018) simplified the sensitivity analysis, and overly damped the sensitivity numbers in order to make the BESO procedure stable.

Hence, in this research, we proposed the fatigue and stress based BESO method to optimize the structure with no fatigue and stress failure. In the proposed stress-based method, the stress vectors of the material have been fully considered in the sensitivity analysis, and then, the current BESO method has been extended to find a design without large stress concentration, and with local stress close to the stress limit. In the fatigue-based approach, the aim is to provide a preliminary optimal solution for helping engineers to achieve stiff and fatigue-resistant structural components. The methods have been verified numerically and the results obtained are appealing, where for comparison the traditional compliance-based BESO method has been solved in each case.

1.3 Organisation of the thesis

The research is organized as follows. In Chapter 2, the literature review of the related researches is presented. Firstly, stress constrained topology optimization introduced in this chapter in which we reviewed different stress–based methods, along with the challenges that need to be overcome for effectively solving optimization problems which are based on stress. Then the fatigue constrained topology optimization with different fatigue failure criteria and methodology, has been reviewed at the end of this chapter.

Chapter 3 describes the evolutionary optimization procedures. The problem formulation of the original BESO method has been discussed in this chapter. Since BESO method is the foundation of our proposed method, therefore we also reviewed the sensitivity analysis of the traditional compliance-based BESO method, along with the mesh dependency filter scheme. The elements update scheme has been reviewed in this chapter and the summary of the original BESO method has been discussed at the end.

Chapter 4 presents the proposed stress-based BESO method, in which the three different optimization problem formulations, and the aggregation approaches, have been introduced respectively. The next section of this chapter is related to the calculation of the sensitivity numbers of the elements, derived from the sensitivity analysis which is performed through the adjoint method. The results of the numerical examples for each optimization problems which were introduced at the beginning of this chapter, are presented in the next sections and compared with those from the traditional stiffness optimization. Conclusions and limitations of the proposed topology optimization method are summarized at the end of this chapter.

In Chapter 5 the critical fatigue stress has been considered in the BESO method, where the critical fatigue stress has been used as a stress constraint in the topology optimization process. First, the problem formulation has been defined, and then the sensitivity analysis which is based on the critical fatigue stress, has been calculated to reach the sensitivity numbers of the elements. In the next stage, the numerical implementation procedure and the obtained numerical results of the examples have been discussed respectively. Again, the concluding remarks have been reviewed at the end of this chapter.

The proposed fatigue-based topology optimization in the framework of the BESO, is presented in Chapter 6 where the fatigue failure criteria have been directly applied to the sensitivity analysis. Firstly, the topology optimization problem formulation, different fatigue failure criteria, and the aggregation method of the constraints have been discussed in this chapter respectively, and then the sensitivity number derivation has been calculated based on the fatigue constraint. The optimization procedure and the numerical results have been discussed at the next stage where again the result of the traditional BESO method is available for comparison. The conclusion of the results and limitation of the proposed method has been drawn at the end of this chapter.

Chapter 7 deals with a summary of the study and limitations of the research and suggestions for future work.

Chapter 2

Literature Review

The literature review of the research related to this study is presented in this chapter. In the first part of this chapter, different approaches of stress-constrained topology optimization for continuum structures is reviewed, along with the fundamental difficulties for solving the stress-based topology optimization and the ways to tackle them. The recent development in fatigue constrained topology optimization with different methodologies is examined in the second section of this chapter.

2.1 Stress-constrained topology optimization for continuum structures

Stress-based topology optimization was discussed in many papers, where the majority used the SIMP method along with the Method of Moving Asymptotes (MMA) (Svanberg 1987) to obtain the optimal design, see e.g.(Holmberg, Torstenfelt & Klarbring 2013; Jeong, Choi & Yoon 2014; Jeong et al. 2012; Le et al. 2010; París et al. 2010b). Meanwhile, other topology optimization approaches such as the integer programming method (Svanberg & Werme 2007), the level-set method (Allaire & Jouve 2008; Amstutz & Novotny 2010; Guo et al. 2011) were also applied to solve the stress constraint topology optimization problems. Stress-based BESO has been investigated recently by Xia et al. (2018) in which the sensitivity analysis was simplified in order to make the BESO procedure stable.

2.1.1 Stress-based topology optimization using SIMP method

As mentioned earlier, most of the stress-based topology optimizations are based on the SIMP method which is a continuous density approach. The optimization problem aims to reach a black and white design, while satisfying stress constraints, where the final optimization problem is solved by the MMA (Svanberg 1987). Also, the design variable filtering (Bruns & Tortorelli 2001) is used rather than sensitivity filtering, which is used in compliance-based approaches. The optimization problem formulation reads:

$$\begin{cases} \text{Minimize}: \quad f(\boldsymbol{\rho}) \quad (\boldsymbol{\rho}: \text{Filtered density}) \\ \text{subject to}: \quad \sigma_e \le \sigma^* \quad (\text{e} = 1,2,\ldots\ldots, \text{NE}): \text{Local constraint} \\ \boldsymbol{\rho} = [\rho_1(x), \rho_2(x), \ldots\ldots\ldots, \rho_{NE}(x)] \quad (\varepsilon < \mathbf{x} \le 1, \ \varepsilon: \text{a lower bound}) \end{cases} \tag{2-1}$$

where $\boldsymbol{\rho}$ is the vector of filtered elements densities and $\boldsymbol{x}$ is the vector of design variables. The filtered densities can be defined as follows:

$$\rho_e(x) = \frac{\sum_{j \in \Omega_e} w_j x_j}{\sum_{j \in \Omega_e} w_j} \tag{2-2}$$

where x_j denotes the design variables and w_j is weight factor which reads:

$$w_j = \frac{r_0 - r_j}{r_0} \tag{2-3}$$

where r_0 is the filter radius and the distance between the design variables e and j is denoted by r_j. Ω_e is the set of design variables which are in a circle with the radius of r_0. The static equilibrium must be satisfied at each iteration of the optimization problem, which reads:

$$\mathbf{K}(\rho(x))\mathbf{u}(\rho(x)) = \mathbf{F} \tag{2-4}$$

where $\boldsymbol{K}$ is the global stiffness matrix and $\boldsymbol{u}$ and $\boldsymbol{F}$ are the vectors of displacement and applied load respectively. In the density-based optimization approach (SIMP) the penalization method applies to the global stiffness matrix to penalize the intermediate design variables stiffness which can be defined as follows:

$$\mathbf{K}(\rho(x)) = \sum_{e=1}^{n_e} \eta_K(\rho_e(x))\hat{\mathbf{K}}_e \tag{2-5}$$

the penalization function which is denoted by $\eta_K(\rho_e(x))$ reads:

$$\eta_K(\rho_e(x)) = (\rho_e(x))^q \tag{2-6}$$

where q is a penalization factor and should be defined larger than 1 (q >1) and as explained in Holmberg et al. (2013), it has been proven by several authors that setting q=3 works well. Hence, by calculating the global stiffness matrix and applying the finite element analysis (FEA), one can calculate the displacement vectors of the elements and the stress vectors accordingly. As mentioned earlier, applying the obtained stress of the elements directly in the optimization problem is not possible and some difficulties will arise. In the next section, we discuss the strategies to tackle these difficulties and how to apply the stress constraint in topology optimization procedure.

2.1.1.1 Fundamental difficulties

There are three significant challenges that need to be overcome for effectively solving stress-based optimization problems (Bendsøe, MP 2004). The first is related to the so-called "singularity" phenomenon (Cheng, G. & Guo 1997; Cheng, Gengdong & Jiang 1992; Rozvany 2001). The second is related to the local nature of the constraint, and the third is related to the highly non-linear stress behavior. The "singularity" problem was first encountered when designing trusses subject to stress constraints where the n-dimensional feasible design space contains degenerate subspaces of dimension less than n (Cheng, Gengdong & Jiang 1992; Kirsch 1990). In the discrete density approaches like the BESO approach, two phases, typically representing void and solid materials, are used and no singularity problem occurs because the stress constraint is only applied to the solid phase. The final design is also free from the intermediate design variable values between solid and void, that is remained for the continuous density formulation.

To overcome the singularity phenomenon, the relaxation technique was used to reach accessible design in topology optimization. This means that in the topology optimization problem the original constraint will be changed to the smooth approximation by using the relaxation methods. There are different relaxation approaches, e.g. ε-relaxation (Cheng, G. & Guo 1997) and qp-approach (Bruggi 2008). Recently 'relaxed stress' (Le et al. 2010) or 'penalized stress' (Holmberg, Torstenfelt &

Klarbring 2013) has been used extensively in stress-constrained topology optimization problems with the continuous density approach to overcome the singularity problem.

In the 'penalized stress' approach, the relaxed stress vector of elements will be used rather than the real stress vector of the elements. The real stress vector of the elements reads:

$$\hat{\boldsymbol{\sigma}}(x) = \mathbf{DBu}(x) \tag{2-7}$$

where ***D*** and ***B*** are the constitutive and stress displacement matrixes of the elements respectively. The penalizes stress reads:

$$\boldsymbol{\sigma}(x) = \eta_s(\rho_e(x))\hat{\boldsymbol{\sigma}}(x) \tag{2-8}$$

where the filtered design variable is denoted by $\rho_e(x)$ and the stress penalization factor $\eta_s(\rho_e(x))$ is defined for increasing the stress value of the intermediate densities and can be defined as follows see e.g. (Holmberg, Torstenfelt & Klarbring 2013; Jeong, Choi & Yoon 2014; Jeong et al. 2012):

$$\eta_s(\rho_e(x)) = (\rho_e(x))^{\frac{1}{2}} \tag{2-9}$$

As explained in (Holmberg, Torstenfelt & Klarbring 2013) the stress penalization that is defined in Equation (2-8) is the penalization in (Bruggi 2008), but with a specific exponent which is suggested in (Le et al. 2010). Comparing the stress which is obtained by penalization (2-8) with stress calculation by (Duysinx & Bendsøe 1998), the penalized stress is non-physical for intermediate density values.

The second difficulty of stress-based topology optimization is due to the local nature of the stress constraint, which means that a large number of failure criteria should be defined for every element in a sub-optimization problem, which is difficult for a gradient-based optimizer to solve efficiently. To remedy this situation some different aggregation methods have been introduced which aggregate many local constraints into one global function, for example *p*-norm (Duysinx & Sigmund 1998; Le et al. 2010), *p*-mean (Duysinx & Sigmund 1998), KS-function (Kreisselmeier & Steinhauser 1979; Yang & Chen 1996) and lower bound KS-function (Luo & Kang 2012; Paris et al. 2009). All the mentioned

aggregations functions are based on the aggregation parameters *P>0* which converge to the maximum local constraint value:

$$\lim_{p\to\infty} \Psi(f_1, f_2, f_3, \ldots\ldots\ldots, f_N ; P) = \max(f_1, f_2, f_3, \ldots\ldots\ldots, f_N) \tag{2-10}$$

where the maximum local constraint is approximated by the aggregation function of Ψ which is scalar. Next, we discuss the *p*-norm and *p*-mean aggregation function and the strategies to enhance their performance. For more discussion on other aggregation methods such as KS-function and lower bound KS-function we refer to (Kreisselmeier & Steinhauser 1979; Luo & Kang 2012; Paris et al. 2009; Yang & Chen 1996).

The *p*-norm function (Duysinx & Sigmund 1998; Le et al. 2010) can be defined as follows:

$$\Psi_{PN} = \left(\sum_{e=1}^{N} f_e^{\,p} \right)^{\frac{1}{p}} \tag{2-11}$$

where the *P*-mean function (Duysinx & Sigmund 1998) reads:

$$\Psi_{PM} = \left(\frac{1}{N} \sum_{e=1}^{N} f_e^{\,p} \right)^{\frac{1}{p}} \tag{2-12}$$

The lower and upper boundary of the maximum local constraint can be defined as *p*-mean and *p*-norm respectively (Duysinx & Sigmund 1998):

$$\Psi_{PM} = \left(\frac{1}{N} \sum_{e=1}^{N} f_e^{\,p} \right)^{\frac{1}{p}} \le \max(f_1, f_2, f_3, \ldots\ldots\ldots, f_N) \le \Psi_{PN} = \left(\sum_{e=1}^{N} f_e^{\,p} \right)^{\frac{1}{p}} \tag{2-13}$$

According to (Le et al. 2010), both *p*-norm and *p*-mean functions can be used effectively to aggregate the local functions into a global function but the stress function must be positive such as von Mises stress. In addition (Holmberg, Torstenfelt & Klarbring 2013) investigated that using the *1/N* term which changes the *p*-norm function to *p*-mean, works as a 'built-in' scaling of the limit value and has

a positive effect on the convergence. It also avoids troubles in the first iterations of the optimization where we have high stresses value in some points.

When all the local functions have the same values, the *p*-mean function will have the value of the maximum local function. By increasing the *p* value, we will reach the maximum local function value. However, the nonlinearity of the problem will be increased by choosing the higher value of the *p,* due to the discontinuity of the local functions intersection point, which approximates by aggregation functions. In many pieces of research, limited values of *p* are used to avoid the high nonlinearity problem, for example, $p \epsilon$ [3, 12]. Hence the aggregation functions such as *p*-mean and *p*-norm cannot calculate the maximum local stress constraint accurately. In the case of the *p*-norm method, since the maximum local constraint is less than the *p*-norm constraint, the optimal design is conservative. However, in the case of the *p*-mean approach, the maximum stress of the optimal design is higher than the allowable stress limit, since the *P*-mean constraint value is less than the maximum local constraint value.

Since the numbers of the local constraints are very large in stress-constrained topology optimization, the aggregation approaches overestimate or underestimate the maximum local stress constraint. To remedy this problem, some solutions have been proposed for the accurate aggregation function approximation. One solution is dividing the design domain into *m* sub-domains where the aggregation function will assemble the local constraints of each sub-domain into separate function (*m* functions) rather than assembling all the local constraints into one global function (París et al. 2010a). Increasing the number of sub-domains better approximates the maximum local constraint but leads to increase in the number of the constraint in the topology optimization problem and increase the computational cost accordingly. Different approaches for subdividing the design domain have been introduced. The subdividing approach first introduced by París et al. (2010a) where the design domain divided into ‘blocks’, which were the neighboring elements region. Another strategy was proposed by Le et al. (2010) in which the element was sorted based on their stress level at each iteration as follows:

$$\{e_1, e_2, e_3, ..., e_n : \sigma_1 \le \sigma_2 \le \sigma_3 \le ..... \le \sigma_n\} \tag{2-14}$$

and then the *m* region defined as:

$$\Omega_k \equiv \{e_k, e_{m+k}, e_{2m+k}, ...\}, k = 1, 2, ..., m \tag{2-15}$$

where the number of m must not be too large because of the computational cost, for example, $m \in [1, 16]$. As explained in (Le et al. 2010), considering the regional constraints in the topology optimization problem leads to better optimization results, when compared with one global constraint with the same function. However, they reported that when the number of sub-regions increases further, the better optimal design cannot necessarily be reached.

Recently, (Holmberg, Torstenfelt & Klarbring 2013) proposed the so-called 'stress level techniques', in which the dividing order is based on the stress level of the elements, where the elements with similar stress value were in the same sub-region. The sub-domain dividing reads as:

$$\underbrace{\sigma_1 \ge \sigma_2 \ge \sigma_3 \ge ..... \ge \sigma_{\frac{n_e}{n_c}}}_{sub-region1} \ge ..... \ge \underbrace{\sigma_{\frac{2n_e}{n_c}} \ge ..... \ge \sigma_{\frac{(n_c-1)n_e}{n_c}}}_{sub-region2} \ge ..... \ge \underbrace{\sigma_{n_e}}_{sub-region n_c} \tag{2-16}$$

where n_c is the number of sub-regions and n_e is the number of elements. As explained in (Holmberg, Torstenfelt & Klarbring 2013), by considering the 'stress level techniques' in topology optimization problems, the better optimal design can be obtained while comparing it with the regional constraint approach which has been used by Le et al. (2010). However, this comparison was not quantitative and was based on the visual comparison of the plots of the stress field.

Considering the sub-domain strategies lead to a better approximation of the maximum local constraint, which is close to the real maximum local stress constraint, but it does not have the same value. To overcome this difficulty, Le et al. (2010) proposed the normalization approach, in which the aggregated constraints were normalized as follows:

$$\sigma_{\max} \approx c\Psi_{PN} \tag{2-17}$$

where *c* is the normalization factor and can be defined as follows:

$$c^I = \alpha^I \frac{\sigma_{\max}^{I-1}}{\Psi_{PN}^{I-1}} + (1-\alpha^I)\, c^{I-1} \quad , \quad 0 < \alpha^I < 1 \tag{2-18}$$

where the maximum local stress at previous iteration denoted by $\sigma^{I\text{-}1}{}_{max}$ and the oscillations of the *c* can be controlled by factor α, which should have a value between 0 and 1, while *c* oscillates, otherwise it should be set to 1. Since the normalization factor is not differentiable, it causes inconsistency, which results in different optimization problem at each iteration. As explained in (Le et al. 2010) any convergence issues will happen and the final optimization problem will converge.

The last issue with the stress constraint is its highly nonlinear dependence on the design. According to (Jeong et al. 2012), a highly non-linear stress constraint is often observed when relaxation techniques are employed to cope with the singularity issue. As a result, the convergence problems may occur for the optimization problem. To remedy this issue and avoid non-convergence cases the algorithm should be robust, and the optimization solution should be consistent numerically. Consequently, the aforementioned challenges clearly highlight the complexity of obtaining a global optimum through stress-based topology optimization. After addressing these challenges, the next section discusses the recent research by Xia et al. (2018) in which they investigated the stress optimization problem using the BESO method.

2.1.2 Stress-based topology optimization using the BESO method

As mentioned earlier, stress constraint has rarely been used in terms of the BESO method. Recently, Xia et al. (2018) investigated the stress optimization problem using the BESO method, since BESO enables a solid/void optimized topology. The optimization problem has been formulated to minimize the *p*-norm stress (Duysinx & Sigmund 1998; Le et al. 2010) while satisfying the volume constraint which reads:

$$\begin{cases} \text{Minimize}: \quad \sigma_{PN} \\ \text{subject to}: \begin{cases} \mathbf{KU} = \mathbf{F} \\ V(x) = \sum x_i v_i = V_{req} \\ x_i = 0 \ or \ 1 \ , \ i = 1,.....,nel \end{cases} \end{cases} \tag{2-19}$$

where ***K***, ***U***, and ***F*** are the global stiffness matrix, displacement matrix and external load respectively and $V(x)$ and V_{req} are the total and prescribed volume. The *p*-norm stress approximation (σ_{PN}) was performed to estimate the maximum stress value, where the local von Mises stresses of the elements have been assembled in one global function as follows:

$$\sigma_{PN} = \left(\sum_{i=1}^{nel} \sigma_{vm,i}^{p} \right)^{\frac{1}{p}} \tag{2-20}$$

Since the BESO method (Huang, X & Xie, YM 2007, 2010) is a gradient-based topology optimization, the optimization problem should be solved by deriving the objective function over design variables, and then the sensitivity numbers of the elements can be calculated based on the sensitivity analysis. The BESO method and its procedure will be discussed completely later in Chapter 4. To avoid the checkerboard patterns and mesh-dependency, the sensitivity filtering (Huang, X & Xie, YM 2007, 2010) was used by Xia et al. (2018) to filter the sensitivity numbers of the elements, rather than design variable filtering, which is used in the continuous density approaches (SIMP). In addition, they have also used an additional filtering approach on design variables to overcome the nonlinearity of stress behaviour as follows:

$$x_i = \frac{\sum_{j=1}^{nel} w_{ij}^{den} x_j}{\sum_{j=1}^{nel} w_{ij}^{den}} \tag{2-21}$$

where w_{ij}^{den} is the linear weight factor and can be defined as:

$$w_{ij}^{den} = \max(0, r_{den} - \Delta(i, j)) \quad , \quad r_{den} > r_{sen} > h_e \tag{2-22}$$

where the sensitivity filter radius and element length are denoted by r_{sen} and h_e respectively. Therefore Xia et al. (2018) used both sensitivity and design variables filtering scheme to solve the optimization problem. Also, to improve the convergence, they used the average of the current sensitivity numbers with the historical information of the last two iterations as follows:

$$\alpha_i^l = \frac{\alpha_i^{(l)} + \alpha_i^{(l-1)} + \alpha_i^{(l-2)}}{3}, \text{ for } l > 2 \tag{2-23}$$

where α_i is the sensitivity numbers of the element *i.*

Due to the complexity of the stress-based topology optimization problems, Xia et al. (2018) simplified the sensitivity analysis and overly damped the sensitivity numbers, in order to make the BESO procedure stable. However, in our research, the stress-based topology optimization problem is formulated the same as the problem formulation, which was done by Xia et al. (2018), however, we have considered the full stress vectors of the material in the sensitivity analysis rather than simplifying the sensitivity analysis. Then, the current BESO method will be extended to find a design without large stress concentration and with local stress close to the stress limit. We will later discuss our proposed method in Chapter 5 where we have solved different stress-based optimization problems including the problem formulation which has been solved by Xia et al. (2018).

In the next section, the fatigue constraint topology optimization has been reviewed where we discuss different approaches and strategies for applying the fatigue constraints in topology optimization along with their limitations and drawbacks.

2.2 Fatigue-constrained topology optimization for continuum structures

2.2.1 Overview of various methods and applications

In recent years, the fatigue-based optimization was addressed in various ways. The shape optimization with fatigue consideration was studied by (Grunwald & Schnack 1998; Kaya, Karen & Öztürk 2010; Mrzyglod & Zielinski 2007). For topology optimization, Sherif et al. (2010) explored the dynamic

fatigue load, using the equivalent static loads (Kim & Park 2010; Park & Kang 2003). In the next section, we introduce the most recent progress for the fatigue constrained topology optimization and review their methodology and their limitations.

Holmberg et al. (2014) investigated the fatigue-based topology optimization, in which the fatigue analysis and topology optimization were conducted in two separate steps. The maximum principal stress, representing the allowable cumulative damage, was calculated for a specific number of cycles, and then it was used as a fatigue constraint in the topology optimization problem. It indicated that the fatigue constraint was equivalent to the maximum principal stress constraint, where the problem was formulated to minimize the weight of the structure while fulfilling the fatigue and static stress constraints. The problem formulation reads:

$$\begin{cases} \min : \sum_{e=1}^{n_e} m_e \rho_e(x) \\ \text{subject to}: \begin{cases} \sigma_j^f(x) \le \bar{\sigma}^f \quad j = 1,.....n_{fc} \\ \sigma_j^s(x) \le \bar{\sigma}^s \quad i = 1,.....n_{sc} \\ \varepsilon \le x_e \le 1 \quad e = 1,....., n_e \end{cases} \end{cases} \tag{2-24}$$

where the numbers of fatigue and static stress constraints have been denoted by n_{fc} and n_{sc}. The fatigue failure measurement of the elements was defined by using the *p*-norm function as follows:

$$\sigma_j^f(x) = \left(\frac{1}{N_j} \sum_{a \in \Omega_j} (\sigma_a^1(x))^p \right)^{\frac{1}{p}} \tag{2-25}$$

where the highest tensile principal stress of point *a* and the set of fatigue evaluation point which belongs to the clusters *j* has been denoted by $\sigma^1{}_a$and $\Omega_{j.}$ respectively. The critical fatigue stress in Equation (2-24) was calculated based on high-cycle fatigue analysis, by solving a problem in which the objective function was to maximize the critical fatigue stress, while fulfilling the cumulative fatigue damage constraint as follows:

$$\begin{cases} \text{Maximize}: \quad \overline{\sigma}^{f} \\ \text{subject to}: \begin{cases} \sum_{l=1}^{L} \frac{n_l}{N_l} \le \overline{D}, \quad D \le \overline{D} \le 1 \end{cases} \end{cases} \tag{2-26}$$

where n_l and N_l are the number of load cycles and the number of cycles to failure respectively. For solving the optimization problem in Equation (2-24), the continuous density approach (SIMP) was used along with the MMA (Svanberg 1987) as an optimizer. Also, to avoid the checkerboard solution, the design variable filtering approach (Bruns & Tortorelli 2001) was used rather than the sensitivity filtering, and the sensitivity analysis of the fatigue constraints was based on the maximum tensile principal stress. For calculation of the regional fatigue constraints, the 'stress level techniques' (Holmberg, Torstenfelt & Klarbring 2013) has been used in which the clusters have been defined based on the stress values of the elements. As discussed in (Holmberg, Torstenfelt & Klarbring 2014) the final optimal design is free from the large stress concentration, but the local fatigue and stress values can be above the constraints values due to applying the regional constraints approach. Hence, (Holmberg, Torstenfelt & Klarbring 2014) proposed a method in which the fatigue analysis is separate from the topology optimization problem, and the fatigue constraint can be used as stress constraint in the topology optimization problem. We also have applied this methodology as used in (Holmberg, Torstenfelt & Klarbring 2014), but by considering the BESO method rather than the SIMP method, which is discussed in Chapter 5.

In (Jeong, Choi & Yoon 2015), the fatigue-based topology optimization was investigated with the constant-proportional loading condition. The fatigue failure criteria were calculated based on the stress-life method, by using dynamic and static analysis to overcome the non-differentiability of the fatigue constraint, based on the Modified Goodman, Soderberg, and Gerber theories, where the signed von Mises mean stress was calculated by static analysis and harmonic analysis was used to calculate the von Mises alternating stress. The topology optimization problem was formulated to minimize the volume of the structure subject to the fatigue constraints. Also, additional static stress constraint was applied to avoid static failures. The optimization problem is as follows:

$$\begin{cases} \text{Minimize}: V(\boldsymbol{\gamma}) = \sum_{e=1}^{NE} \tilde{\gamma}_e v_e & \tilde{\gamma}_e = \text{Filtered density} \\ \text{subject to}: \begin{cases} f_{1,e} = L_e(\sigma_a, \sigma_m) \le 1 \\ f_{2,e} = \dfrac{\sigma_a + \sigma_m}{\sigma_y} \le 1 \\ f_{3,e} = \dfrac{\sigma_a - \sigma_m}{\sigma_y} \le 1 \\ \varepsilon \le \gamma_e \le 1 \quad e = 1,\ldots..,n_e \end{cases} \end{cases} \tag{2-27}$$

where $f_{2,e}$, $f_{3,e}$ are the static stress constraints which can be defined based on the yield stress of the material (σ_y) to avoid static failures, and $f_{1,e}$ is the fatigue constraint which is the maximum fatigue criteria among the Gerber, Soderberg and Modified Goodman criteria as follows:

$$f_{1,e} = \max\left(\begin{array}{l} \text{Modified Goodman}: \ \dfrac{\sigma_a}{\sigma_{se}} + \dfrac{\max[\sigma_m, 0]}{\sigma_{TS}} \le 1 \\ \text{Gerber}: \ \dfrac{\sigma_a}{\sigma_{se}} + \left(\dfrac{\max[\sigma_m, 0]}{\sigma_{TS}} \right)^2 \le 1 \\ \text{Soderberg}: \ \dfrac{\sigma_a}{\sigma_{se}} + \dfrac{\max[\sigma_m, 0]}{\sigma_y} \le 1 \end{array} \right) \tag{2-28}$$

where σ_{TS} and σ_y represent the tensile and yield stress. Alternating and mean stresses are denoted by σ_a and σ_m respectively, and σ_{se} is the stress amplitude with no mean stress in the case of the fully reversed loading condition. For more details regarding the Goodman, Gerber and Soderberg theory we refer to (Aliabadi 1992; Lee, Barkey & Kang 2012; Suresh 1998).

The normalized *p*-norm approach was applied to assemble the local constraints in one function as follows:

$$(f_i^{\max})_{PN} = c_i^{iteration} \left(\sum_e (f_{i,e})^p \tilde{\gamma}_e \right)^{\frac{1}{p}} \tag{2-29}$$

where $c_i^{iteration}$ is the normalization factor (Le et al. 2010) and can be defined as:

$$c_i^{iteration} = \alpha^{iteration} \frac{\sigma_{\max}^{iteration-1}}{f_{i,PN}^{iteration-1}} + (1-\alpha^{iteration})\, c^{iteration-1} \quad , \quad 0 < \alpha^{iteration} < 1 \tag{2-30}$$

Since the fatigue failure criteria are non-differentiable with respect to the design variables and stress components, Jeong et al. (2015) proposed their own differentiable fatigue and static failure criteria, by using the differentiable signed von Mises criterion. To approximate the local constraint better, Jeong et al. (2015) used the same approach of the regional constraint, which is used in (Le et al. 2010). Finally, the dynamic optimization problem with fatigue constraint, is solved based on the continuous density approach (SIMP) by using the MMA (Svanberg 1987) as a solver where different values of the *p* factor in *p*-norm function led to different optimal layouts. Therefore, comparing with (Holmberg, Torstenfelt & Klarbring 2014), (Jeong, Choi & Yoon 2015) were able to apply the fatigue constraints directly in topology optimization problems and develop a new dynamic fatigue-base topology optimization, based on the SIMP method.

Collet et al. (2017) proposed a fatigue constraint topology optimization, in which the modified Goodman method was used, along with the Sine method to calculate failure criteria. The problem was defined as minimizing the weight of the structure with a set of local stress constraints to represent the fatigue resistibility of the optimal design. The equivalent static analysis has been used to calculate the alternating and mean stress of the elements and then compared with the modified Goodman diagram. As explained in (Collet, Bruggi & Duysinx 2017) to avoid fatigue failure the mean and alternating stress of all the elements must be in the safe region of the Goodman diagram. According to (Collet, Bruggi & Duysinx 2017) the safe region of the Goodman diagram can be defined as follows:

$$\begin{cases} \dfrac{\sigma_a}{S_e} + \dfrac{\sigma_m}{S_{ut}} \le 1 \\ \dfrac{\sigma_a}{S_y} - \dfrac{\sigma_m}{S_{yc}} \le 1 \\ \dfrac{\sigma_a}{S_e} \le 1 \end{cases} \tag{2-31}$$

where S_{ut}, Sy and S_{yc} represent the tensile stress, yielding stress in tension and yielding stress in comparison respectively. The endurance limit of the elements denoted by S_e, and σ_m and σ_a are the equivalent mean and alternating stress of the elements. The optimization problem reads:

$$\begin{cases} \text{Minimize } : W = \sum_{e=1}^{NE} x_e v_e \\ \text{subject to}: \begin{cases} \dfrac{\sigma_a}{S_e} + \dfrac{\sigma_m}{S_{ut}} \le 1 \\ \dfrac{\sigma_a}{S_y} - \dfrac{\sigma_m}{S_{yc}} \le 1 \\ \dfrac{\sigma_a}{S_e} \le 1 \\ \varepsilon \le x_e \le 1 \quad e = 1,\ldots..,NE \end{cases} \end{cases} \tag{2-32}$$

The density filtering approach (Bruns & Tortorelli 2001) was used to avoid the checkerboard pattern for the optimal design. As with (Holmberg, Torstenfelt & Klarbring 2014; Jeong, Choi & Yoon 2015), the optimization problem was solved based on the continuous density approach (SIMP) by considering the MMA (Svanberg 1987) as an optimization solver. The relaxation method (Le et al. 2010) was used to overcome the so-called 'singularity' phenomenon of fatigue constraints. Collet et al. (2017) investigated a fatigue-based topology optimization method, in which they applied the fatigue constraint directly in the topology optimization process but again the fatigue constrained topology optimization has been considered in terms of continuous density (SIMP) rather than the discrete density approach. We have also used the same equivalent static analysis (Collet, Bruggi & Duysinx 2017) for our fatigue-based proposed method which has been discussed in Chapter 6.

Recently, Oest and Lund (Oest & Lund 2017) applied a method by considering the fatigue life of the elements in topology optimization. The quasi-static analysis was used for the finite element analysis and the fatigue failure criteria were determined using the traditional rain-flow counting. The optimization problem was then formulated to minimize the mass while enduring the accumulated damage under the proportional loading condition and reads:

$$\begin{cases} \min : \sum_{e=1}^{n_e} m_e \rho_e(x) \\ \text{subject to}: \begin{cases} g_D(x) \le 1 \\ \varepsilon \le x_e \le 1 \quad e = 1,\ldots..,n_e \end{cases} \end{cases} \tag{2-33}$$

where g_D is the *p*-norm function of the fatigue constraint that can be defined as:

$$g_D(x) = \left(\sum_{e=1}^{ne} (D_e)^p \right)^{\frac{1}{p}} \tag{2-34}$$

and D_e is the accumulated damage in element *e* which is caused by each load cycle *i* as follows:

$$D_e = \sum_{i=1}^{n_{RF}} \left(\frac{n_i}{N_{ei}} \right) \tag{2-35}$$

For solving the optimization problem Oest and Lund (Oest & Lund 2017) applied the MMA solver along with the SIMP method where the density filtering approach was used to overcome the checker-board pattern. In conclusion Oest and Lund (Oest & Lund 2017) proposed a new gradient-based method which considers the finite-life fatigue constraint directly in the topology optimization. The high-cycle fatigue analysis, along with the rain-follow counting, was used to calculate the accumulated damage of elements in the design process.

As stated earlier, all the fatigue-based topology optimization methods were based on continuous densities of elements with MMA, and fatigue constraint has never been used in discrete densities topology optimization problems e.g. BESO method. Hence, in this research, we have applied the fatigue constraint directly in topology optimization problem where the sensitivity filtering has been applied, rather than design variable filtering approach, as used in the continuous density method (SIMP). The proposed BESO method is explained and discussed in Chapter 7 where different numerical examples are available to show the validity of the proposed method. In Chapter 3 we review the original BESO method where we discuss each step of the BESO procedure in detail.

Chapter 3

Bi-directional evolutionary topology optimization methods

3.1 The BESO method

Bi-directional evolutionary structural optimization (BESO) was first introduced by Yang et al. (1999) for compliance optimization. In their study, the solid element with the lowest sensitivity number changed to void elements, and the void elements with the highest sensitivity number changed to solid. In addition, the sensitivity numbers of the void elements were calculated after finite element analysis by using the linear displacement filed extrapolation. Later Querin et al. (2000) applied the von Mises stress criterion in the BESO algorithm, in which the void elements were the elements with the lowest von Mises stress, and the void elements with the stress near to the highest stress changed to solids. The early versions of the BESO method, which ranked the elements separately, for addition and removal purposes were illogical and cumbersome. In addition, due to the large number of iterations, their computational efficiency was low and in some case the convergence history was disordered. Huang and Xie (Huang, X & Xie, Y 2007) proposed a new BESO method for stiffness optimization in which they addressed many issues of the topology optimization method and also resolved the problems of the early BESO versions. In this study, we developed the BESO (Huang & Xie, 2007) for stress and fatigue optimization. Hence, we review the original BESO method (Huang, X & Xie, Y 2007) in this chapter, and in the next chapters we will extend the BESO method for stress and fatigue optimization.

3.1.1 Optimization problem

In the BESO method, (Huang, X & Xie, Y 2007), the aim is to minimize the compliance while satisfying a volume constraint. This means that we seek the stiffest structure with the prescribed volume and problem formulation which reads:

$$\begin{cases} \text{Minimize} : \quad C = \dfrac{1}{2}\mathbf{f}^T\mathbf{u} \\ \text{subject to}: \begin{cases} \mathbf{KU} = \mathbf{F} \\ V(x) = \sum x_i v_i = V_{req} \\ x_i = 0 \ or \ 1 \ , \ i = 1,.....,nel \end{cases} \end{cases} \tag{3-1}$$

where **u** and **f** are the displacement and applied load vectors respectively, and *C* is the mean compliance which has an inverse relation with structure stiffness. This means by minimizing the compliance, the stiffness of the structure will be maximized. V_{req} is the prescribed volume which uses a constraint in the original BESO method, and x_i is the binary design variables for each element in the design space, where 0 represents the void elements and the solid elements are denoted by 1. The application of $x_i = 0$ for the void elements leads to inaccurate design due to missing the void elements design information, therefore Huang and Xie (Huang, X & Xie, Y 2007), used x_{min} which is a small value (e.g. 0.001)rather than 0 for void elements. This means that instead of removing the void elements completely from the design domain, they will be replaced by a soft material. Then the necessary information for sensitivity analysis can be calculated from the finite element analysis. The BESO method is a gradient-based optimization method in which the sensitivity number of the elements is calculated, based on the objective function to remove and add the elements to the design space simultaneously, while satisfying the volume constraint. The sensitivity number can be calculated based on the sensitivity analysis by deriving the objective function over design variables. In the next section, the details of the BESO sensitivity analysis and the sensitivity numbers are reviewed for the compliance-based BESO.

3.1.2 Sensitivity analysis

As mentioned earlier, the BESO method is a gradient-based optimization method and the sensitivity numbers can be calculated by deriving the objective function, which is compliance in the original BESO method over changing the design variables. This means that the variation of the objective function will be calculated based on the variation of the design variables, which is due to adding and removing elements from the design domain. The general form of the sensitivity numbers reads

$$\alpha_i' = \alpha_i . \Delta x_i = \frac{\partial f\left(x_1, x_2, ..., x_N\right)}{\partial x_i} . \Delta x_i \tag{3-2}$$

where α_i is the sensitivity of the elements and α'_i denotes the sensitivity number of the elements in the design domain. As explained in (Huang, X & Xie, Y 2007), The sensitivity number of the compliance-based BESO method can be calculated as follows:

$$\alpha_i = \frac{\partial C}{\partial x_i} = -\frac{1}{2}\mathbf{U}^T \frac{\partial \mathbf{K}}{\partial x_i}\mathbf{U} \tag{3-3}$$

where ***U*** and ***K*** are the displacement and the general stiffness matrix of the structure respectively. In the BESO procedure, the removal and addition of the material into the design domain is based on the relative ranking of the sensitivity numbers. For calculating the sensitivity number of the void elements Huang and Xie (Huang, X & Xie, Y 2007) proposed a new filter scheme which also helps the smoothness of the sensitivity number of all the elements in the design domain. Additionally, it overcomes the "mesh-dependency" and the "checkerboard patterns" problems.

3.1.3 BESO filter scheme

As mentioned earlier, the filter scheme was proposed by Hunag and Xie (Huang, X & Xie, Y 2007) will improve the sensitivity numbers and also overcome the checkerboard pattern and mesh-dependency problems. The so-called "mesh-dependency problem" arises from the obtained different optimal design, while having different mesh sizes for design domain. The heuristic filter scheme (Huang, X & Xie, Y 2007) was used to improve the sensitivity number and overcome the mesh related problems. Therefore, the same optimal design should be obtained, when different mesh sizes have been used for topology optimization problem. The improved sensitivity number reads:

$$\hat{\alpha}_i = \frac{\sum_{j=1}^{N} w(r_{ij})\alpha_i}{\sum_{j=1}^{M} w(r_{ij})} \tag{3-4}$$

where r_{ij} denotes the distance between the center of the element i and element j. $w(r_{ij})$ is the weight factor given as

$$w(r_{ij}) = \begin{cases} r_{\min} - r_{ij} & \text{for } r_{ij} < r_{\min} \\ 0 & \text{for } r_{ij} \geq r_{\min} \end{cases} \tag{3-5}$$

where r_{min} is the filter radius. As mentioned in (Huang, X & Xie, Y 2007) the value of r_{min} which does not change when the finer mesh is used, should be large enough to cover more than one element in the sub-domain of Ω_i.($\Omega_i \in \Omega$). Subsequently the size of the sub-domain Ω_i. which is shown in Fig. 3-1 does not change by changing the mesh size. Hence the improved sensitivity number can be calculated by the contribution of the nodes which are located inside the sub-domain Ω_i. by using the filter scheme.

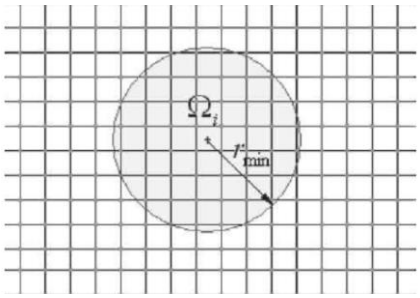

Fig. 3-1. Sub-domain Ω_i., which using for filter scheme (Huang, X & Xie, Y 2007)

3.1.4 Stabilization of the solution

The BESO algorithm has difficulty with convergence if the original sensitivity numbers are used. This problem arises since the sensitivity numbers calculations are based on the absence and presence of the elements, which makes the topology difficult to be converged. To remedy this problem Huang and Xie (Huang, X & Xie, Y 2007) proposed the averaging scheme, in which the elemental sensitivity number can be further modified, by averaging its historical information to improve the convergence of the solution. That is, the sensitivity number after the first iteration is calculated by

$$\alpha_i = \frac{1}{2}(\alpha_{i,k} + \alpha_{i,k-1}) \tag{3-6}$$

where $\alpha_{i,k}$ and $\alpha_{i,k-1}$ are the sensitivity numbers of the current and previous iteration respectively. Thus the modified sensitivity number considers the sensitivity information in the previous iterations and it will be used as a new modified sensitivity number for the next iteration.

3.1.5 Element addition/removal scheme and convergence criterion

The BESO approach is based on the relative ranking of the sensitivity numbers which allows the void and solid elements to be added and removed from the design domain simultaneously. The material is removed from the design domain gradually and step by step by comparing the target volume of the next iteration (V_{k+1}) with the volume constraint V^* where the target volume for the next iteration can be obtained as follows:

$$V_{k+1} = V_k(1 \pm ER) \qquad k = 1,2,3,..... \tag{3-7}$$

where the evolutionary ratio is denoted by *ER*. The volume for the next iteration will be set to the volume constraint V^* for the rest of iterations while the volume constraint satisfies as follows:

$$V_{k+1} = V^* \tag{3-8}$$

As explained in (Huang, X & Xie, Y 2007), for solid elements, the elemental density is switched from 1 to x_{min} if the following criterion is satisfied.

$$\alpha_i \le \alpha_{th} \tag{3-9}$$

and for void elements, the elemental density is switched from x_{min} to 1 if the following criterion is satisfied

$$\alpha_i > \alpha_{th} \tag{3-10}$$

where α_{th} is the threshold of the sensitivity number, which is determined by the target material volume V_{k+1} and the relative ranking of the sensitivity numbers. The calculation of the threshold of the sensitivity number (α_{th}) is very simple in the BESO procedure. For example, the design domain includes 2000 elements and the sensitivity numbers sort such that $\alpha_1 > \alpha_2 > \alpha_3 > \ldots\ldots\ldots > \alpha_{2000}$, if for

calculating the V_{k+1}, 1200 elements should be in the design domain, therefore, $\alpha_{th} = \alpha_{1200}$. Using the mentioned threshold for adding and removing the elements from design domain, might lead to the addition or removal of a large number of materials from the design domain in a single iteration and cause the structure to lose its integrity. To remedy this situation and guarantee the gradual evolution process, Huang and Xie (Huang, X & Xie, Y 2007) used the "maximum volume addition ratio" (AR_{max}) which is normally greater than 1%. In the BESO method, the gradual material removal will be stopped, while the algorithm reaches the objective volume (V^*) and the whole optimization process will end if the following convergence criterion is satisfied:

$$error = \left| \frac{\sum_{i=1}^{N} C_{k-i+1} - \sum_{i=1}^{N} C_{k-N-i+1}}{\sum_{i=1}^{N} C_{k-i+1}} \right| \leq tolerance \tag{3-11}$$

where k and C are the number of the current iteration and objective function respectively, and tolerance is the prescribed tolerance which is defined for convergence. The speed of the convergence depends on N which is the integer number and normally has the value of 5 (Huang, X & Xie, Y 2007) which means the small violation of the mean compliance is acceptable over the last 10 iterations.

3.2 The general overview of the BESO procedure

The evolutionary iteration procedure can be outlined as follows:

Step 1: Discretize the whole design domain using a finite element mesh.

Step 2: Define the BESO parameters such as objective volume, V^*, evolutionary ratio ER.

Step 3: Carry out finite element analysis (FEA) for calculating the sensitivity numbers.

Step 4: Determine the target volume for the next design. When the current volume V_k is larger than the objective volume V^*, the target volume for the next design can be calculated by Equation (3-7).

Step 5: Filter sensitivity numbers in the whole design domain to obtain the improved sensitivity numbers by Equation (3-4) and average the obtained sensitivity number by its previous iterations history by Equation (3-6).

Step 6: Reset the design variables of all elements by switching the solid elements to voids and vice versa based on Equations (3-9 and 3-10).

Step 7: Repeat 3–6 until the solution is convergent.

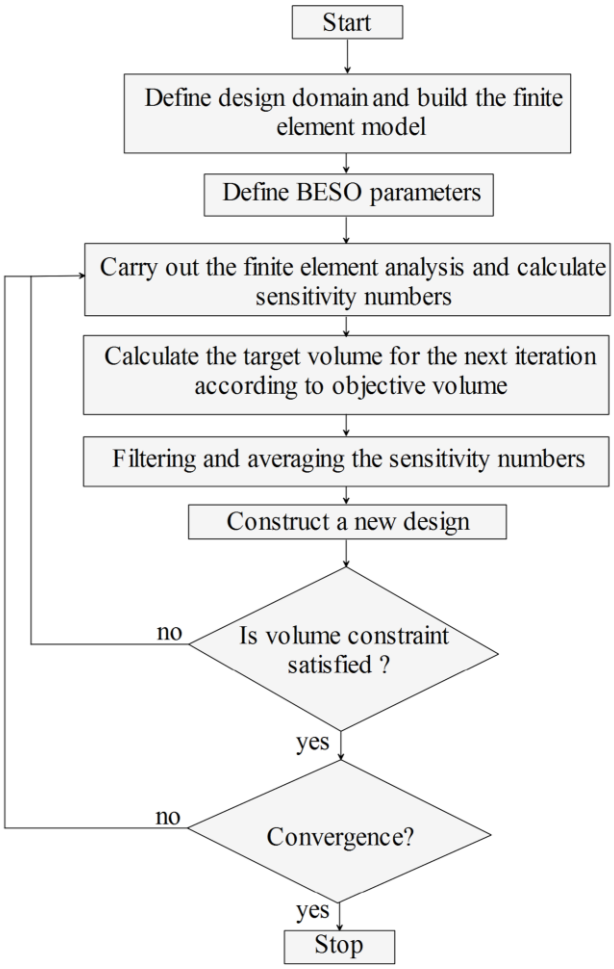

Fig. 3-2. Flowchart of the BESO procedure

The BESO procedure can be depicted in a flowchart as in Fig. 3-2.

3.3 BESO with an additional constraint

For adding a local constraint to the original BESO problem, Huang and Xie (Huang, X & Xie, Y 2010a) introduced the Lagrangian multiplier (λ). They added a local displacement constraint to their original BESO problem, in which they sought the stiffest structure while satisfying the volume and displacement constraints simultaneously. The optimization problem with additional displacement constraint is as follows:

$$\begin{cases} \text{Minimize} : \quad C = \dfrac{1}{2}\mathbf{f}^T\mathbf{u} \\ \text{subject to}: \begin{cases} u_j \le u_j^* \\ V(x) = \sum x_i v_i = V_{req} \\ x_i = 0 \ or \ 1 \ , \ i = 1,.....,nel \end{cases} \end{cases} \tag{3-12}$$

The modified objective function, considering the local displacement constraints reads:

$$f_1(x) = C + \lambda(u_j - u_j^*) \tag{3-13}$$

where $0 \le \lambda \le 1$. The modified objective function could have the same value as the original one, when the displacement value and the constraint value are equal. If $u_j < u_j^*$ the displacement constraint is satisfied and λ should set to 0 (λ=0). Hence the Lagrangian multiplier will act as a compromise between the local displacement constraint and the objective function. Since it has an effective role in calculating the sensitivity numbers it should be defined prior to the calculation of the sensitivity numbers.

3.3.1 Calculation of the Lagrangian multiplier

As explained in (Huang, X & Xie, Y 2010a) the calculation of the Lagrangian multiplier is based on the volume and additional constraint (displacement). This means the proper value of the Lagrangian multiplier (λ) can be calculated while both constraints are satisfied. λ can be defined as follows:

$$\lambda = \frac{1-\omega}{\omega} \tag{3-14}$$

where $\omega_{min} \le \omega \le 1$ and ω_{min} can have the small value e.g. $10^{-10.}$ The procedure of calculating the appropriate value for λ is as follows:

Step 1: The first lower bound value of ω is set to $\omega_{lower} = \omega_{min}$ and the upper bound value is set to be $\omega_{upper} = 1$.

Step 2: Start the program and calculate the sensitivity numbers based on the modified objective function (Equation (3-13)) and calculate the displacement for the next iteration (u_j^{k+1}) as follows:

$$u_j^{k+1} \approx u_j^k + \sum_i \frac{d\,u_j^k}{d\,x_i}\,\Delta x_i \tag{3-15}$$

Step 3: If the estimated displacement of the next iteration (u_j^{k+1}) is larger than its constraint value (u_j^*) then ω should be updated with a smaller value as follows:

$$\hat{\omega} = \frac{\omega + \omega_{lower}}{2} \tag{3-16}$$

and ω_{upper} should be set to ω at the same time. If u_j^{k+1} is less than the displacement constraint value, then ω should be updated with a larger value as follows:

$$\hat{\omega} = \frac{\omega + \omega_{upper}}{2} \tag{3-17}$$

and at the same time, ω_{lower} should be updated to ω.

Step 4: The above steps should be repeated until the difference between the upper and lower bounds of ω is less than10^{-5} (Huang, X & Xie, Y 2010a).

By using a Lagrangian multiplier, one can add an additional constraint to the topology optimization problem. Hence, if different constraints are added to the optimization problem, different Lagrangian multipliers must be applied rather than one, and the algorithm should be enhanced to have efficient computational cost. According to (Huang, X & Xie, Y 2010a) the computational cost for calculating the Lagrangian multiplier, while having one additional constraint is negligible because the calculation just updates the ranking of the sensitivity numbers based on the modified objective function (Equation (3-13)). In Chapter 4, we introduce our proposed stress-based BESO approach in which we have extended the BESO method by using the stress constraint to develop a stress-based BESO method.

Chapter 4

Bi-directional evolutionary topology optimization method based on stress

Stress-based topology optimization has been done by many authors during past decades but as stated earlier, the majority of the approaches are based on the SIMP method which is a continuous density approach. There was no report on considering stress constraint in term of the BESO methods, which is a discrete density and binary approach until recently when Xia et al. (2018) investigated the stress-based optimization problem in terms of BESO method. As explained in Chapter 2, Xia et al. (2018) simplified the sensitivity analysis and damped the sensitivity number for making the BESO procedure stable, meaning that they did not use the full stress vector in the sensitivity analysis. In this study, we have proposed a stress-based BESO method in which the sensitivity analysis has not been simplified, and the stress vectors of the material have been fully considered in the sensitivity analysis. Hence the BESO method has been used to find an optimal design without stress concentration where the stresses of the elements are close to the stress limit. As discussed later in this chapter, our proposed stress-based BESO method was able to reduce the maximum stress and consequently the stress concentration more than the method which was introduced by Xia et al. (2018) while compared with the original compliance-based BESO method.

4.1 Optimization problems formulation

In this chapter, three different optimization problems have been solved by considering the stress constraint in the BESO procedure. The first optimization problem which is called $\boldsymbol{P1_{stress}}$ is regarding the minimization of the compliance while satisfying volume and stress constraints. The problem is equal to the original BESO with an additional stress constraint as follows:

$$\mathbf{P1}_{\mathbf{stress}}: \begin{cases} \text{Minimize}: \ \mathrm{C} = f(x) = \dfrac{1}{2}\mathbf{u}^{\mathrm{T}}\mathbf{k}\mathbf{u} \\ \text{subject to}: \begin{cases} \sigma_G^{PN}{}_{(\max)} \le \sigma^* \\ V^* - \sum_{i=1}^{N_i} V_i x_i = 0 \\ x_i = x_{\min} \text{ or } 1 \end{cases} \end{cases} \tag{4-1}$$

The second problem is called ***P2*$_{stress}$** and deals with the minimization of the stress subject to the volume constraint as follows:

$$\mathbf{P2}_{\mathbf{stress}}: \begin{cases} \text{Minimize}: \ \sigma_G^{PN}(x) = \left(\dfrac{1}{N_i} \sum_{i=1}^{N_i} (\sigma_i^{vm}(x))^P \right) \\ \text{subject to}: \begin{cases} V^* - \sum_{i=1}^{N_i} V_i x_i = 0 \\ x_i = x_{\min} \text{ or } 1 \end{cases} \end{cases} \tag{4-2}$$

The third and last topology optimization problem which is called ***P3*$_{stress}$** is regarding the minimization of the structure volume while satisfying the stress constraint and reads:

$$\mathbf{P3}_{\mathbf{stress}}: \begin{cases} \text{Minimize}: \ V = \sum_{i=1}^{N_i} V_i x_i \\ \text{subject to}: \begin{cases} \sigma_G^{PN}{}_{(\max)} \le \sigma^* \\ x_i = x_{\min} \text{ or } 1 \end{cases} \end{cases} \tag{4-3}$$

In all the above optimization problems (***P1*$_{stress}$ – *P3*$_{stress}$**), V^*, V_i and x_i are the volume constraint, individual elements volume, and binary design variables respectively. The stress constraint is denoted by σ^*, and σ_G^{PN} is the global modified *p*-norm stress function which is based on the von Mises stresses of the elements and is discussed in the next section. To show the validity of our proposed method the above optimization problems have been solved for different numerical examples and are illustrated in the next sections. For showing the effectiveness of the proposed approach in reducing the stress concentration, the obtained results are compared with the original compliance–based BESO method (Huang, X & Xie, Y 2007) which is called ***P*$_{compliance}$** in this chapter and was introduced earlier in Chapter 3 (Equation (3-1)).

4.2 Local stresses aggregation method

Since the BESO method is a discrete density approach in which two phases representing void and solid materials are used and the final design is also free from intermediate material, no “singularity” problem occurs because the stress constraint is only applied to the solid phase. Regarding the local nature of the constraints in the stress-based topology optimization problems, the BESO cannot be exempted from this phenomenon like the continuous density approaches e.g. SIMP. To remedy this problem, the global approach of the local stress aggregation has been used, by adopting the *p*-norm aggregation function used by many authors see e.g.(Holmberg, Torstenfelt & Klarbring 2013; Jeong, Choi & Yoon 2014; Jeong et al. 2012; Le et al. 2010; Xia et al. 2018).

4.2.1 *p*-norm approach

To overcome the local nature of stress constraint and consequently decrease the computational cost for solving the optimization problems in this chapter, the modified *p*-norm function has been used to assemble the von Mises stresses of the elements, which are evaluated at the center of the elements in one global function. The *p*-norm stress is defined as:

$$\sigma_G^{PN}(x) = \left(\frac{1}{N_i} \sum_{i=1}^{N_i} (\sigma_i^{vm}(x))^p \right)^{\frac{1}{p}} \tag{4-4}$$

where the number of the stress evaluation points is denoted by N_i and σ_i^{vm} is the von Mises stress of the elements, which reads:

$$\sigma_i^{vm} = (\sigma_{ix}^2 - \sigma_{ix}\sigma_{iy} + \sigma_{iy}^2 + 3\tau_{ixy}^2)^{0.5} \tag{4-5}$$

The *p*-norm factor is denoted by p which should be infinite in principle, but some authors have reported that in practice a value from 3 to 4 works properly see e.g. (Jeong, Choi & Yoon 2014; Jeong et al. 2012; Le et al. 2010). According to (Le et al. 2010) many local optimums will occur if the value of the p increases and the optimization problem converge to a local optimum with a high maximum stress. In this research, our numerical experiences show that choosing a value from 3 to 5 for *p*-norm

factor (p) is acceptable for the proposed stress-based BESO problems. However, by changing the p value and selecting the other values, a different optimal design maybe obtained because of the change of the objective function.

4.3 Stress measurement

In this chapter for solving the stress-based optimization problem, the linear static analysis has been used to evaluate the displacement and stress of the elements and other quantities where the finite element analysis (FEA) reads:

$$\mathbf{KU} = \mathbf{F} \tag{4-6}$$

where **U** and **K** are the displacement and global stiffness matrix respectively and the vector of the applied load is denoted by **F**. Using the four nodes bilinear quadrilateral elements in FEA is simple and decreases the computational cost, while having promising results. It has also been used earlier in stress-constraint topology optimization e.g. (Jeong, Choi & Yoon 2014; Le et al. 2010) , therefore we have also employed it in our FEA. In this research, for solving the optimization problem, the material interpolation scheme (SIMP) is also adopted which reads:

$$E(x_i) = E^0 x_i^{\,q} \tag{4-7}$$

where the penalty exponent is denoted by q and is set to 3 unless stated. E^0 is Young's modulus of the solid material. To assemble the global stiffness matrix, the interpolation scheme has been used as follows:

$$\mathbf{K} = \sum_i x_i^{\,q}\, \mathbf{K}_i^0 \tag{4-8}$$

where the design variables of the element i is denoted by x_i and $\mathbf{K}_i^0$ is the elemental stiffness matrix of the solid elements.

For calculating the von Mises stress of the elements (Equation (4-5)) the stress vectors of the elements have been obtained in the centroid of the elements in the FEA as follows:

$$\boldsymbol{\sigma}_i = \mathbf{D}_i \mathbf{B}_i \mathbf{u}_i = \{\sigma_{ix}, \sigma_{iy}, \tau_{ixy}\} \tag{4-9}$$

where $\mathbf{B}_i$, $\mathbf{D}_i$, and $\mathbf{u}_i$ are the strain displacement matrix, constructive matrix and displacement vector respectively. By assuming the plane stress problem, the constructive matrix $\mathbf{D}_i$ can be defined as:

$$\mathbf{D}_i = \frac{E^0 x_i}{1-\nu^2}\begin{bmatrix} 1 & \nu & 0 \\ \nu & 1 & 0 \\ 0 & 0 & (1-\nu)/2 \end{bmatrix} \tag{4-10}$$

Hence, von Mises stress of each element in the design domain can be calculated based on the stress and displacement vectors which are calculated from FEA. Consequently, they can be applied to the *p*-norm function to reach a global stress constraint.

4.4 Sensitivity derivation

In order to solve the proposed stress-based BESO method problems, which were discussed earlier, the sensitivity numbers of the elements in the design domain should be calculated based on the derivative of the *p*-norm stress with respect to design variables. Hence the gradient of the *p*-norm stress (Equation (4-4)), calculated by applying the chain rule and can be defined as follows:

$$\frac{\partial \sigma_G^{PN}(x)}{\partial x_i} = \frac{\partial \sigma_G^{PN}(x)}{\partial \sigma_i^{vm}} \frac{\partial \sigma_i^{vm}(x)}{\partial x_i} = \frac{\partial \sigma_G^{PN}(x)}{\partial \sigma_i^{vm}} \left(\frac{\partial \sigma_i^{vm}(x)}{\partial \boldsymbol{\sigma}_i} \right) \frac{\partial \boldsymbol{\sigma}_i(x)^T}{\partial x_i} \tag{4-11}$$

where the term $\partial \sigma_G^{PN}(x) / \partial \sigma_i^{vm}$ can be defined as:

$$\frac{\partial \sigma_G^{PN}(x)}{\partial \sigma_i^{vm}} = \left(\frac{1}{N_i} \sum_{i=1}^{N_i} (\sigma_i^{vm}(x))^P \right)^{\left(\frac{1}{P}-1\right)} \times \frac{1}{N_i} \left(\sigma_i^{vm}(x)\right)^{P-1} \tag{4-12}$$

Since our topology optimization problems are in the 2D case, the derivative of the von Mises stress over the stress vector ($\partial \sigma_i^{vm}(x) / \partial \boldsymbol{\sigma}_i$) in Equation (4-11) can be defined as:

$$\frac{\partial \sigma_i^{vm}(x)}{\partial \boldsymbol{\sigma}_i} = \begin{cases} \dfrac{\partial \sigma_i^{vm}(x)}{\partial \sigma_{ix}} = \dfrac{1}{2\sigma_i^{vm}(x)}\left(2\sigma_{ix}(x) - \sigma_{iy}(x)\right) \\ \dfrac{\partial \sigma_i^{vm}(x)}{\partial \sigma_{iy}} = \dfrac{1}{2\sigma_i^{vm}(x)}\left(2\sigma_{iy}(x) - \sigma_{ix}(x)\right) \\ \dfrac{\partial \sigma_i^{vm}(x)}{\partial \tau_{ixy}} = \dfrac{3}{\sigma_i^{vm}(x)}\tau_{ixy}(x) \end{cases} \tag{4-13}$$

The term $\partial \boldsymbol{\sigma}_i(x)/\partial x_i$ in Equation (4-11), which is the derivative of the stress vector with respect to the design variables, can be defined as follows:

$$\frac{\partial \boldsymbol{\sigma}_i(x)}{\partial x_i} = \frac{\partial \mathbf{D}(x)}{\partial x_i}\mathbf{B}\mathbf{u} + \mathbf{D}\mathbf{B}\frac{\partial \mathbf{u}(x)}{\partial x_i} \tag{4-14}$$

The term $\partial \mathbf{D}(x)/\partial x_i$ can be easily calculated from Equation (4-10), but the term $\partial \mathbf{u}(x)/\partial x_i$ cannot easily be derived. For solving Equation (4-14) the adjoint method should be used to calculate the derivative of the displacement vectors over the design variables. Hence, when calculating the term $\partial \mathbf{u}(x)/\partial x_i$, the chain rule can be applied to the global Equation (4-6) as follows:

$$\frac{\partial \mathbf{F}}{\partial x_i} = \frac{\partial \mathbf{K}(x)}{\partial x_i}\mathbf{u} + \mathbf{K}\frac{\partial \mathbf{u}(x)}{\partial x_i} \tag{4-15}$$

then from Equation (4-15), the term $\partial \mathbf{u}(x)/\partial x_i$ can be calculated as:

$$\frac{\partial \mathbf{u}(x)}{\partial x_i} = -\mathbf{K}^{-1}\frac{\partial \mathbf{K}(x)}{\partial x_i}\mathbf{u} \tag{4-16}$$

Substituting Equation (4-16) into Equation (4-14) and then Equation (4-14) into Equation (4-11) gives:

$$\frac{\partial \sigma_G^{PN}(x)}{\partial x_i} = \frac{\partial \sigma_G^{PN}(x)}{\partial \sigma_i^{vm}}\left(\frac{\partial \sigma_i^{vm}(x)}{\partial \boldsymbol{\sigma}_i}\right)^T \times \left(\frac{\partial \mathbf{D}(x)}{\partial x_i}\mathbf{B}\mathbf{u} - \mathbf{D}\mathbf{B}\mathbf{K}^{-1}\frac{\partial \mathbf{K}(x)}{\partial x_i}\mathbf{u}\right) \tag{4-17}$$

By adopting the global stress constraint measurement (*p*-norm) the number of the stress constraint is less than the number of design variables x_i, therefore the adjoint method can be applied for solving the Equation (4-17) where the adjoint variable $\boldsymbol{\lambda}$ is defined as:

$$\boldsymbol{\lambda}^T = \frac{\partial \sigma_G^{PN}(x)}{\partial \sigma_i^{vm}} \left(\frac{\partial \sigma_i^{vm}(x)}{\partial \boldsymbol{\sigma}_i} \right)^T \mathbf{DBK}^{-1} \tag{4-18}$$

where λ can be calculated by the adjoint equation as follows:

$$\mathbf{K}\boldsymbol{\lambda} = \frac{\partial \sigma_G^{PN}(x)}{\partial \sigma_i^{vm}} \mathbf{DB} \frac{\partial \sigma_i^{vm}(x)}{\partial \boldsymbol{\sigma}_i} \tag{4-19}$$

By inserting $\boldsymbol{\lambda}$ into Equation (4-17) the final gradient of the *p*-norm stress reads:

$$\frac{\partial \sigma_G^{PN}(x)}{\partial x_i} = \frac{\partial \sigma_G^{PN}(x)}{\partial \sigma_i^{vm}} \left(\frac{\partial \sigma_i^{vm}(x)}{\partial \boldsymbol{\sigma}_i} \right)^T \frac{\partial \mathbf{D}(x)}{\partial x_i} \mathbf{Bu} - \boldsymbol{\lambda}^T \left(\frac{\partial \mathbf{K}(x)}{\partial x_i} \mathbf{u} \right) \tag{4-20}$$

As explained earlier, since the *p*-norm approach has been used to assemble the local stresses of the elements in one global function, the derivative of the *p*-norm stress with respect to the design variables x_i (Equation (4-20)) should be used for evaluating the sensitivity numbers. Hence Equation (4-20) is common in all the stress-based optimization problems of this chapter (***P1***$_{stress}$ **–** ***P3***$_{stress}$). However, depending on the objective function of the problems; the calculation of the sensitivity numbers might be different in each case, but the sensitivity of the *p*-norm (Equation (4-20)) plays the main role in the evaluation of their sensitivity numbers. In the next sections, we investigate the different stress-based topology optimization problems (***P1***$_{stress}$ **–** ***P3***$_{stress}$) along with different numerical examples to show the validity and effectiveness of the proposed method.

4.5 Stiffness optimization with an additional stress constraint

In this section, the first proposed optimization problem (**P1**$_{\mathbf{stress}}$) which is shown in Equation (4-1) was solved where the compliance has been minimized subject to the volume and stress constraints. This means that an additional stress constraint has been added to the original BESO problem. As discussed

earlier in Chapter 3, the Lagrangian multiplier is used for adding an extra constraint to the original BESO problem and the derivative of the modified objective function will be considered for the calculation of the sensitivity numbers. In addition, in order to show the effectiveness of the proposed approach, the stress distribution of the element in the original BESO problem (***P*** $_{compliance}$) has been compared with the ***P1*** $_{stress}$ problem.

4.5.1 Numerical procedure

To solve the ***P1*** $_{stress}$ problem, the sensitivity numbers of the elements should be defined based on the derivative of the objective function. Since an extra stress constraint has been added to the original BESO problem, the objective function should be modified as follows:

$$f_1(x) = C + \lambda(\sigma_G^{PN}{}_{(\max)} - \sigma^*) \tag{4-21}$$

where C, $\sigma_G^{PN}{}_{(max)}$ and σ^* are the compliance, normalized p-norm stress, and stress constraint respectively. The Lagrangian multiplier is denoted by λ which calculates based on the volume and stress constraints and is discussed later in the next section. According to the Equation (4-21), when the p-norm stress is equal to the stress constraint, the modified objective function will be the same as the original BESO objective function. In addition, when $\sigma_G^{PN}{}_{(max)} < \sigma^*$, the Lagrangian multiplier will be set to zero ($\lambda=0$), meaning that the stress constraint has already been satisfied. However, the value of λ will tend to infinity if $\sigma_G^{PN}{}_{(max)} > \sigma^*$ which means that $\sigma_G^{PN}{}_{(max)}$ is minimized to satisfy the stress constraint in later iterations. Hence the Lagrangian multiplier will act as a compromise between the local stress constraint and the objective function. As it has an effective role in calculating the sensitivity numbers it should be defined prior to the calculation of the sensitivity numbers. Thus, the sensitivity of the modified objective function is:

$$\frac{df_1}{dx_i} = q\, x_i^{\,q-1}\left(-\frac{1}{2}\mathbf{u}^{\mathbf{T}}\mathbf{K}\mathbf{u} + \lambda \frac{\sigma_G^{PN}{}_{(\max)}(x)}{\partial x_i}\right) \tag{4-22}$$

where the sensitivity number of the elements used in BESO can be expressed by:

$$\alpha_i = -\frac{1}{q}\frac{df_1}{dx_i} = x_i^{q-1}\left(\frac{1}{2}\mathbf{u}^{\mathbf{T}}\mathbf{K}\mathbf{u} - \lambda\frac{\sigma_{G\ (\max)}^{PN}(x)}{\partial x_i}\right) \tag{4-23}$$

In the BESO method, the optimal design is obtained by adding and removing the elements from the design domain (solid and void elements). Therefore, the sensitivity numbers for solid and void elements can be defined as:

$$\alpha_i = \begin{cases} \frac{1}{2}\mathbf{u}^{\mathbf{T}}\mathbf{K}\mathbf{u} - \lambda\frac{\sigma_{G\ (\max)}^{PN}(x)}{\partial x_i} & \text{for} \quad x_i = 1 \\ x_i^{q-1}\left(\frac{1}{2}\mathbf{u}^{\mathbf{T}}\mathbf{K}\mathbf{u} - \lambda\frac{\sigma_{G\ (\max)}^{PN}(x)}{\partial x_i}\right) & \text{for} \quad x_i = x_{\min} \end{cases} \tag{4-24}$$

where the normalized *p*-norm stress $\sigma_G^{PN}{}_{(max)}$ has been used to better approximate the maximum local stress value, and according to (Le et al. 2010) leads to better designs, when using the lower *p*-norm factor (*p*). The normalized *p*-norm stress can be defined as follows

$$\sigma_{G\ (\max)}^{PN} \approx c^I\ (\sigma_G^{PN})^I \tag{4-25}$$

where I denotes the iteration number and c^I can be evaluated according to the following equation when I >1.

$$c = \alpha^I\ \frac{\sigma_{\max}^{I-1}}{(\sigma_G^{PN})^{I-1}} + (1-\alpha^I)\ c^{I-1} \quad , \quad 0 < \alpha^I < 1 \tag{4-26}$$

Therefore, the derivative of the normalized *p*-norm stress in Equation (4-24) can be calculated by calculating the derivative of the *p*-norm stress (Equation (4-17)) and *c* as above.

4.5.2 Calculation of the Lagrangian multiplier

According to (Huang, X & Xie, Y 2010a) the Lagrangian multiplier (λ) can be calculated based on the volume and additional constraint which means that the proper value of the λ can be obtained while both constraints are satisfied. Hence by considering the stress and volume constraints, λ can be defined as follows

$$\lambda = \frac{1-\omega}{\omega} \tag{4-27}$$

where $\omega_{min} \leq \omega \leq 1$ and ω_{min} can has the small value e.g. 10^{-10}. The procedure of calculating the appropriate value for λ is as follows:

Step 1: The first upper and lower bound values of ω are set to be ω_{upper} = 1 and ω_{lower} = ω_{min} respectively.

Step 2: Calculate the sensitivity numbers of the elements based on the modified objective function and estimate the *p*-norm stress for the next iteration ($(\sigma_G^{PN})_{\max}^{I+1}$) as follows:

$$(\sigma_G^{PN})_{\max}^{I+1} \approx (\sigma_G^{PN})_{\max}^{I} + \sum_i \frac{\sigma_G^{PN}}{\partial x_i} \Delta x_i \tag{4-28}$$

Step 3: If $(\sigma_G^{PN})_{\max}^{I+1} > \sigma^*$, then the smaller value should be chosen for ω as follows:

$$\hat{\omega} = \frac{\omega + \omega_{lower}}{2} \tag{4-29}$$

and at the same time, ω_{upper} should be set to ω. If $(\sigma_G^{PN})_{\max}^{I+1} < \sigma^*$ then a larger value should be used for ω as follows:

$$\hat{\omega} = \frac{\omega + \omega_{upper}}{2} \tag{4-30}$$

and at the same time, ω_{lower} should be set to ω.

Step 4: The above steps should be repeated until the difference between the upper and lower bounds of ω is less than10^{-5} and a proper value of λ was obtained. Since the current stress-based BESO only needs to update the relative ranking of sensitivity numbers, the cost of Lagrangian multiplier calculation is negligible in the proposed method.

4.5.3 BESO procedure with an additional stress constraint

The proposed stress-based BESO method procedure for solving problem ***P1***$_{stress}$ is similar to the procedure of the original BESO method, which was discussed in Chapter 3, the difference being that the sensitivity numbers of the elements are based on the stress and volume constraints where the Lagrangian multiplier is used to add the additional stress constraint to the original BESO problem. In addition, the convergence criteria are based on both the volume and stress constraints. In the original BESO algorithm, the sensitivity numbers and convergence criterion are calculated based on the volume constraint. Since in both the original BESO method and the proposed stress-based approach the BESO optimizer is used, the relative ranking of the sensitivity numbers leads to the optimal design in both approaches. Hence in the proposed stress-based approach, the sensitivity numbers filtering used is the same as the original BESO method (Huang, X & Xie, YM 2010) which discussed in Chapter 3. Also, the sensitivity numbers have been modified by averaging their values at their previous iteration to improve the convergence of BESO. In the proposed stress-based BESO method, the gradual material removal is stopped when the algorithm reaches the objective volume (V^*) and the whole optimization process will end if the following convergence criteria are satisfied.

$$error_1 = \frac{\left| \sum_{i=1}^{N} C_{k-i+1} - \sum_{i=1}^{N} C_{k-N-i+1} \right|}{\sum_{i=1}^{N} C_{k-i+1}} \leq 0.01 \tag{4-31}$$

$$error_2 = \frac{\left| \sum_{i=1}^{N} (\sigma_{\max,\,k-i+1} - \sigma_{\max,\,k-N-i+1}) \right|}{\sum_{i=1}^{N} \sigma_{\max,\,k-i+1}} \leq 0.01 \tag{4-32}$$

where $N = 5$ is used in this problem.

The stress-based BESO procedure for solving the optimization problem ***P1***$_{stress}$ can be depicted in a flowchart as Fig. 4-1 where the procedure can be outlined as follows:

Step 1: Discretize the whole design domain using a finite element mesh.

Step 2: Define the BESO parameters such as objective volume, V^*, stress constraint σ^* and evolutionary ratio *ER*.

Step 3: Carry out finite element analysis (FEA) for calculating the sensitivity numbers which are based on stress.

Step 4: Determine the target volume for the next design according to the volume constraint.

Step 5: Update Lagrangian multiplier of the constraints (volume and stress).

Step 6: Filter sensitivity numbers in the whole design domain to obtain the improved sensitivity numbers and average the obtained sensitivity number by its previous iterations history.

Step 7: Reset the design variables of all elements by switching the solid elements to voids and vice versa.

Step 8: Repeat 3–6 until the solution is convergent.

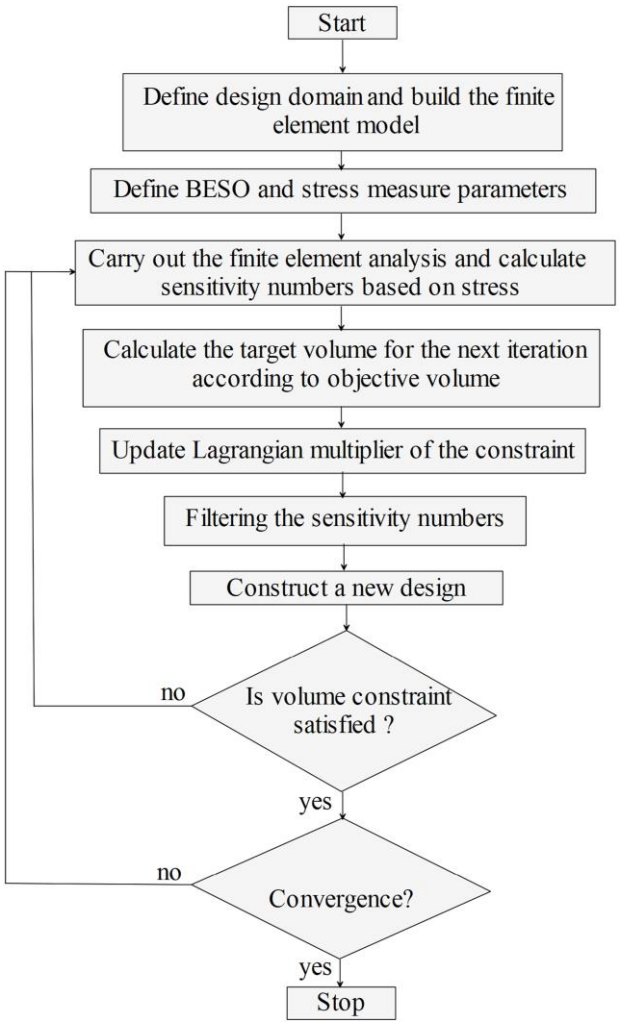

Fig. 4-1. Flowchart of the BESO procedure with an additional stress constraint

4.5.4 Numerical examples

To show the effectiveness of the proposed stress-based BESO approach, the optimal layouts for the 2D examples in the plane stress are provided in this section where the $\mathbf{P1}_{\mathbf{stress}}$ problem has been solved and compared with the traditional compliance-based problem $\mathbf{P}_{\mathbf{compliance}}$. The same loading condition, BESO parameters, and volume constraint, have been used in both optimization problems ($\mathbf{P1}_{\mathbf{stress}}$& $\mathbf{P}_{\mathbf{compliance}}$) to better compare the final stress distribution of the elements and the compliance of the optimal designs. A developed Matlab code has been implemented to solve the optimization problem. Since in the numerical examples the point load has been applied to the structure, which will cause an irreducible high local stress at the position of the point load (even if the entire domain becomes solid), therefore the elements in the neighborhood of the point load are excluded from the design space, which means that they are kept as solid elements during the entire optimization process.

4.5.4.1 L-bracket beam (center load)

The first example is the benchmark example of the stress constraint topology optimization and has been considered by many authors see e.g. (Holmberg, Torstenfelt & Klarbring 2013; Jeong, Choi & Yoon 2014; Jeong et al. 2012; Le et al. 2010; Xia et al. 2018). This example is the L-bracket beam with a point load on the middle of the right side with a fixed edge as shown in Fig. 4-2.

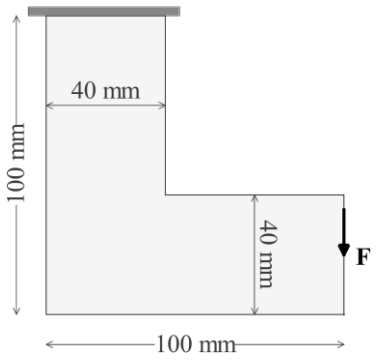

Fig. 4-2. L-Bracket beam

The design space consists of 6400 four-node plane stress elements in total, which are of equal size (1 mm × 1 mm) with a 1 mm thickness. The applied point load has been set to be 500 N in this example,

and to avoid stress concentration in the vicinity of the point load, 3 × 2 elements (six elements) around the applied point load are excluded from the design space and fixed as solid elements during the optimization process. The evolutionary rate (*ER*) and the filter radius (r_{min}) are set to be 0.02 and 1.5 mm respectively. Carbon steel 1018 with Young's modulus 210,000 MPa and Poisson's ratio 0.3 has been used as the material reference. The optimization problems have been solved for two different volume constraints 0.32 and 0.4 where the stress constraint has been set to be 358 MPa, which is the material's yield limit.

	$\mathbf{P1}_{\mathbf{stress}}$ (V/V_0=0.32)	$\mathbf{P}_{\mathbf{compliance}}$ (V/V_0=0.32)
Optimized layout & von Mises stress plot	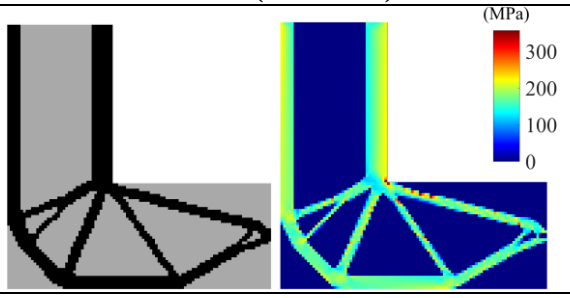	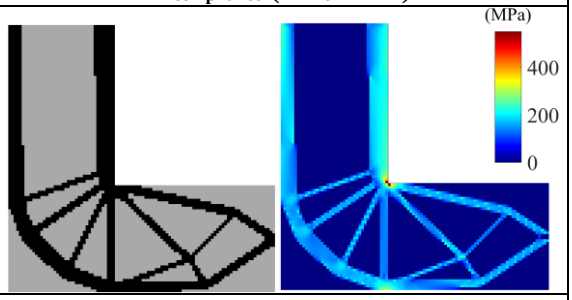
	σ_{max} = 356.4 [MPa], C = 295.5 [N mm]	σ_{max} = 551 [MPa], C = 283.7 [N mm]

Fig. 4-3. Optimal layouts for L-bracket (V/V_0=0.32)

The topology optimization results for volume constraint 0.32 is shown in Fig. 4-3 and the convergence plots are provided in Fig. 4-4. As it can be seen from the results, the maximum stress has been reduced by 35 % compared to the original BESO problem ($\mathbf{P}_{\mathbf{compliance}}$), however the difference between the compliance in both approaches is less than 4.5%. The convergence plots which are shown in Fig. 4-3 are based on the convergence criteria defined in Equations (4-31) and (4-32). The convergence criterion which is based on the *p*-norm stress is also depicted for the $\mathbf{P}_{\mathbf{compliance}}$ problem to compare the evolution of the stress in both approaches.

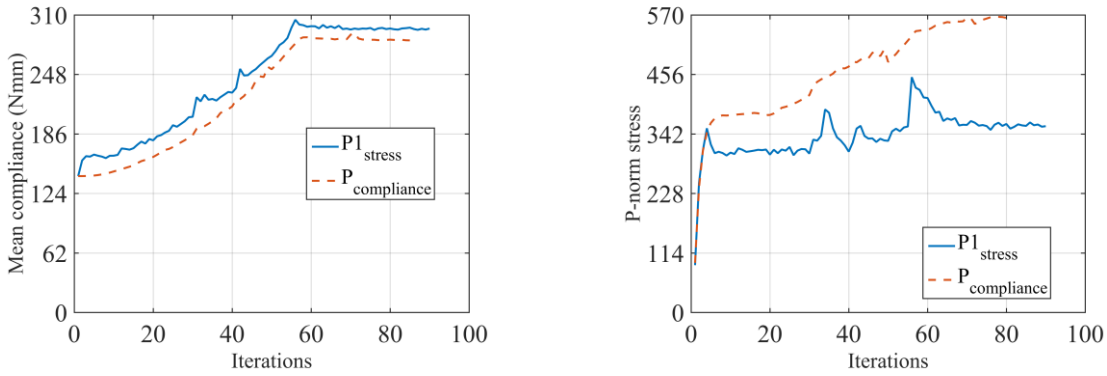

(a) (b)

Fig. 4-4. Convergence plots for L-bracket (V/V_0=0.32) (a) mean compliance, (b)*p*-norm stress

The optimized layouts and the convergence plots for the volume constraint 0.4 (V/V_0=0.4) is also depicted in Figs. 4-5 and 4-6. According to the results, the difference between the mean compliance in both approaches is less than 5.5%. However, the maximum von Mises stress has been decreased significantly (29%) while compared with the compliance-based method (**P**$_{\textbf{compliance}}$). The evolution of the *p*-norm stress and the optimization layout of the proposed problem with volume constraint 0.32 is shown in Fig. 4-7.

	P1$_{\textbf{stress}}$ (V/V_0=0.4)	**P**$_{\textbf{compliance}}$ (V/V_0=0.4)
Optimized layout & von Mises stress plot	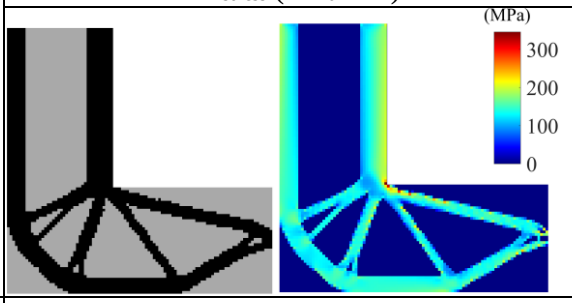	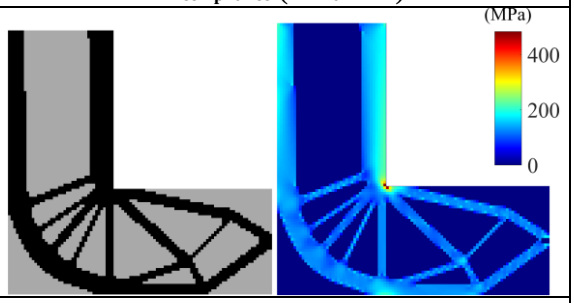
	σ_{max} = 345.4 [MPa], C = 245.9 [N mm]	σ_{max} = 483.5 [MPa], C = 233.9 [N mm]

Fig. 4-5. Optimal layouts for L-bracket (V/V_0=0.4)

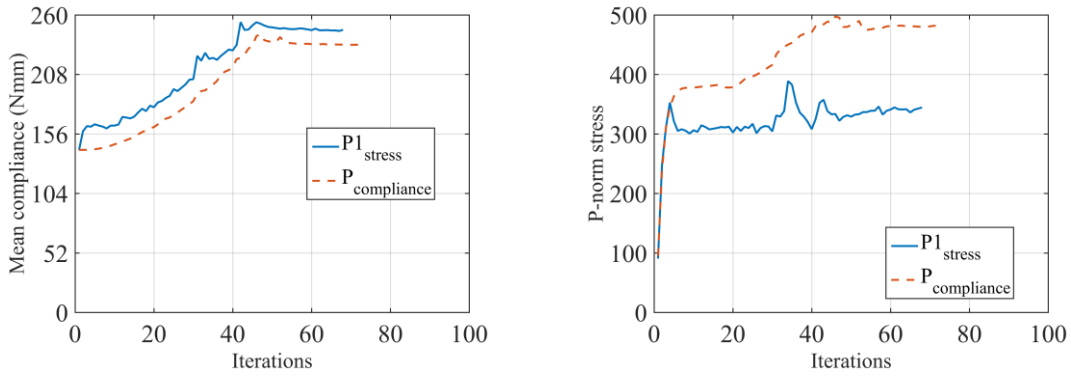

(a) (b)

Fig. 4-6. Convergence plots for L-bracket (V/V_0=0.4) (a) mean compliance, (b)*p*-norm stress

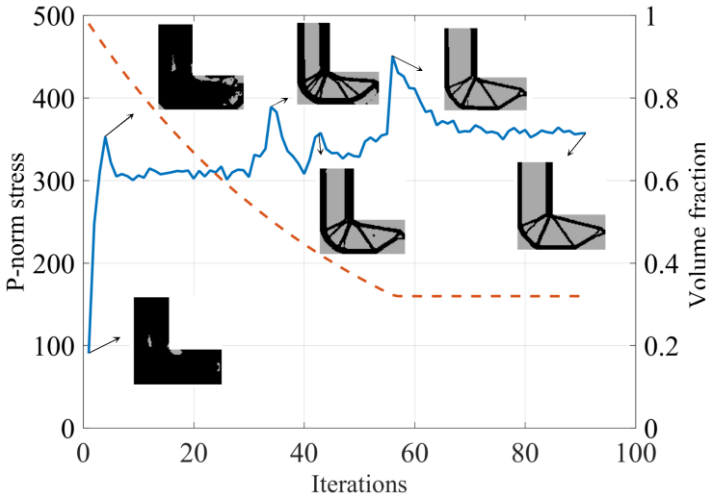

Fig. 4-7. Evolution of optimized layout and *p*-norm stress for L-bracket (V/V_0=0.32)

4.5.4.2 Long-clamped beam

The second example, which is represented in Fig. 4-8, deals with the optimization of a long clamped beam that is clamped on both sides, with a point load applied at the center of the beam where L = 200 mm and the thickness is 1 mm. The design domain is discretized by 6000, 1×1 mm quadrilateral Q4 plane stress elements. The sensitivity filter radius (r_{min}) and the evolutionary ratio (ER) are chosen to be 2 mm and 0.02 respectively. A 1000 N point load has been applied in the middle of the beam. As explained earlier in this chapter, due to applying the point load, 12 elements (3×4) in the vicinity of the applied load are not used as design variables to avoid the high local stress concentrations.

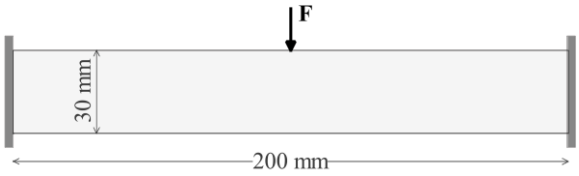

Fig. 4-8. Long clamped beam

Solutions for the long clamped beam problem for minimizing compliance are shown in Figs. 4-9 and 4-11 for different volume constraints 0.33 and 0.42. As mentioned before, in each example we have the optimal design of the traditional compliance-based optimization problem ($\mathbf{P}_{\mathbf{compliance}}$) which has the same load and volume constraint as the examples which have been solved in $\mathbf{P1}_{\mathbf{sress}}$ problems.

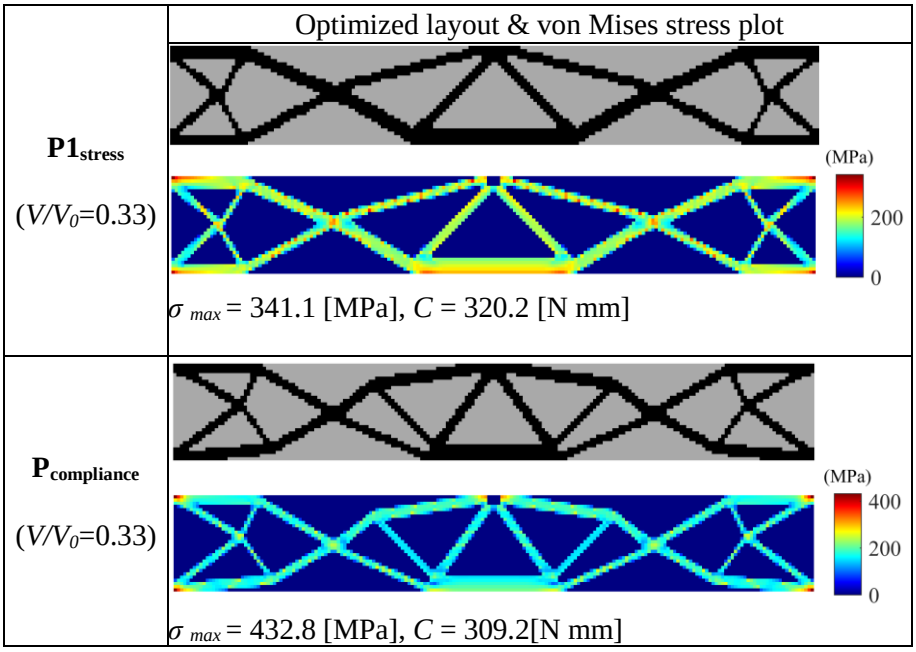

Fig. 4-9. Optimal layouts for the long clamped beam (V/V_0=0.33)

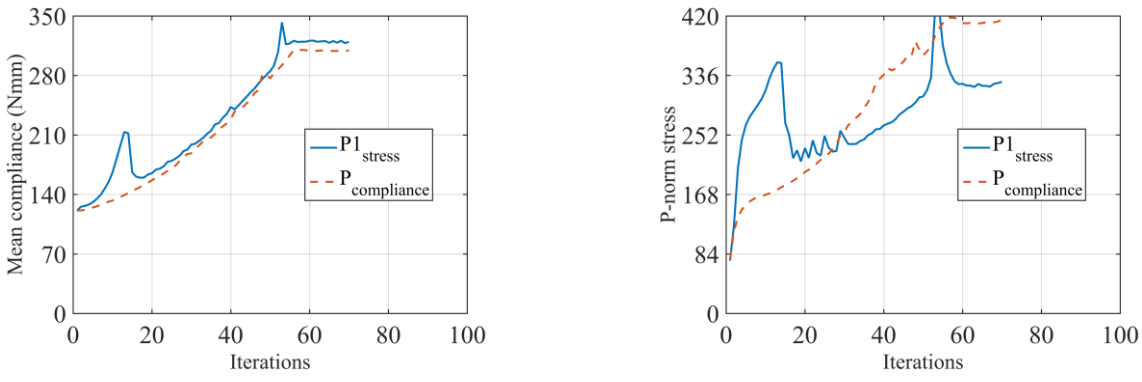

(a) (b)

Fig. 4-10. Convergence plots for the long clamped beam (V/V_0=0.33) (a) mean compliance, (b) *p*-norm stress

According to the results, the difference between the mean compliance of the $\mathbf{P1}_{\mathbf{stress}}$ and $\mathbf{P}_{\mathbf{compliance}}$ problems is 3%-4% while the maximum stress in the proposed approach ($\mathbf{P1}_{\mathbf{stress}}$) has been reduced by 20%-22% compared with the compliance-based BESO problem ($\mathbf{P}_{\mathbf{compliance}}$). The convergence plots of the problem solution are shown in Figs. 4-10 and 4-12 where the case of the compliance problem $\mathbf{P}_{\mathbf{compliance}}$ is also available for comparison.

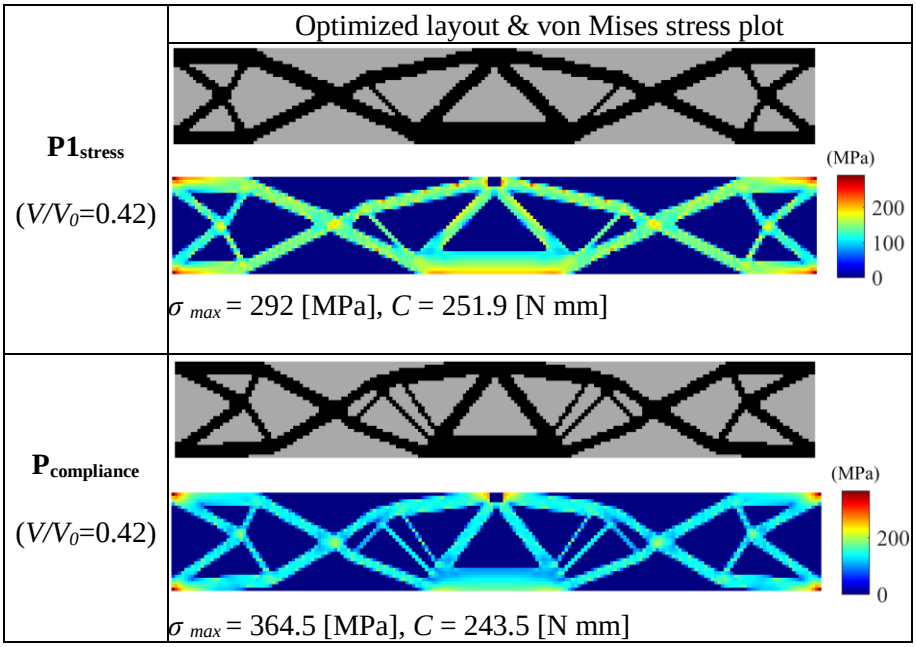

Fig. 4-11. Optimal layouts for the long clamped beam (V/V_0=0.42)

The evolution of the *p*-norm stress and the optimal design layouts for specific iterations are also illustrated in Fig. 4-13 for the volume constraint 0.33(V/V_0=0.33).

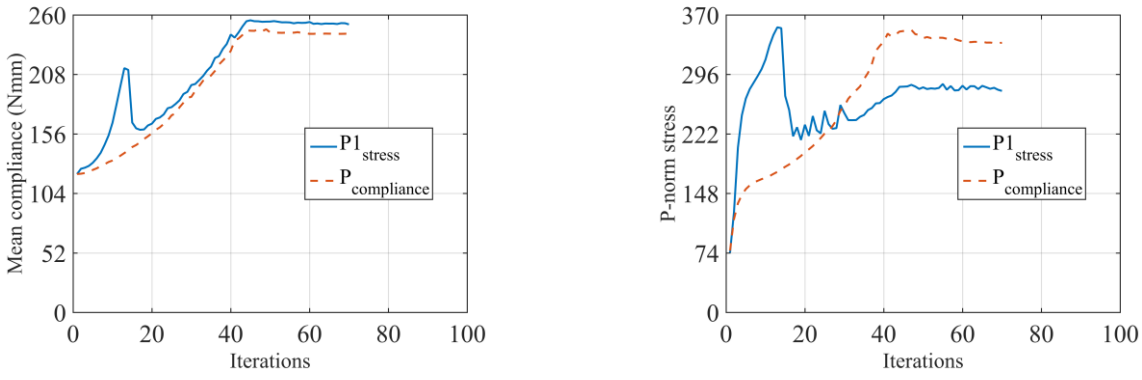

(a) (b)

Fig. 4-12. Convergence plots for the long clamped beam (V/V_0=0.42) (a) mean compliance, (b) *p*-norm stress

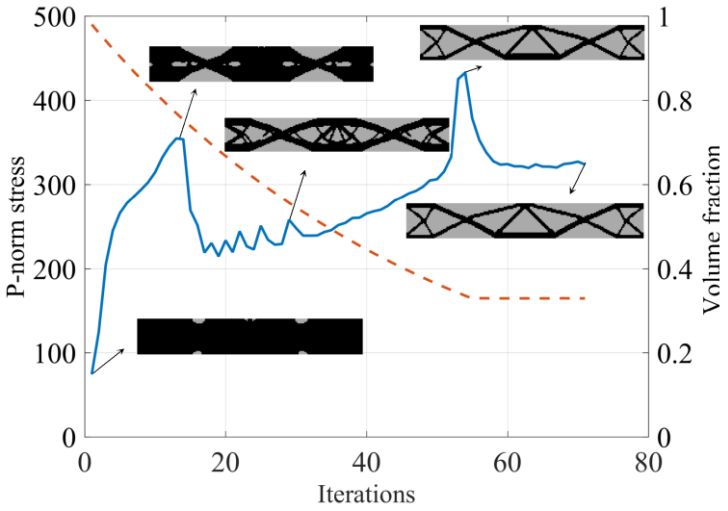

Fig. 4-13. Evolution of optimized layout and *p*-norm stress for the long clamped beam (V/V_0=0.33)

It can be seen from the results that optimal designs of the traditional BESO stiffness problem contain high-stress concentration, in which the maximum stress is larger than the material stress limit which has been set to the yield limit of the materials in this chapter. This means that the optimal design is not resistant for the stress failure. However, in the results which were obtained from the proposed method, all of the maximum stresses are below the yield limit threshold, while the structure has the highest stiffness, and the difference between the proposed method stiffness and which has obtained from the original BESO approach is about 3%- 4%.

4.5.4.3 Cantilever Beam

A cantilever beam, which is shown in Fig. 4-14, has been considered as the third example in this chapter where a 650 N point load is applied at the middle of the right-hand side and the design space has meshed into 5000 quadrilateral plane stress elements (1×1 mm). Again to avoid the stress concentration, the eight elements (4×2) which are at the neighborhood of the applied load are excluded from the design space. The thickness, sensitivity filter radius (r_{min}) and the evolutionary rate (*ER*) are set to be 1 mm, 2 mm and 0.02 respectively. The numerical results from the optimization

problems $\mathbf{P1}_{\mathbf{stress}}$ and $\mathbf{P}_{\mathbf{compliance}}$ are shown in Figs. 4-15 and 4-17 for different volume constraints 0.25 and 0.4.

As can be seen from the results, the maximum stress has decreased from 31% - 36% compared with the traditional compliance-based method, however the compliance value in the case of the proposed approach is 1.5%- 4% higher than the compliance values which were obtained from the $\mathbf{P1}_{\mathbf{stress}}$ due to the applied stress constraint and consequently the modified objective function.

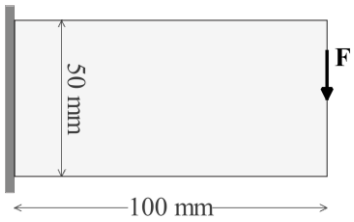

Fig. 4-14. Cantilever Beam

	Optimized layout & von Mises stress plot
$\mathbf{P1}_{\mathbf{stress}}$ (V/V_0=0.25)	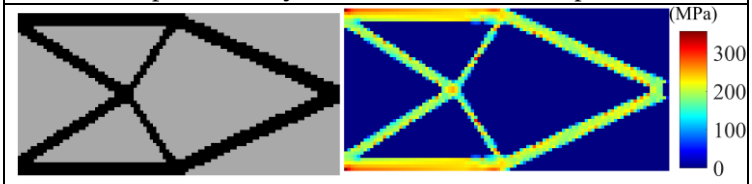 σ_{max} = 356.7 [MPa], C = 246.4 [N mm]
$\mathbf{P}_{\mathbf{compliance}}$ (V/V_0=0.25)	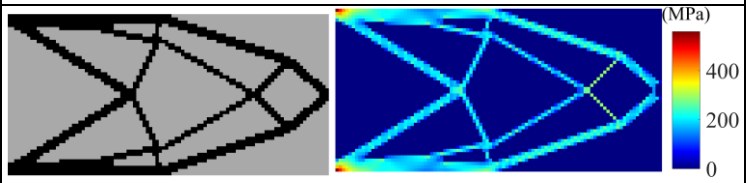 σ_{max} = 558.9 [MPa], C = 243.3 [N mm]

Fig. 4-15. Optimal layouts for cantilever beam (V/V_0=0.25)

The convergence plots are shown in Figs. 4-16 and 4-18 where the *p*-norm stress evolution is also provided for the compliance-based approach ($\mathbf{P}_{\mathbf{complince}}$) for comparison.

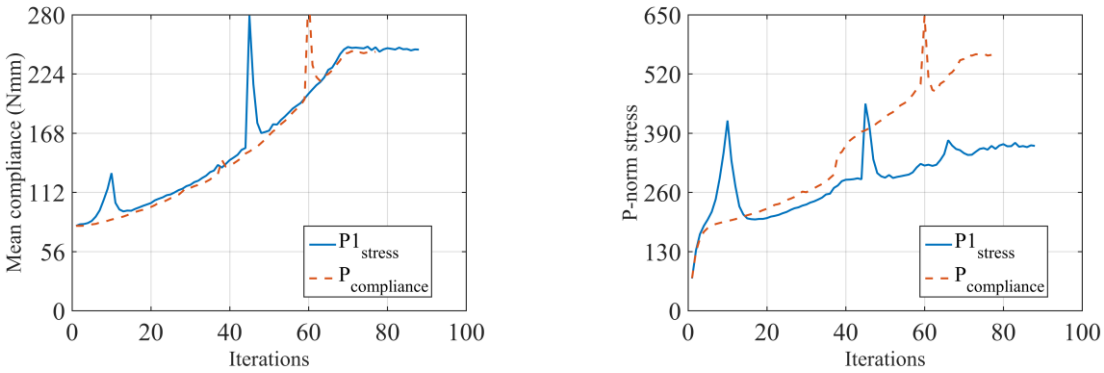

(a) (b)

Fig. 4-16. Convergence plots for cantilever beam (V/V_0=0.25) (a) mean compliance, (b) *p*-norm stress

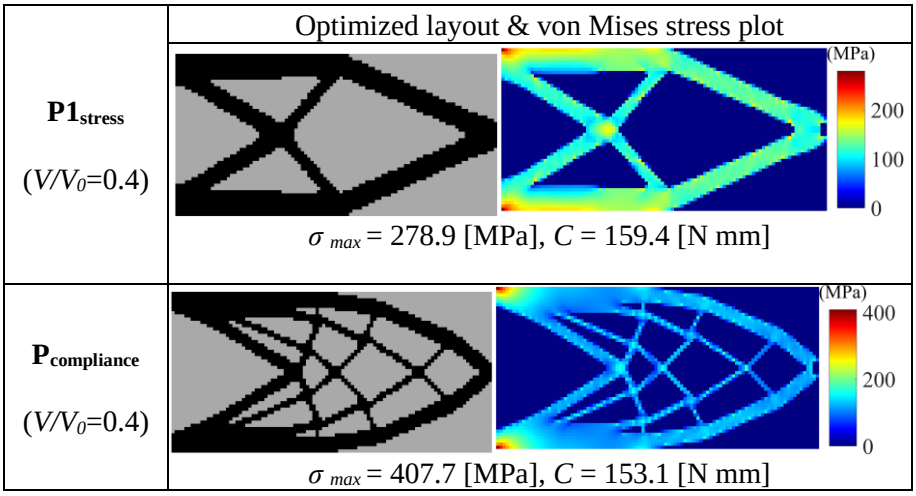

Fig. 4-17. Optimal layouts for cantilever beam (V/V_0=0.35)

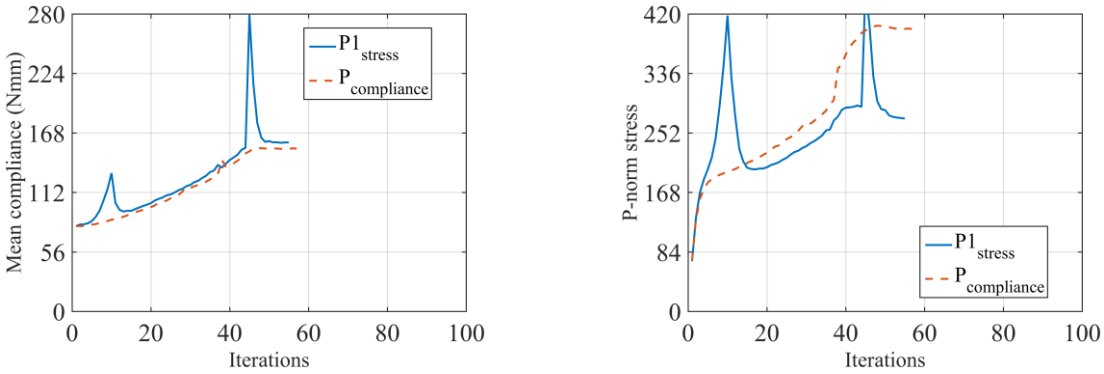

(a) (b)

Fig. 4-18. Convergence plots for cantilever beam (V/V_0=0.35) (a) mean compliance, (b) *p*-norm stress

The evolution of the *p*-norm stress and some specific design layouts are shown in Fig. 4-19 for the $\mathbf{P1}_{\mathbf{stress}}$ problem with volume constraint 0.25. According to the afore-mentioned results, again in this example, the stress consternation has been reduced significantly, while the stiffness of the structure is very close to the stiffness which is obtained from the original stiffness optimization in the framework of the BESO method. This means that the optimal structure obtained from $\mathbf{P1}_{\mathbf{stress}}$ problem is stress-failure resistant.

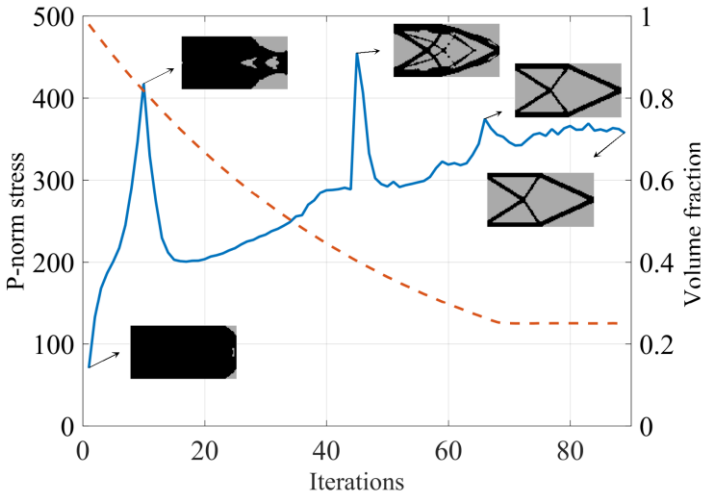

Fig. 4-19. Evolution of optimized layout and *p*-norm stress for long clamped beam (V/V_0=0.25)

4.5.5 Concluding remarks

Bi-directional evolutionary topology optimization (BESO) with an additional stress constraint was addressed in the previous sections of this chapter. The aim was to seek the stiffest structure while volume and stress constraints were satisfied. Since stress is one of the most important criteria in the engineering applications, it is essential for it to be considered in terms of topology optimization, to avoid stress failure of the optimal design. In addition, it is not enough to use the BESO purely for stiffness optimization. The stress constraint should be applied as a constraint in the original BESO problem to seek the stiffest optimal design which is resistant to stress failure.

The numerical results in the above sections show the efficiency of the proposed stress-based BESO method where the maximum stress was constrained to the yield limit of the materials. It was seen

from the results that the mean compliance values of the optimal structure in the proposed method with the original BESO method were very close (difference < 4%). The maximum stress in the proposed method reduced significantly (all the stresses < yield limit) when compared with the original BESO approach. Hence the proposed approach was able to solve the BESO problem with an additional stress constraint.

4.6 Stress minimization of the structures considering the BESO method

In this section, the optimization problem is as defined in Equation (4-2) where the *p*-norm stress is minimized subject to a volume constraint. The problem formulation is called $\mathbf{P2_{sterss}}$ in this chapter, and again the results are compared with the BESO traditional stiffness optimization ($\mathbf{P_{compliance}}$) which has been defined in Equation (3-1). Again, the material chosen is carbon steel 1018 and to avoid stress concentration, the elements in the vicinity of the applied loads are excluded from the design space.

4.6.1 Procedure summary

To solve the $\mathbf{P2_{sterss}}$ optimization problem which is shown in Equation (4-2), the gradient of the modified *p*-norm stress should be derived in Equation (4-20). Since the *p*-norm stress is minimized, subject to the volume constraint, a negative value of the sensitivity number should be used as follows:

$$\alpha_i = -\frac{\partial \sigma_G^{PN}(x)}{\partial x_i} = -\left[\frac{\partial \sigma_G^{PN}(x)}{\partial \sigma_i^{vm}} \left(\frac{\partial \sigma_i^{vm}(x)}{\partial \boldsymbol{\sigma}_i} \right)^T \frac{\partial \mathbf{D}(x)}{\partial x_i} \mathbf{Bu} - \boldsymbol{\lambda}^T \left(\frac{\partial \mathbf{K}(x)}{\partial x_i} \mathbf{u} \right) \right] \tag{4-33}$$

The sensitivity numbers in Equation (4-33) consist of two terms where the first term is the variation of the stress itself. Recently Xia et al. (2018) addressed the same optimization problem as $\mathbf{P2_{sterss}}$ in their research. As mentioned previously, they simplified the sensitivity analysis, due to the complexity of the stress sensitivity analysis. The sensitivity number is only considered the second term of the Equation (4-33) and the first term is totally ignored due to the artificial material interpolation scheme.

The BESO procedure for solving the $\mathbf{P2_{sterss}}$ is the same as the original BESO procedure, which was discussed in Chapter 3, however, with the difference that the sensitivity numbers are calculated based on the stress (Equation (4-33)) rather than compliance. Again, the sensitivity numbers have been modified by averaging their values at their previous iteration to improve the convergence of the BESO. As discussed in Chapter 3, the sensitivity filtering approach has been used to avoid the checkerboard patterns (Huang, X & Xie, YM 2007, 2010). Additionally, the absolute difference of the maximum stresses between two sequential iterations is considered as a convergence criterion when the volume constraint is satisfied and can be defined as follows:

$$error = \frac{\left|\sum_{i=1}^{N}(\sigma_{\max,\,k-i+1} - \sigma_{\max,\,k-N-i+1})\right|}{\sum_{i=1}^{N}\sigma_{\max,\,k-i+1}} \leq 0.01 \tag{4-34}$$

where $N = 5$ is used in this problem.

4.6.2 Numerical examples

To show the effectiveness of the proposed stress-based BESO approach, again the optimal layouts for the 2D examples in the plane stress are provided in this section, where the $\mathbf{P2_{stress}}$ problem (Equation (4-2)) has been solved and compared with the traditional compliance-based problem $\mathbf{P_{compliance}}$ (Equation (3-1)). The same loading condition, BESO parameters, and volume constraint have been used in both optimization problems ($\mathbf{P1_{stress}}$ & $\mathbf{P_{compliance}}$) to better compare the final stress concentration of the optimal design.

4.6.2.1 L-bracket beam (top load)

The L-bracket with the top load and fixed edge is considered as the first example. This is the most popular example for the stress constraint topology optimization problem, due to the stress concentration at the kink of the L-beam. This has been addressed by many authors in their research

see e.g. (Bruggi & Duysinx 2012; Holmberg, Torstenfelt & Klarbring 2013; Jensen 2016; Jeong et al. 2012; Le et al. 2010). The geometry and the dimensions of the L-bracket beam are shown in Fig. 4-20 where the thickness is 1 mm, and the design domain consists of 6400 elements which have 4 nodes and are equal sized (1 mm × 1 mm). The point load is 500 N and applied at the top of the right-hand side of the L-bracket. Again, to avoid the stress concentration, six elements (2×3) are excluded from the design space. The stress limit, evolutionary rate (*ER*) and the sensitivity filter (r_{min}) are set to be 358 MPa, 0.02 and 1.5 mm respectively.

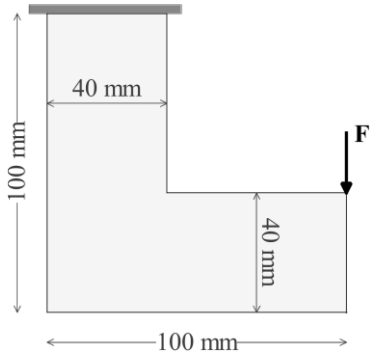

Fig. 4-20. L-Bracket beam

The optimization problem aims to minimize the *p*-norm stress while satisfying the prescribed volume constraint. The optimal solutions of the L-bracket example are illustrated in Figs. 4-21 and 4-24. As it can be seen from the result in the stress-based approach, the stress values of the elements have been reduced significantly, compared with the compliance-based BESO method. In addition, as shown in Fig. 4-22, the stress concentration at the kink of the L-bracket has also been alleviated, however, $\mathbf{P}_{\mathbf{complince}}$ optimal design suffers from the high-stress concentration at the kink of the L-bracket. According to the numerical results, the maximum stress has been reduced from 36% - 37% in comparison with the traditional BESO method. The value of the mean compliance is higher than the traditional compliance-based approach, due to the different objective functions in both optimization problem ($\mathbf{P2}_{\mathbf{stress}}$ & $\mathbf{P}_{\mathbf{compliance}}$).

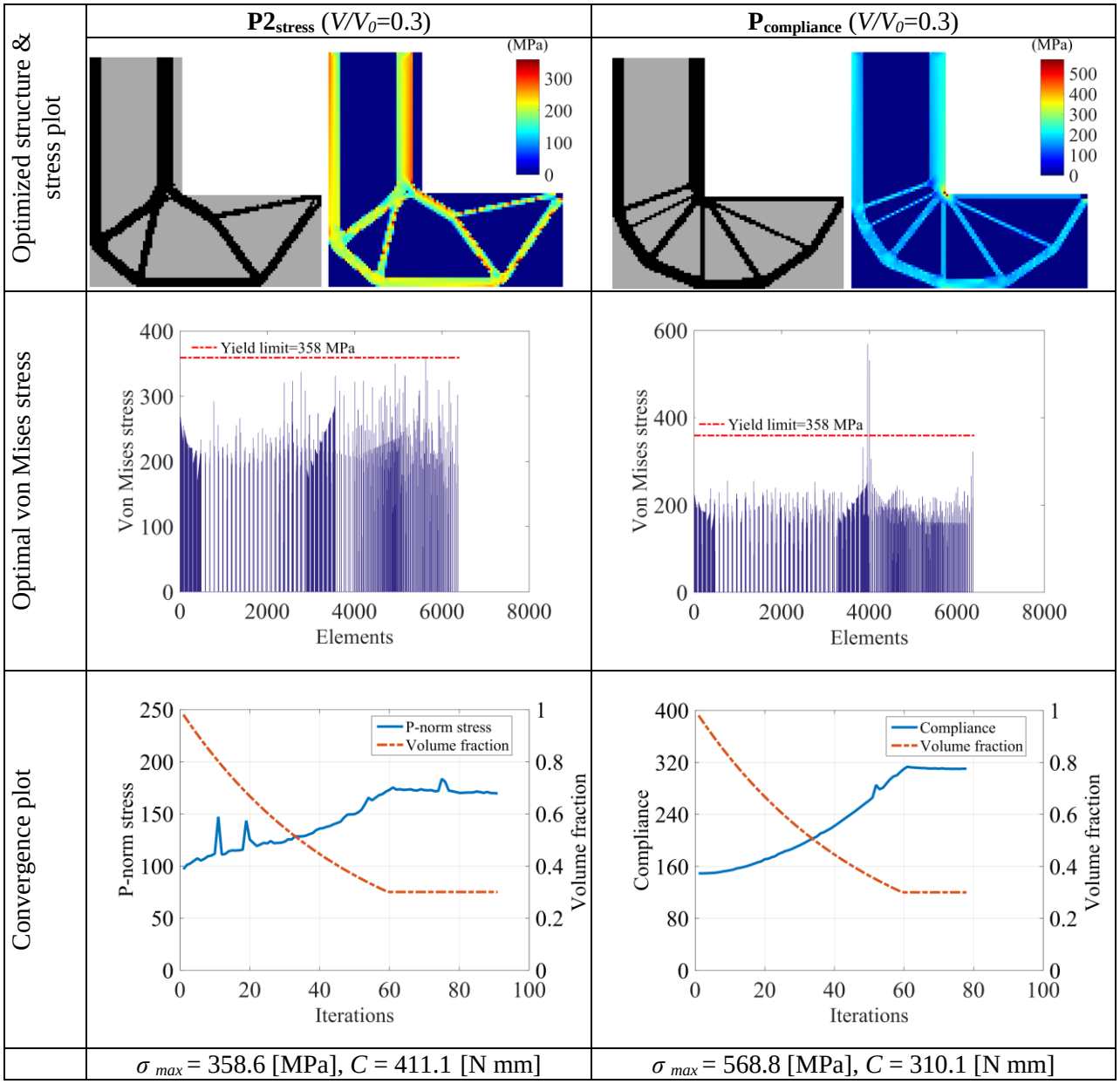

Fig. 4-21. Optimal layouts for L- bracket beam with top load (V/V_0=0.3)

The optimization evolution history of the L-bracket with volume constraint 0.3 is shown in Fig. 4-23, to show how the proposed approach reaches the optimal design during the optimization process. Different from the original BESO method, in the developed stress-based BESO approach, adding and removing of the material from design space, is based on the sensitivity number which depends on stress rather than strain energy. According to the results (Fig. 4-23), the sensitivity numbers of the elements at the kink of the L-bracket are the lowest in the design space, which then caused them to be removed in the first iteration. In the case of the traditional stiffness optimization in which the

sensitivity numbers are based on the elements strain energies, the strain energies of the elements at the kink are the highest in the design space, which would not be removed from the design space during the optimization processes. Hence the optimal design obtained from the stiffness optimization, suffers from the high-stress concentration compared with the developed stress-based approach. For comparison, the optimal design obtained from the developed BESO approach has been compared with the best discrete optimal design in (Xia et al. 2018) where the maximum stress in (Xia et al. 2018) has been reduced by 27.8%, while in the proposed method of this research, the maximum stress has been reduced around 37% .

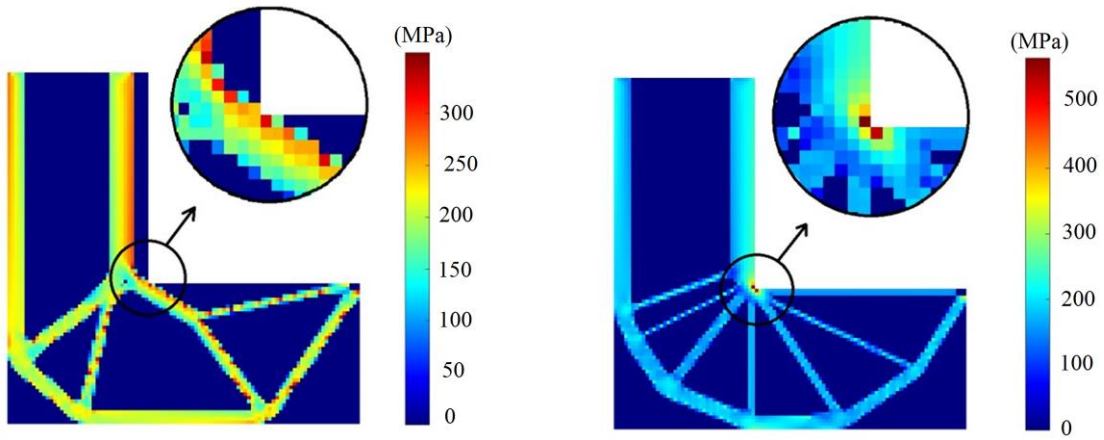

(a) (b)

Fig. 4-22. Comparing the stress concentration of the L-bracket (a) $\mathbf{P2}_{\mathbf{stress}}$ (V/V_0=0.3) (b) $\mathbf{P}_{\mathbf{compliance}}$ (V/V_0=0.3)

The effects of the different BESO parameter on the final optimal design are also depicted in Figs. 4-26 to 4-28 where different evolutionary rate and filter radius have been applied to reach the optimal designs for volume fraction 0.35. Since the BESO method is a discrete design optimization solution, the Zig-Zag boundaries of the optimal designs are inevitable compared with the continuous density approaches e.g. SIMP method. According to the results, the larger filter radius leads to the design with a higher maximum and fewer members. Applying a smaller filter radius causes the maximum stress to be lower, but the optimized design contains more members which may be costly for manufacturing. The evolutionary rate (*ER*) does not lead to major changes to the final design but applying the smaller

value of the *ER* leads to an increase in the computational cost due to the slow evolution of the volume fraction. The afore-mentioned results show that the developed BESO problem can effectively decrease the maximum stress of the final optimized structure and the stress concentration at the kink of the L-bracket can be alleviated significantly when compared with the results of the BESO stiffness optimization ($\mathbf{P}_{\mathbf{copliance}}$). In the next section another example has been solved for $\mathbf{P2}_{\mathbf{stress}}$ and again the results have been compared with the compliance-based BESO approach to better show the effectiveness of the proposed approach in the stress minimization of the optimal designs.

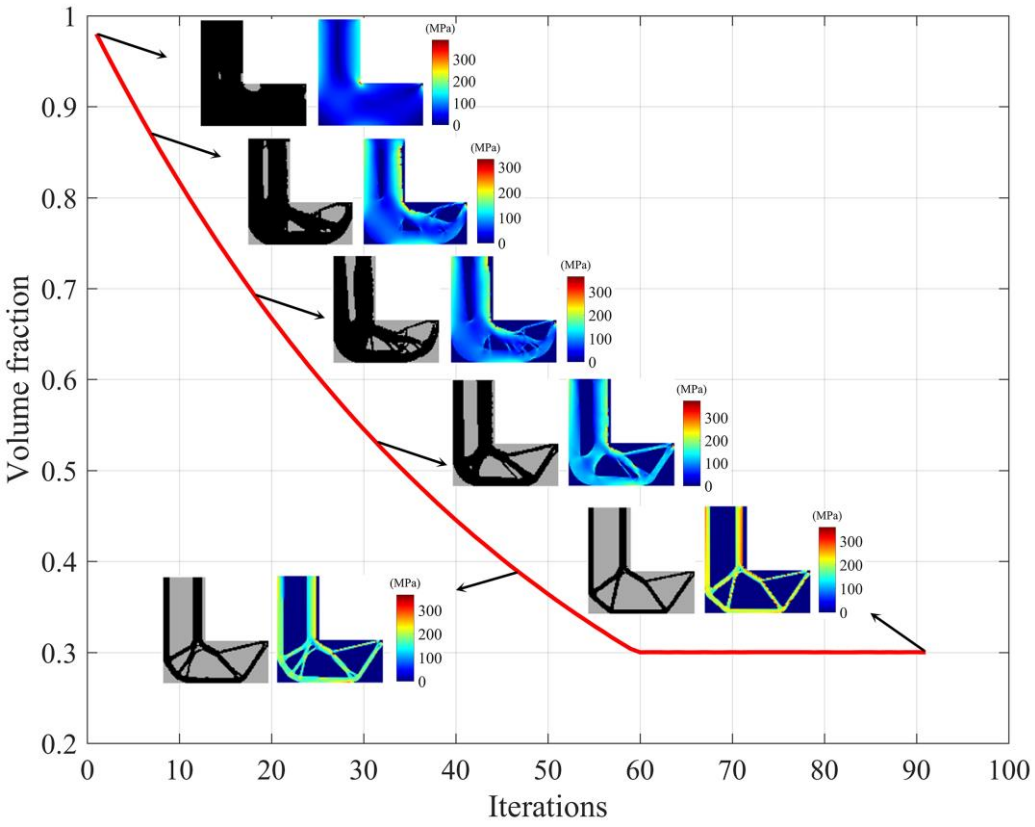

Fig. 4-23. Evolution of topology for optimizing the L-bracket (V/V_0=0.3)

	P2$_{stress}$ (V/V_0=0.4)	**P$_{compliance}$** (V/V_0=0.4)
Optimized structure & stress plot	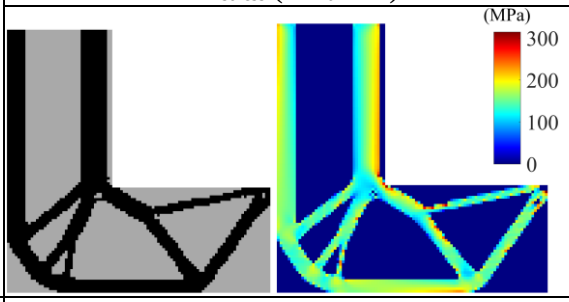	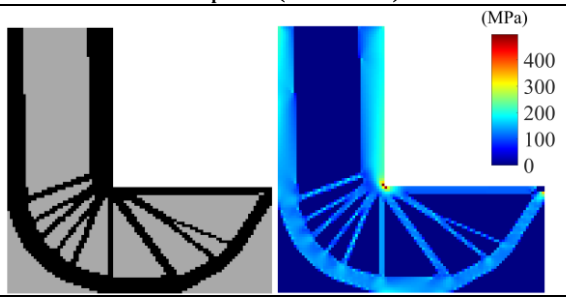
Optimal von Mises stress	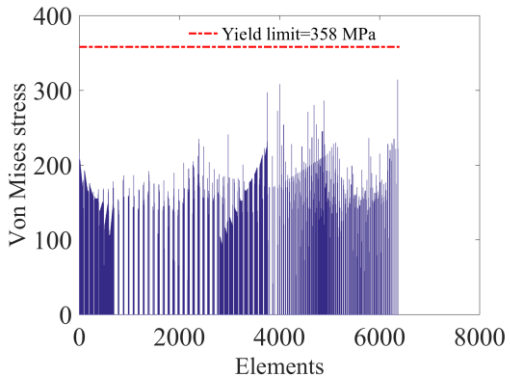	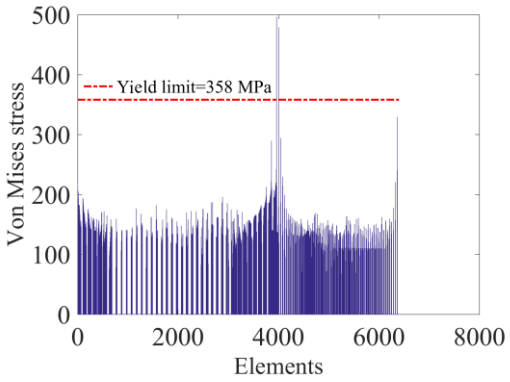
Convergence plot	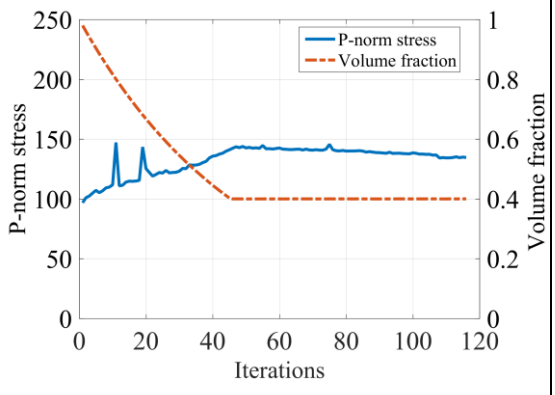	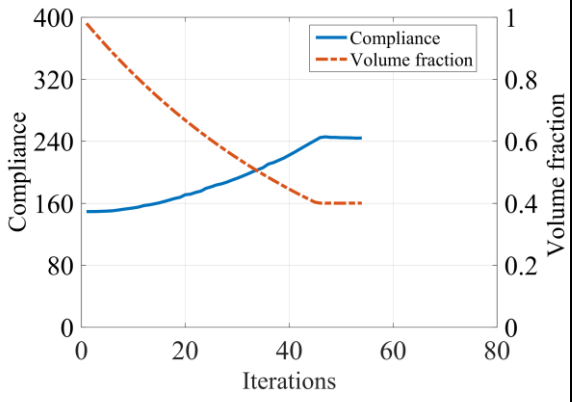
	σ_{max} = 314.3 [MPa], C = 297.8 [N mm]	σ_{max} = 496.2 [MPa], C = 244.1 [N mm]

Fig. 4-24. Optimal layouts for L- bracket beam with top load (V/V_0=0.4)

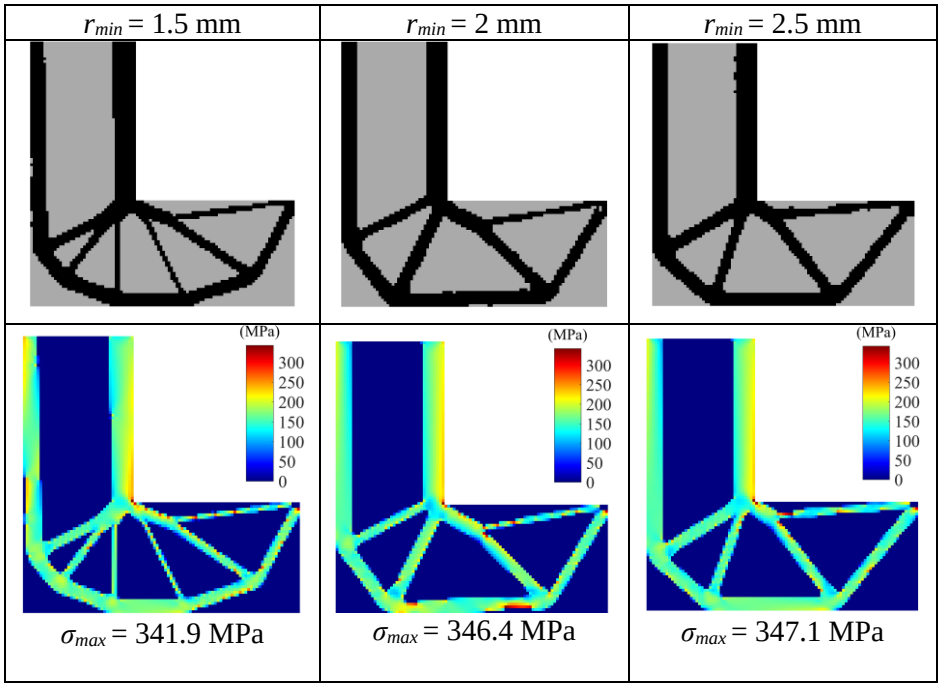

Fig. 4-25. Optimization layouts for L-bracket with **ER = 0.01** (V/V_0 = 0.35)

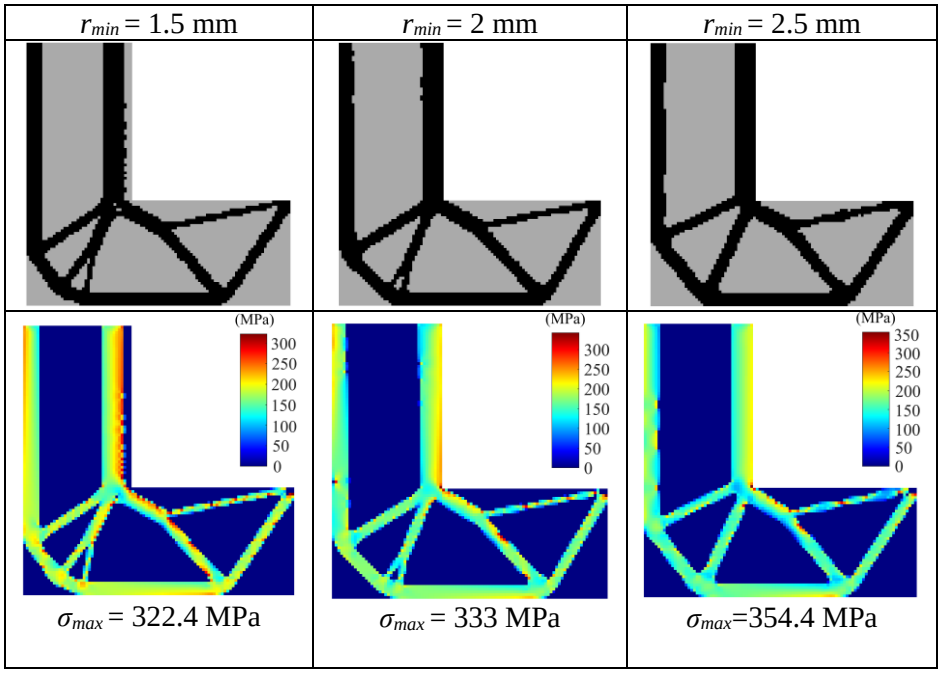

Fig. 4-26. Optimization layouts for L-bracket with **ER = 0.02** (V/V_0 = 0.35)

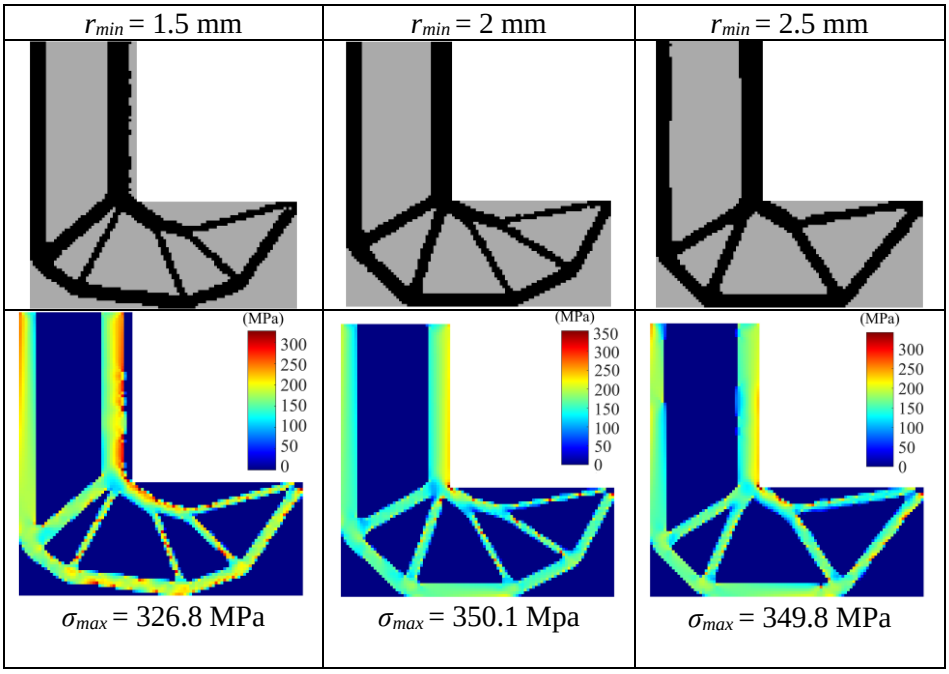

Fig. 4-27. Optimization layouts for L-bracket with **ER = 0.025** (V/V_0 = 0.35)

4.6.2.2 Cantilever Beam

The second example, which is the benchmark problem for the original BESO approach, deals with the optimization of the cantilever beam as shown in Fig. 4-14. A 1500 N point load is applied at the middle of the right-hand side and the design space has meshed into 5000 quadrilateral plane stress elements (1×1 mm). Again, to avoid the stress concentration, the eight elements (4×2) which are at the neighborhood of the applied load, are excluded from the design space. Also, the thickness, sensitivity filter radius (r_{min}) and the evolutionary rate (ER) are set to be 1 mm, 2 mm and 0.02 respectively. The numerical results from the optimization problems $\mathbf{P2_{stress}}$ and $\mathbf{P_{compliance}}$ are shown in Figs. 4-28 and 4-29 for different volume constraints 0.3 and 0.43. According to the results, the maximum stress with volume constraint 0.3 has been reduced by 42% compared with the stiffness optimization problem with the same volume constraint. However, the mean compliance value is larger in the case of the $\mathbf{P2_{stress}}$ problem, due to the stress-based objective function rather than compliance-based one. According to the results which have been obtained with the volume constraint 0.43, it can be seen that the maximum stress value has been decreased by around 27% compared to the original BESO method. Since the sensitivity numbers of the elements in the proposed method are based on the

stress, the elements with the lowest sensitivity numbers have been removed from the design space, while the elements with the highest sensitivity numbers have been kept as solid elements. The optimization layout's history of the cantilever beam with volume constraint 0.3, is also illustrated in Fig. 4-30 which shows how the algorithm reaches the final optimal design during the optimization process.

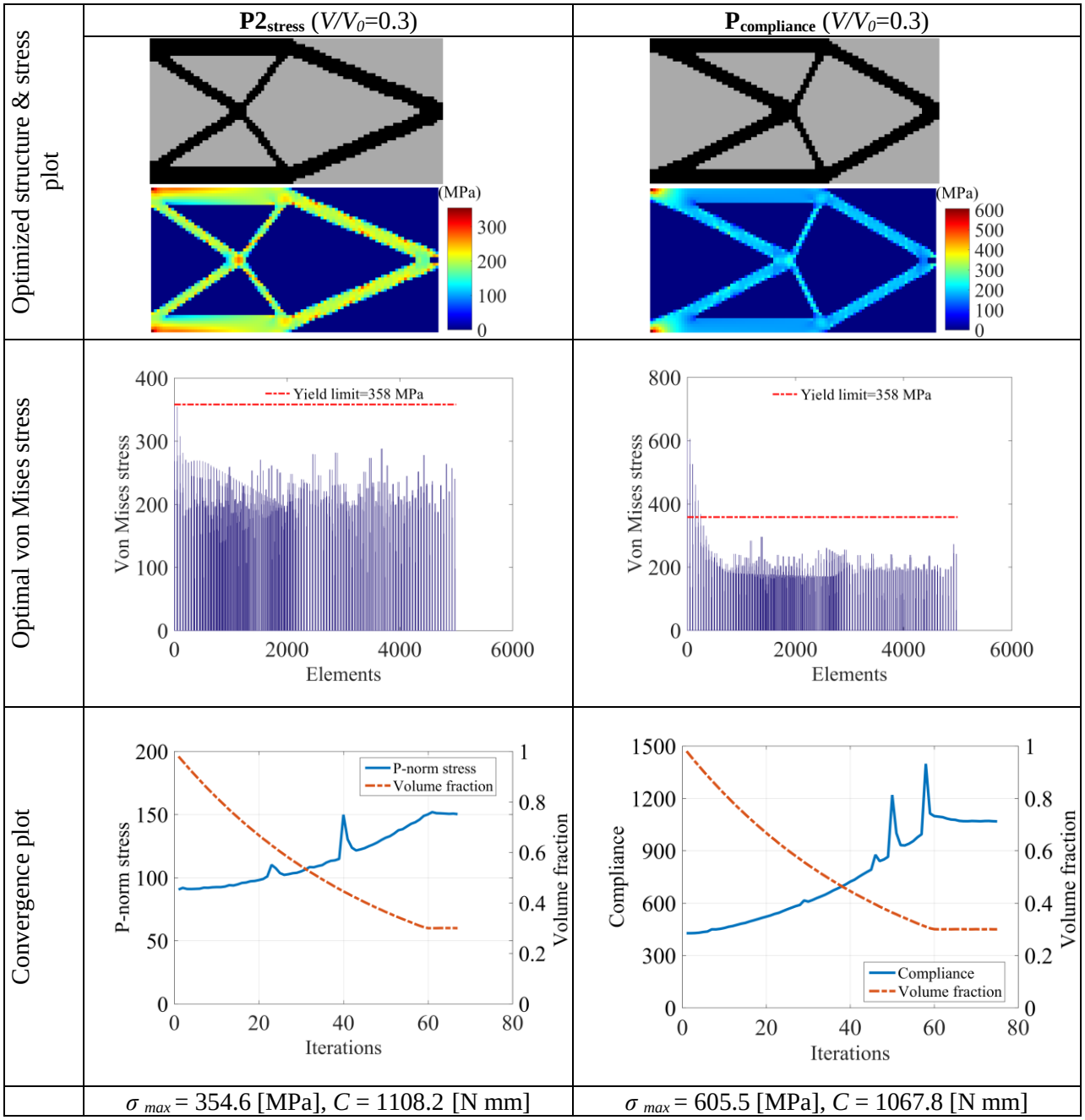

Fig. 4-28. Optimal layouts for Cantilever beam (V/V_0=0.3)

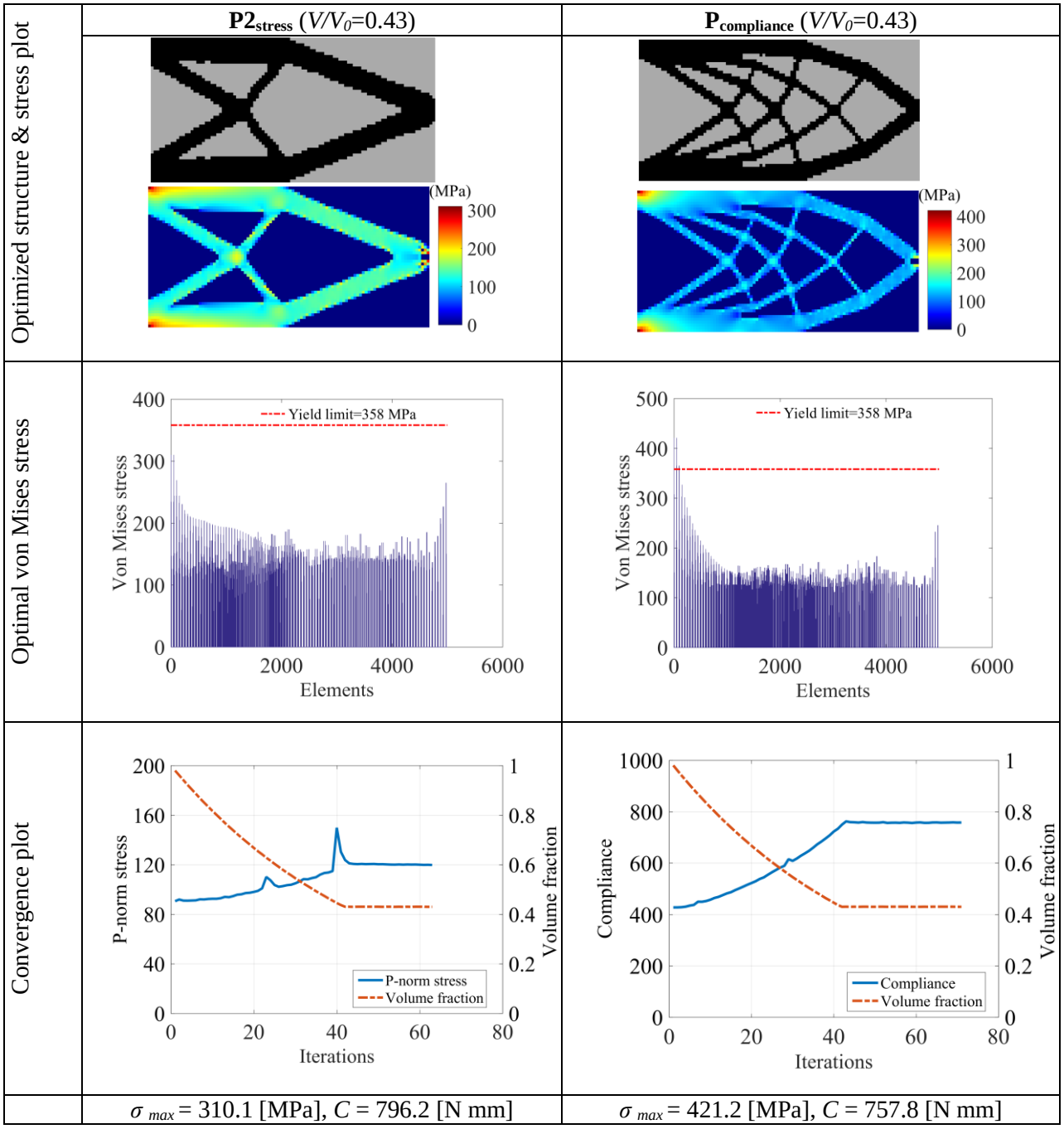

Fig. 4-29. Optimal layouts for Cantilever beam (V/V_0=0.43)

Again, it can be seen from the results that the proposed approach is able to reduce the maximum stress of the optimal design significantly, and all the optimized designs are free from large stress concentration when compared with the original BESO method. In the next section, another rare example has been solved for **P2**$_{\text{stress}}$ problem where again the results are compared with the compliance-based BESO to show the validity of the proposed method.

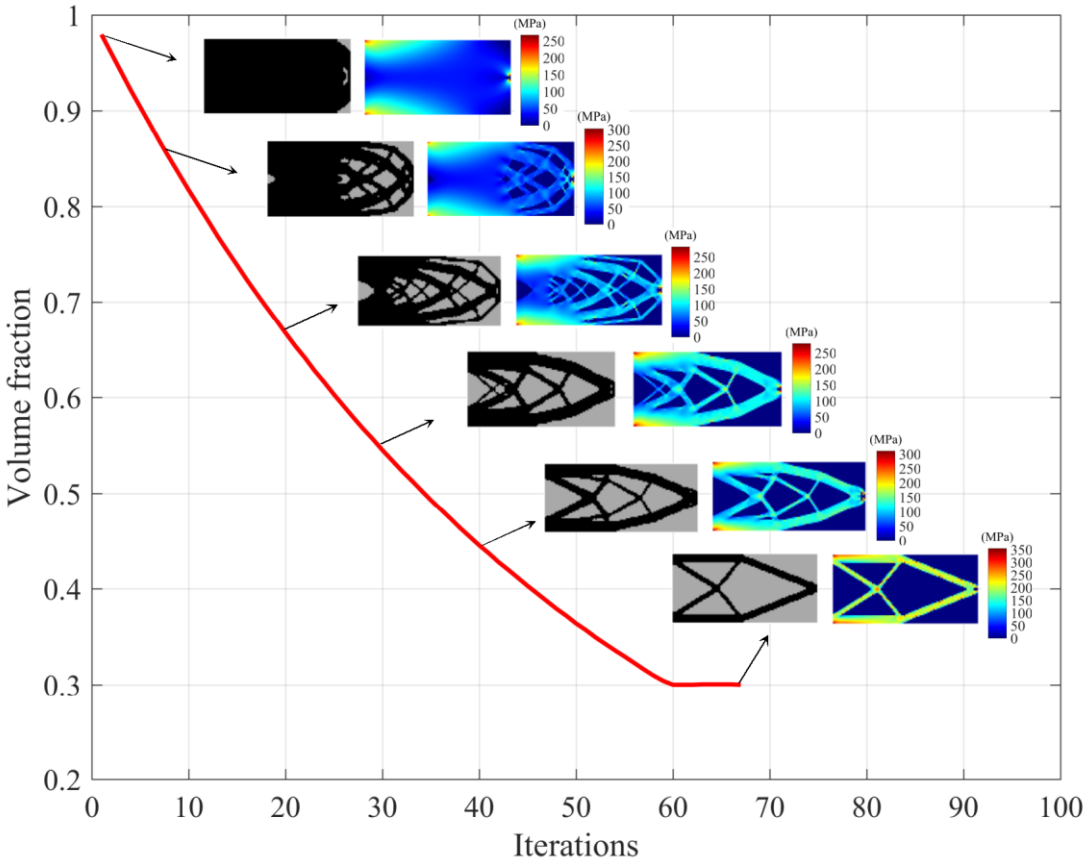

Fig. 4-30. Evolution of topology for optimizing the L-bracket (V/V_0=0.3)

4.6.2.3 Eyebar beam

This example deals with the optimization of the Eyebar beam which also has been used by (Amstutz & Novotny 2010) in their research. The design domain consists of the quadrilateral Q4 plane stress elements (1×1 mm), with a circular hole with radius 15 mm excluded from the design domain. The geometry and the boundary condition can be seen in Fig. 4-31, where the thickness has been set to 1 mm and 20 mm of the beam is clamped along a segment. A horizontal load function with the density of $F(x,y) = (73((y^2 - 15^2)\ if\ x \le 0\ ,\ 0\ if\ x > 0)$ is applied at the centre of the hole. The load is distributed to mimic the contact produced by the pin-joint with the origin of the Cartesian coordinate system ((x, y)) at the center of the hole. The sensitivity filter and the evolutionary rate have been set to 2mm and 0.02 respectively.

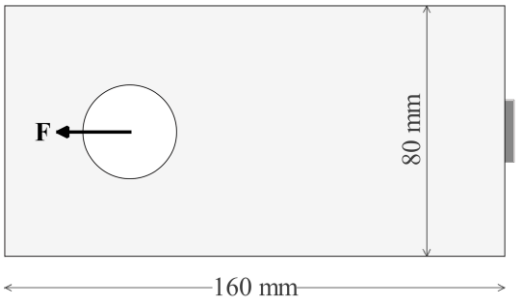

Fig. 4-31. Eyebar beam

The topology optimization results for two different volume constraints 0.39 and 0.5 have been shown in Figs. 4-32 and 4-33. According to the results obtained from the volume constraint 0.39, the high-stress concentration around the bar eye in the case of the $\mathbf{P}_{\mathbf{complice}}$ has been alleviated to around 42% in the case of $\mathbf{P2}_{\mathbf{sterss}}$. A**s** discussed earlier, the mean compliance values in the case of the proposed approach ($\mathbf{P2}_{\mathbf{sterss}}$) is higher than the original BESO method. The maximum stress with the volume fraction 0.5 has been reduced around 24% compared with the maximum stress which was obtained from the $\mathbf{P}_{\mathbf{compliance}}$ problem. The optimization layout history is also depicted in Fig. 4-34 where the optimization process of the Eyebar with volume fraction 0.39, has been shown for specific iterations. According to the results obtained, the proposed stress-based approach was again able to reduce the maximum stress of the elements, and consequently the stress concentration of the final optimized structure.

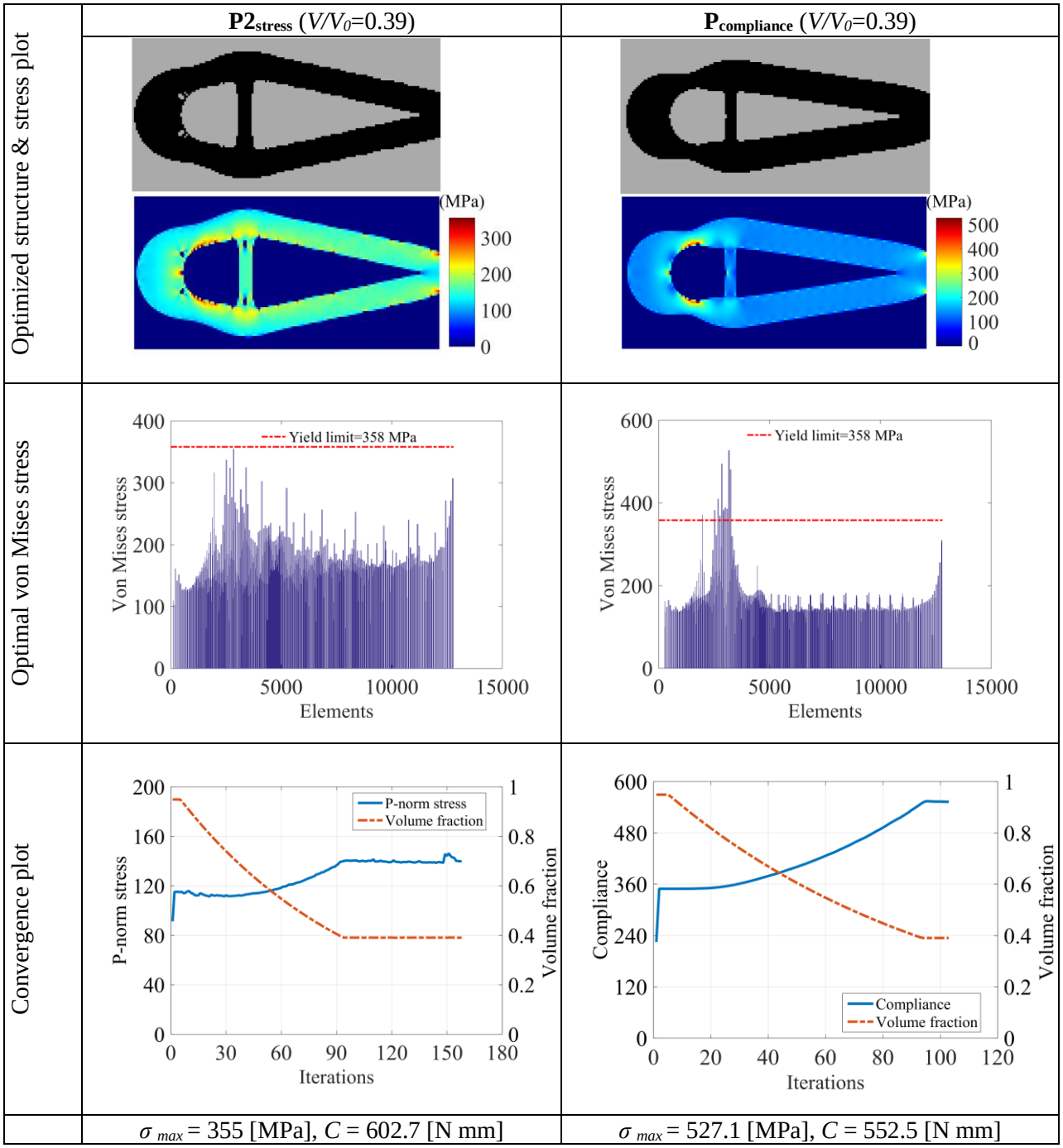

Fig. 4-32. Optimal layouts for Eyebar beam (V/V_0=0.39)

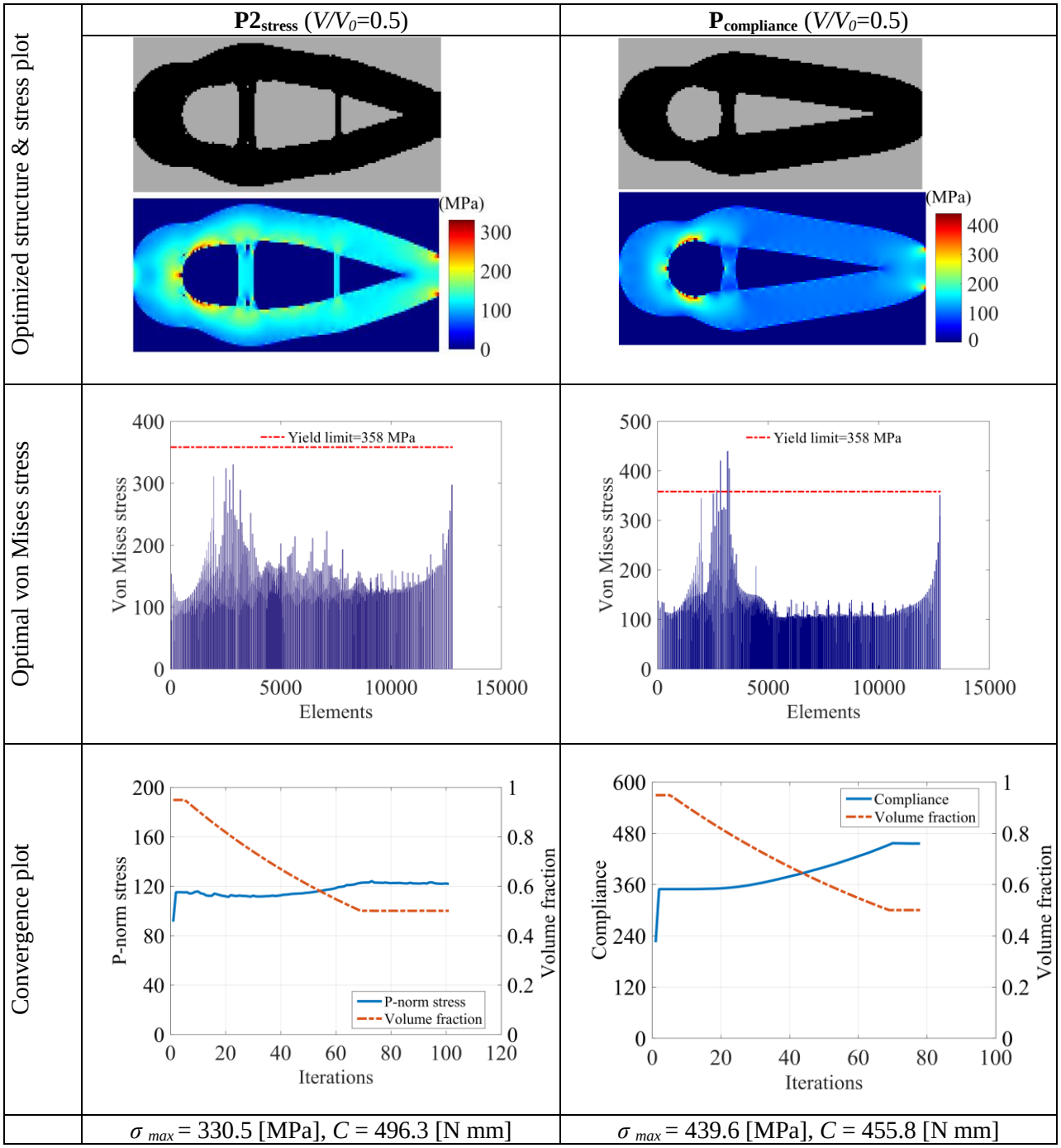

Fig. 4-33. Optimal layouts for Eyebar beam (V/V_0=0.5)

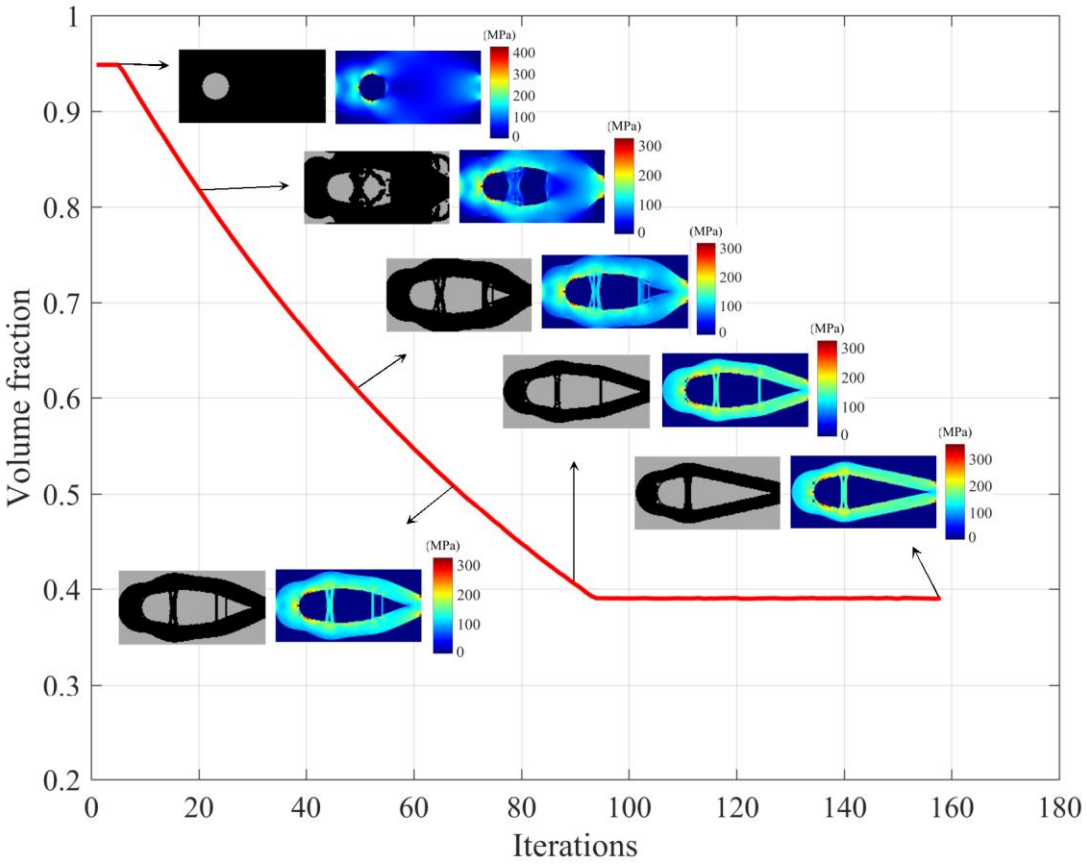

Fig. 4-34. Evolution of topology for optimizing the Eyebar (V/V_0=0.39)

4.6.3 Concluding remarks

In the previous sections, the proposed stress-based BESO method was formulated to minimize the stress to obtain an optimized structure without large stress concentration, while satisfying volume constraint. Compared to the original BESO method where the optimal design may contain high-stress concentrations, the numerical results show that by considering the stress sensitivity analysis in the BESO method, one can reach an optimal design without large stress concentration and with the local stresses closer to the stress limit of the elements. Since stress is one of the most important criteria in engineering application, it is not sufficient to optimize structure purely for stiffness without considering stress failure in the original BESO method. Hence the application of the proposed stress-based BESO method leads to a better optimal design which is resistant to stress failure and is closer to

a practical engineering design. In the next section, another topology optimization, is called **P3$_{sterss}$** in this research has been solved for different numerical examples.

4.7 Volume minimization by considering stress constraint

In practice, the proposed stress-based BESO approach can also be formulated to minimize the volume of the structure while satisfying a predefined stress constraint. In this section, to demonstrate the effectiveness of the developed BESO approach, the **P3$_{stress}$** has been solved for the numerical examples as was shown earlier in Equation (4-3). For comparison, the volume constraint in the original BESO problem (**P$_{compliance}$**) has been set to the optimized volume, which is obtained from the **P3$_{stress}$** optimization problem.

4.7.1 Procedure summary

To solve the **P3$_{sterss}$** optimization problem as shown in Equation (4-3), the volume is minimized, subject to stress constraint. The stress constraint should be added to the objective function by using the Lagrangian multiplier (λ), therefore the modified objective function can be defined as follows:

$$f_3(x) = \sum_{i=1}^{N} v_i x_i + \lambda(\sigma_G^{PN}(x) - \sigma^*) \tag{4-35}$$

where $\sigma_G{}^{PN}$ and σ^* are the *p*-norm stress and predefined stress constraint respectively. According to Equation (4-35), if the stress constraint is satisfied, the modified objective function will be equal to the original objective function, and the Lagrangian multiplier (λ), can set to any constant. To solve the optimization problem, the sensitivity numbers of the elements should be calculated, by calculating the derivative of the objective function as follows:

$$\frac{d\ f_3(x)}{d\ x_i} = V_i + \lambda\left(\frac{\partial \sigma_G^{PN}(x)}{\partial x_i}\right) \tag{4-36}$$

where the gradient of the modified *p*-norm stress can be calculated as per Equation (4-20). Substituting Equation (4-20) into Equation (4-36) the final derivative of the objective function reads:

$$\frac{d\ f_3(x)}{d\ x_i} = V_i + \lambda \left[\frac{\partial \sigma_G^{PN}(x)}{\partial \sigma_i^{vm}} \left(\frac{\partial \sigma_i^{vm}(x)}{\partial \boldsymbol{\sigma}_i} \right)^T \frac{\partial \mathbf{D}(x)}{\partial x_i} \mathbf{Bu} - \boldsymbol{\lambda}^T \left(\frac{\partial \mathbf{K}(x)}{\partial x_i} \mathbf{u} \right) \right] \tag{4-37}$$

By using the uniform mesh in the FEA analysis, the volume of the elements is the same and therefore the final sensitivity number reads as follows:

$$\alpha_i = -\frac{1}{\lambda} \left(\frac{d\ f_3(x)}{d\ x_i} - V_i \right) = - \left[\frac{\partial \sigma_G^{PN}(x)}{\partial \sigma_i^{vm}} \left(\frac{\partial \sigma_i^{vm}(x)}{\partial \boldsymbol{\sigma}_i} \right)^T \frac{\partial \mathbf{D}(x)}{\partial x_i} \mathbf{Bu} - \boldsymbol{\lambda}^T \left(\frac{\partial \mathbf{K}(x)}{\partial x_i} \mathbf{u} \right) \right] \tag{4-38}$$

Compared with the BESO procedure of the $\mathbf{P2_{sterss}}$ problem (Equation (4-2)), in the $\mathbf{P3_{sterss}}$ problem the BESO algorithm is slightly different, where the calculation of the target volume for the next iteration depends on the stress constraint value, by applying a function (G_s) which indicate the relative gap between the stress constraint and the maximum stress values. The target volume of the next iteration can be calculated as follows:

$$V_{k+1} = V_k \left(1 - ER \times G_s\right) \tag{4-39}$$

where V_k and ER are the current iteration volume and evolutionary rate respectively. G_s is the gap function which controls the volume fraction of the structure during the optimization progress by comparing the maximum stress value of the current iteration with the stress constraint. If the maximum stress is violated and is larger than the stress constraint, then G_s will be set to a negative value, which increases the structural volume automatically to reduce the maximum stress. G_s can be defined as follows:

$$G_s = \begin{cases} 1 \quad if \quad \dfrac{\left|\sigma^* - \partial\sigma_{G\ (\max)}^{PN}\right|}{\sigma^*} \le tolerance \\ \dfrac{(\sigma^* - \partial\sigma_{G\ (\max)}^{PN})/\sigma^*}{tolerance} \quad if \quad \dfrac{\left|\sigma^* - \partial\sigma_{G\ (\max)}^{PN}\right|}{\sigma^*} \le tolerance \end{cases} \tag{4-40}$$

where *tolerance* is a user-defined parameter which has been set to 0.05 in this research. When the maximum stress reaches the stress constraint, the volume fraction will be stopped, but the optimization progress will be continued with the constant volume to be converged. The convergence criteria are based on the volume and stress as follows:

$$error_1 = \left| \frac{\sum_{i=1}^{N} V_{k-i+1} - \sum_{i=1}^{N} V_{k-N-i+1}}{\sum_{i=1}^{N} V_{k-i+1}} \right| \le 0.01 \tag{4-41}$$

$$error_2 = \frac{\left| \sum_{i=1}^{N} (\sigma_{\max,\,k-i+1} - \sigma_{\max,\,k-N-i+1}) \right|}{\sum_{i=1}^{N} \sigma_{\max,\,k-i+1}} \le 0.01 \tag{4-42}$$

where $N = 5$ is used in this problem. Again the sensitivity numbers have been modified by averaging their values at their previous iteration to improve the convergence of BESO. As discussed in Chapter 3, the sensitivity filtering approach has been used to avoid the checkerboard patterns (Huang, X & Xie, YM 2007, 2010). The BESO procedure for solving the optimization problem $\mathbf{P3_{stress}}$ can be depicted in a flowchart (Fig. 4-35). In the next section, the $\mathbf{P3_{stress}}$ has been solved for different numerical examples, and previously stated, the topology optimization results have been compared with the traditional stiffness approach to show the validity of the proposed method.

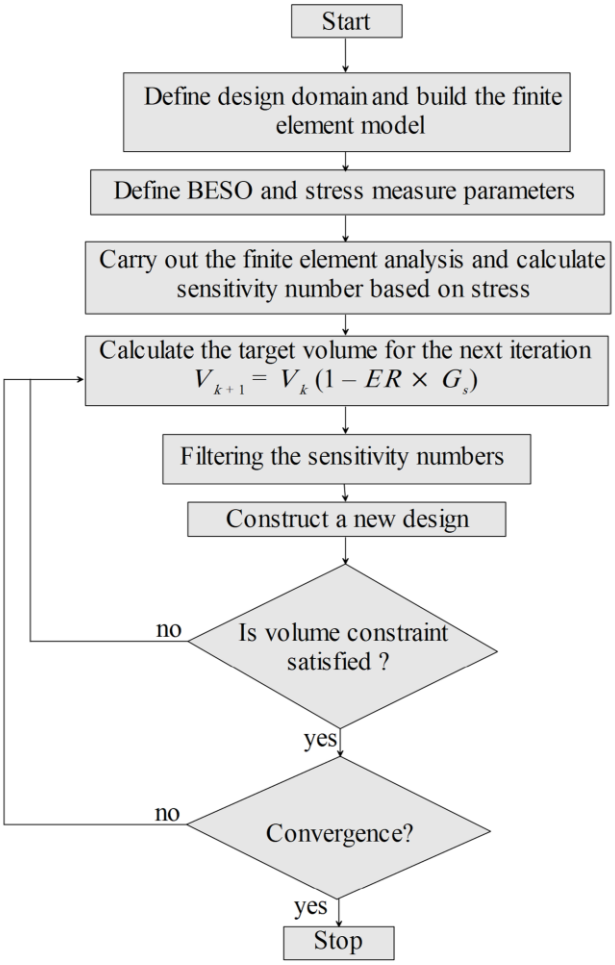

Fig. 4-35. Flowchart of the BESO procedure for solving the **P3**$_{\mathbf{stress}}$ optimization problem

4.7.2 Numerical implementation

In this section, the **P3**$_{\mathbf{stress}}$ optimization problem has been solved for the cantilever beam and the long clamped beam as shown in Figs. 4-33 and 4-8, where the structural volume is minimized while satisfying the stress constraint (σ^*).

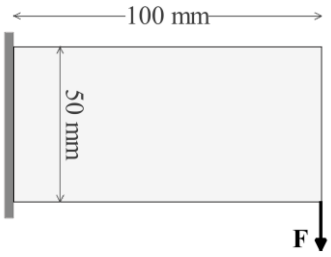

Fig. 4-36. L-Bracket beam

For the cantilever beam example, a 700 N point load has been applied to the bottom corner of the right side and the design space has meshed into 5000 quadrilateral plane stress elements (1×1 mm), where again to avoid the stress concentration, six elements (3×2) in the vicinity of the point load are excluded from the design space during the optimization process.

	P3$_{\mathbf{stress}}$ (σ^* = 370 MPa)	**P**$_{\mathbf{compliance}}$ (V/V_0 = 0.312)
Optimized structure & stress plot	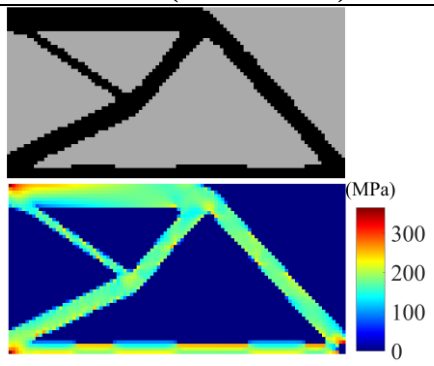	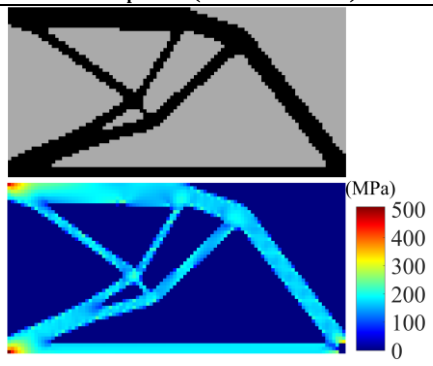
Optimal von Mises stress	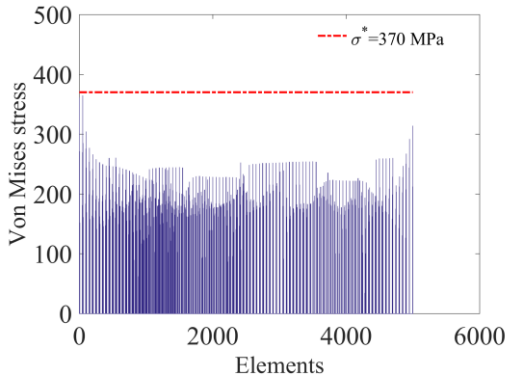	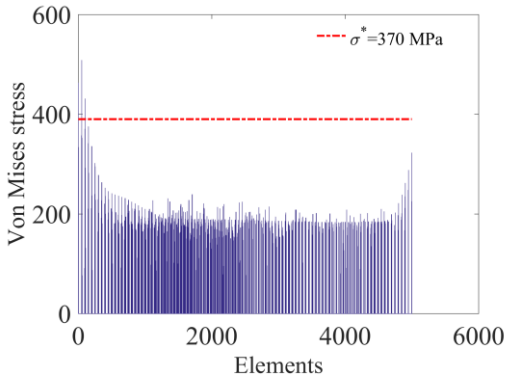
Convergence plot	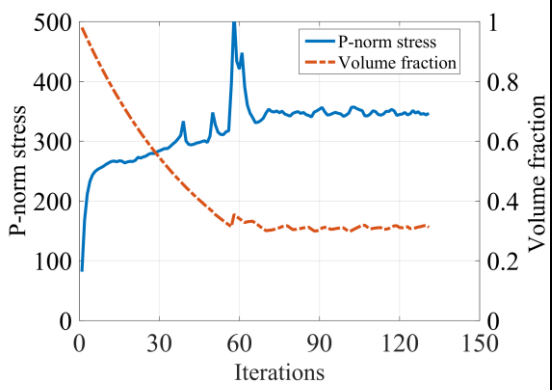	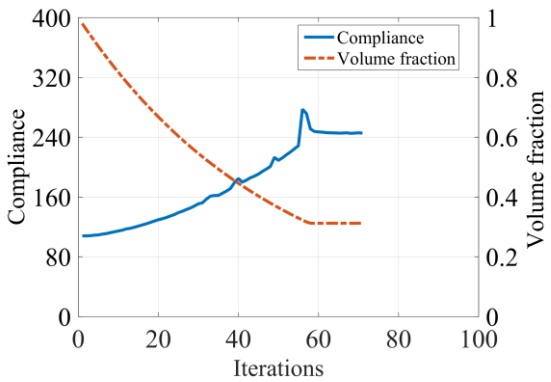
	σ_{max} = 364.9 [MPa], C = 252.1[N mm], $V_{optimal}/V_0$ = 0.312	σ_{max} = 508.8 [MPa], C = 245.3 [N mm]

Fig. 4-37. Optimal layouts for cantilever beam (σ^* = 370 MPa)

The boundary condition, geometry and the applied load for the long clamped beam example is the same as Fig. 4-8 which has shown before. A 1000 N point load applied to the middle of the beam and 12 elements (3×4) are excluded from the design space to avoid the stress concentration around the point load. The material is carbon steel 1018 and the evolutionary rate (*ER*) and the sensitivity filter radius (r_{min}) have been set to be 0.02 and 2 mm for both examples.

The optimization solution results for the cantilever beam have been shown in Figs. 4-37 to 4-39 for different stress constraints values of 450 MPa, 390 MPa, and 370 MPa. As stated earlier, when comparing the obtained results with the original BESO method, the volume constraints of the $\mathbf{P}_{\mathbf{compliance}}$ have been set to the optimal volumes, which have been calculated from the $\mathbf{P3}_{\mathbf{stress}}$ problem. It can be seen from the results that the problem of minimizing volume subject to stress constraint ($\mathbf{P3}_{\mathbf{stress}}$) can effectively constrain the maximum stress which means this satisfies the stress constraints. The maximum stress of the final optimal designs in the $\mathbf{P3}_{\mathbf{stress}}$ problem, has been reduced significantly (28% - 32%) while compared with the stiffness optimization problem results in the $\mathbf{P}_{\mathbf{compliance}}$ problem with the same volume. However, the mean compliance values in the $\mathbf{P3}_{\mathbf{stress}}$ problem are slightly higher than the values of the original BESO approach due to the different objective functions. In addition, the convergence plots show how the *Gs* gap functions increased the structural volume to control the maximum stress and constrain it to below the prescribed stress constraint during optimization progress.

The topology optimization results for the long clamped beam example (Fig. 4-8) with different stress constraints 345 MPa,400 MPa, and 450 MPa have been depicted in Figs. 4-40 to 4-43. According to the numerical results for each stress constraint, different optimal volumes have been obtained. In all cases the stress constraint has been satisfied and the maximum stress of the final design is less than the stress constraints value. However, in the case of the stiffness optimization ($\mathbf{P}_{\mathbf{compliance}}$), although the optimal design has the same volume as was obtained from the $\mathbf{P3}_{\mathbf{stress}}$ solution, the maximum stress in all the optimal designs is larger than the stress constraint. Hence the proposed approach which was used to solve the $\mathbf{P3}_{\mathbf{stress}}$ was able to reduce the maximum stress and constrain it to a value which is

less than the stress constraint value where the maximum stress has been decreased by 20% - 30% when compared to the traditional BESO stiffness optimization. The role of the *Gs* gap function can be seen from the convergence plots where the structural volume has been increased to overcome the violation of the maximum stress.

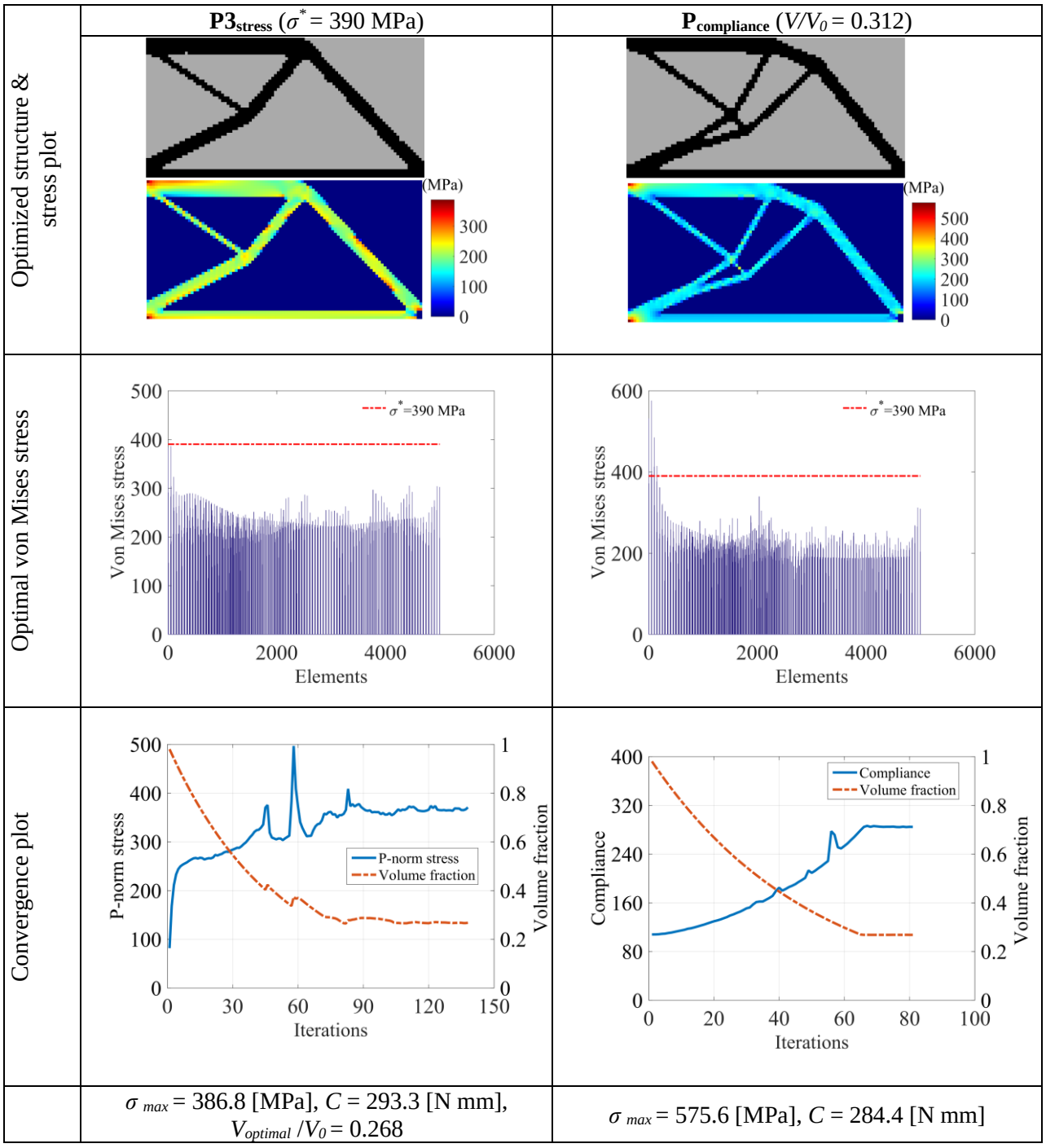

Fig. 4-38. Optimal layouts for cantilever beam (σ^* = 390 MPa)

	P3$_{stress}$ (σ^* = 450 MPa)	**P$_{compliance}$** (V/V_0 = 0.242)
Optimized structure & stress plot	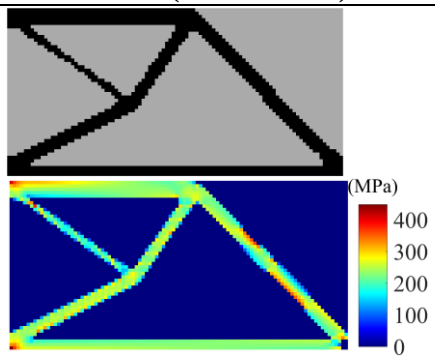	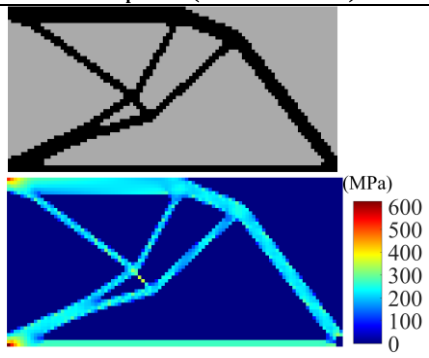
Optimal von Mises stress	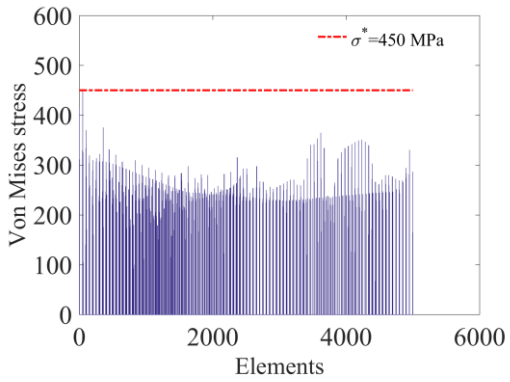	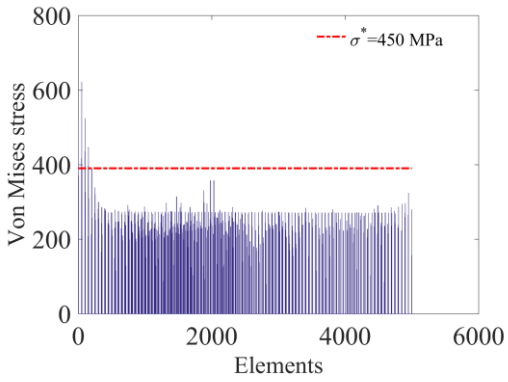
Convergence plot	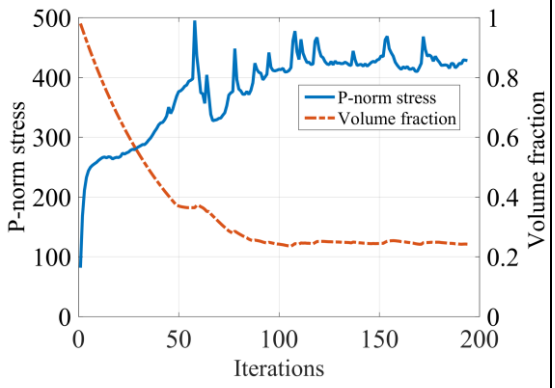	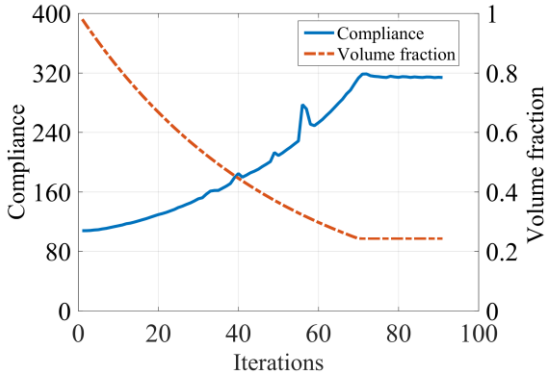
	σ_{max} = 448 [MPa], C = 321.4 [N mm], $V_{optimal}/V_0$ = 0.242	σ_{max} = 622.5 [MPa], C = 313.7 [N mm]

Fig. 4-39. Optimal layouts for cantilever beam (σ^* = 450 MPa)

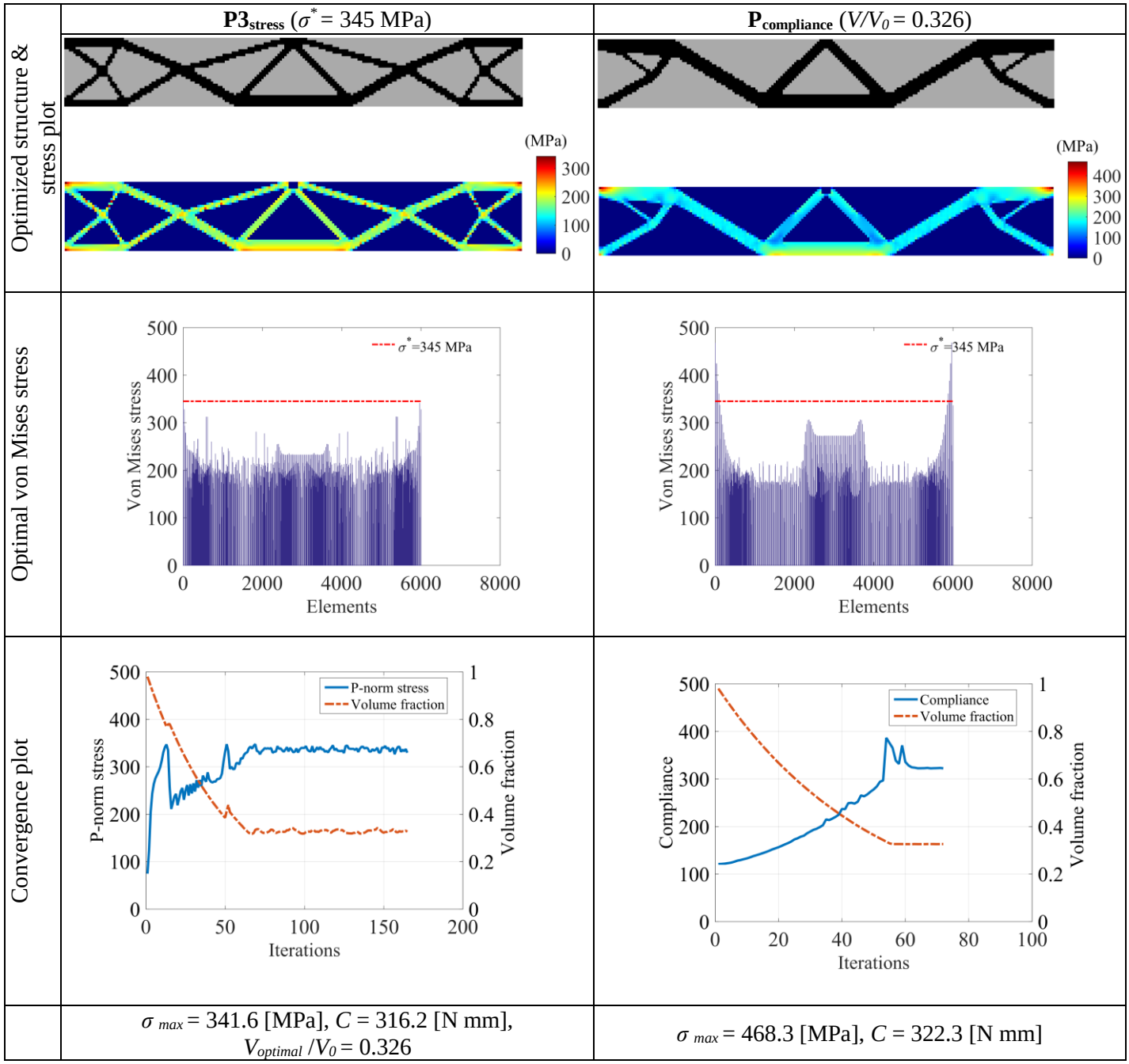

Fig. 4-40. Optimal layouts for the long clamped beam (σ^*=345 MPa)

	P3$_{stress}$ (σ^* = 400 MPa)	**P$_{compliance}$** (V/V_0 = 0.289)
Optimized structure & stress plot	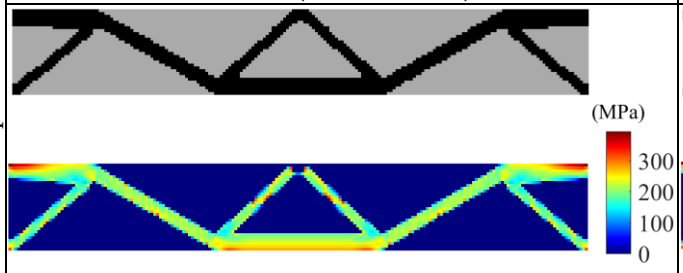	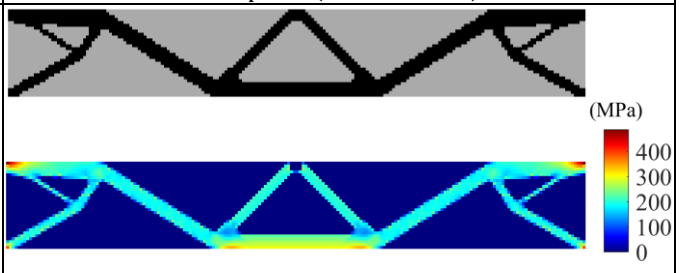
Optimal von Mises stress	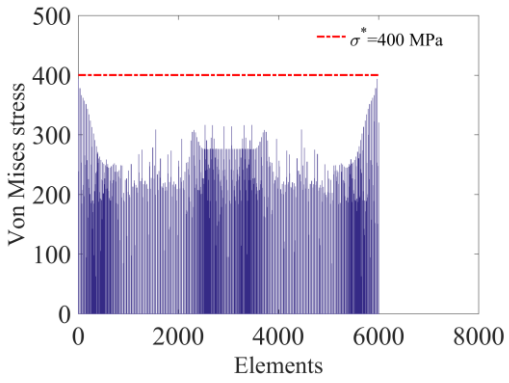	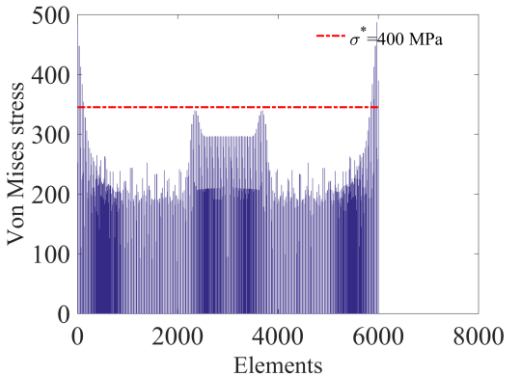
Convergence plot	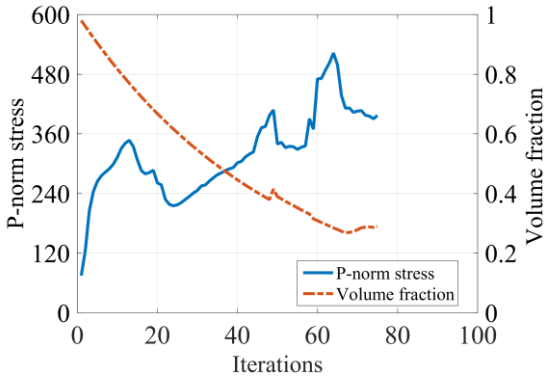	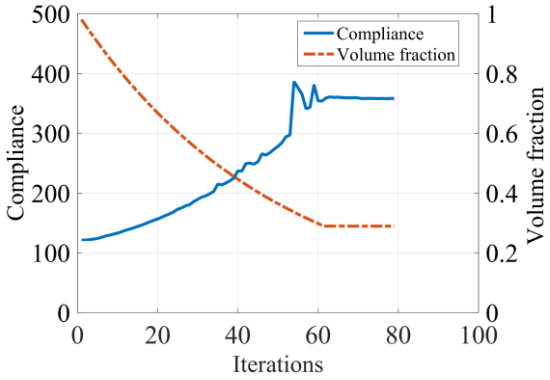
	σ_{max} = 393.9 [MPa], C = 374.3 [N mm], $V_{optimal}/V_0$ = 0.289	σ_{max} = 487.2 [MPa], C = 358 [N mm]

Fig. 4-41. Optimal layouts for the long clamped beam (σ^* = 400MPa)

	P3$_{stress}$ (σ^* = 450 MPa)	**P$_{compliance}$** (V/V_0 = 0.236)
Optimized structure & stress plot	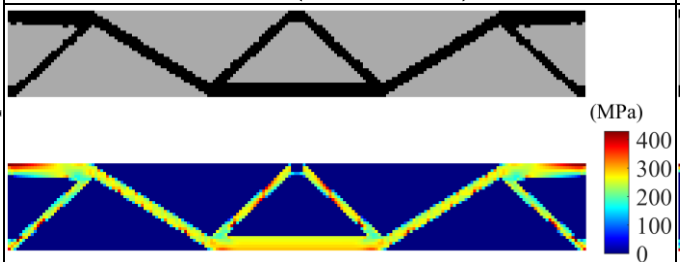	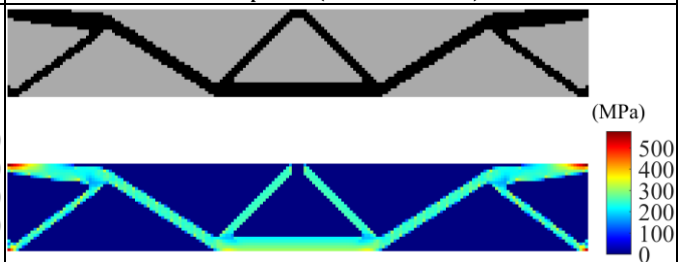
Optimal von Mises stress	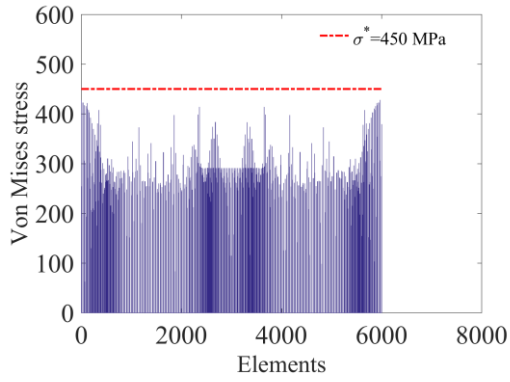	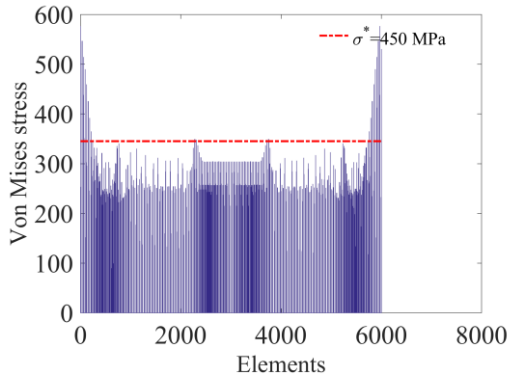
Convergence plot	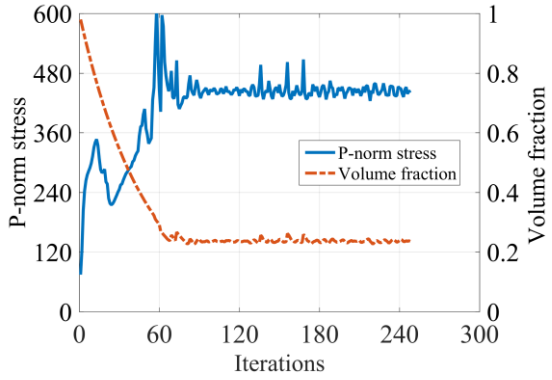	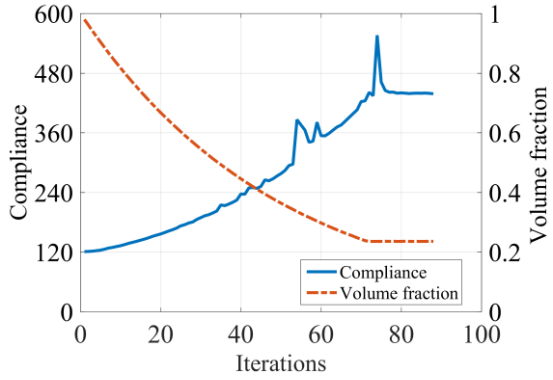
	σ_{max} = 428.3 [MPa], C = 446.9 [N mm], $V_{optimal}/V_0$ = 0.236	σ_{max} = 576.8 [MPa], C = 438.3 [N mm]

Fig. 4-42. Optimal layouts for the long clamped beam (σ^* = 450MPa)

4.8 Computational cost

In this section the computational effort of the developed stress-based BESO method has been compared with the original stiffness optimization BESO approach. Tables 1 and 2 show the CPU times which are needed to run the Matlab code. Compared to the original BESO approach the costliest part of the proposed approach, is the solution of the adjoint equilibrium equation which is used in this research to calculate the derivative of the displacement vector in all three optimization problems (**P1**$_{\mathbf{stress}}$**, P2** $_{\mathbf{stress}}$**,** and **P3**$_{\mathbf{stress}}$).

Table 4-1. CPU time (seconds) for solving the **P2**$_{\mathbf{stress}}$ problem (L-bracket (V/V_0=0.3))

Iteration	BESO considering stress (**P2**$_{\mathbf{stress}}$)		BESO considering compliance (**P**$_{\mathbf{compliance}}$)	
	Total time	Time to solve equilibrium equations. (Including adjoint system).	Total time	Time to solve equilibrium equations.
5	1.176	0.779	0.836	0.612
11	0.955	0.802	0.794	0.675
22	1.691	1.587	1.386	1.295
45	3.586	3.398	2.885	2.824
91	7.323	7.159	5.884	5.746

To better compare the computational effort of the proposed method with the traditional compliance-based BESO approach (**P**$_{\mathbf{compliance}}$), the number of the iteration in the **P**$_{\mathbf{compliance}}$ solutions has been set to the final iteration number of the **P2** $_{\mathbf{stress}}$ problem, where the optimization problem has been converged. According to the results, the computational effort of the proposed method is slightly higher than the original BESO method due to the application of the adjoint method for calculating the

derivative of the displacement vector in the sensitivity analysis. When comparing the total CPU times for both solutions, the difference between the CPU times are negligible and are acceptable

Table 4-2. Summary of the total computing time for solving the **P2**$_{\mathbf{stress}}$ problem (L-bracket (V/V_0=0.3))

L-bracket	BESO considering stress	BESO considering compliance
Number of elements	6400	6400
Number of iterations	91	91
Volume fraction	0.3	0.3
Computing time (second)	14.731	11.785

4.9 Mesh quality effect

In this section the mesh quality effects have been investigated for the proposed stress-based BESO method, where the **P1**$_{\mathbf{stress}}$ problem has been solved with different mesh sizes of 80×40, 100×50, 140×70 and 200×100 for the cantilever example, which has been shown earlier in Fig. 4-14. As explained earlier a 650 N point load is applied at the middle of the right-hand side and the design space has meshed into 5000 quadrilateral plane stress elements (1×1 mm). Again, to avoid the stress concentration, the eight elements (4×2) which are at the neighborhood of the applied load, are excluded from the design space. The thickness and the evolutionary rate (*ER*) are set to be 1 mm, and 0.02 respectively. The sensitivity filter radius (r_{min}) has been set to 1.5 mm for all mesh sizes. Different from the original BESO method (Huang, X & Xie, YM 2007, 2010) which is a mesh-independent approach, the proposed stress-based approach is not mesh-independent. Although in the proposed method, the mesh-independent filter has been used to reach the optimal designs, as it can be seen from the results, different optimal layouts are obtained while using different mesh sizes, and as

explained in (Jeong, Choi & Yoon 2015) this is because of the so-called “local optima issue”. This occurs in the stress and fatigue-based topology optimization due to the local and nonlinearity nature of the stress and fatigue constraints. The results for applying the different mesh sizes are depicted in Fig. 4-43. The results of the original BESO method are also provided to show the validity of the stress-based proposed method in minimizing the stress while the mesh sizes have been changed. Although in the traditional BESO method, the relatively similar filtering radius should be used to achieve the same optimized result which is mesh-independent, in order to better compare the final maximum stress, the filter radius of the $\mathbf{P}_{\mathbf{compliance}}$ is set to be the same as the filter radius of $\mathbf{P1}_{\mathbf{stress}}$, which is 1.5 mm in this section. According to the results, the maximum stress has been reduced in comparison to the traditional BESO method, while the mesh dimensions have been changed. By changing the same relative filtering radius, the optimal final designs cannot be the same which is different from the original BESO method (Huang, X & Xie, YM 2007, 2010). By setting the filter radius to larger higher values than 1.5 mm, the relatively similar results might be obtained in which the changing of the filter radius is not based on the relative change of the mesh sizes. This means that for obtaining the same topology, changing of the filter radius does not depend on the mesh sizes as is in the traditional BESO method, and the same topology cannot be obtained due to the local optima. In addition, the same topology may be obtained by defining the larger filter values while using the finer mesh sizes which are not based on the sizes of the mesh but based on experience as shown in Fig. 4-44. The results of the original BESO method in Fig. 4-44 have been obtained by changing the filter radius based on the relative change of the mesh sizes which leads to the same final topology in all cases. However, the results which are obtained from the proposed method, are based on setting the filter radius to larger values according to experience to obtain the same topology.

Mesh size	r_{min} & σ_{max}	Optimized structure & Stress plot (**P1$_{stress}$**)	Optimized structure & Stress plot (**P$_{compliance}$**)
80×40	$(r_{min})_{stress}$ = 1.5 mm $(\sigma_{max})_{stress}$ = 320.1 [MPa] $(C)_{stress}$ = 185.5 [N mm]	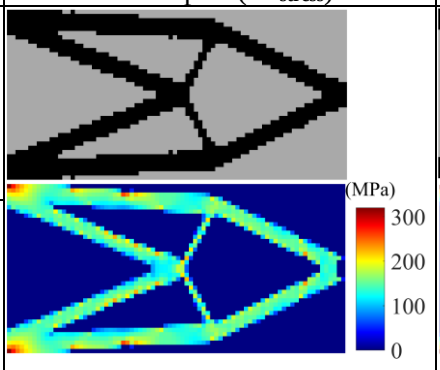	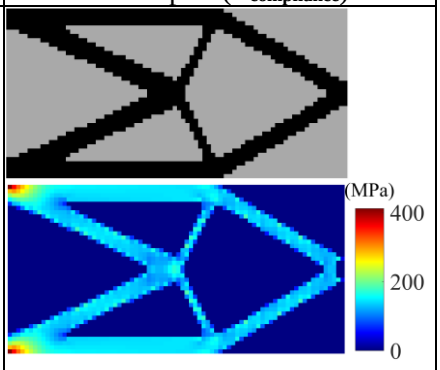
	$(r_{min})_{compliance}$ = 1.5 mm $(\sigma_{max})_{compliance}$ = 411.7 [MPa] $(C)_{compliance}$ = 173 [N mm]		
100×50	$(r_{min})_{stress}$ = 1.5 mm $(\sigma_{max})_{stress}$ = 295.9 [MPa] $(C)_{stress}$ = 178.2 [N mm]	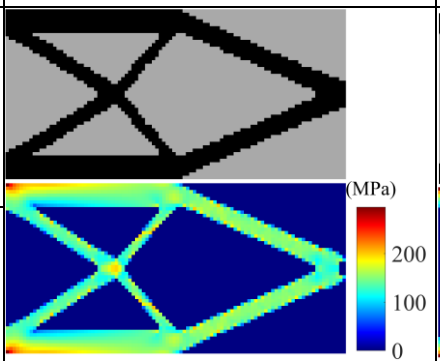	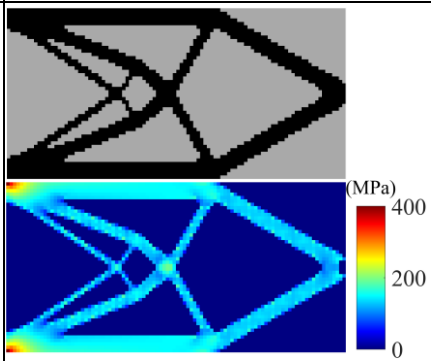
	$(r_{min})_{compliance}$ = 1.5 mm $(\sigma_{max})_{compliance}$ = 400.4 [MPa] $(C)_{compliance}$ = 171.5 [N mm]		
140×70	$(r_{min})_{stress}$ = 1.5 mm $(\sigma_{max})_{stress}$ = 307.5 [MPa] $(C)_{stress}$ = 175.1 [N mm]	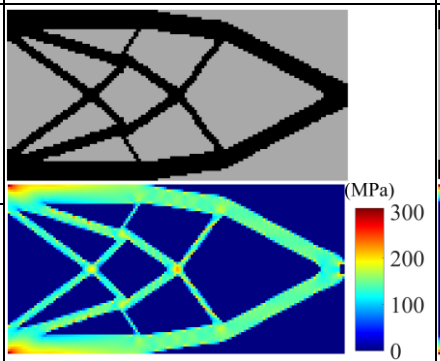	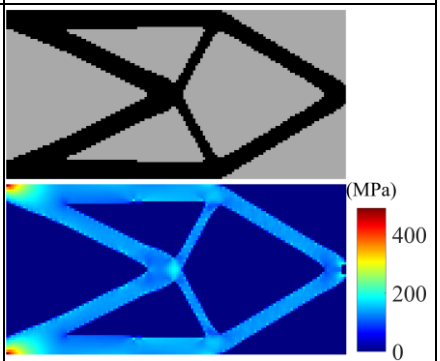
	$(r_{min})_{compliance}$ = 1.5 mm $(\sigma_{max})_{compliance}$ = 490.7 [MPa] $(C)_{compliance}$ = 171.6 [N mm]		
200×100	$(r_{min})_{stress}$ = 1.5 mm $(\sigma_{max})_{stress}$ = 349.4[MPa] $(C)_{stress}$ = 183.1[N mm]	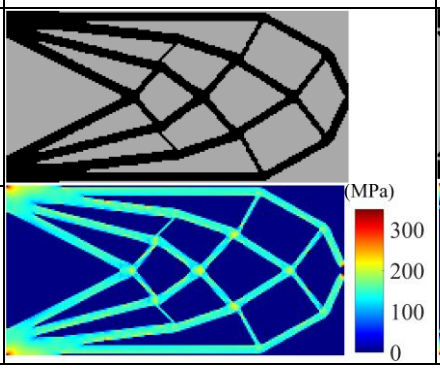	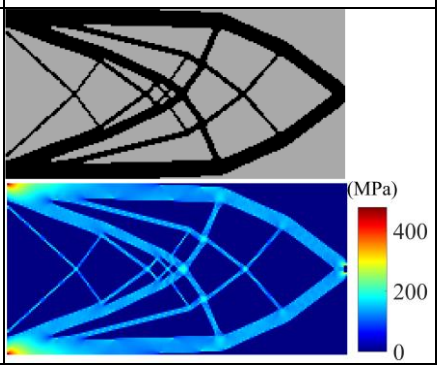
	$(r_{min})_{compliance}$ = 1.5mm $(\sigma_{max})_{compliance}$ = 477.3 [MPa] $(C)_{compliance}$ = 170.8 [N mm]		

Fig. 4-43. Optimal layouts for the cantilever beam with the same filter radius 1.5 mm (σ^* = 358MPa, V/V_0=0.35)

Mesh size	r_{min} & σ_{max}	Optimized structure & Stress plot (**P1**$_{\mathbf{stress}}$)	Optimized structure & Stress plot (**P**$_{\mathbf{compliance}}$)
80×40	$(r_{min})_{stress}$ = 2 mm $(\sigma_{max})_{stress}$ = 314.6 [MPa] $(C)_{stress}$ = 177.1 [N mm]	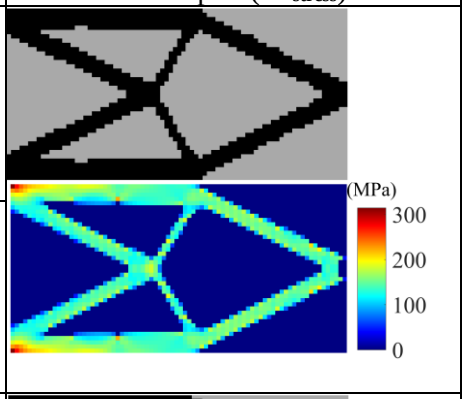	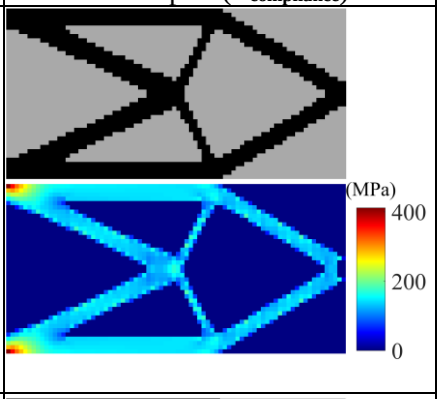
	$(r_{min})_{compliance}$ = 2 mm $(\sigma_{max})_{compliance}$ = 411.7 [MPa] $(C)_{compliance}$ = 173 [N mm]		
100×50	$(r_{min})_{stress}$ = 2 mm $(\sigma_{max})_{stress}$ = 344 [MPa] $(C)_{stress}$ = 175.2 [N mm]	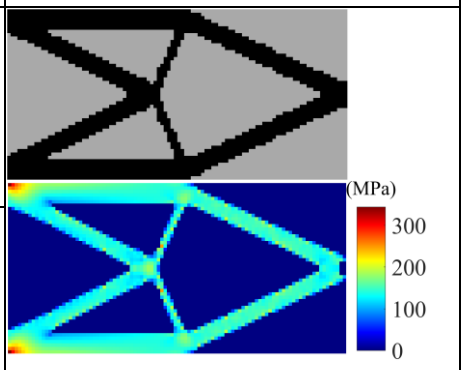	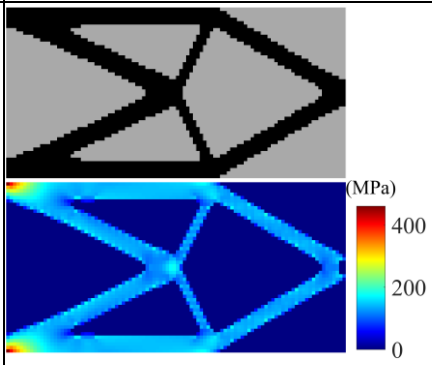
	$(r_{min})_{compliance}$ = 2.5 mm $(\sigma_{max})_{compliance}$ = 460.5 [MPa] $(C)_{compliance}$ = 173 [N mm]		
140×70	$(r_{min})_{stress}$ = 2.5 mm $(\sigma_{max})_{stress}$ = 341.9 [MPa] $(C)_{stress}$ = 174.2 [N mm]	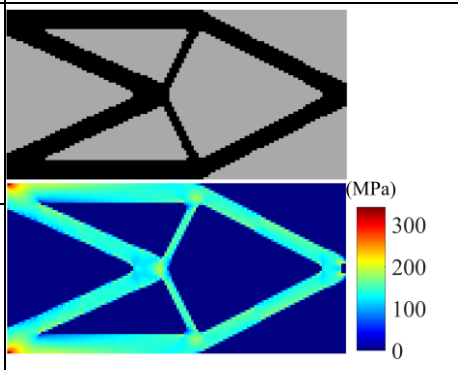	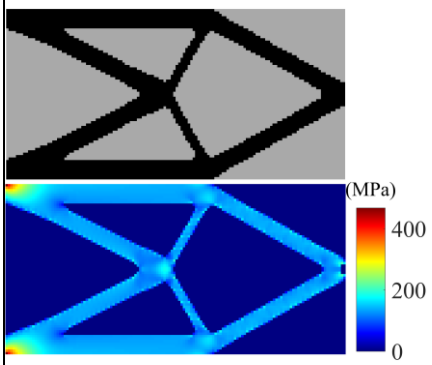
	$(r_{min})_{compliance}$ = 3.5 mm $(\sigma_{max})_{compliance}$ = 467.9 [MPa] $(C)_{compliance}$ = 170.4 [N mm]		
200×100	$(r_{min})_{stress}$ = 5.5 mm $(\sigma_{max})_{stress}$ = 355.4 [MPa] $(C)_{stress}$ = 174.9 [N mm]	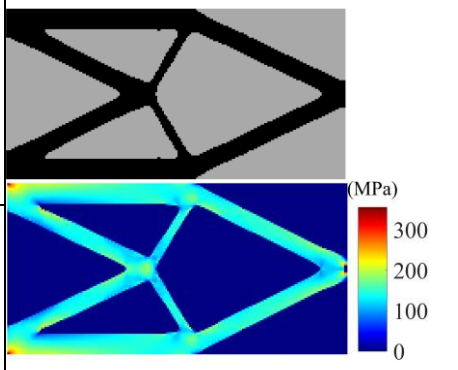	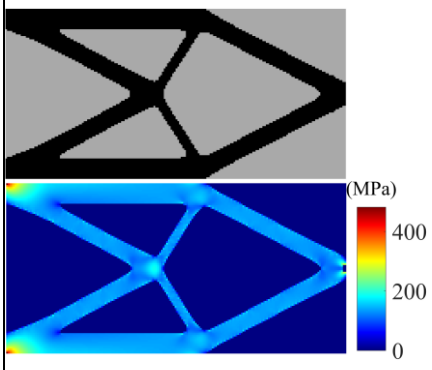
	$(r_{min})_{compliance}$ = 5mm $(\sigma_{max})_{compliance}$ = 481.9 [MPa] $(C)_{compliance}$ = 169.7 [N mm]		

Fig. 4-44. Optimal design layouts for the cantilever beam with different filtering radius (σ^* = 358MPa, V/V_0=0.35)

4.10 Conclusion

In this chapter of this research, the BESO approach was developed to solve the stress-based topology optimization problems. Three different optimization problems which are called $\mathbf{P1}_{\mathbf{stress}}$, $\mathbf{P2}_{\mathbf{stress}}$ and $\mathbf{P3}_{\mathbf{stress}}$ were solved for different numerical examples to show the validity and merit of the stress-based BESO approach. In the $\mathbf{P1}_{\mathbf{stress}}$ problem, the aim was to seek the stiffest structure while satisfying the prescribed stress and volume constraints. In the $\mathbf{P2}_{\mathbf{stress}}$ problem the *p*-norm stress was minimized subject to the volume constraint and in the last problem ($\mathbf{P3}_{\mathbf{stress}}$) the minimum volume of the structure was sought while satisfying the stress constraint. In addition, all the solutions of the above-mentioned problems have been compared with the original BESO approach ($\mathbf{P}_{\mathbf{compliance}}$). The numerical examples show that the proposed stress-based approach is able to reduce the high-stress concentration, and also minimize the maximum stress values when compared to the traditional BESO approach. Although $\mathbf{P1}_{\mathbf{stress}}$ and $\mathbf{P2}_{\mathbf{stress}}$ problems are different, both have a volume constraint which can be set to the same value for comparison. However, in the $\mathbf{P3}_{\mathbf{stress}}$ problem the volume is the objective function and by tailoring the stress constraint to reach the same volume as $\mathbf{P1}_{\mathbf{stress}}$ and $\mathbf{P2}_{\mathbf{stress}}$ problems the stress value and the mean compliance will be completely different, and it is not a possible to compare the results. Therefore, the results of the $\mathbf{P3}_{\mathbf{stress}}$ problem cannot compare with the $\mathbf{P1}_{\mathbf{stress}}$ and $\mathbf{P2}_{\mathbf{stress}}$. According to the results the $\mathbf{P1}_{\mathbf{stress}}$ leads to stiffest structure while compare to the $\mathbf{P2}_{\mathbf{stress}}$, however the maximum stress in $\mathbf{P1}_{\mathbf{stress}}$ is higher than the $\mathbf{P2}_{\mathbf{stress}}$ where both problems satisfied the stress constraints.

Since stress failure plays a fundamental role in engineering application, the optimal designs which are obtained from the proposed method are closer to the engineering needs. Hence the proposed stress-based BESO method can be used as a tool to optimize the structures in the framework of the BESO method, in which the optimized structure is resistant to the stress failure, when compared with the BESO stiffness optimization. In short, this research has developed a new stress-based BESO approach.In the next chapter the critical fatigue stress will be applied as a stress constraint in the BESO topology optimization problem, where the sensitivity analysis is based on the principal stress, rather than the von Mises stress to reach the optimized structure which is fatigue-resistant.

Chapter 5

BESO method based on critical fatigue stress

In this chapter, the critical fatigue stress has been applied as a stress constraint in the original BESO approach, which means the BESO optimization problem has been solved for additional fatigue stress constraint to minimize the compliance while satisfying the fatigue stress. The stress constraint in this chapter, is based on the critical fatigue stress for the specific life cycles. Different from the stress-based topology optimization of the previous chapter, (Chapter 4), in this chapter the calculation of the sensitivity numbers is based on the principal stress sensitivity analysis rather than von Mises stress sensitivity analysis. Since the compressive principal stresses generally do not have any role in the fatigue failure of the structures, the highest tensile principal stresses of the elements have been considered in the sensitivity analysis to obtain the sensitivity numbers. The critical fatigue stress has been calculated based on the high cycle fatigue approach, in which the highest tensile principal stress which causes the fatigue failure in the structure, has been calculated based on the Goodman fatigue failure criteria for a predefined number of cycles. Different numerical examples have been solved to show the effectiveness of the fatigue-based approach, where the results are compared with both the compliance-based and the stress-based reproaches.

5.1 Introduction

The idea of separating the fatigue analysis from the topology optimization was proposed by Holmberg et al. (2014) where the critical fatigue stress was calculated prior to the optimization process and then used as a stress constraint in the topology optimization problem to reach the fatigue-resistant optimized structures. The high-cycle fatigue regime was used to calculate the critical fatigue stress. The sensitivity analysis was based on the maximum principal tensile stress since the fatigue failure does not accrue with compressive stress. They used the fatigue accumulation damage approach to seek the highest tensile principal stress which caused the allowable cumulative damage to the

structure. This means that to calculate the critical fatigue stress another problem was solved prior to the optimization solution as follows:

$$(\mathrm{P}_{\mathrm{crit}}) \begin{cases} \max\ \sigma_f^* \\ s.t.\ D = \dfrac{\sigma_a}{\sigma_{nf}} + \dfrac{\sigma_m}{\sigma_{ut}} \le 1 \end{cases} \tag{5-1}$$

where D is the cumulative damage and must be less than 1 in order to avoid fatigue failure. For solving the optimization problem, Holmberg et al. (2014) used the *p*-norm approach to gather the critical fatigue stress of the elements in one function. In addition, they used the method of moving asymptotes (MMA) (Svanberg 1987) to solve the gradient-based topology optimization in the framework of the SIMP method, where the minimum volume of the structure was sought while satisfying the prescribed life cycles. The optimization problem was solved in the same way as stress constraint topology optimization (Holmberg, Torstenfelt & Klarbring 2013), the main difference being that the stress constraint was substituted with the critical fatigue stress and the sensitivity analysis was based on the principal tensile stress, rather than the von Mises stress. The results obtained were compared with the stress-based topology optimization based on the von Mises stress to show the effectiveness of their new approach. The method was based on continuous density, and as mentioned before, there is no report on using fatigue constraint in discrete density approaches such as the BESO method. Therefore, in this chapter, we used the methodology which has been used in (Holmberg, Torstenfelt & Klarbring 2013) to solve the BESO optimization problem, which is based on the critical fatigue stress. Our approach differs from (Holmberg, Torstenfelt & Klarbring 2013) in that the critical fatigue stress has been calculated based on the Goodman fatigue failure criterion rather than cumulative damage. Hence the critical fatigue stress can be calculated as follows:

$$(\mathrm{P}_{\mathrm{crit}}) \begin{cases} \max\ \sigma_f^* \\ s.t.\ Goodman\ fatigue\ criterion: \dfrac{\sigma_a}{S_n} + \dfrac{\sigma_m}{S_u} \le 1 \end{cases} \tag{5-2}$$

where the ultimate tensile stress and the fatigue limits of the elements are denoted by S_{ut} and S_n respectively, and σ_a and σ_m are the alternating and mean stress which are discussed later in this chapter. The S_n, which is the fatigue limits of the elements, is calculated based on the desired life which is expected from the structure. To avoid fatigue failure, the Goodman fatigue criterion must be less than 1 (Aliabadi 1992; Jeong, Choi & Yoon 2015; Suresh 1998). Therefore, according to Equation (5-2), the highest tensile principal stress should be calculated for the specific life cycle, which applies as stress constraint in the topology optimization problem.

5.2 Problem statement

The topology optimization problem which has been solved in this chapter deals with minimization of the compliance while fulfilling the critical fatigue stress. The optimization problem reads:

$$\mathbf{P}_{\textbf{fatigue stress}}: \begin{cases} \text{Minimize}: \ \mathrm{C} = f(x) = \dfrac{1}{2}\mathbf{u}^{\mathrm{T}}\mathbf{k}\mathbf{u} \\ \text{subject to}: \begin{cases} \sigma_f^{PN} \le \sigma_f^{*} \\ V^{*} - \displaystyle\sum_{i=1}^{N_i} V_i x_i = 0 \\ x_i = x_{\min} \text{ or } 1 \end{cases} \end{cases} \tag{5-3}$$

where V^{*}, V_i and x_i are the volume constraint, individual elements volume and binary design variables respectively and the critical fatigue stress constraint is denoted by σ_f^{*}. σ_f^{PN} is the global modified *p*-norm stress function which is based on the maximum principal tensile stresses of the elements and is discussed in the next section. Since using the local constraints of each element in the topology optimization problem leads to a huge computational cost and is nearly impossible, the global approach of gathering the constraints by using the *p*-norm function has been used in this research (Holmberg, Torstenfelt & Klarbring 2013). The optimization problem is called $\mathbf{P}_{\textbf{fatigue stress}}$ in this chapter, and different numerical examples have been solved for this optimization problem. The results have been compared with the $\mathbf{P1}_{\textbf{stress}}$ problem which was shown in Equation (4-1), and the stress

constraint in the $\mathbf{P1_{stress}}$ problem has been set to the critical fatigue stress value which has been applied in the $\mathbf{P_{fatigue\ stress}}$ problem.

5.3 Stress measurement for calculating the critical fatigue stress

As mentioned earlier in this chapter, fatigue analysis and topology optimization have been performed in two separate steps (Holmberg, Torstenfelt & Klarbring 2014), where the maximum tensile principal stress, referred to as critical fatigue stress in this chapter, has been calculated based on the Goodman fatigue failure criterion which reads

$$\left(\frac{\sigma_a}{\sigma_{nf}} + \frac{\sigma_m}{\sigma_{ut}} \leq 1\right) \tag{5-4}$$

where the alternating and mean stress of the elements can be defined as follows:

$$\sigma_a = \frac{\sigma_{\max} - \sigma_{\min}}{2} \tag{5-5}$$

$$\sigma_m = \frac{\sigma_{\max} + \sigma_{\min}}{2} \tag{5-6}$$

The σ_{nf}, which is related to the fatigue limit of the elements for allowable life cycles, can be defined based on the *Basquin* Equation (Aliabadi 1992; Lee, Barkey & Kang 2012; Suresh 1998) as follows:

$$\sigma_{nf} = \sigma'_f (2N_f)^b \tag{5-7}$$

$$\sigma'_f = \frac{(f\ \sigma_{ut})^2}{\sigma_e} \tag{5-8}$$

$$b = -\frac{1}{3}\log\frac{(f\ \sigma_{ut})}{\sigma_e} \tag{5-9}$$

where σ'_f and b are the fatigue strength coefficient and fatigue strength exponents which are based on the material properties, and N_f represents the number of cycles to failure at stress amplitude σ_{nf}.

σ_e is the endurance limit of the material which can be calculated as follows

$$\sigma_e = 0.5\sigma_{ut} \quad for \quad \sigma_{ut} < 1379\ MPa \tag{5-10}$$

Also, σ_{ut} is the ultimate tensile strength of the materials, where f represents the fraction of σ_{ut} and can be calculated as follows (Aliabadi 1992; Lee, Barkey & Kang 2012; Suresh 1998).

$$f = 0.9 \quad for \quad \sigma_{ut} < 480\ Mpa \tag{5-11}$$

In principle, the modified endurance limit ($\overline{\sigma}_e$) should be calculated by applying the correction factor to the actual endurance limit σ_e, as used and explained in (Aliabadi 1992; Lee, Barkey & Kang 2012; Suresh 1998). Then the fatigue strength exponent (b) and fatigue strength (σ'_f) should be calculated accordingly based on $\overline{\sigma}_e$. Since the proposed method, which is based on the critical fatigue stress, aims to reach a preliminary optimized structure in the first stage of the fatigue design process, in this research the actual endurance limit is used rather than $\overline{\sigma}_e$ which means that none of these correction factors have been applied for the proposed method. By defining the *Basquin* Equation parameters, the fatigue limit of the N_f cycles (σ_n) can be obtained easily. The critical fatigue stress calculation only needs to be done once during the optimization. For avoiding fatigue failure, the highest tensile principal stress for allowable life cycles has been sought, based on the Goodman fatigue criteria, which means that the highest tensile principal stress should fulfill the Goodman equation. Finally, this critical tensile stress can be used in the topology optimization problem as a stress constraint. The *p*-norm global approach has been used to gather all the local critical fatigue stresses in one function to reduce the computational cost as follows:

$$\sigma_{cfs}^{PN}(x) = \left(\frac{1}{N_i} \sum_{i=1}^{N_i} (\sigma_a^1(x))^P \right)^{\frac{1}{P}} \tag{5-12}$$

where σ_a^1 the maximum tensile principal stress and can be defined as:

$$\begin{cases} \sigma_a^1 = \max(\lambda^1, 0) \\ \lambda^1 > \lambda^2 > \lambda^3 \end{cases} \tag{5-13}$$

Where λ^1, λ^2 and λ^3 are the eigenvalues of the stress tensor:

$$S = \begin{bmatrix} S_{11} & S_{12} & S_{13} \\ S_{12} & S_{22} & S_{23} \\ S_{13} & S_{23} & S_{33} \end{bmatrix} \tag{5-14}$$

As explained in Chapter 4, the *p* factor of the *p*-norm function should be infinite in principle to reach the maximum stress, but in practice, a value from 3 to 4 has been used by many other authors. In this research, our numerical experiences show that choosing a value from 3 to 5 for *p*-norm factor (*p*) works well for the BESO method based on the critical fatigue stress. However, by changing the *p* value and selecting the other values, different optimal designs maybe obtained because of the change of the objective function. The finite elements analysis (FEA) is performed based on the static finite element analysis based on Equation (4-6) and again, for solving the optimization problem, the material interpolation scheme (SIMP) is also adopted based on Equations (4-7) and (4-8). For solving the optimization problem which has shown in Equation 5-3 the sensitivity numbers of the elements should be calculated based on the tensile principal stress sensitivity analysis, which is discussed in the next section. The high cycle fatigue approach with the constant proportional loading condition has been used to reach the alternating and mean stress of the elements. According to Collet et al. (2017) the equivalent static analysis could be applied to fatigue analysis by considering the amplitude of the static stress state, if the material behaviour is assumed to be elastic, and there is no crack initiation assumption. Furthermore, the loading condition must be constant proportional loading case. Hence the equivalent static analysis has been used to calculate the critical fatigue stress of the elements.

5.4 Sensitivity analysis based on critical fatigue stress

For solving the BESO optimization problem which considers the fatigue stress as a constraint, the sensitivity numbers of the elements should be calculated based on the derivative of the *p*-norm stress

with respect to design variables. Hence the gradient of the *p*-norm stress by applying the chain rule can be defined as follows:

$$\frac{\partial \sigma_{cfs}^{PN}(x)}{\partial x_i} = \frac{\partial \sigma_{cfs}^{PN}(x)}{\partial \sigma_a^1} \frac{\partial \sigma_a^1(x)}{\partial x_i} \tag{5-15}$$

where the term $\partial \sigma_f^{PN}(x) / \partial \sigma_a^1$ can be defined by taking the derivative of Equation (5-12) as follows:

$$\frac{\partial \sigma_{cfs}^{PN}(x)}{\partial \sigma_a^1} = \left(\frac{1}{N_i} \sum_{i=1}^{N_i} (\sigma_a^1(x))^P \right)^{\left(\frac{1}{P}-1\right)} \times \frac{1}{N_i} \left(\sigma_a^1(x)\right)^{P-1} \tag{5-16}$$

The derivative of the σ_a^1 with respect to design variables x_i reads:

$$\frac{\partial \sigma_a^1(x)}{\partial x_i} = \phi_i \frac{\partial S_{ij}}{\partial x_i} \phi_j = \mathbf{\Lambda}_t \frac{\partial \sigma_t}{\partial x_i} = \mathbf{\Lambda}_a \frac{\partial \boldsymbol{\sigma}_a(x)}{\partial x_i} \tag{5-17}$$

$$\mathbf{\Lambda} = (\phi_1{}^2, \phi_2{}^2, \phi_3{}^2, 2\phi_1\phi_2, 2\phi_2\phi_3, 2\phi_1\phi_3)^T \tag{5-18}$$

$$\frac{\partial \boldsymbol{\sigma}_a(x)}{\partial x_i} = \frac{\partial \mathbf{D}(x)}{\partial x_i} \mathbf{B}\mathbf{u} + \mathbf{D}\mathbf{B} \frac{\partial \mathbf{u}(x)}{\partial x_i} \tag{5-19}$$

where $\mathbf{\Lambda}$ is the transformation vector in which the component of the corresponding eigenvector is denoted by ϕ_i and **u**, **B** and **D**, which are the displacement, strain displacement, and the constitutive matrices respectively. The term $\partial \mathbf{D}(x) / \partial x_i$ can be easily calculated from Equation (4-10) as mentioned before, but the term $\partial \mathbf{u}(x) / \partial x_i$ cannot easily be derived. For solving Equation (5-15) the adjoint method should be used to calculate the derivative of the displacement vectors over the design variables. Hence for calculating the term $\partial \mathbf{u}(x) / \partial x_i$, the chain rule can be applied to the global Equation (4-6) which was discussed in Chapter 4 as follows:

$$\frac{\partial \mathbf{F}}{\partial x_i} = \frac{\partial \mathbf{K}(x)}{\partial x_i} \mathbf{u} + \mathbf{K} \frac{\partial \mathbf{u}(x)}{\partial x_i} \tag{5-20}$$

from which the derivative of the displacement matrix over design variables can be obtained as follows:

$$\frac{\partial \mathbf{u}(x)}{\partial x_i} = -\mathbf{K}^{-1} \frac{\partial \mathbf{K}(x)}{\partial x_i} \mathbf{u} \tag{5-21}$$

By substituting Equation (5-17) into Equation (5-15) and then (5-15) into (5-13) and finally Equations (5-13) and (5-12) into (5-11) the derivative of the *p*-norm stress reads:

$$\frac{\partial \sigma_{cfs}^{PN}(x)}{\partial x_i} = \frac{\partial \sigma_{cfs}^{PN}(x)}{\partial \sigma_a^1} \times \mathbf{\Lambda}_a \left(\frac{\partial \mathbf{D}(x)}{\partial x_i} \mathbf{B}\mathbf{u} - \mathbf{D}\mathbf{B}\mathbf{K}^{-1} \frac{\partial \mathbf{K}(x)}{\partial x_i} \mathbf{u} \right) \tag{5-22}$$

where the adjoint equation can be defined as follows:

$$\mathbf{K}\boldsymbol{\lambda}^T = \mathbf{B}^T \mathbf{D}^T \mathbf{\Lambda}_a \frac{\partial \sigma_{cfs}^{PN}(x)}{\partial \sigma_a^1} \tag{5-23}$$

Therefore, by inserting the adjoint variable $\boldsymbol{\lambda}$ in Equation 5-18 the final gradient reads

$$\frac{\partial \sigma_{cfs}^{PN}(x)}{\partial x_i} = \left[\frac{\partial \sigma_{cfs}^{PN}(x)}{\partial \sigma_a^1} \mathbf{\Lambda}_a{}^T \frac{\partial \mathbf{D}(x)}{\partial x_i} \mathbf{B}\mathbf{u} - \boldsymbol{\lambda}^T \left(\frac{\partial \mathbf{K}(x)}{\partial x_i} \mathbf{u} \right) \right] \tag{5-24}$$

5.5 Numerical implementation procedure

To solve the $\mathbf{P}_{\text{fatigue stress}}$ problem, the sensitivity numbers of the elements should be defined based on the derivative of the objective function. Since an extra critical fatigue stress constraint has been added to the original BESO problem, the objective function should be modified as follows:

$$f(x) = C + \lambda(\sigma_{cfs}^{PN} - \sigma_f{}^*) \tag{5-25}$$

where C, $\sigma_{cfs}{}^{PN}$ and σ_f^* are the compliance, *p*-norm fatigue stress, and critical fatigue stress constraint respectively. λ represents the Lagrangian multiplier which calculates based on the volume and critical fatigue stress constraints as discussed in section 4-5-2. According to Equation (5-25), when the *p*-norm stress is equal to the critical fatigue stress constraint, the modified objective function will be the same as the original BESO objective function. In addition, while $\sigma_{cfs}{}^{PN} < \sigma_f^*$, the Lagrangian multiplier will be set to zero ($\lambda=0$), meaning that the stress constraint has been already satisfied. However, the

value of λ will tend to infinity if $\sigma_{cfs}^{PN} > \sigma_f^*$, which means that σ_{cfs}^{PN} is minimized to satisfy the critical fatigue stress constraint in later iterations. The Lagrangian multiplier should be defined prior to the calculation of the sensitivity numbers, where the sensitivity of the modified objective function is:

$$\frac{df}{dx_i} = q\, x_i^{q-1}\left(-\frac{1}{2}\mathbf{u}^{\mathrm{T}}\mathbf{K}\mathbf{u} + \lambda \frac{\sigma_{cfs}^{PN}(x)}{\partial x_i}\right) \tag{5-26}$$

where the sensitivity number of the elements used in BESO can be expressed by:

$$\alpha_i = -\frac{1}{q}\frac{df}{dx_i} = x_i^{q-1}\left(\frac{1}{2}\mathbf{u}^{\mathrm{T}}\mathbf{K}\mathbf{u} - \lambda \frac{\sigma_{cfs}^{PN}(x)}{\partial x_i}\right) \tag{5-27}$$

Finally, the the sensitivity numbers for solid and void elements can be defined as

$$\alpha_i = \begin{cases} \dfrac{1}{2}\mathbf{u}^{\mathrm{T}}\mathbf{K}\mathbf{u} - \lambda \dfrac{\sigma_{cfs}^{PN}(x)}{\partial x_i} & \text{for} \quad x_i = 1 \\ x_i^{q-1}\left(\dfrac{1}{2}\mathbf{u}^{\mathrm{T}}\mathbf{K}\mathbf{u} - \lambda \dfrac{\sigma_{cfs}^{PN}(x)}{\partial x_i}\right) & \text{for} \quad x_i = x_{\min} \end{cases} \tag{5-28}$$

The procedure for the calculation of the Lagrangian multiplier is the same as the stress-based approach which was discussed in Chapter 4, with the exception of the calculation of the *p*-norm critical fatigue stress for the next iteration ($(\sigma_{cfs}^{PN})^{I+1}$), which is based on the critical fatigue stress rather than von Mises stress as follows:

$$(\sigma_{cfs}^{PN})^{I+1} \approx (\sigma_{cfs}^{PN})^{I+1} + \sum_i \frac{\sigma_{cfs}^{PN}}{\partial x_i}\,\Delta x_i \tag{5-29}$$

The BESO procedure for solving the optimization problem $\mathbf{P}_{\text{fatigue stress}}$ is the same flowchart which has been depicted in Fig. 4-1, where only the sensitivity analysis is based on the critical fatigue stress rather than von Mises stress.In the proposed BESO method which considers the critical fatigue stress the gradual material removing will be stopped while the algorithm reaches the objective volume (V^*) and the whole optimization process will end if the following convergence criteria are satisfied:

$$error_1 = \left| \frac{\sum_{i=1}^{N} C_{k-i+1} - \sum_{i=1}^{N} C_{k-N-i+1}}{\sum_{i=1}^{N} C_{k-i+1}} \right| \leq 0.01 \quad (5\text{-}30)$$

$$error_2 = \frac{\left| \sum_{i=1}^{N} (\sigma_{\max,\, k-i+1} - \sigma_{\max,\, k-N-i+1}) \right|}{\sum_{i=1}^{N} \sigma_{\max,\, k-i+1}} \leq 0.01 \quad (5\text{-}31)$$

where $N = 5$ is used in this problem.

5.6 Numerical examples

In this section, to show the validity and merit of the BESO method, which is based on the critical fatigue stress, the $\mathbf{P}_{\mathbf{fatigue\ stress}}$ problem (Equation (5-3)) has been solved for different 2D numerical examples. Since the constant proportional loading condition has been applied and, it was assumed that the materials remain elastic with no crack initiation, the static analysis has been used to calculate the critical fatigue stress of the elements by considering the amplitude of the stress state. The results of the $\mathbf{P}_{\mathbf{fatigue\ stress}}$ problem have been compared with the results of the $\mathbf{P1}_{\mathbf{stress}}$, where the same stress constraints have been applied. Additionally, the results have been compared with the original BESO method.

5.6.1 L-Bracket beam (center load)

The $\mathbf{P}_{\mathbf{fatigue\ stress}}$ problem has been solved for the L-bracket beam of Fig. 4-2 in this section, where the design space consists of a total of 6400 four-node plane stress elements, which are equal sized (1 mm × 1 mm) with the thickness of 1 mm. To avoid stress concentration in the vicinity of the point load, 3 × 2 elements (six elements) around the applied point load are excluded from the design space and fixed as solid elements during the optimization process. The evolutionary rate (*ER*) and the filter radius (r_{min}) are set to be 0.02 and 1.5 mm respectively. Carbon steel 1018 with Young's modulus 210,000 MPa and Poisson's ratio 0.3 has been used as the material reference. The constant

proportional load with the maximum of 400 N and minimum of 220 N has been applied in the middle of the right-hand side of the L-bracket beam. σ_{ut}, σ'_f and b have been set to be 440 MPa, 712.8 MPa and -0.851 respectively.

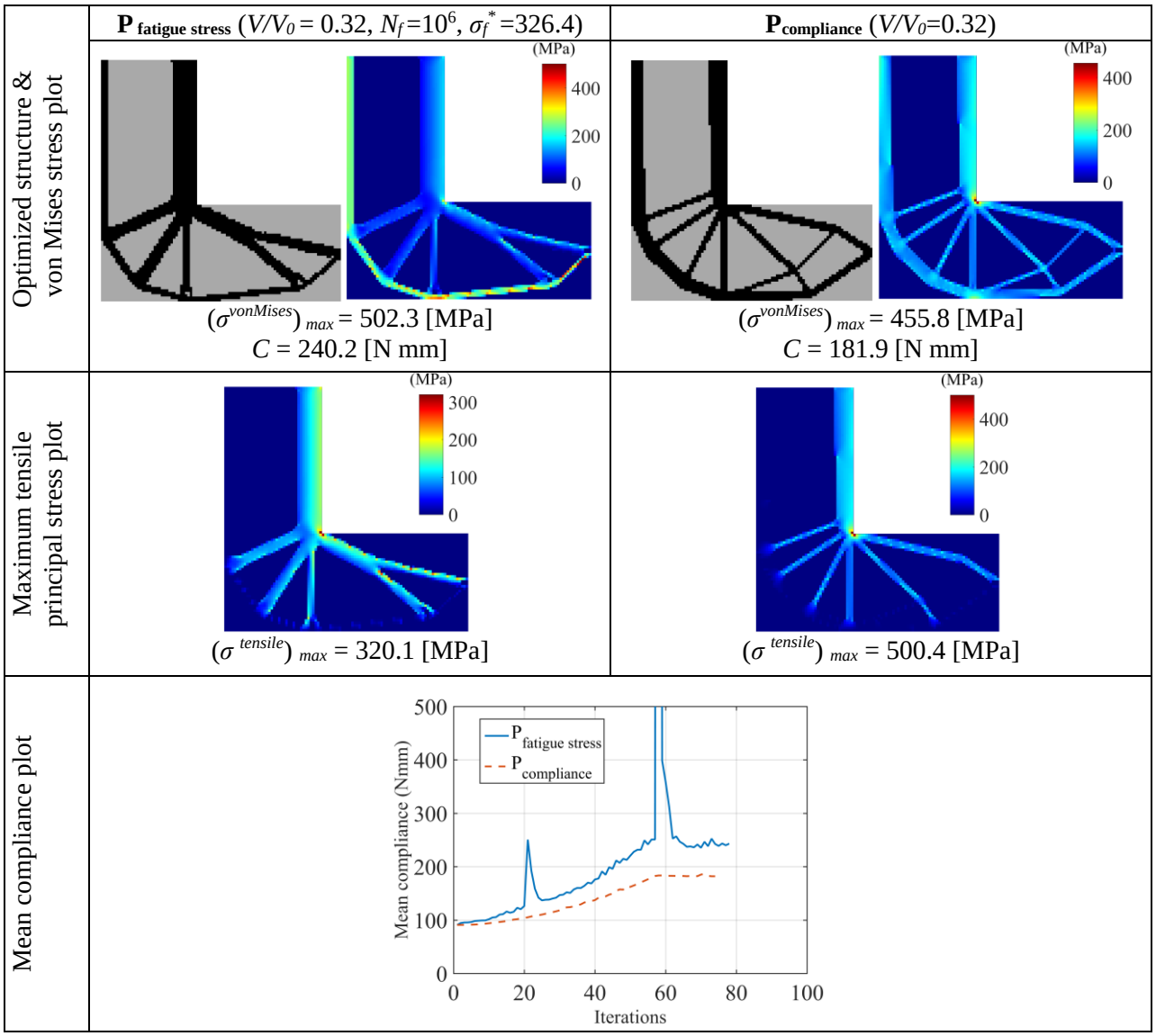

Fig. 5-1. Optimal layouts for the L-bracket beam with center load (V/V_0=0.32, N_f=10^6, σ_f^*=326.4 MPa)

According to the applied load and the *Basquin* Equation parameters, which are defined above, the critical fatigue stresses for N_f =10^6 and N_f =10^7 which are calculated by the Matlab code, are σ_f^* = 326.4 MPa and σ_f^* = 299.1 MPa respectively, where these stresses have been used as stress constraints to solve the optimization problems for two different volume constraints 0.32 and 0.45. Therefore, the optimization problem aims to seek the stiffest structure, which the highest tensile principal stress in

the entire design space is less than the value of σ_f^*=326.4 MPa for the volume constraint 0.32 and σ_f^*=299.1 MPa for the volume constraint 0.45.

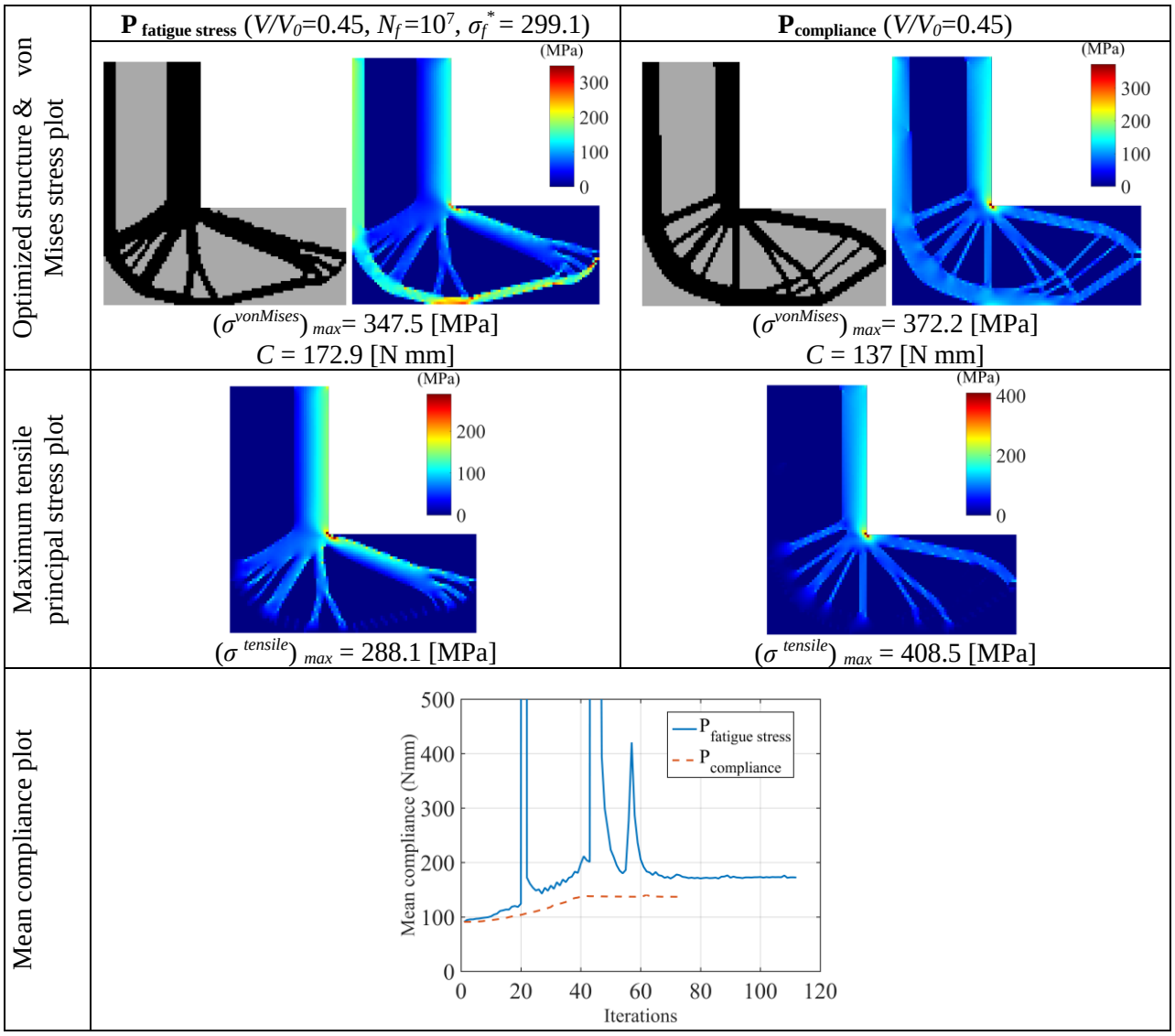

Fig. 5-2. Optimal layouts for the L-bracket beam with center load (V/V_0=0.45, N_f=10^7, σ_f^*=299.1 MPa)

Solutions for the L-bracket beam with the center load problem in which the compliance has been minimized, based on the critical fatigue stress are shown in Figs. 5-1 and 5-2 for different volume constraints 0.32 and 0.45. As previously mentioned, in each example there is the optimal design of the traditional compliance-based optimization problem ($\mathbf{P}_{\mathbf{compliance}}$) which has the same load and volume constraint as the examples which have been solved in $\mathbf{P}_{\mathbf{fatigue\ stress}}$ problems. According to the results, the maximum tensile principal stress has been decreased from 36% - 29% compared with the $\mathbf{P}_{\mathbf{compliance}}$ results. In addition, all the maximum tensile principal stresses values of the optimal designs

in the proposed BESO approach ($\mathbf{P}_{\text{fatigue stress}}$) are less than the critical fatigue constraint value. However, the mean compliance values are higher than the values which were obtained in the original BESO method due to the application of an additional fatigue constraint in the original BESO method. Since the sensitivity analysis is based on tensile principal stress rather than von Mises stress, it can be seen from the results that the maximum von Mises stress values are higher than the tensile principal stress in the proposed BESO approach. In addition, compared with the optimal design of the original BESO method, it can be seen that the vertical bars of the L-bracket have different thicknesses where the bars which are on tension are thicker than the bars which are on compression.

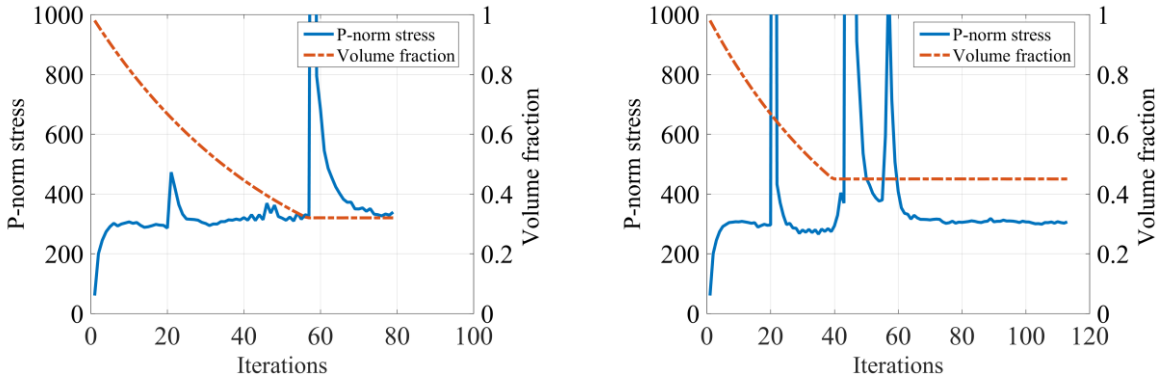

(a) (b)

Fig. 5-3.Convergence plots for L-bracket with center load (a) (V/V_0=0.32), (b) (V/V_0=0.45)

The convergence plots of the problems which are based on the *p*-norm stress evolution in each iteration are depicted in Fig. 5-3. In the next optimization example, the L-bracket beam has again been solved, where the position of the load has been changed from the center to the top of the right-hand side of the L-bracket.

5.6.2 L-Bracket beam (top load)

For the second example, the L-bracket beam of Fig. 4-20 has been solved for the $\mathbf{P}_{\text{fatigue stress}}$ problem. Again, to avoid stress concentration in the vicinity of the point load, 3 × 2 elements (six elements) around the applied point load are excluded from the design space and fixed as solid elements during optimization process where the design space consists of a total of 6400 four-node plane stress

elements, which are equal sized (1 mm × 1 mm) with the thickness of 1 mm. The filter radius (r_{min}) and the evolutionary rate (ER) are set to be 1.5 mm and 0.02 respectively.

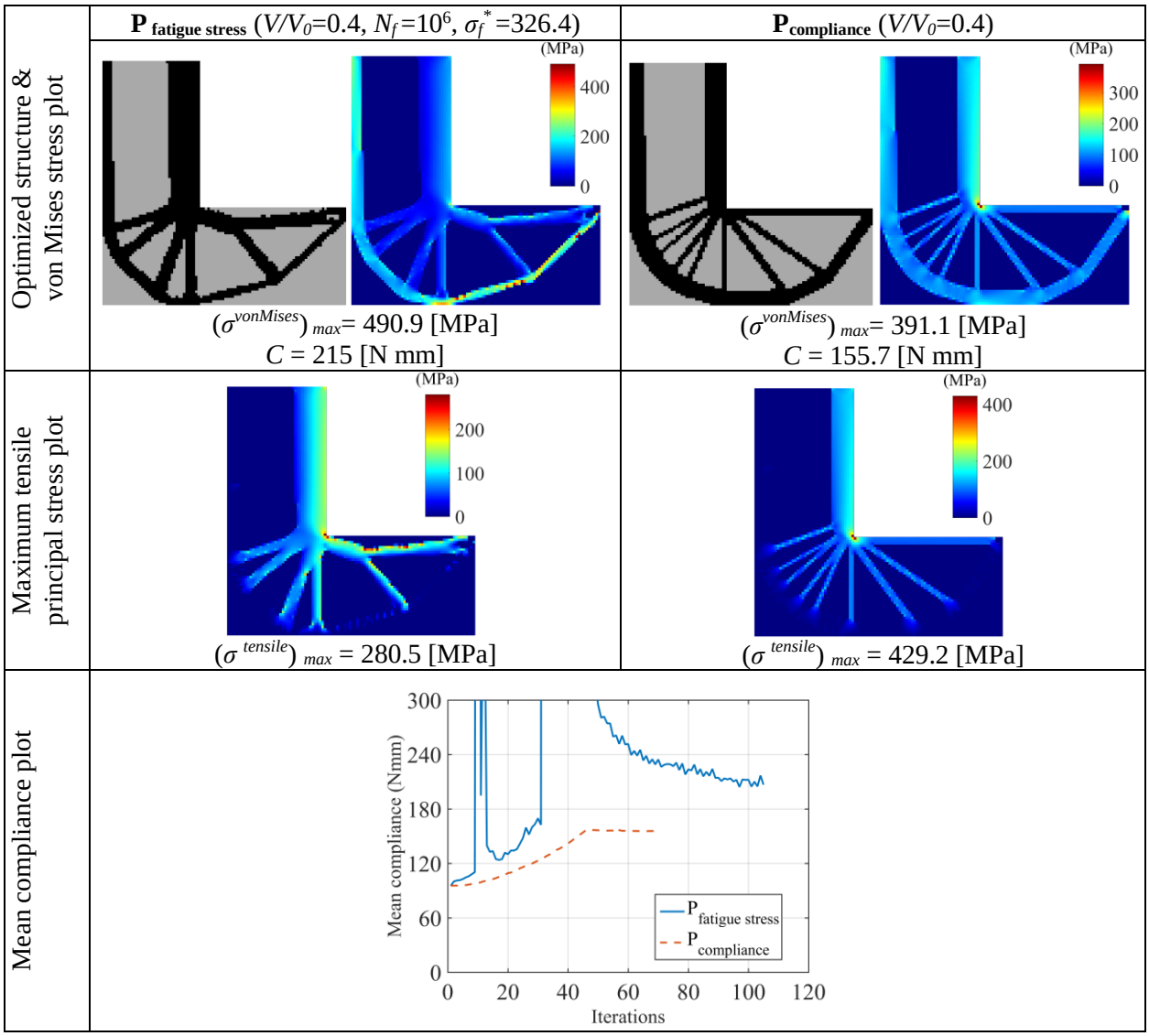

Fig. 5-4. Optimal layouts for the L-bracket beam with top load (V/V_0 = 0.4, N_f=10^6, σ_f^*=326.4 MPa)

The material reference is carbon steel 1018 with Young's modulus 210,000 MPa and Poisson's ratio 0.3. Again, the constant proportional load with the maximum of 400 N and minimum of 220 N has used in this example where the load has been applied in the top of the right-hand side of the L-bracket beam as shown in Fig. 4-20. b, σ'_f and σ_{ut} are set to be -0.0851, 712.8 MPa and 440 MPa respectively. The critical fatigue stresses constraints have been calculated as σ_f^* = 299.158 MPa and σ_f^* = 326.4 MPa for N_f =10^7 and N_f =10^6 respectively.

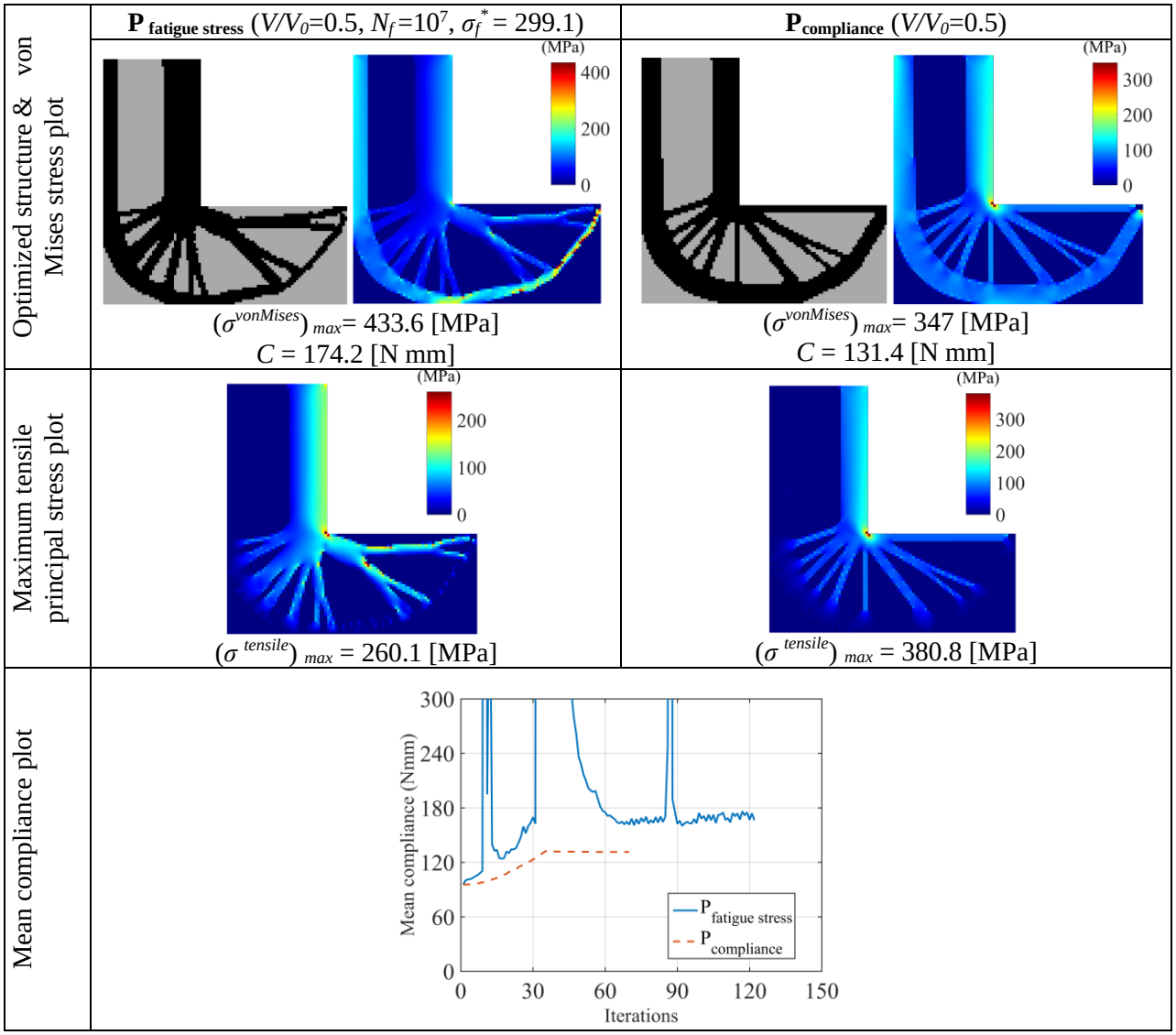

Fig. 5-5. Optimal layouts for the L-bracket beam with top load (V/V_0=0.5, N_f=10^7, σ_f^*=299.1 MPa)

The optimization problem has been solved for two different volume constraints 0.4 and 0.5. For the volume constraint 0.4, the fatigue constraint 326.4 MPa has been used and the fatigue constraint 299.1 MPa has been used for the volume constraint 0.5. Solutions for the L-bracket beam with the top load problem are shown in Figs. 5-4 and 5-5. Again, in each example, the original BESO method results have been compared with the proposed BESO method which is based on the critical fatigue stress constraint. As can be seen from the results, the maximum tensile principal stress has decreased from 34% - 32% compared with the maximum tensile principal stress value of the original BESO method ($\mathbf{P}_{\mathbf{compliance}}$), where in the case of the proposed BESO method, all the maximum tensile stress values are below the fatigue failure threshold. The mean compliance values are again higher than the values

which were obtained in the original BESO method, due to modifying the original objective function by using the fatigue stress constraint. Again, as can be seen from the results, the von Mises stress values are higher than the tensile principal stress in the proposed BESO approach.

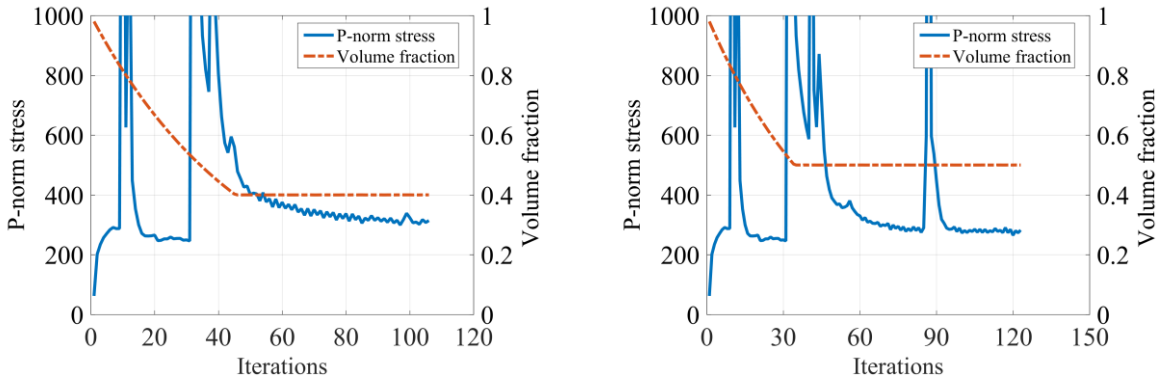

(a) (b)

Fig. 5-6. Convergence plots for L-bracket with top load (a) (V/V_0=0.4), (b) (V/V_0=0.5)

The convergence plots of the problems for the volume constraints 0.4 and 0.5 are shown in Figs. 5-6a and 5-6b where the significant jumps in the mean compliance can be seen in comparison to the traditional BESO approach. The jumps in the mean compliance during the fatigue-based optimization process are caused by a significant change of topology resulting from the elimination of one or more bars in one iteration. Following the significant jumps, the mean compliance quickly recovers and resumes a smooth ascent. In the next optimization example, the long clamp beam has been solved for the proposed optimization problem where again, the aim is to seek the stiffest structure while satisfying the fatigue stress and volume constraints simultaneously.

5.6.3 Long clamp beam

For the third example, again the long-clamped beam which has been shown in Fig. 4-8 is solved with the proposed BESO approach where the maximum stiffness is sought subject to volume and fatigue stress constraints. The design domain is discretized by 6000, 1×1 mm quadrilateral Q4 plane stress elements, with thickness set at 1 mm. The evolutionary ratio (ER) and sensitivity filter radius (r_{min}) and are chosen to be 2 and 0.02 respectively. The constant proportional load with the maximum of

800 N and minimum of 440 N, has been used in this example to calculate the stress state of the elements. To avoid the high local stress concentrations due to applying the point load, 12 elements (3×4) in the vicinity of the applied load are not used as design variables. σ_{ut}, σ'_f and b have been set to be 440 MPa, 712.8 MPa and -0.851 respectively.

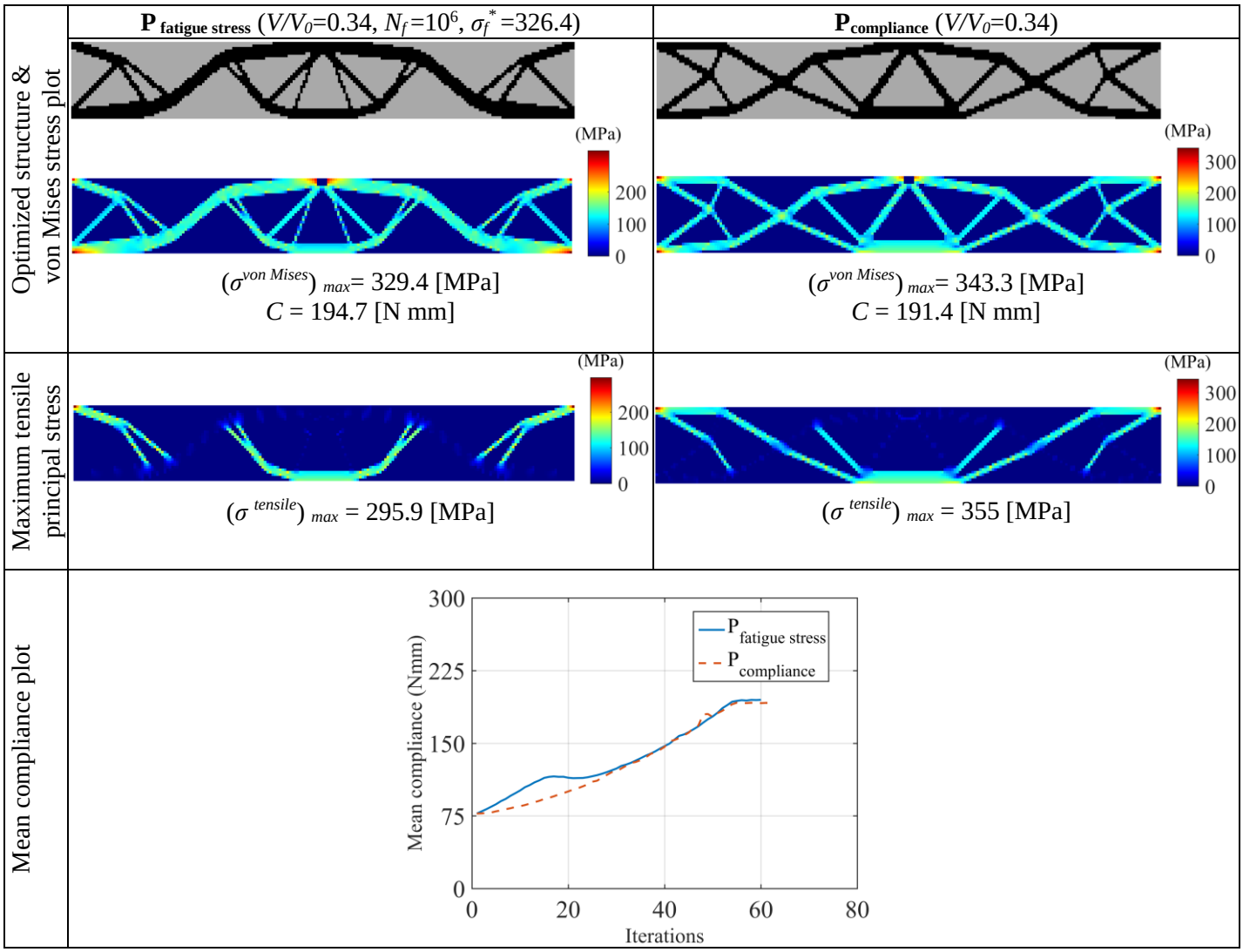

Fig. 5-7. Optimal layouts for long clamped beam (V/V_0=0.34, N_f=10^6, σ_f^*=326.4 MPa)

The optimization problem has been solved for two different volume constraints of 0.34 and 0.44 where N_f =10^6 has been used for volume constraint 0.34 and N_f =10^7 for volume constraint 0.44. Again, the critical fatigue stress has been calculated as σ_f^*=326.4 MPa for N_f =10^6 and σ_f^*=299.1 for N_f =10^7. The solutions to the problem are depicted in Figs. 5-7 and 5-8.

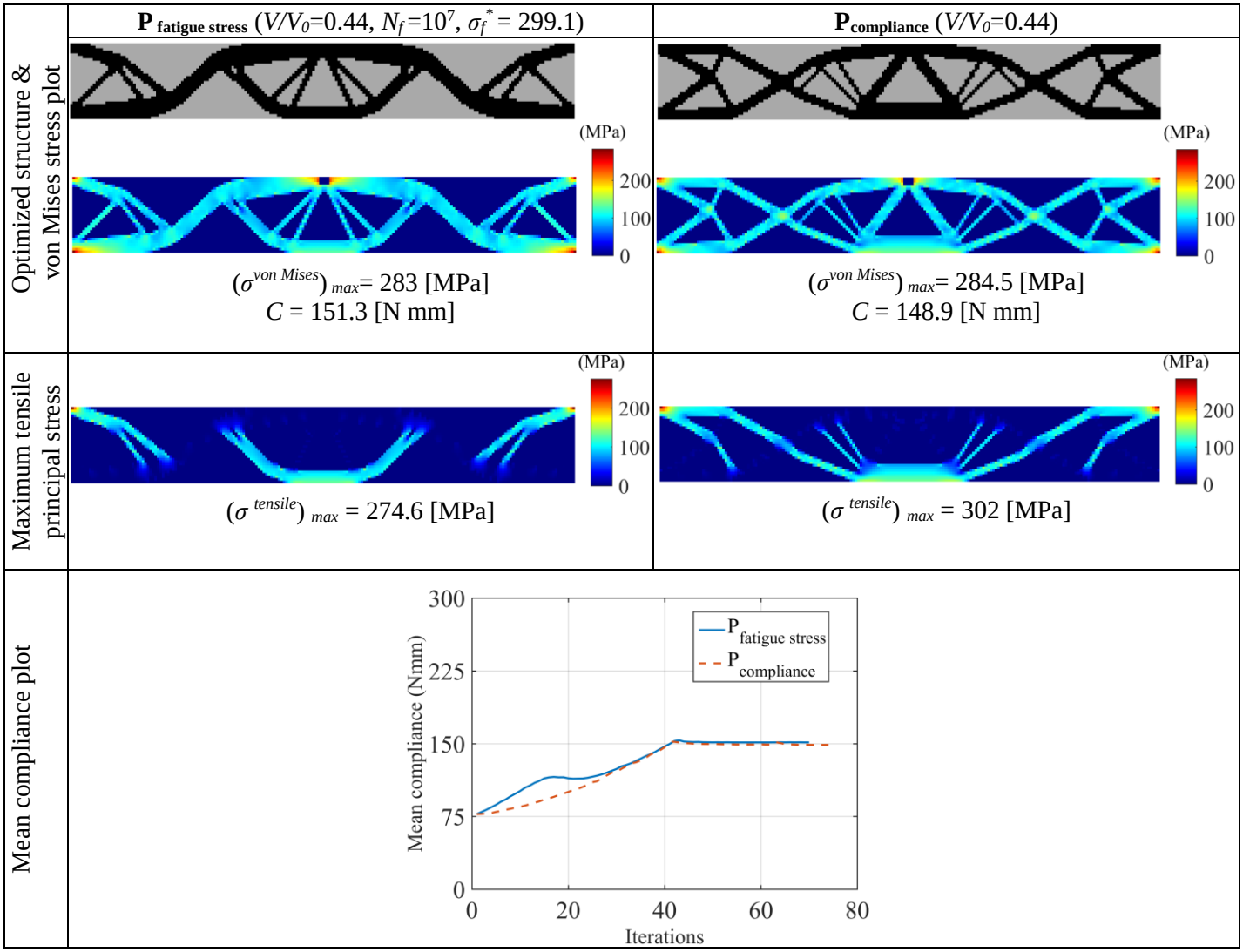

Fig. 5-8. Optimal layouts for long clamped beam (V/V_0=0.44, N_f=10^7, σ_f^*=299.1 MPa)

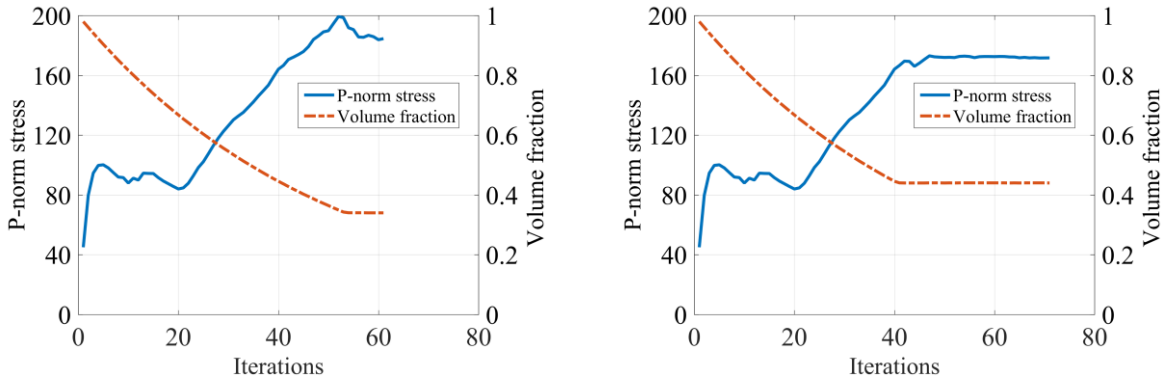

(a) (b)

Fig. 5-9. Convergence plots for long clamped beam (a) (V/V_0=0.34), (b) (V/V_0=0.44)

As can be seen from the results, the maximum tensile principal stress value in the case of the proposed BESO method, is less than the critical fatigue stress threshold. In the case of the original BESO method, the tensile principal stress value is larger than the threshold. However, the mean compliance values are larger than the values of the original BESO method, due to modification of the original objective function. Also, the values of the von Mises stress are higher than the values of the tensile principal stresses and the critical fatigue stress due to the application of the sensitivity numbers, which are based on the principal tensile stress rather than the von Mises stress. The convergence plots are also depicted in Fig. 5-9.

5.7 Concluding remarks

In this chapter, the BESO method has been developed for considering the critical fatigue stress in the optimization problem to reach the fatigue-resistant optimized design, based on the methodology which was proposed by Holmberg et al. (Holmberg, Torstenfelt & Klarbring 2014). Since the tensile principal stresses are the main causes of the fatigue failure, and generally the compressive stresses do not have the main role in fatigue failures (Holmberg, Torstenfelt & Klarbring 2014), the sensitivity analysis was based on the tensile principal stress. The high cycle fatigue along with the constant proportional loading condition has been used to calculate the critical fatigue stress. In addition, the Goodman fatigue failure criteria used to calculate the maximum tensile principal stress, has been used as stress constraint in the topology optimization problem. Different numerical examples have been solved to show the merit of the proposed method in the framework of the BESO method where the results have been compared with the traditional BESO problem results. As seen from the results, the maximum tensile principal stress in all the optimized structures are less than the critical fatigue stress threshold, while in the case of the original BESO method all are higher than the threshold limit. However, the mean compliance in the proposed method, is higher than the traditional BESO method, due to adding the extra fatigue stress constraint and modifying the objective function. As discussed previously, the Goodman fatigue failure criteria show the interaction of the alternating stress and mean stress in fatigue failure of materials. According to the Goodman diagram, is depicted in Fig. 5-

10, the fatigue failure will occur while the combination of the mean and alternating stress of an element lies in the safe zone of the Goodman diagram.

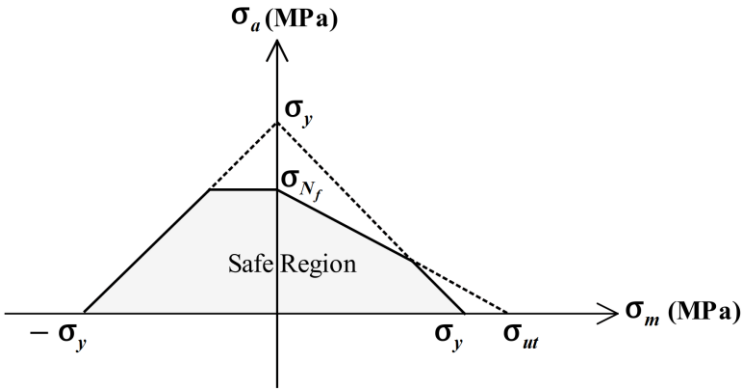

Fig. 5-10. Goodman diagram

Hence, to reach the optimized structure with no fatigue failure, different combinations of the alternating and mean stresses should be taken in to account, where the combination of all stresses must be in the safe fatigue zone of the Goodman diagram. Since in the proposed BESO method of this chapter, the sensitivity analysis is based on the tensile principal stress and the fatigue failure criteria is not considered directly in calculating the sensitivity numbers of the elements, and, because the critical fatigue stress which is based on the maximum tensile principal stress has been used as stress constraint in the topology optimization problem, the optimized structure is fatigue-resistant just for the tensile principal stresses. This means that in the case of the interaction of the mean and alternating stresses with other stress combinations (e.g. von Mises, Signed von Mises (Jeong, Choi & Yoon 2015) and Sines theory (Collet, Bruggi & Duysinx 2017)) it is not possible to reach the fatigue-resistant optimized structure due to not considering the fatigue failure criteria directly in the sensitivity analysis. The different alternating and mean stresses combination can be defined as follows

$$(Von\,Mises)\begin{cases}\sigma_a=\sqrt{{\sigma_{1a}}^2+{\sigma_{2a}}^2-2\sigma_{1a}\sigma_{2a}}\\ \sigma_m=\sqrt{{\sigma_{1m}}^2+{\sigma_{2m}}^2-2\sigma_{1m}\sigma_{2m}}\end{cases} \tag{5-32}$$

$$(Sines theory)\begin{cases}\sigma_a=\sqrt{{\sigma_{1a}}^2+{\sigma_{2a}}^2-2\sigma_{1a}\sigma_{2a}}\\ {\sigma_m}^{eq}=\sigma_{1m}+\sigma_{2m}\end{cases} \tag{5-33}$$

$$(Signed\ von Mises)\begin{cases}\sigma_a = \sqrt{{\sigma_{1a}}^2 + {\sigma_{2a}}^2 - 2\sigma_{1a}\sigma_{2a}} \\ {\sigma_m}^{signedvonMises} = \begin{cases}\sqrt{{\sigma_{1m}}^2 + {\sigma_{2m}}^2 - 2\sigma_{1m}\sigma_{2m}} & if\ |\sigma_{1m}| \geq 0 \\ -\sqrt{{\sigma_{1m}}^2 + {\sigma_{2m}}^2 - 2\sigma_{1m}\sigma_{2m}} & if\ |\sigma_{1m}| < 0\end{cases}\end{cases} \quad (5\text{-}34)$$

where σ_{1m}, σ_{2m}, σ_{1a} and σ_{2a} are principal mean and alternating stresses respectively.

Hence, the optimized structure for the L-bracket example with the center load which has been depicted in Fig. 5-2, is checked for the above combination and also for the combination of the maximum tensile principal stress as well. The Goodman diagrams for the different combinations have been shown in Fig. 5-11. As can be seen from the results, in the case of the maximum tensile principal stress, all combinations lie in the safe zone of the Goodman diagram, but in other combination cases, the scatters of the mean and alternating stresses have violated the Goodman fatigue failure criterion. Therefore, we can conclude that although the maximum principal stress is the main cause of the fatigue failure of the elements, by considering the maximum tensile principal stress in the sensitivity analysis, it is not possible to reach the fatigue-resistant optimized structure while considering the others mean and alternating stress combination (von Mises, signed von Mises and sines theory). The obtained optimized structure is only fatigue-resistant against the maximum tensile principal stress. To remedy this drawback, we should apply the fatigue failure criteria directly in the sensitivity analysis, where the sensitivity numbers of the elements are based on the fatigue failure criteria and are updated at each iteration of the optimization.

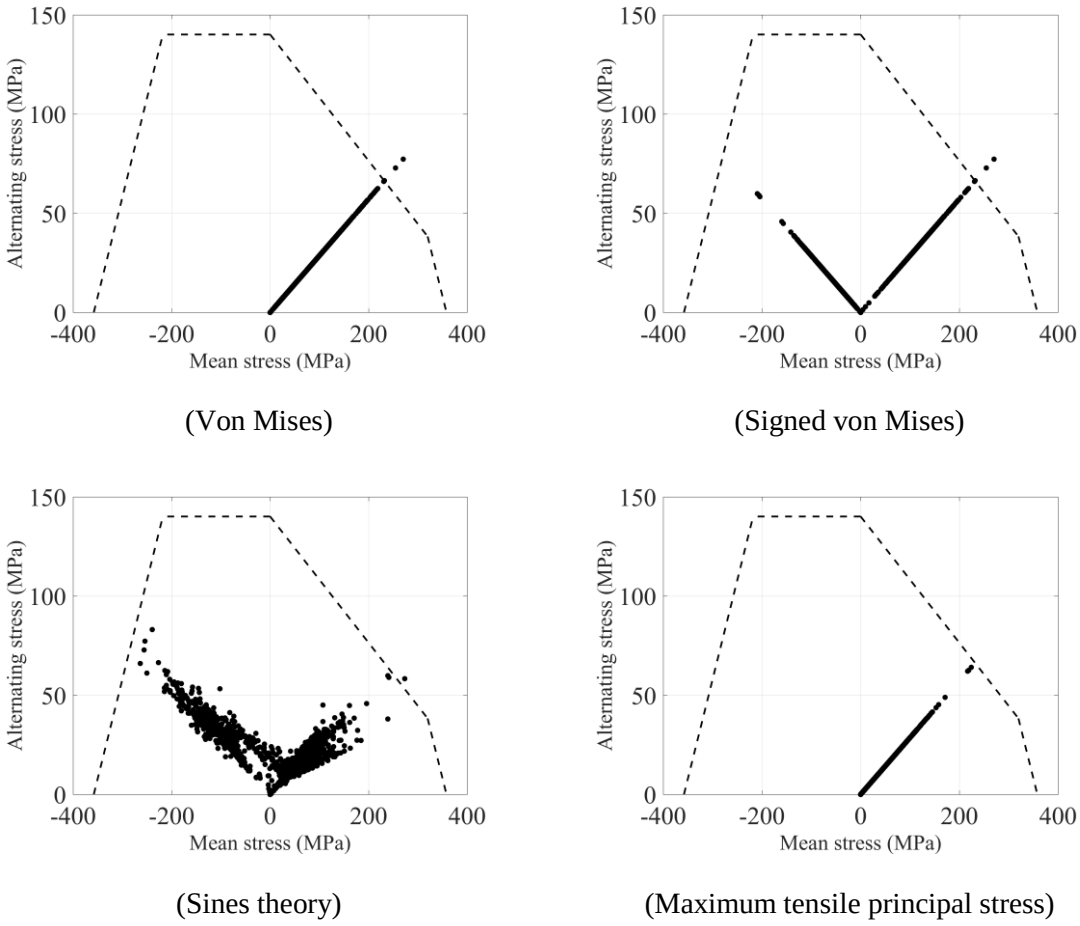

(Von Mises) (Signed von Mises)

(Sines theory) (Maximum tensile principal stress)

Fig. 5-11. Goodman diagram for the example of Fig. 5-2 with different alternating and mean stress combination

In the next chapter a newly developed fatigue-based BESO method is considered, where the fatigue failure criteria are directly used in the sensitivity analysis to calculate the sensitivity numbers of the elements, and also different numerical examples have been solved for the proposed method, in which different alternating and mean stress combinations (Equations (5-32) to (5-34)) have been checked for the results obtained to show the merit and validity of the proposed approach.

Chapter 6

Fatigue constraint topology optimization in the framework of the BESO method

6.1 Introduction

In this chapter, a simplified fatigue based BESO approach is developed where the modified Goodman fatigue failure criterion has been considered to calculate the sensitivity numbers of the elements. In the currently proposed approach, which is different from the BESO approach with critical fatigue stress, which has been discussed in Chapter 5, the fatigue failure criterion has been used directly in the sensitivity analysis, in which the sensitivity numbers of the elements are based on the modified Goodman fatigue failure criterion rather than maximum tensile principal stress. The high-cycle fatigue approach along with the constant proportional loading condition, has been used for the fatigue analysis. The global approach of assembling the local fatigue constraints has been applied by using the modified *p*-norm which assembles all the local fatigue constraints in one function to decrease the computational cost. The equivalent linear static analysis has been used to obtain the fatigue failure criteria of the elements where the material behaviour has been assumed to remain elastic with no crack initiation. The optimization problem is defined to minimize the mean compliance of the structure while satisfying the volume and the fatigue failure criterion simultaneously. The proposed method also has been developed for Gerber fatigue criteria, in which the sensitivity numbers are calculated based on the Gerber equation rather than the Modified Goodman. Different numerical examples have been solved in this chapter to show the effectiveness and merit of the proposed fatigue-based BESO approach, where the obtained results have been compared with the results of the traditional BESO method, with the same volume constraint and loading condition. In addition, the interaction of the mean and alternating stress has been checked for different combinations, (von Mises, signed von Mises and sines theory) as discussed in Chapter 5. The proposed method in the framework of BESO aims to provide a preliminary optimal solution for helping engineers to achieve stiff and fatigue-resistant structural components.

6.2 Problem statement

In this chapter the main topology optimization formulation deals with maximizing the stiffness of the structure, subject to the volume and fatigue constraints which can be defined as follows:

$$(\mathbf{P_{fatigue}}) \quad \begin{cases} \text{Minimize} \ : \ \mathrm{C} = f(x) = \dfrac{1}{2}\mathbf{u}^{\mathbf{T}}\mathbf{k}\mathbf{u} \\ \text{subject to:} \begin{cases} (f_{PN})_{\max} \le 1 \\ V^{*} - \sum_{i=1}^{N_i} V_i x_i = 0 \\ x_i = x_{\min} \text{ or } 1 \end{cases} \end{cases} \tag{6-1}$$

where V^{*}, V_i and x_i are the volume constraint, individual elements volume and binary design variables respectively. $(f_{PN})_{\max}$ is the global modified *p*-norm function of the local fatigue constraints and is discussed in the next section. It is based on the modified Goodman fatigue failure criteria of the elements and must be less than 1 to avoid the fatigue failure. In contrast, the traditional compliance-based BESO approach ($\mathbf{P_{complinace}}$) which was introduced in Chapter 3 (Equation (3-1)) deals with minimizing the compliance with volume constraint only and has been used for comparison in this chapter. To show the merit of our proposed method, the $\mathbf{P_{fatigue}}$ optimization problem has been solved for different numerical examples where the results are compared with the $\mathbf{P_{complince.}}$

6.3 Fatigue failure criteria

Considering the fatigue failure criteria in the topology optimization problem, the global approach of assembling the local fatigue criteria has been used by using the *p*-norm approach (Le et al. 2010) as follows:

$$f_{PN}(x) = \left(\sum_{i=1}^{N_i} \left(L_i^{\,GM}(x) \right)^{p} \right)^{\frac{1}{p}} \tag{6-2}$$

where L_i^{GM} is the modified Goodman fatigue failure criterion for each element, and p is the p-norm coefficient. The p-norm function has been successfully applied in stress-based and fatigue-based topology optimization by some authors see e.g. (Holmberg, Torstenfelt & Klarbring 2014; Jeong, Choi & Yoon 2015; Oest & Lund 2017). As discussed in Chapter 4, the value of the p is selected to be a constant between 3 and 5 for the topology optimization problems in this research. The normalized p-norm approach (Le et al. 2010) which better approximates the maximum local constraint as explained in (Le et al. 2010), has been used in this chapter, where the normalized p-norm function reads:

$$(f_{PN}^{I})_{\max} \approx c^{I}\ f_{PN}^{I} \tag{6-3}$$

where the iteration number is denoted by I and c^I is a coefficient and can be calculated according to the following equation when I >1.

$$c^{I} = \alpha^{I}\ \frac{\sigma_{\max}^{I-1}}{f_{PN}^{I-1}} + (1-\alpha^{I})\ c^{I-1} \quad , \quad 0 < \alpha^{I} < 1 \tag{6-4}$$

6.3.1 Fatigue analysis

In this chapter, the high cycle fatigue approach (HCF) which is only valid for the stress-life method, (Budynas, Nisbett & Shigley 2011; Norton 2005) has been used for fatigue analysis, where the applied loading condition is constant and proportional. According to (Collet, Bruggi & Duysinx 2017; Norton 2005), if the materials' behavior is elastic, and there is no assumption of crack initiation, the high cycle fatigue approach works well, and the amplitude of the stress state can be applied for the fatigue analysis which has been obtained from the equivalent static analysis. In addition, the "quiescence of the solicitation" has no effects on the fatigue life at room temperature, while the loading condition is constant, with no corrosion. Hence, in this chapter, the equivalent static analysis has been used for the fatigue analysis, to obtain the fatigue failure criteria of the elements. To solve the optimization problem in this chapter, the applied load which is shown in Fig. 6-1 is used, where the load F_{min}< 0 represented the combination of tension-compression and F_{min}> 0 is considered as tension only.

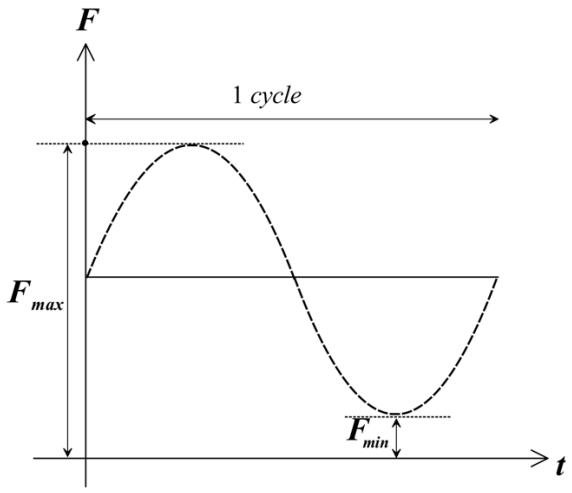

Fig. 6-1. One cycle of the applied load

By applying the above applied load to the structure, the stress state history which is shown in Fig. 6-2 can be obtained where the alternating and mean stress can be calculated from the minimum (σ_{min}) and maximum (σ_{max}) values as follows:

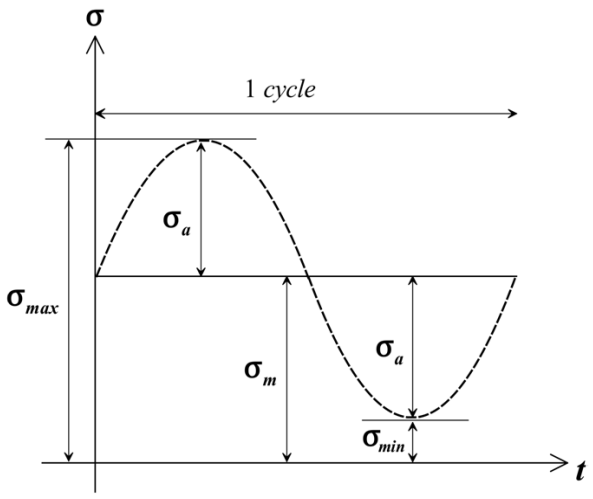

Fig. 6-2. One cycle of the stress history

$$\sigma_a = \frac{\sigma_{\max} - \sigma_{\min}}{2} \tag{6-5}$$

$$\sigma_m = \frac{\sigma_{\max} + \sigma_{\min}}{2} \tag{6-6}$$

The modified Goodman theory, which shows the interaction of the mean and alternating stresses and is used for evaluating the fatigue failure criteria as follows:

$$L_i^{GM}(x) = \frac{\sigma_{a_i}^{vonMises}}{(\sigma_i)_{Nf}} + \frac{\sigma_{m_i}^{vonMises}}{\sigma_{ut}} \leq 1 \tag{6-7}$$

where σ_{ut}, $\sigma_{m_i}^{vonMises}$ and $\sigma_{a_i}^{vonMises}$ represent the tensile strength of each element, von Mises mean stress and von Mises alternating stress respectively. $(\sigma_i)_{Nf}$ is the critical fatigue stress for a prescribed number of cycles(N_f) which can be calculated by the *Basquin* Equation (Aliabadi 1992; Lee, Barkey & Kang 2012; Suresh 1998) as discussed in Chapter 5 (Equations (5-7) to (5-11)). To evaluate the alternating and mean stress of the elements, the von Mises stress measurement has been used as follows:

$$\sigma_{a_i}^{vonMises} = \sqrt{\sigma^2{}_{x_{a_i}} + \sigma^2{}_{y_{a_i}} - \sigma_{x_{a_i}}\sigma_{y_{a_i}} + 3\tau_{xy_{a_i}}} \tag{6-8}$$

$$\sigma_{m_i}^{vonMises} = \sqrt{\sigma^2{}_{x_{m_i}} + \sigma^2{}_{y_{m_i}} - \sigma_{x_{mi}}\sigma_{y_{mi}} + 3\tau_{xy_{m_i}}} \tag{6-9}$$

$$\sigma_{a_i} = c_a \boldsymbol{\sigma}_i = \begin{bmatrix} \sigma_{x_{a_i}} \\ \sigma_{y_{a_i}} \\ \tau_{xy_{a_i}} \end{bmatrix} \tag{6-10}$$

$$\sigma_{m_i} = c_m \boldsymbol{\sigma}_i = \begin{bmatrix} \sigma_{x_{m_i}} \\ \sigma_{y_{m_i}} \\ \tau_{xy_{m_i}} \end{bmatrix} \tag{6-11}$$

$$\boldsymbol{\sigma}_i = \mathbf{D}_i \mathbf{B}_i \mathbf{u}_i \tag{6-12}$$

where c_m and c_a are the mean and alternating stress scaling factors which can be calculated as follows

$$c_a = \frac{1-(F_{\min}/F_{\max})}{2} \tag{6-13}$$

$$c_m = \frac{1+(F_{\min}/F_{\max})}{2} \tag{6-14}$$

The stress vectors of the elements which are given in Equation (6-12) are evaluated at the center of the elements, where $\mathbf{D}_i$ and $\mathbf{B}_i$ denote the constitutive and strain displacement matrixes of the *i*th

element respectively. Since in the fatigue-based BESO approach, which is a binary approach, the so-called "singularity" issue will not occur for the solution of the problem, no penalty exponent has been used for the stress vectors. For the plane stress problem, the constitutive matrix $\mathbf{D}_i$ can be defined as follows:

$$\mathbf{D}_i = \frac{E^0 x_i}{1-\nu^2}\begin{bmatrix} 1 & \nu & 0 \\ \nu & 1 & 0 \\ 0 & 0 & (1-\nu)/2 \end{bmatrix} \tag{6-15}$$

As discussed earlier in this chapter, an equivalent static analysis is performed to obtain the displacement vectors and other quantities. The static FE analysis is performed as follows:

$$\mathbf{KU} = \mathbf{F}_{\max} \tag{6-16}$$

where **U** is the displacement vector and **K** is the global stiffness matrix of the structure. The mean and alternating stress scaling factors c_m and c_a (Equations (6-12) and (6-13)) can be calculated based on the maximum applied load ($\mathbf{F}_{max}$) where the maximum force is applied statically to the structure according to Equation 6-16. Note that in the FE analysis, the maximum force ($\mathbf{F}_{max}$) can be substituted by the minimum force ($\mathbf{F}_{min}$) which leads to obtaining different scaling factors that are based on $\mathbf{F}_{min}$ rather than $\mathbf{F}_{max}$, with the same results obtained in both cases. As mentioned in Chapter 4, again in this chapter, the material interpolation scheme (SIMP) is adopted for solving the optimization problem (Equations (4-7) and (4-8)).

Furthermore, the modified Goodman diagram, shown in Fig. 5-10 in the previous chapter, is used to evaluate the interaction of the mean and alternating stress of the final optimized design, where all the scatters of the mean and alternating stresses of the final design must lie in the safe zone of the Goodman diagram, in order to avoid the fatigue failure. Different combinations of mean and alternating stress (Equations (5-32) to (5-34)) which discussed before are used to check the fatigue failure of the final optimal structures' elements. The alternating stress in the Goodman diagram for the examples of this chapter is bounded by the fatigue stress ($(\sigma_i)_{Nf}$) which is calculated by considering the infinite life cycles ($N_f > 10^7$).

6.4 Sensitivity analysis with the fatigue constraint

To solve the optimization problem, the sensitivity numbers should be evaluated from the sensitivity analysis, where the gradient of the modified *p*-norm fatigue criteria in Equation (6-2), is derived from the chain rule:

$$\frac{\partial f_{PN}(x)}{\partial x_i} = \frac{\partial f_{PN}(x)}{\partial {L_i}^{GM}} \frac{\partial {L_i}^{GM}(x)}{\partial x_i} \tag{6-17}$$

By taking the derivative of Equation (6-17), the term $\partial f_{PN}(x) / \partial {L_i}^{GM}$ can be calculated as:

$$\frac{\partial f_{PN}(x)}{\partial {L_i}^{GM}} = \left(\sum_{i=1}^{N_i} \left({L_i}^{GM}(x) \right)^p \right)^{(\frac{1}{p}-1)} \left({L_i}^{GM}(x) \right)^{(p-1)} \tag{6-18}$$

where the derivative of the term $\partial {L_i}^{GM}(x) / \partial x_i$ is as follows:

$$\frac{\partial {L_i}^{GM}(x)}{\partial x_i} = \frac{\partial {L_i}^{GM}(x)}{\partial {\sigma_{a_i}}^{vonMises}} \frac{\partial {\sigma_{a_i}}^{vonMises}}{\partial x_i} + \frac{\partial {L_i}^{GM}(x)}{\partial {\sigma_{m_i}}^{vonMises}} \frac{\partial {\sigma_{m_i}}^{vonMises}}{\partial x_i} \tag{6-19}$$

$$\frac{\partial {L_i}^{GM}(x)}{\partial {\sigma_{a_i}}^{vonMises}} = \frac{1}{(\sigma_i)_{Nf}} \tag{6-20}$$

$$\frac{\partial {L_i}^{GM}(x)}{\partial {\sigma_{m_i}}^{vonMises}} = \frac{1}{\sigma_{ut}} \tag{6-21}$$

$$\frac{\partial {\sigma_{a_i}}^{vonMises}}{\partial x_i} = \frac{\partial {\sigma_{a_i}}^{vonMises}}{\partial \sigma_{a_i}} \frac{\partial \sigma_{a_i}}{\partial \boldsymbol{\sigma}_i} \frac{\partial \boldsymbol{\sigma}_i}{\partial x_i} \tag{6-22}$$

$$\frac{\partial {\sigma_{m_i}}^{vonMises}}{\partial x_i} = \frac{\partial {\sigma_{m_i}}^{vonMises}}{\partial \sigma_{m_i}} \frac{\partial \sigma_{m_i}}{\partial \boldsymbol{\sigma}_i} \frac{\partial \boldsymbol{\sigma}_i}{\partial x_i} \tag{6-23}$$

For the 2D cases, the derivatives of the von Mises alternating and mean stress in Equations (6-22) and (6-23) are:

$$\frac{\partial \sigma_{a_i}^{vonMises}}{\partial \sigma_{a_i}} = \begin{cases} \dfrac{\partial \sigma_{a_i}^{vonMises}}{\partial \sigma_{x_{a_i}}} = \dfrac{1}{2\sigma_{a_i}^{vonMises}}(2\sigma_{x_{a_i}} - \sigma_{y_{a_i}}) \\ \dfrac{\partial \sigma_{a_i}^{vonMises}}{\partial \sigma_{y_{a_i}}} = \dfrac{1}{2\sigma_{a_i}^{vonMises}}(2\sigma_{y_{a_i}} - \sigma_{x_{a_i}}) \\ \dfrac{\partial \sigma_{a_i}^{vonMises}}{\partial \tau_{xy_{a_i}}} = \dfrac{1}{\sigma_{a_i}^{vonMises}}(3\tau_{xy_{a_i}}) \end{cases} \tag{6-24}$$

$$\frac{\partial \sigma_{m_i}^{vonMises}}{\partial \sigma_{m_i}} = \begin{cases} \dfrac{\partial \sigma_{m_i}^{vonMises}}{\partial \sigma_{x_{m_i}}} = \dfrac{1}{2\sigma_{m_i}^{vonMises}}(2\sigma_{x_{m_i}} - \sigma_{y_{m_i}}) \\ \dfrac{\partial \sigma_{m_i}^{vonMises}}{\partial \sigma_{y_{m_i}}} = \dfrac{1}{2\sigma_{m_i}^{vonMises}}(2\sigma_{y_{m_i}} - \sigma_{x_{m_i}}) \\ \dfrac{\partial \sigma_{m_i}^{vonMises}}{\partial \tau_{xy_{m_i}}} = \dfrac{1}{\sigma_{m_i}^{vonMises}}(3\tau_{xy_{m_i}}) \end{cases} \tag{6-25}$$

The derivatives of $\sigma_{a_i} / \partial \boldsymbol{\sigma}_i$ and $\sigma_{m_i} / \partial \boldsymbol{\sigma}_i$ are as follows:

$$\frac{\sigma_{a_i}}{\partial \boldsymbol{\sigma}_i} = c_a \tag{6-26}$$

$$\frac{\sigma_{m_i}}{\partial \boldsymbol{\sigma}_i} = c_m \tag{6-27}$$

The derivative of the stress vectors in Equations (6-22) and (6-23)) with respect to design variable x_i gives:

$$\frac{\partial \boldsymbol{\sigma}_i}{\partial x_i} = \frac{\partial \mathbf{D}}{\partial x_i}\mathbf{B}\mathbf{u} + \mathbf{D}\mathbf{B}\frac{\partial \mathbf{u}}{\partial x_i} \tag{6-28}$$

where the term $\partial \mathbf{u} / \partial x_i$ can be calculated by using the chain rule from the Equation (6-16) as follows:

$$\frac{\partial \mathbf{u}}{\partial x_i} = -\mathbf{K}^{-1}\frac{\partial \mathbf{K}}{\partial x_i}\mathbf{u} \tag{6-29}$$

Combining Equations (6-19), (6-22), (6-23), (6-28) and (6-29), the gradient of the modified *p*-norm fatigue criteria reads:

$$\frac{\partial f_{PN}(x)}{\partial x_i} = \left(\sum_{i=1}^{N_i} \left(L_i{}^{GM}(x) \right)^p \right)^{(\frac{1}{p}-1)} \left(L_i{}^{GM}(x) \right)^{(p-1)} \times$$
$$\left[\frac{1}{(\sigma_i)_{Nf}} \frac{\partial \sigma_{a_i}{}^{vonMises}}{\partial \sigma_{a_i}} c_a \left(\frac{\partial \mathbf{D}}{\partial x_i}\mathbf{Bu} - \mathbf{DBK}^{-1}\frac{\partial \mathbf{K}}{\partial x_i}\mathbf{u} \right) + \right. \tag{6-30}$$
$$\left. \frac{1}{\sigma_{ut}} \frac{\partial \sigma_{m_i}{}^{vonMises}}{\partial \sigma_{m_i}} c_m \left(\frac{\partial \mathbf{D}}{\partial x_i}\mathbf{Bu} - \mathbf{DBK}^{-1}\frac{\partial \mathbf{K}}{\partial x_i}\mathbf{u} \right) \right].$$

To avoid the calculation of the inverse **K**, we defined the adjoint variable $\boldsymbol{\lambda}_a$ and $\boldsymbol{\lambda}_m$ by:

$$\boldsymbol{\lambda}_a{}^T = \frac{1}{(\sigma_i)_{Nf}} c_a \left(\frac{\partial \sigma_{a_i}{}^{vonMises}}{\partial \sigma_{a_i}} \right)^T \mathbf{DBK}^{-1} \tag{6-31}$$

$$\boldsymbol{\lambda}_m{}^T = \frac{1}{\sigma_{ut}} c_m \left(\frac{\partial \sigma_{m_i}{}^{vonMises}}{\partial \sigma_{m_i}} \right)^T \mathbf{DBK}^{-1} \tag{6-32}$$

which was calculated from the adjoint equation:

$$\mathbf{K}\boldsymbol{\lambda}_a = \frac{1}{(\sigma_i)_{Nf}} c_a \mathbf{DB} \frac{\partial \sigma_{a_i}{}^{vonMises}}{\partial \sigma_{a_i}} \tag{6-33}$$

$$\mathbf{K}\boldsymbol{\lambda}_m = \frac{1}{\sigma_{ut}} c_m \mathbf{DB} \frac{\partial \sigma_{m_i}{}^{vonMises}}{\partial \sigma_{m_i}} \tag{6-34}$$

Equations (6-33) and (6-34) are the standard finite element analysis of the adjoint systems, where the term on the right-hand side denotes the equivalent external loads. By inserting the adjoint variables into Equation (6-30) the final gradient reads:

$$\frac{\partial f_{PN}(x)}{\partial x_i} = \left(\sum_{i=1}^{N_i} \left(L_i{}^{GM}(x) \right)^p \right)^{(\frac{1}{p}-1)} \left(L_i{}^{GM}(x) \right)^{(p-1)} \times$$
$$\left[\frac{1}{(\sigma_i)_{Nf}} c_a \frac{\partial \sigma_{a_i}{}^{vonMises}}{\partial \sigma_{a_i}} \frac{\partial \mathbf{D}}{\partial x_i}\mathbf{Bu} - \boldsymbol{\lambda}_a{}^T \left(\frac{\partial \mathbf{K}}{\partial x_i}\mathbf{u} \right) + \right. \tag{6-35}$$
$$\left. \frac{1}{\sigma_{ut}} c_m \frac{\partial \sigma_{m_i}{}^{vonMises}}{\partial \sigma_{m_i}} \frac{\partial \mathbf{D}}{\partial x_i}\mathbf{Bu} - \boldsymbol{\lambda}_m{}^T \left(\frac{\partial \mathbf{K}}{\partial x_i}\mathbf{u} \right) \right].$$

Also as explained in (Huang, X & Xie, YM 2010) the sensitivity of the compliance can be calculated as:

$$\frac{\partial C}{\partial x_i} = \frac{1}{2}\mathbf{u}_i{}^{\mathrm{T}}\mathbf{K}_i\mathbf{u}_i \tag{6-36}$$

Hence, to calculate the sensitivity numbers of the elements, the gradients of the *p*-norm fatigue criteria and the compliance have been obtained in this section.

6.4.1 Sensitivity numbers

The Lagrangian multiplier (λ) has been introduced to consider the additional displacement constraint (Huang, X & Xie, Y 2010a), as discussed in Chapter 4. In this chapter, this method is again extended to consider the additional fatigue constraint. To do so, the original objective function is modified by adding a Lagrangian multiplier, λ, as

$$f_1(x) = C + \lambda((f_{PN})_{\max} - 1) \tag{6-37}$$

where $0 \le \lambda \le 1$. The modified objective function could be the same value as the original value when the $(f_{PN})_{max}$ is equal to 1. If $(f_{PN})_{max} < 1$ the fatigue constraint is satisfied, λ should set to 0 (λ=0). Hence the Lagrangian multiplier will act as a compromise between the local displacement constraint and the objective function. Since λ has an effective role in calculating the sensitivity numbers it should be defined prior to the calculation of the sensitivity numbers. Thus, the sensitivity of the modified objective function is:

$$\frac{df_1}{dx_i} = q\,x_i{}^{q-1}\left(-\frac{1}{2}\mathbf{u}_i{}^{\mathrm{T}}\mathbf{K}_i\mathbf{u}_i + \lambda\frac{\partial f_{PN}(x)}{\partial x_i}\right) \tag{6-38}$$

Thus, the sensitivity number of the elements used in BESO can be expressed by:

$$\alpha_i = -\frac{1}{q}\frac{df_1}{dx_i} = x_i{}^{q-1}\left(\frac{1}{2}\mathbf{u}_i{}^{\mathrm{T}}\mathbf{K}_i\mathbf{u}_i - \lambda\frac{\partial f_{PN}(x)}{\partial x_i}\right) \tag{6-39}$$

where the calculation of the Lagrangian multiplier (λ) is based on the volume constraint and the additional fatigue constraint, which means that the proper value of the Lagrangian multiplier (λ) can be calculated while both constraints are satisfied. Therefore, λ can be defined as follows:

$$\lambda = \frac{1-\omega}{\omega} \tag{6-40}$$

where $\omega_{min} \leq \omega \leq 1$ and $\omega_{\min}$ can have the small value e.g. 10^{-10}. The procedure of calculating the appropriate value for λ is as follows:

Step 1: The first lower bound value of ω is set to $\omega_{lower} = \omega_{min}$ and the upper bound value is set to be $\omega_{upper} = 1$.

Step 2: Start the program and calculate the sensitivity numbers based on the modified objective function and estimate the fatigue failure criterion for the next iteration ($(f_{PN})_{\max}^{I+1}$) as follows:

$$(f_{PN})_{\max}^{I+1} \approx (f_{PN})_{\max}^{I} + \sum_i \frac{\partial f_{PN}}{\partial x_i} \Delta x_i \tag{6-41}$$

Step 3: If the estimated fatigue failure of the next iteration ($(f_{PN})_{\max}^{I+1}$) is larger than 1 then ω should be updated with a smaller value as follows:

$$\hat{\omega} = \frac{\omega + \omega_{lower}}{2} \tag{6-42}$$

and ω_{upper} should be set to ω at the same time. If $(f_{PN})_{\max}^{I+1}$ is less than 1 then ω should be updated with a larger value as follows:

$$\hat{\omega} = \frac{\omega + \omega_{upper}}{2} \tag{6-43}$$

and at the same time, ω_{lower} should be updated to ω.

Step 4 : The above steps should be repeated until the difference between the upper and lower bounds of ω is less than10^{-5} and a proper value of λ was obtained (Huang, X & Xie, Y 2010a).

6.5 Bi-directional evolutionary structural optimization procedure with fatigue constraint

The fatigue-based evolutionary optimization flowchart, which is used in this chapter, is shown in Fig. 6-3. The procedure for the proposed algorithm was based on the BESO method algorithm (Huang, X & Xie, Y 2010a) and also the procedure which was used in Chapter 4 for problem **P1$_{\text{stress}}$**, except for the determination of the sensitivity numbers and the Lagrangian multiplier, which is based on fatigue

constraint in the proposed algorithm of this chapter. The convergence criteria are based on the compliance and *p*-norm fatigue failure criteria which can be defined as follows:

$$error_1 = \left| \frac{\sum_{i=1}^{N} C_{k-i+1} - \sum_{i=1}^{N} C_{k-N-i+1}}{\sum_{i=1}^{N} C_{k-i+1}} \right| \leq 0.01 \tag{6-44}$$

$$error_2 = \frac{\left| \sum_{i=1}^{N} (f_{PN})_{\max,\, k-i+1} - (f_{PN})_{\max,\, k-N-i+1} \right|}{\sum_{i=1}^{N} (f_{PN})_{\max,\, k-i+1}} \leq 0.01 \tag{6-45}$$

where $N = 5$ is used in this problem as well.

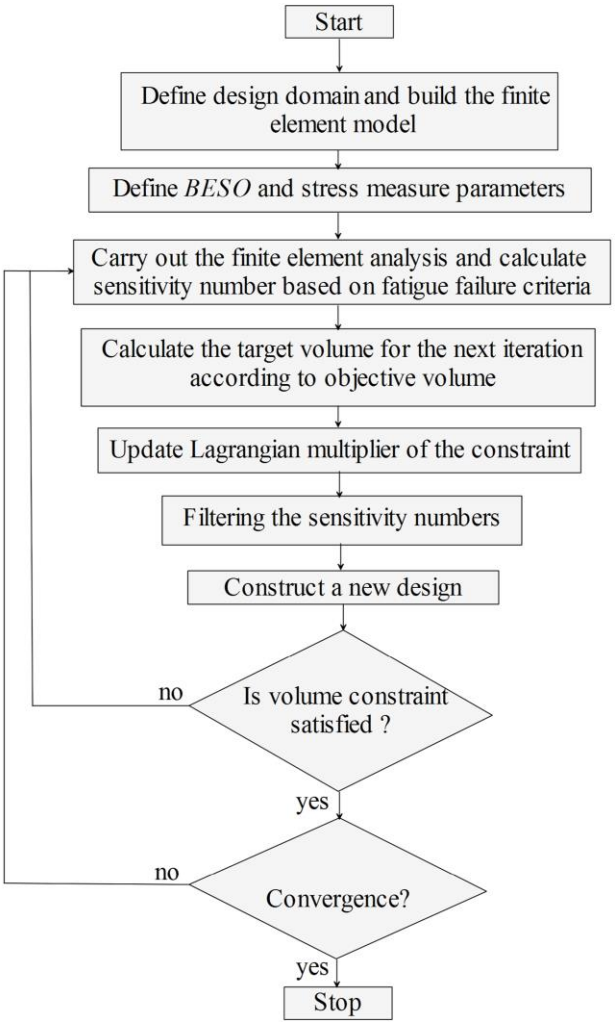

Fig. 6-3. Flowchart of the BESO procedure with an additional fatigue constraint

The gradual material removal will be stopped when the algorithm reaches the objective volume (V^*) and the whole optimization process will end if the above-mentioned convergence criteria are satisfied. As per (Huang, X & Xie, Y 2010b; Huang, X & Xie, YM 2007, 2010; Yi et al. 2013; Zuo, Xie & Huang 2011), the sensitivity numbers were filtered and also modified by averaging their values at their previous iteration to improve the convergence of the proposed BESO.

6.6 Numerical examples

In this section, the fatigue–based problem ($\mathbf{P_{fatigue}}$) is solved for different examples in which the optimized structure with the highest stiffness is sought while the volume and fatigue constraints are satisfied. The constant proportional load which has been shown in Fig. 6-1 is applied to the example in this chapter by considering the maximum ($\mathbf{F}_{max}$) and minimum values ($\mathbf{F}_{min}$) of the loads to evaluate the amplitudes of the stress state. For comparison, the problem of minimizing compliance, subject to the volume constraint ($\mathbf{P_{compliance}}$) is also solved by assuming $\mathbf{F} = \mathbf{F}_{max}$ for each example. The modified Goodman diagram is then used to evaluate both resulting designs by applying the same load. In each example, the tension and tension-compression loads are used to solve the fatigue-based problem $\mathbf{P_{fatigue}}$. The base material of the structure is assumed to be the carbon steel 1018 with Young Modulus E = 210 GPa and Poisson's ratio v = 0.3. Again, the *Basquin* equation (Equation (5-7)) is used to determine the alternating stress value $(\sigma_i)_{Nf}$, which is related to a minimum number of cycles to failure in S_N diagram (Aliabadi 1992; Lee, Barkey & Kang 2012; Suresh 1998). The tensions and compressions yield stresses are assumed to be the same ($\sigma_{ut} = \sigma_y$=358 MPa). As discussed in Chapter 5, and again in this chapter, the proposed fatigue-based ($\mathbf{P_{fatigue}}$) method aims to reach a preliminary optimized structure in the first stage of the fatigue design process, therefore the actual endurance limit is used rather than $\overline{\sigma}_e$ for calculating the σ_{nf}. This means that none of the correction factors of the endurance limit have been applied for the proposed method as well. According to the *Basquin* equation which was defined in previous chapter, σ'_f and b are the fatigue strength coefficient and fatigue strength exponent, which should be calculated accordingly, based on σ_e, and have been set to be 593 MPa and -0.086 in this chapter, respectively. $N_f = 10^7$ is adopted to represent the infinite

loading cycles. To achieve an optimal design with no fatigue failure, the combinations of all mean and alternating stresses of the elements must lie in the safe zone of the modified Goodman diagram, which has been depicted in Chapter 5, Fig. 5-10. To check the fatigue-failure resistance of the optimal design in this chapter, three different combinations of mean and alternating stresses, which have been defined in the previous chapter in Equations (5-32) to (5-34), are checked with the modified Goodman diagram. Also, for comparison, the modified Goodman diagram of the traditional compliance-based method is also available for all the examples where the previously mentioned combinations (Equations (5-32) to (5-34)) have been checked for the final optimal designs.

6.6.1 L-beam with center load

The first example is the same example as shown in Fig. 4-2 which is the L-bracket beam with a fixed edge where the load was applied in the middle of the right-hand side of the beam. The design domain has meshed with a total of 6400 four-node plane stress elements, which have equal sizes of 1 mm × 1 mm. The thickness is assumed to be 1 mm. For avoiding the stress concentration, six elements (3 × 2) around the applied load are excluded from the topology optimization formulation and fixed to be solid. The filter radius and the evolutionary rate in BESO are set to be 1.5 mm and 0.02, respectively. The topology optimization results for the tension and tension-compression loads are shown in Figs. 6-4 and 6-6 in which different volume constraint have been applied for each example.

According to the results, the mean compliance values of the proposed method are 4 – 6% higher than the values obtained from the traditional compliance-based case ($\mathbf{P}_{\mathbf{compliance}}$). However, the fatigue failure criteria in the case of $\mathbf{P}_{\mathbf{fatigue}}$ problems is alleviated significantly in contrast to the results from $\mathbf{P}_{\mathbf{compliance}}$ problems and decreased from 38 – 40% according to the results. This comparison indicated that in the case of the proposed method, the stress concentration was alleviated significantly in the kink edge which led to it being exempted from fatigue failure compared to the traditional compliance-based case.

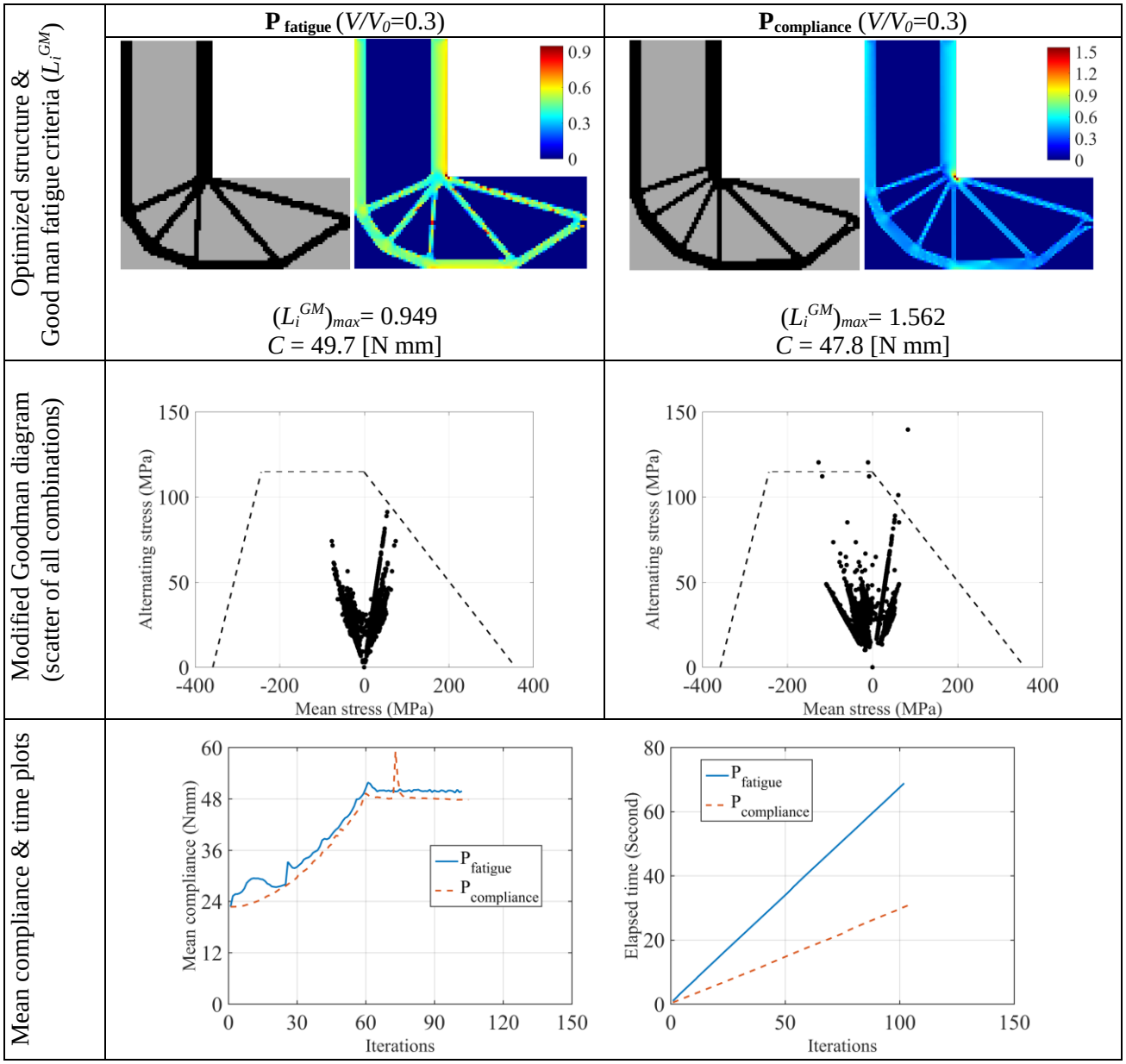

Fig. 6-4.Topology optimization results for L-bracket (F_{max}=200 N, F_{min}= -50 N, V^*=0.3)

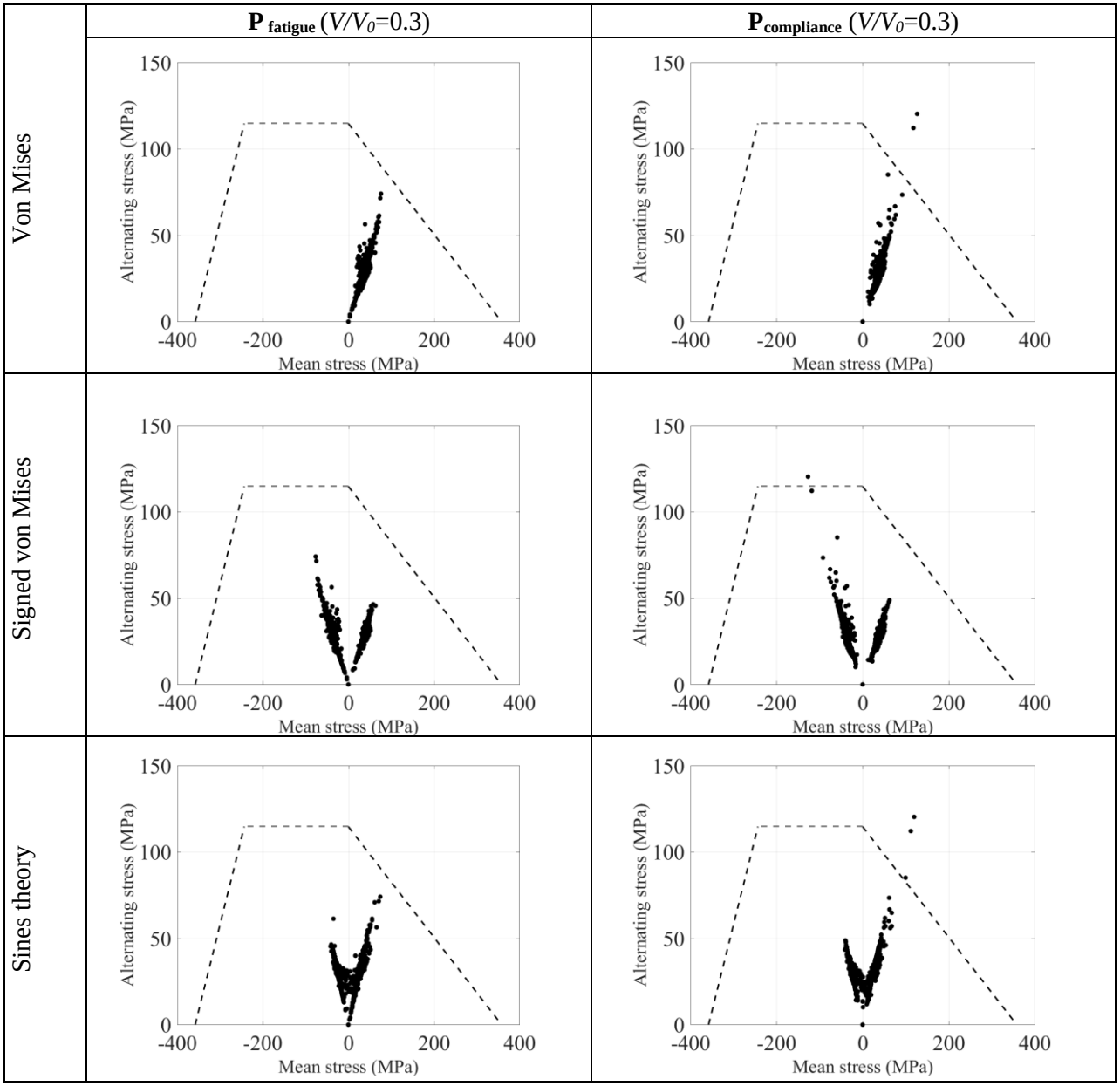

Fig. 6-5. Goodman diagram for L-bracket (F_{max}=200 N, F_{min}= -50 N, V^*=0.3) with different alternating and mean stress combination

According to the results which are shown in Figs. 6-4 and 6-6, the interaction of the mean and alternating stress of all the stress combinations of the final optimal design for the proposed method, lie in the safe zone of the modified Goodman diagram. In the case of the original BESO method without fatigue constraint, the fatigue failure will occur due to the combinations not laying in the safe zone of the Goodman diagram. Also, the interaction scatters of the mean and alternating stresses have been

depicted separately for both optimization problems ($\mathbf{P}_{\mathbf{faigue}}$ & $\mathbf{P}_{\mathbf{compliance}}$) for each combination in Figs. 6-5 and 6-7.

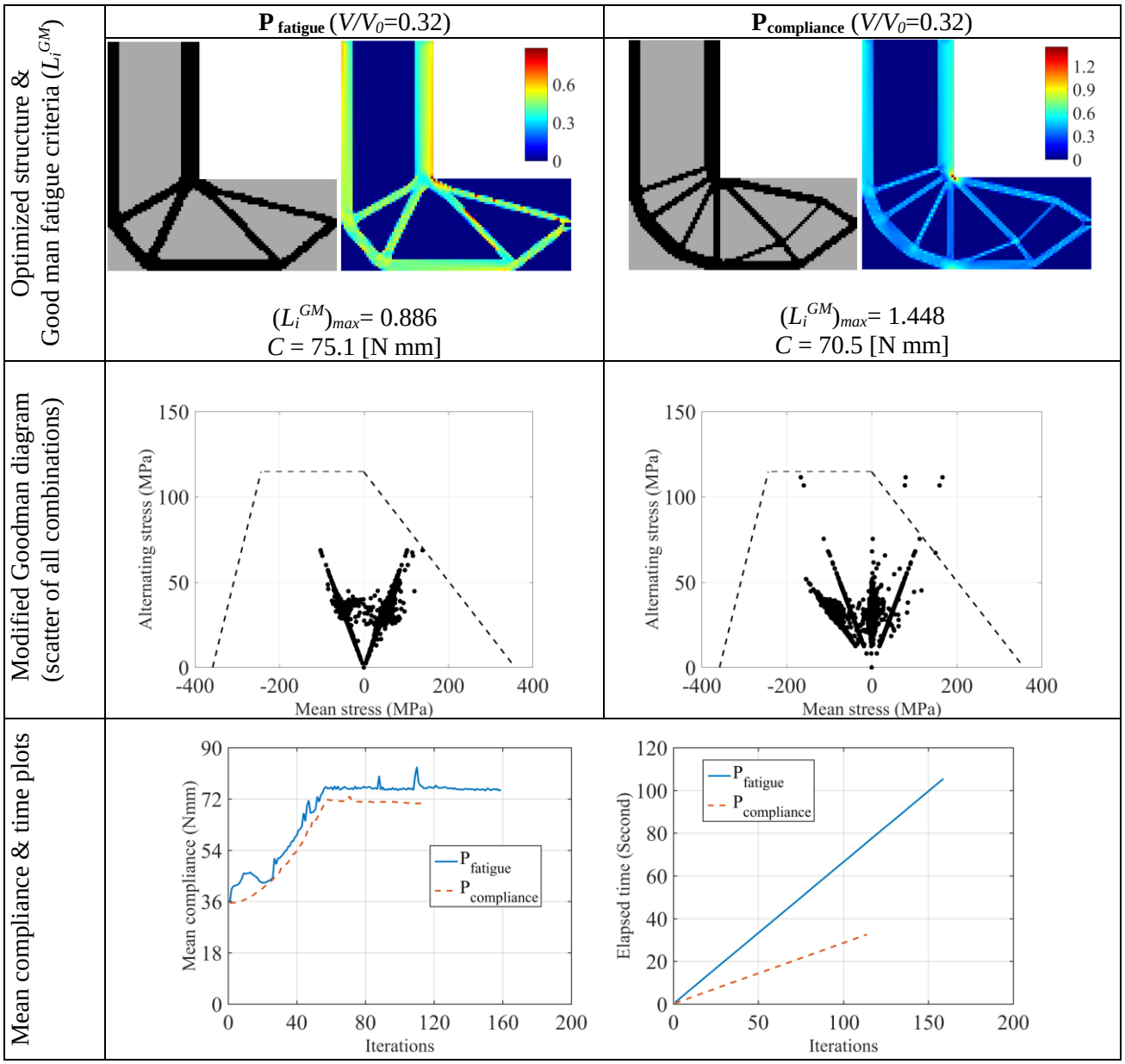

Fig. 6-6. Topology optimization results for L-bracket (F_{max}=250 N, F_{min}= 50 N, V^*=0.32)

The convergence plots of the *p*-norm fatigue constraint for the proposed optimization problem with the volume constraints of 0.3 and 0.32 are depicted in Fig. 6-8. However, the convergence plots of the compliance also have been shown in Figs. 6-4 and 6-6. Additionally, the time plots for solving both optimization problems ($\mathbf{P}_{\mathbf{fatigue}}$ & $\mathbf{P}_{\mathbf{compliance}}$) are depicted in Figs. 6-4 and 6-6 where elapsed time for

solving the proposed optimization problem is more than the original BESO method, due to solving the equilibrium equation of the adjoint method.

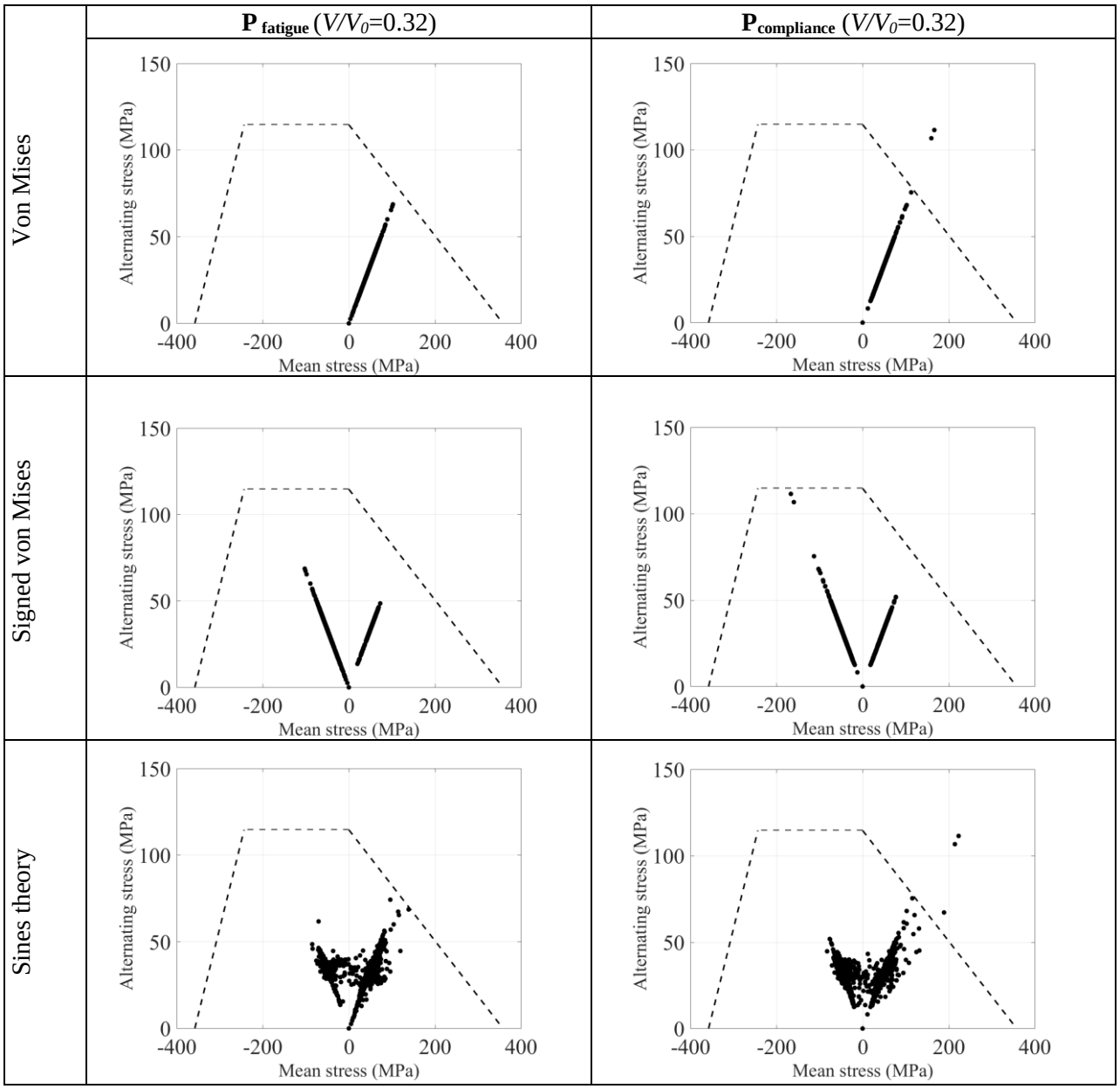

Fig. 6-7. Goodman diagram for L-bracket (F_{max}=250 N, F_{min}= 50 N, V^*=0.32) with different alternating and mean stress combination

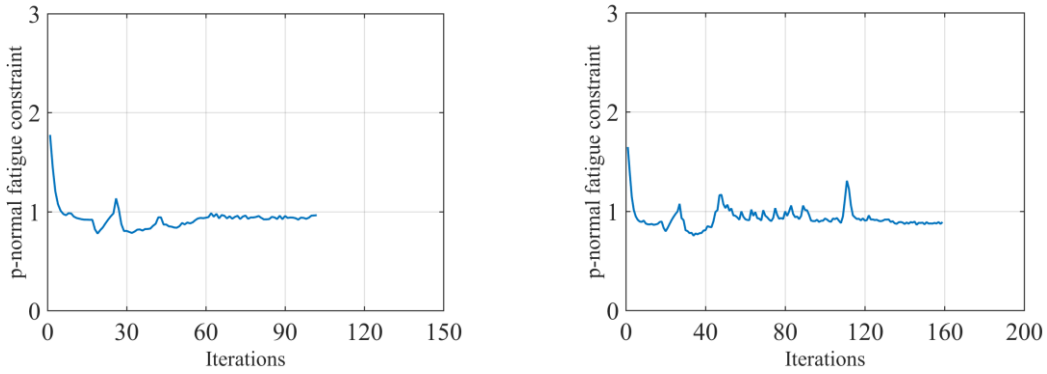

(a) (b)

Fig. 6-8. Convergence plots for L-bracket ($\mathbf{P}_{\mathbf{fatigue}}$) (a) ($V/V_0$=0.3), (b) ($V/V_0$=0.32)

6.6.2 Cantilever Beam

A cantilever beam (Fig. 4-14) in which a point load applied at the right-hand side center has been considered as a second example where the thickness is set to 1 mm. The design domain has been divided into 5000 quadrilateral plane stress elements, where eight elements that are in the vicinity of the applied load have been excluded from the design space to avoid the stress concentration. The evolutionary rate (ER) and sensitivity filter radius (r_{min}) have been set to 0.02 and 2 mm respectively. The numerical results from the optimization problems $\mathbf{P}_{\mathbf{fatigue}}$ and $\mathbf{P}_{\mathbf{compliance}}$ are shown in Figs. 6-9 and 6-13 for different tension and tension-compression load cases, in which different volume constraints have been applied for each fatigue-based example. As can be seen from the results, the fatigue failure criteria have decreased from 35 – 38% when compared with the traditional compliance-based method. The compliance value in the case of the proposed approach, is 11 - 13% higher than the values which were obtained from the $\mathbf{P}_{\mathbf{compliance}}$ optimization problems, due to the application of the fatigue constraint and modifying the original objective function.

According to the results, the interaction of the mean and alternating stress of all the stress combinations of the final optimal design for the proposed method, lie in the safe zone of the modified Goodman diagram. In the case of the traditional BESO method ($\mathbf{P}_{\mathbf{compliance}}$), which is without fatigue constraint, the fatigue failure will occur due to the combinations not lying in the safe zone of the Goodman diagram. Again, the interaction scatters of the alternating and mean stresses have been

shown for both optimization problems ($\mathbf{P_{fatigue}}$ & $\mathbf{P_{compliance}}$) separately, for different combinations in Figs. 6-10 and 6-12.

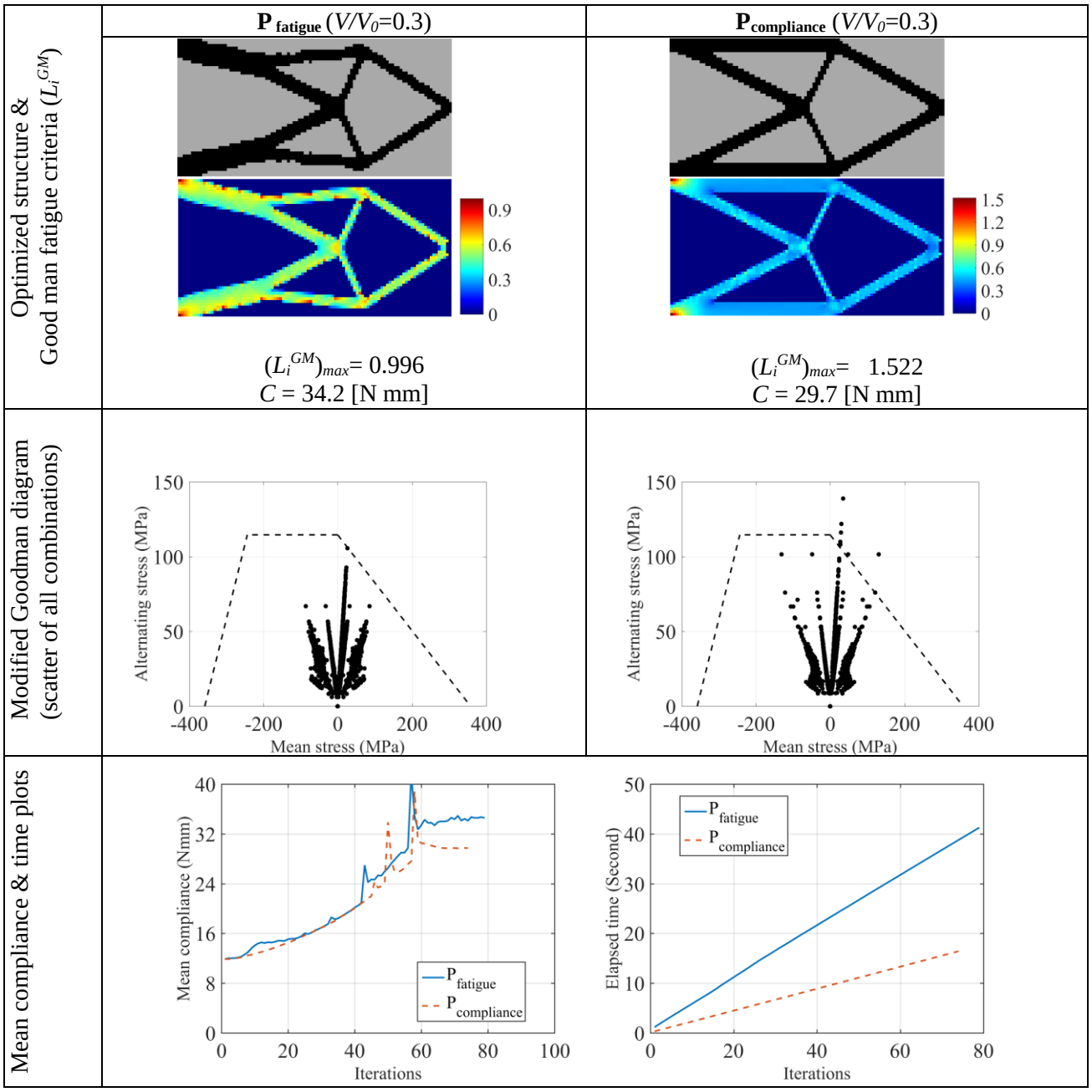

Fig. 6-9. Topology optimization results for cantilever beam (F_{max}=250 N, F_{min}= -150 N, V^*=0.3)

The convergence plots of the *p*-norm fatigue constraint for the $\mathbf{P_{fatigue}}$ problem with the volume constraints of 0.3 and 0.26, are shown in Fig. 6-13. The convergence plots of the mean compliance of both approaches have been shown in Figs. 6-9 and 6-11. The time plots for solving both the optimization problems ($\mathbf{P_{fatigue}}$ & $\mathbf{P_{compliance}}$) are depicted in Figs. 6-9 and 6-11 as well where the

elapsed time for solving the $\mathbf{P}_{\mathbf{fatigue}}$ problem is greater than the $\mathbf{P}_{\mathbf{compliance}}$ problem due to using the adjoint method for calculating the inverse of the global stiffness matrix ($\mathbf{K}^{-1}$) in the sensitivity numbers calculation.

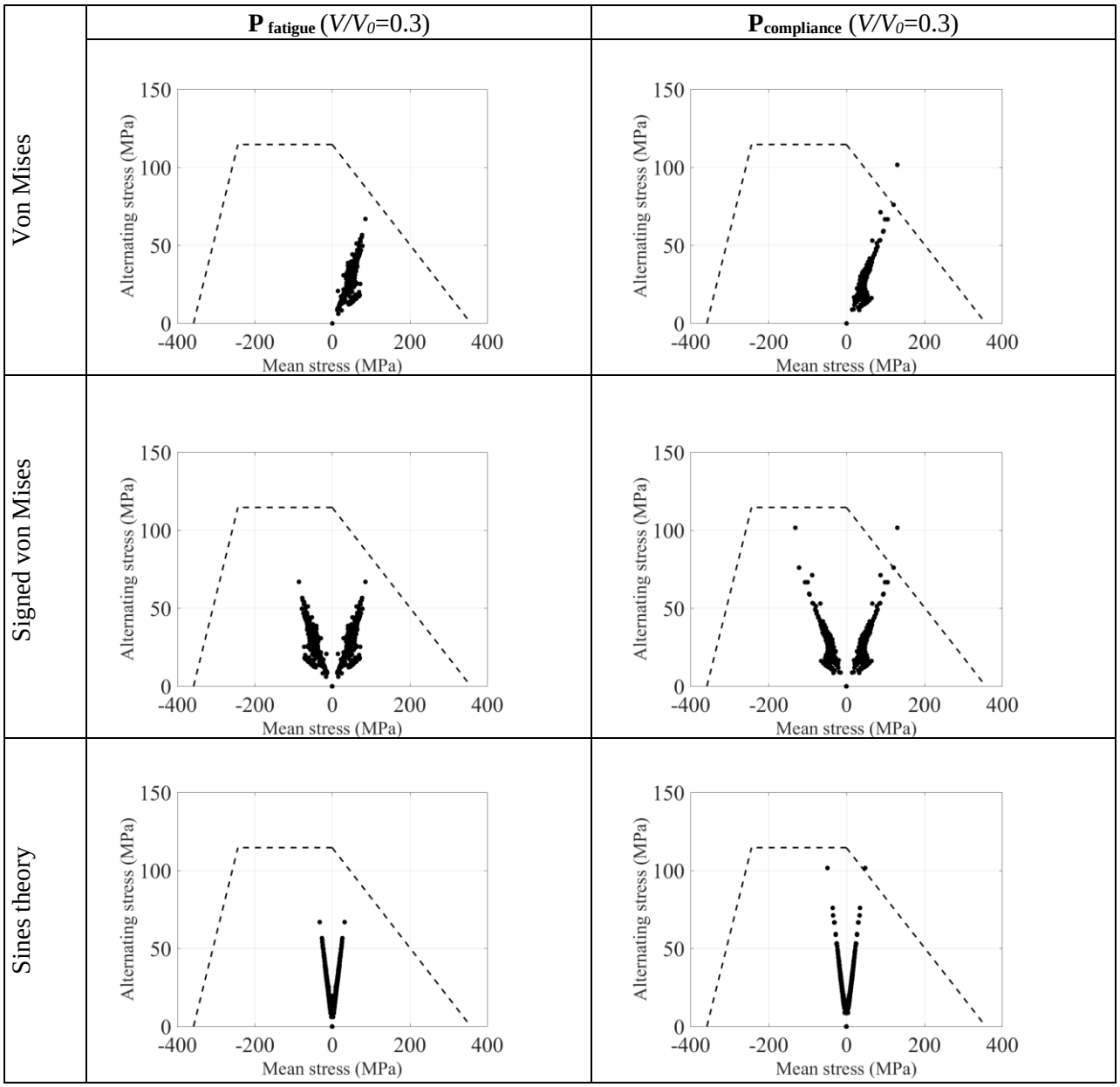

Fig. 6-10. Goodman diagram for cantilever beam (F_{max}=250 N, F_{min}= -150 N, V^*=0.3) with different alternating and mean stress combination

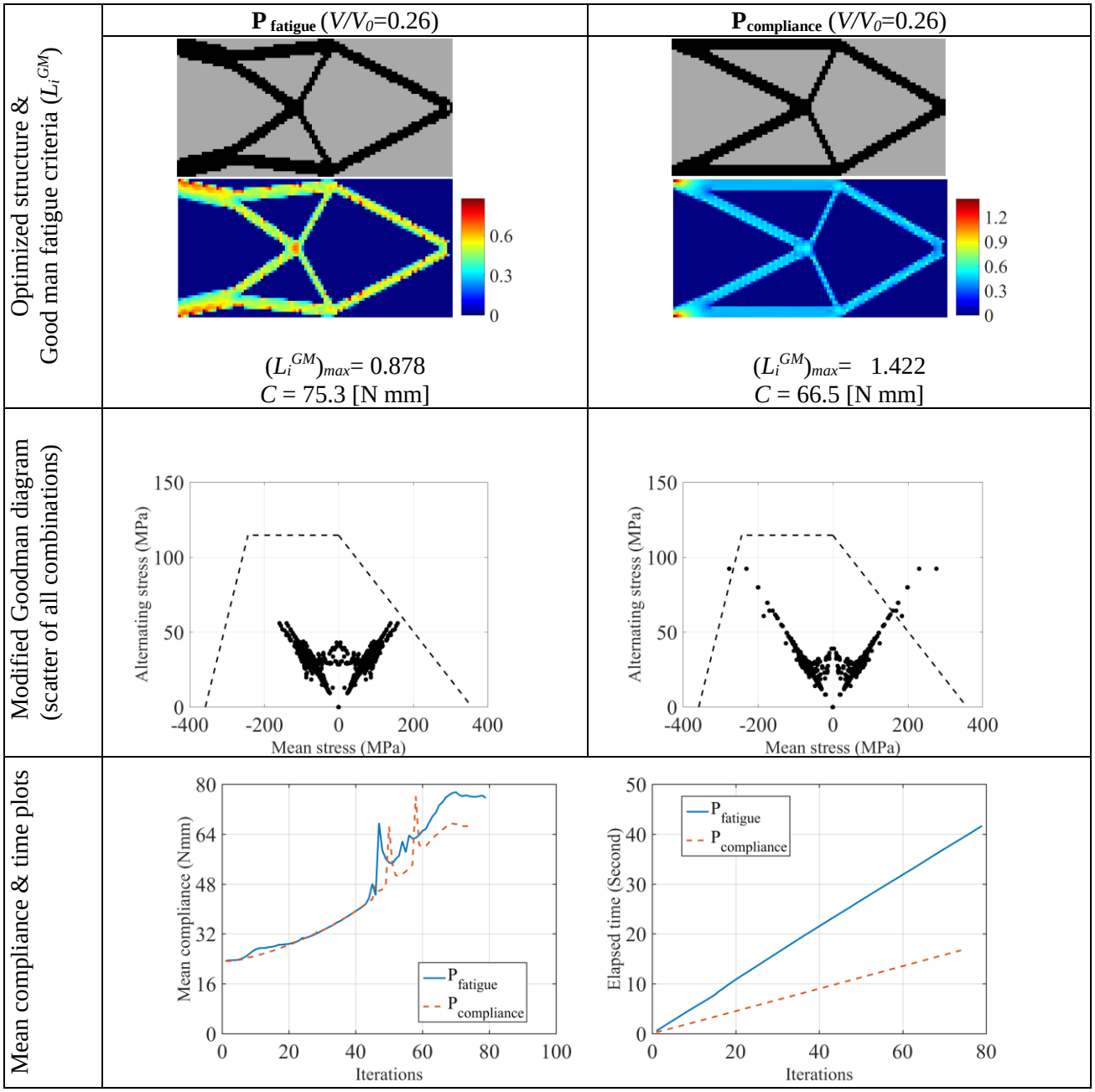

Fig. 6-11. Topology optimization results for cantilever beam (F_{max}=350 N, F_{min}= 150 N, V^*=0.26)

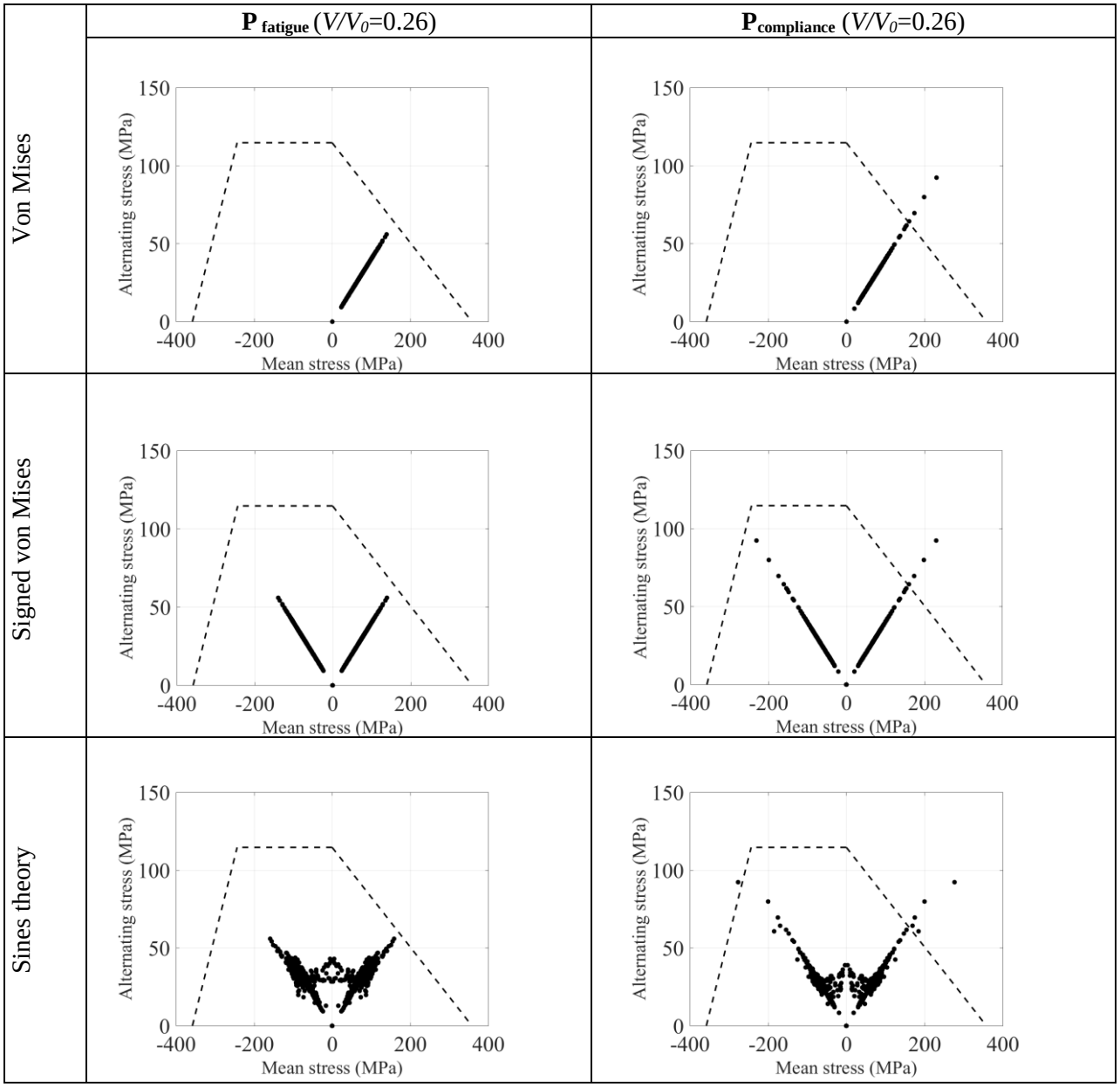

Fig. 6-12. Goodman diagram for cantilever beam (F_{max}=350 N, F_{min}= 150 N, V^*=0.26) with different alternating and mean stress combination

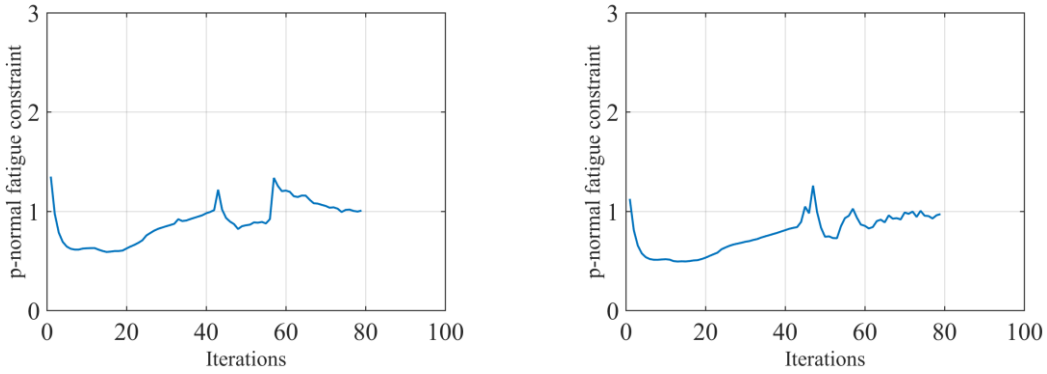

(a) (b)

Fig. 6-13. Convergence plots for cantilever beam ($\mathbf{P_{fatigue}}$) (a) (V/V_0=0.3), (b) (V/V_0=0.26)

6.6.3 Eyebar beam

The third example is the Eyebar beam whose dimensions and boundary condition have been shown in Fig. 4-31 previously. The thickness was 1 mm, and the design domain was discretized with 1 mm × 1 mm quadrilateral Q4 plane stress elements deprived of a circular hole of radius 15 mm. A horizontal load of density $F(x,y)=(F_{max}\ or\ F_{min})((y^2-15^2),_{x\leq 0}\ ,\ 0)$ was applied, where (x, y) denoted the local coordinate system whose origin was located at the center of the hole. The structure was clamped along a segment of length 20 mm on the right-hand side. The alternating and mean stress components were calculated using the scaling factors c_a and c_m which were discussed earlier in this chapter. The sensitivity filter radius and the evolutionary rate in BESO were chosen to be 1.5 and 0.02 respectively. In order to handle the stress concentration, the elements in the vicinity of the applied load remained solid.

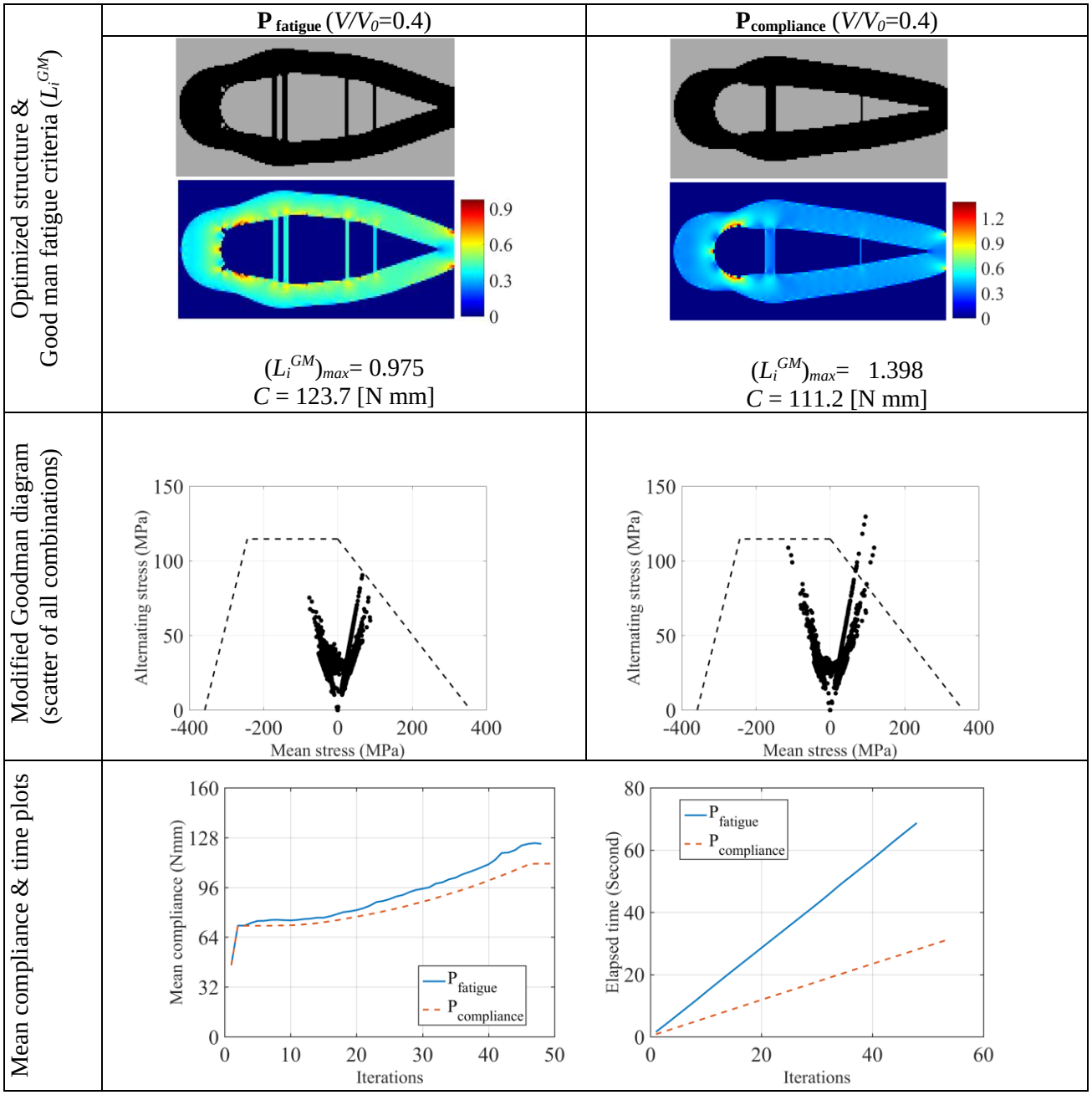

Fig. 6-14. Topology optimization results for Eyebar beam (F_{max}=33 N, F_{min}= -5 N, V^*=0.4)

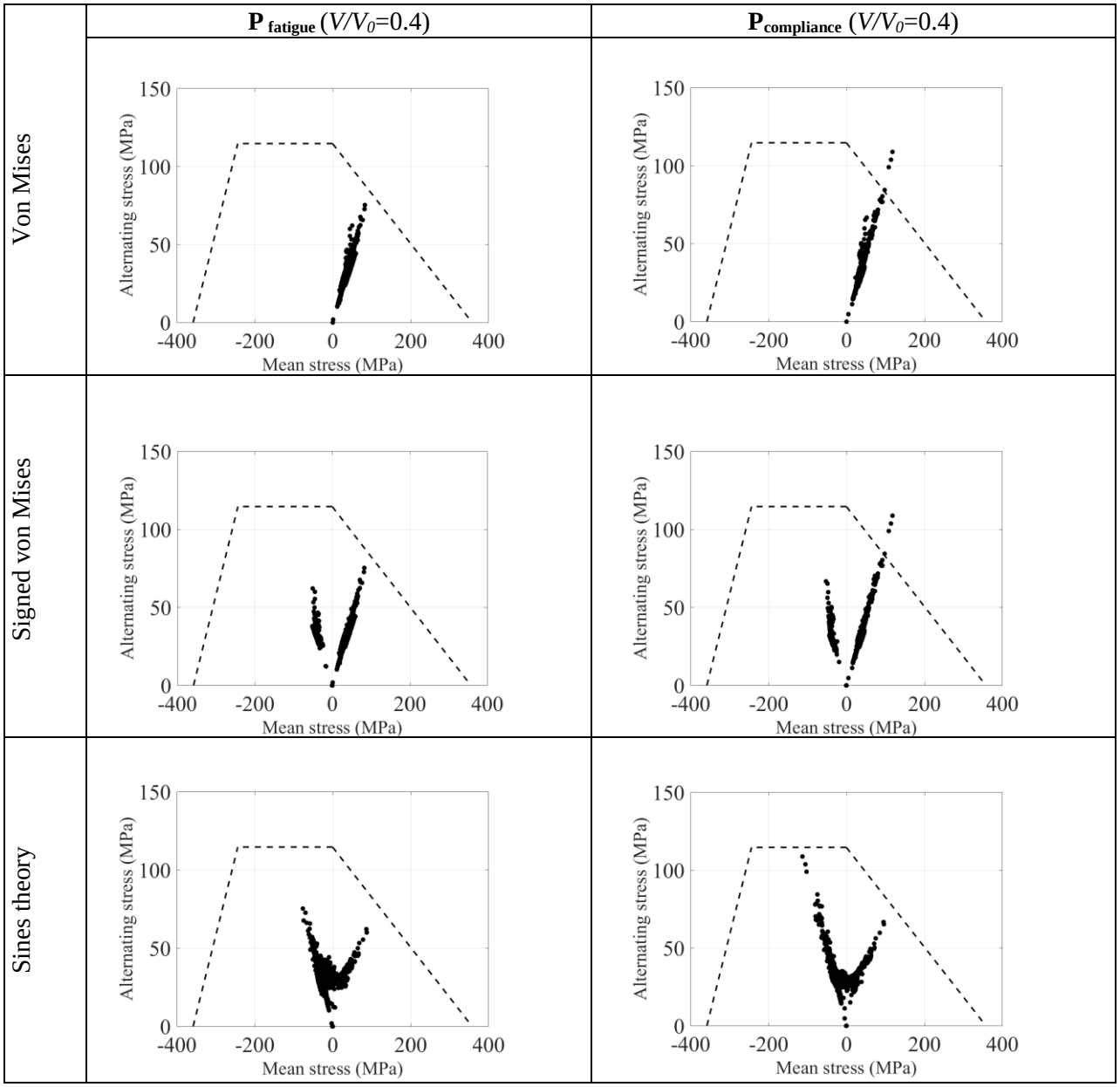

Fig. 6-15. Goodman diagram for Eyebar beam (F_{max}=33 N, F_{min}= -5 N, V^*=0.4) with different alternating and mean stress combination

Solutions for the Eyebar problem for minimizing compliance with and without the fatigue constraint, are shown in Figs. 6-14 and 6-16 where two different load cases (tension and tension-compression loads) have been applied for solving the numerical examples with different volume constraints. Again, for comparison, the volume fractions for $\mathbf{P}_{\mathbf{fatigue}}$ with the fatigue constraint and $\mathbf{P}_{\mathbf{compliance}}$ without the fatigue constraint were the same in each example.

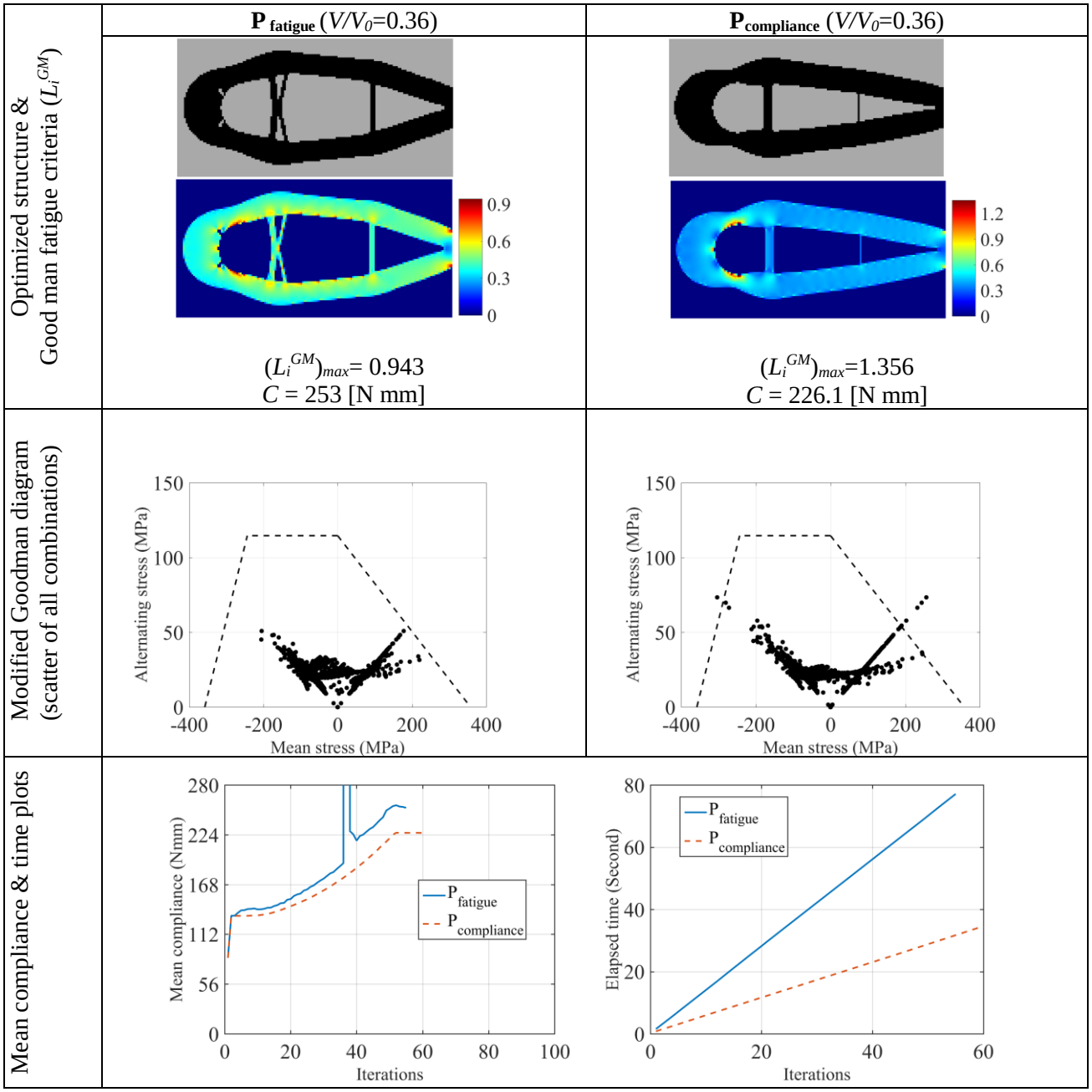

Fig. 6-16.Topology optimization results for Eyebar beam (F_{max}=45 N, F_{min}= 25 N, V^*=0.36)

It can be seen from the results that all combinations of the mean and alternating stresses for the optimal designs obtained from $\mathbf{P}_{\mathbf{fatigue}}$ are within the safe zone of the modified Goodman diagram. It means that the resulting design is fatigue-resistant. However, the optimal designs from the traditional topology optimization, $\mathbf{P}_{\mathbf{compliance}}$, violate the fatigue criteria as shown in Figs. 6-14 and 6-16 for all combinations together and in Figs. 6-15 and 6-17 for different combinations separately, where the Goodman fatigue criteria of the elements which are not in the safe zone are greater than 1.

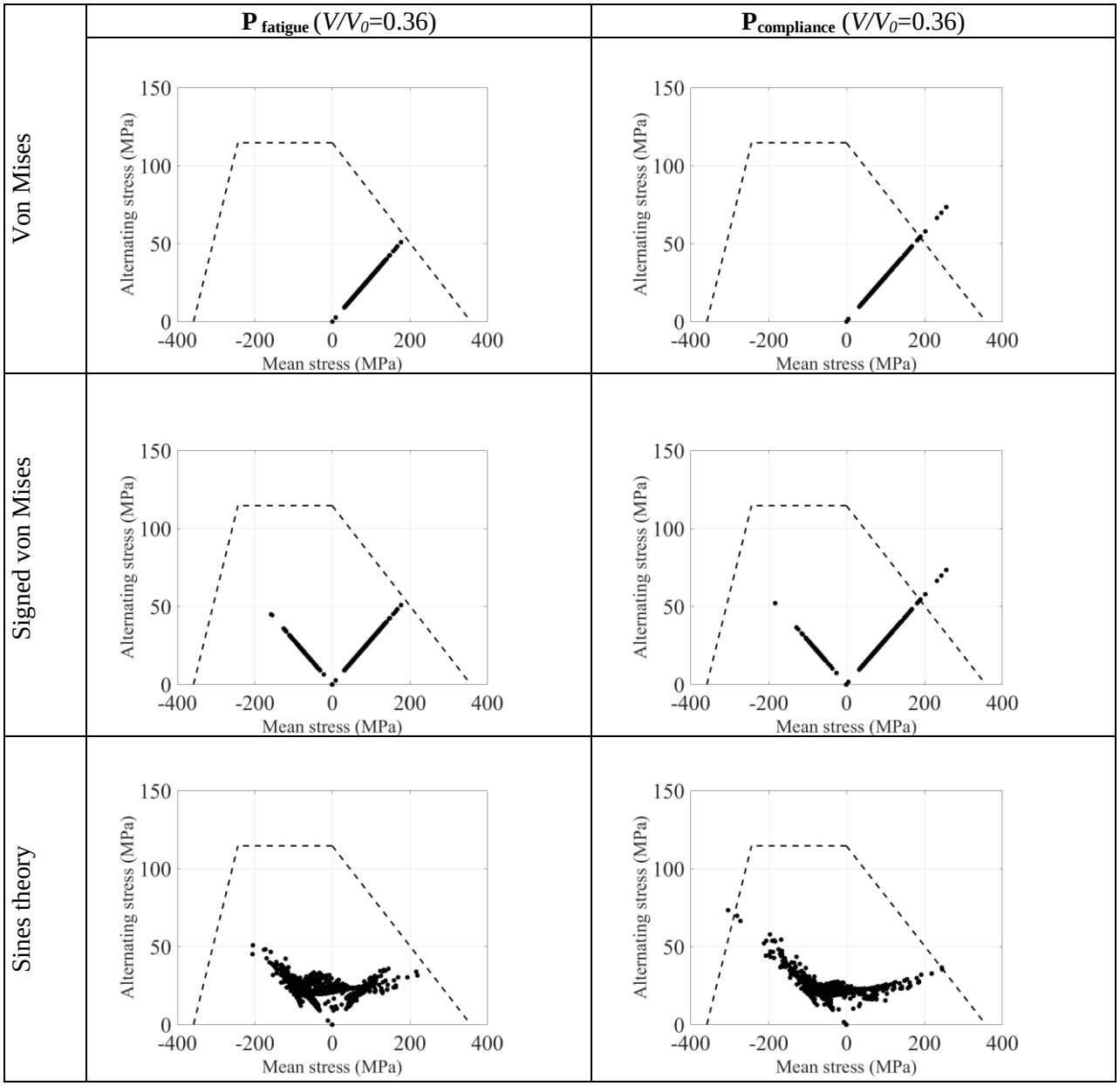

Fig. 6-17. Goodman diagram for Eyebar beam (F_{max}=45 N, F_{min}= 25 N, V^*=0.36) with different alternating and mean stress combination

Hence the proposed fatigue-based approach was able to constrain the fatigue failure criteria below the threshold limit. According to the compliance plots, as shown in Figs. 6-14 and 6-16, the compliance values in the case of the fatigue-based topology optimization ($\mathbf{P_{fatigue}}$) are slightly higher (9 - 10%) than the traditional compliance-based method ($\mathbf{P_{compliance}}$), due to the additional fatigue constraint in $\mathbf{P_{fatigue}}$. However, the fatigue failure criteria have been reduced by 30 - 31% in comparison to the traditional compliance-based problem. The convergence history of the optimization problem $\mathbf{P_{fatigue}}$ is

also given in Fig. 6-18. Additionally, the time plots for solving both optimization problems have been depicted in Figs. 6-14 and 6-16 where the traditional BESO method took less time than the proposed fatigue-base method, as no adjoint equilibrium equation was solved in the $\mathbf{P}_{\mathbf{compliance}}$ problem.

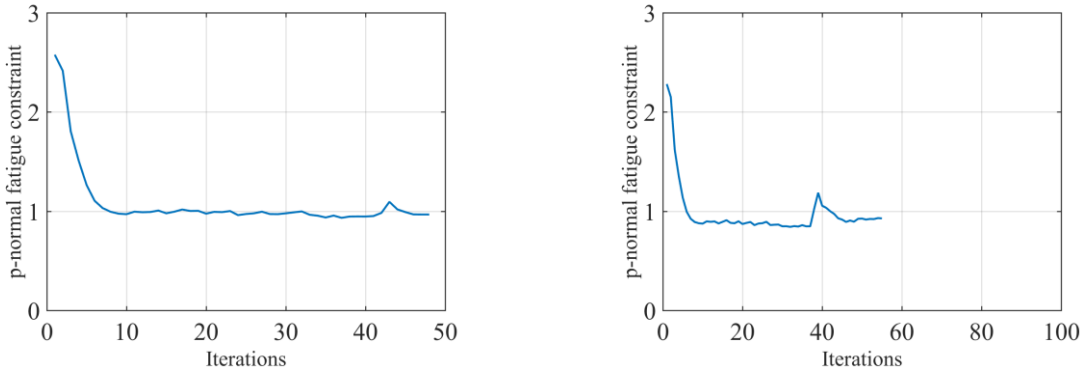

(a) (b)

Fig. 6-18.Convergence plots for Eyebar beam ($\mathbf{P}_{\mathbf{fatigue}}$) (a) ($V/V_0$=0.4), (b) ($V/V_0$=0.36)

6.6.4 Long clamped beam

The last example is the long clamped beam of Chapter 4 (Fig. 4-8) and deals with the optimization of a long clamped beam which is clamped on both sides with a point load applied at the center of the beam where L = 200 mm and the thickness is 1 mm. The design domain is discretized by 6000, 1×1 mm quadrilateral Q4 plane stress elements. The sensitivity filter radius r_{min} and the evolutionary ratio *ER* are chosen to be 2 and 0.02 respectively. The 12 elements (3×4) in the vicinity of the applied load are not used as design variables in order to avoid the stress concentration.

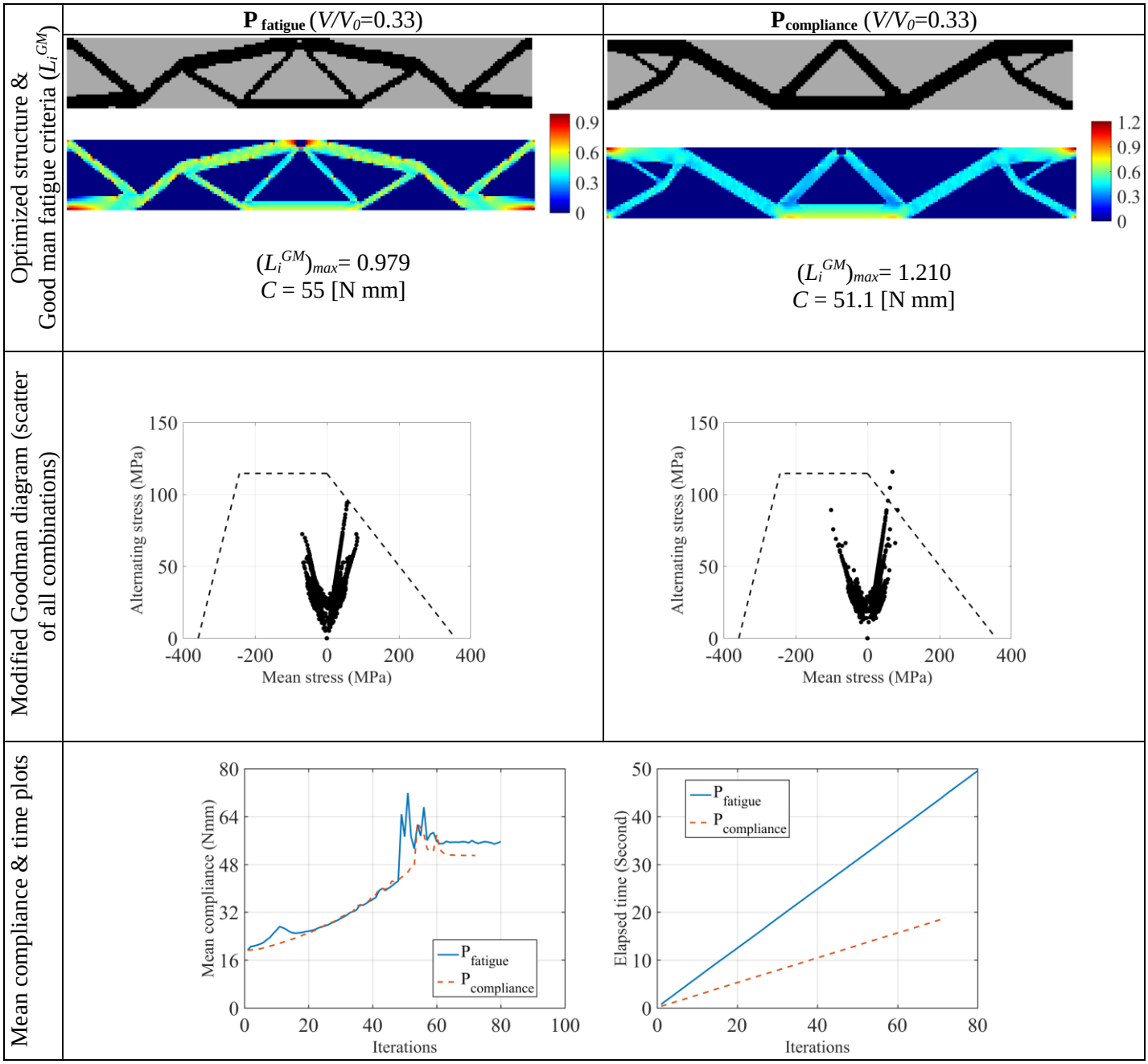

Fig. 6-19.Topology optimization results for Long clamp beam (F_{max}=400 N, F_{min}= -100 N, V^*=0.33)

Solutions for the long clamped beam problem for minimizing compliance are shown in Figs. 6-19 to 6-23, for different volume constraints and loads. As mentioned before, in each example there is the optimal design of the traditional compliance-based optimization problem which has the same volume as the fatigue-based optimization problem. Again, as can be seen from the numerical results, the final optimal designs which were obtained from the traditional stiffness problem (**$\mathbf{P}_{\mathbf{compliance}}$**) are not

fatigue-resistant while they have the same volume as the fatigue-resistant optimal designs which obtained from the proposed fatigue-based optimization problem (**$P_{fatigue}$**).

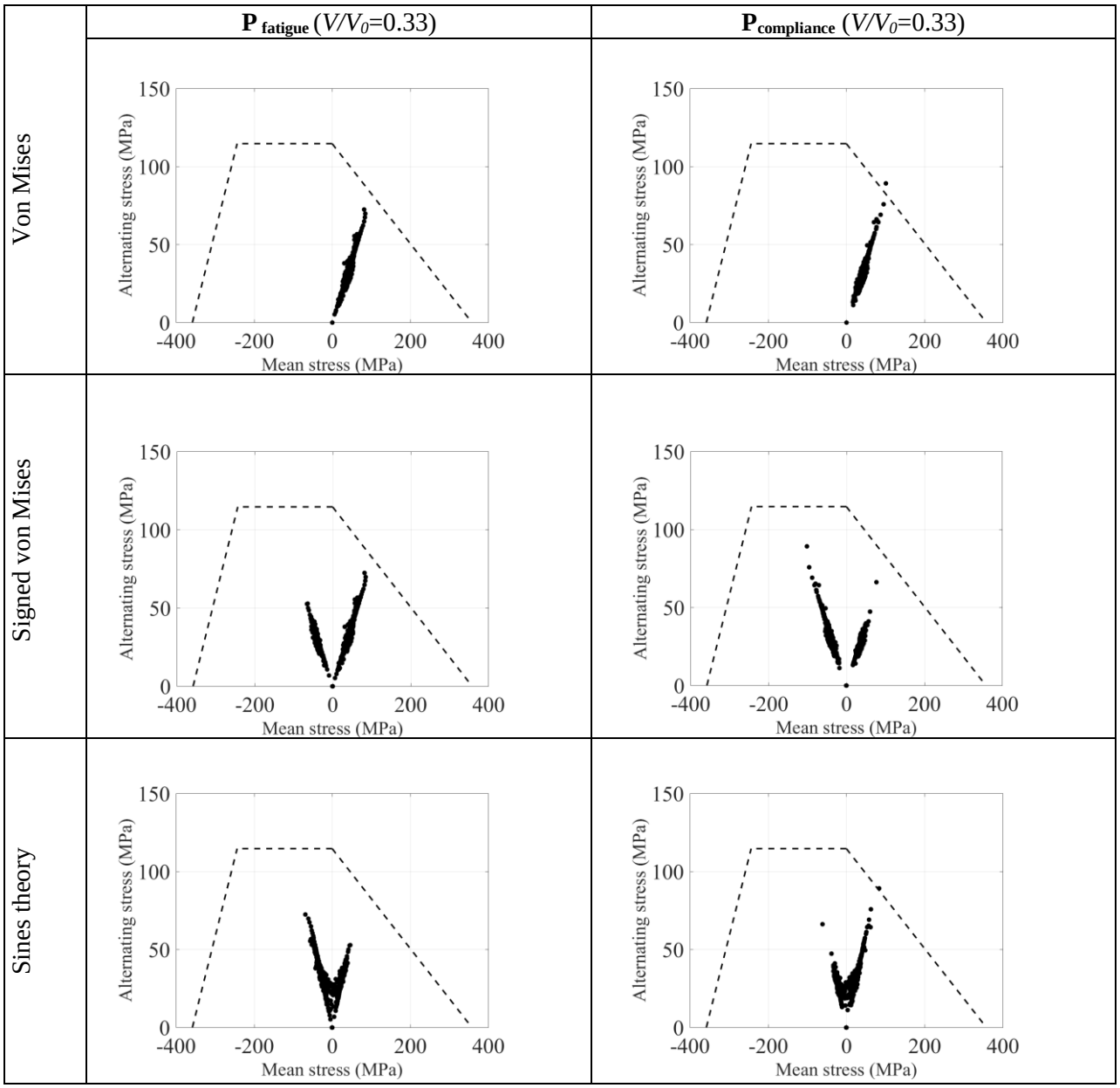

Fig. 6-20.Goodman diagram for Long clamp beam (F_{max}=400 N, F_{min}= -100 N, V^*=0.33) with different alternating and mean stress combination

Notably, the compliance of the proposed fatigue-based approach, is higher than the case of BESO with an additional fatigue constraint. The mean compliance of the examples for both methods and also their time plots, are shown in Figs. 6-19 and 6-21. All combinations of the alternating and mean stress of the examples in the proposed method, lie in the safe zone of the modified Goodman diagram,

which means that the fatigue failure will not occur during the prescribed life cycles. The scatter of the alternating and mean stresses for the different combinations is shown in Figs. 6-20 and 6-22 separately and shown for all combinations in one diagram in Figs. 6-19 and 6-21. In addition, the convergence plots of the proposed fatigue –based approach have been depicted in Fig. 6-23 for different volume constraints 0.33 and 0.25.

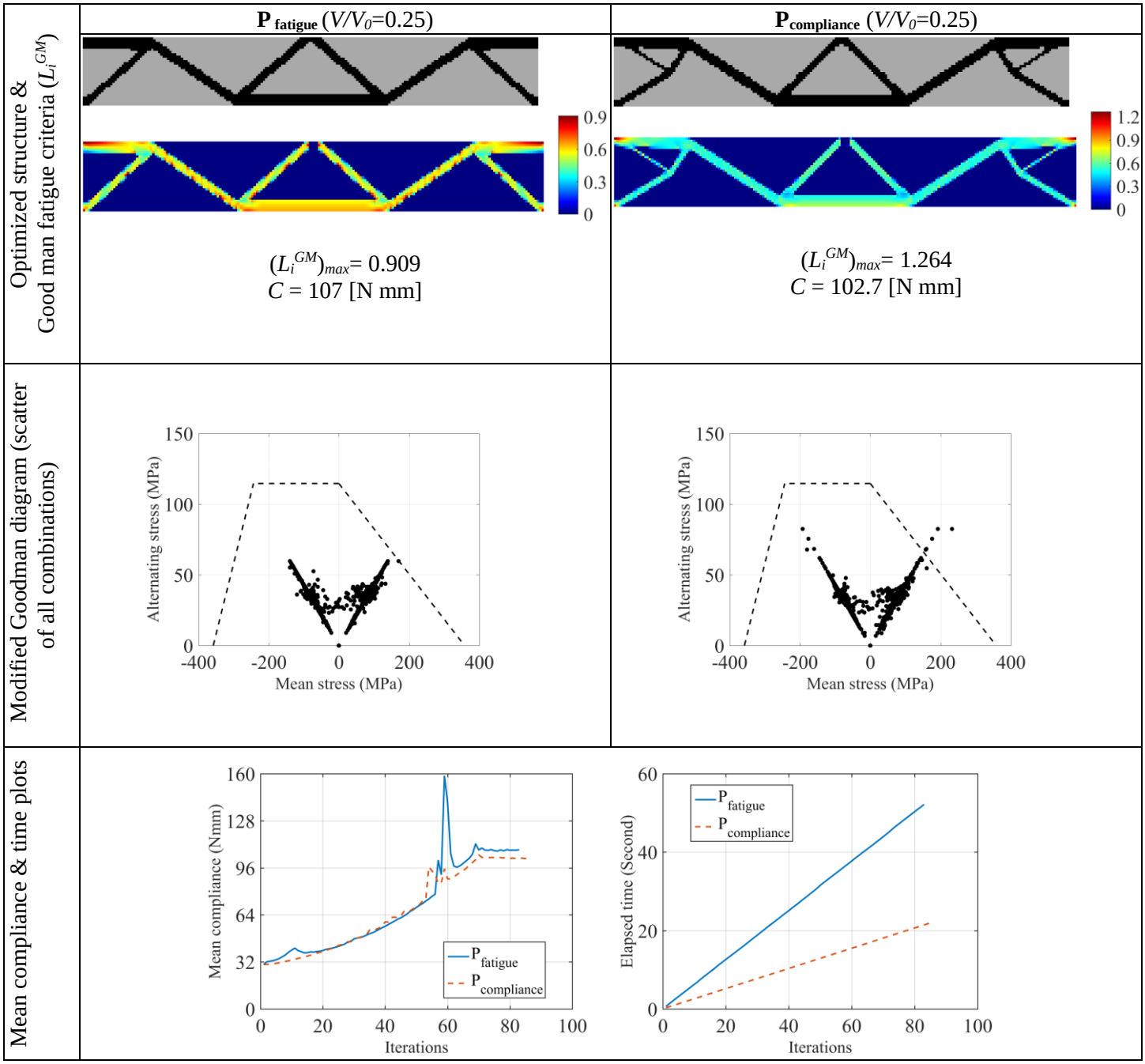

Fig. 6-21. Topology optimization results for Long clamp beam (F_{max}=500 N, F_{min}=200 N, V^*=0.25)

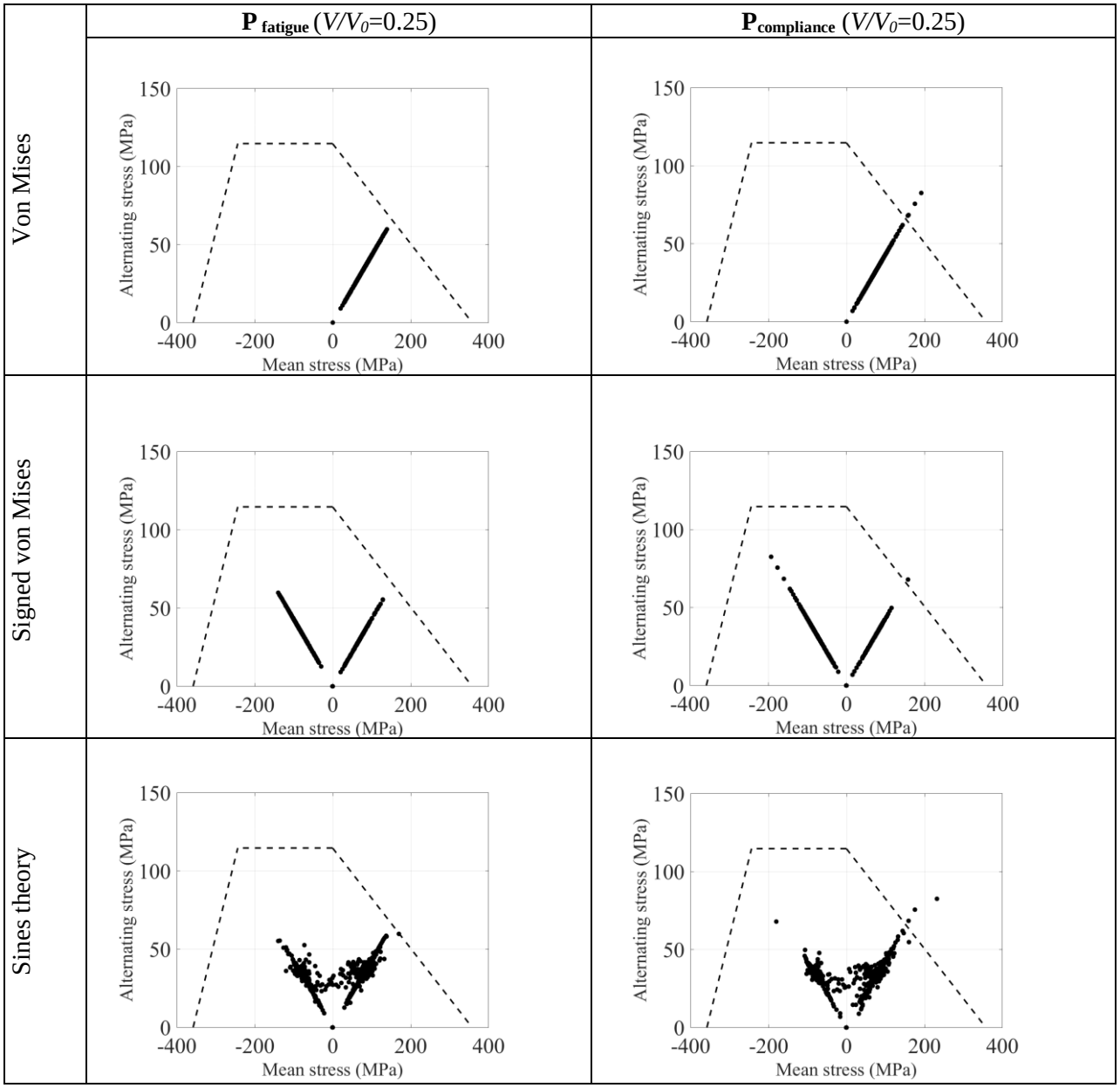

Fig. 6-22. Goodman diagram for Long clamp beam (F_{max}=500 N, F_{min}=200 N, V^*=0.25) with different alternating and mean stress combination

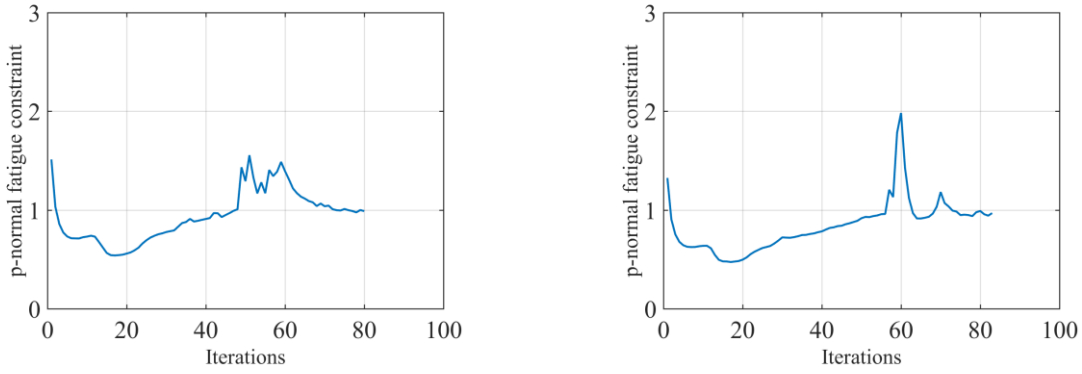

(a) (b)

Fig. 6-23. Convergence plots for Eyebar beam (**P**$_{\textbf{fatigue}}$) (a) (V/V_0=0.33), (b) (V/V_0=0.25)

6.7 Gerber approach

As mentioned earlier in this chapter, the proposed method has been developed for another fatigue failure criteria rather than the modified Goodman to solve the optimization problem **P**$_{\textbf{fatigue}}$**.** In this section the Gerber fatigue failure criterion (Aliabadi 1992; Lee, Barkey & Kang 2012; Suresh 1998) has been used as follows:

$$L_i^{Gerber}(x) = \frac{\sigma_{a_i}^{vonMises}}{(\sigma_i)_{Nf}} + \left(\frac{\sigma_{m_i}^{vonMises}}{\sigma_{ut}}\right)^2 \leq 1 \tag{6-46}$$

Again like the Goodman fatigue criterion σ_{ut}, $\sigma_{m_i}^{vonMises}$ and $\sigma_{a_i}^{vonMises}$ represent the tensile strength of each element, the von-Mises mean stress and the von-Mises alternating stress respectively. $(\sigma_i)_{Nf}$ is the critical fatigue stress for a prescribed number of cycles (N_f) which can be calculated by the *Basquin* Equation (Aliabadi 1992; Lee, Barkey & Kang 2012; Suresh 1998) as discussed in Chapter 5 (Equations (5-7) –(5-11)). The procedure of calculating the sensitivity numbers using the Gerber criterion, is the same as the modified Goodman criterion and just requires the substitution of the Gerber criterion in Equation (6-2) as follows:

$$f_{PN}(x) = \left(\sum_{i=1}^{N_i}\left(L_i^{Gerber}(x)\right)^p\right)^{\frac{1}{p}} \tag{6-47}$$

The derivative of the Gerber criterion with respect to design variables reads:

$$\frac{\partial L_i^{Gerber}(x)}{\partial x_i} = \frac{\partial L_i^{Gerber}(x)}{\partial \sigma_{a_i}^{vonMises}} \frac{\partial \sigma_{a_i}^{vonMises}}{\partial x_i} + \frac{\partial L_i^{Gerber}(x)}{\partial \sigma_{m_i}^{vonMises}} \frac{\partial \sigma_{m_i}^{vonMises}}{\partial x_i} \tag{6-48}$$

Since the first term of the Gerber fatigue criterion is the same as the modified Goodman criteria (Equation (6-7)), all derivatives in Equation (6-48) are the same as Equation (6-19) except the derivative of the term $\partial L_i^{Gerber}(x) \big/ \partial \sigma_{m_i}^{vonMises}$ which reads:

$$\frac{\partial L_i^{Gerber}(x)}{\partial \sigma_{m_i}^{vonMises}} = \frac{2\sigma_{m_i}^{vonMises}}{(\sigma_{ut})^2} \tag{6-49}$$

Hence the final sensitivity numbers can be calculated by modifying the above-mentioned term (Equation (6-49)) in Equation (6-35) which reads:

$$\begin{aligned} \frac{\partial f_{PN}(x)}{\partial x_i} = & \left(\sum_{i=1}^{N_i} \left(L_i^{Gerber}(x) \right)^p \right)^{(\frac{1}{p}-1)} \left(L_i^{Gerber}(x) \right)^{(p-1)} \times \\ & \left[\frac{1}{(\sigma_i)_{Nf}} c_a \frac{\partial \sigma_{a_i}^{vonMises}}{\partial \sigma_{a_i}} \frac{\partial \mathbf{D}}{\partial x_i} \mathbf{B}\mathbf{u} - \boldsymbol{\lambda}_a^T \left(\frac{\partial \mathbf{K}}{\partial x_i} \mathbf{u} \right) + \right. \\ & \left. \frac{2\sigma_{m_i}^{vonMises}}{(\sigma_{ut})^2} c_m \frac{\partial \sigma_{m_i}^{vonMises}}{\partial \sigma_{m_i}} \frac{\partial \mathbf{D}}{\partial x_i} \mathbf{B}\mathbf{u} - \boldsymbol{\lambda}_m^T \left(\frac{\partial \mathbf{K}}{\partial x_i} \mathbf{u} \right) \right]. \end{aligned} \tag{6-50}$$

where the adjoint variable $\boldsymbol{\lambda}_a$ and $\boldsymbol{\lambda}_m$ can be defined by

$$\mathbf{K}\boldsymbol{\lambda}_a = \frac{1}{(\sigma_i)_{Nf}} c_a \mathbf{D}\mathbf{B} \frac{\partial \sigma_{a_i}^{vonMises}}{\partial \sigma_{a_i}} \tag{6-51}$$

$$\mathbf{K}\boldsymbol{\lambda}_m = \frac{2\sigma_{m_i}^{vonMises}}{(\sigma_{ut})^2} c_m \mathbf{D}\mathbf{B} \frac{\partial \sigma_{m_i}^{vonMises}}{\partial \sigma_{m_i}} \tag{6-52}$$

The procedure for calculation of the Lagrangian multiplier for solving the optimization problem is the same as previously and has been discussed earlier in this chapter.

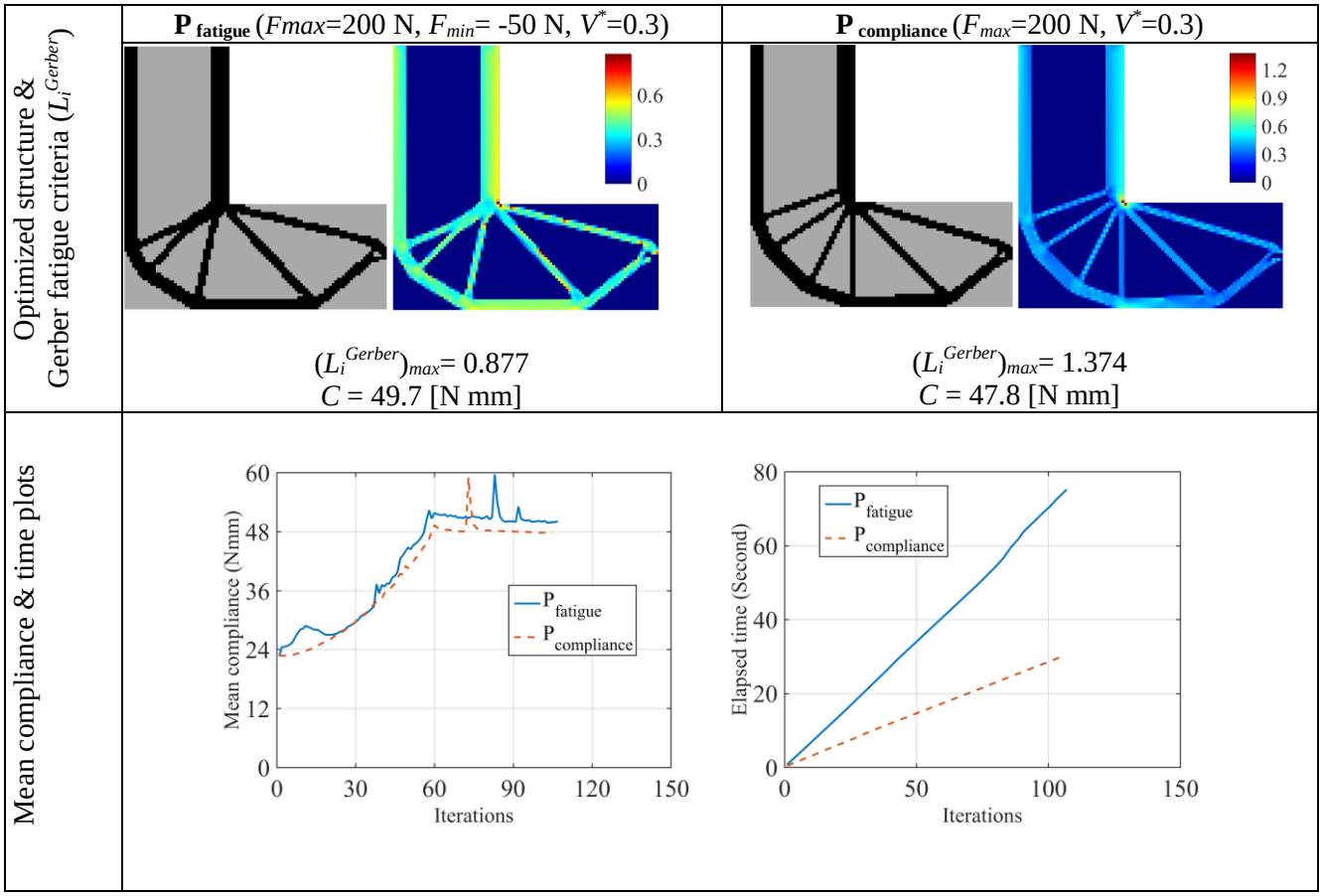

Fig. 6-24.Topology optimization results for L-bracket with Gerber fatigue (F_{max}=200 N, F_{min}= -50 N, V^*=0.3)

In this section, the optimization problem has been solved for the L-bracket beam of Fig. 4-2 which was solved earlier in section 6.6.1 by considering the modified Goodman criterion. All the parameters assumptions for the fatigue analysis are the same as section 6.6.1 including the load value. The topology optimization results for the L-bracket have been shown in Figs. 6-24 and 6-25 where two different loads and volume constraint, have been considered to solve the optimization problem. Again, the traditional BESO method has been solved for comparison. According to the results, the mean compliance values in the proposed method with Gerber fatigue criterion are 4 - 8% higher than the mean compliance values of the original BESO method, due to applying additional fatigue failure constraint. In the case of original BESO method, the maximum fatigue failure criterion is higher than 1, which means that the fatigue failure will occur and is unavoidable, but in the case of the proposed fatigue-based approach it will not occur, since the maximum Gerber criterion is less than 1 for the final optimal designs.

Comparing the computational cost of the proposed fatigue-based approach with the original compliance-based BESO method ($\mathbf{P}_{\mathbf{compliance}}$), the computational efforts of the two examples are illustrated in Figs. 6-24 and 6-25. The algorithms have been run with Matlab codes, in which the total times for solving the optimization problems have been depicted step by step, by calculating the time for each iteration. It can be seen from the result that the computational effort in the proposed approach, is higher than the traditional BESO method, due to the solution of the adjoint equilibrium equation. Also, the convergence plots of the optimization problem $\mathbf{P}_{\mathbf{fatigue}}$, have been depicted in Fig. 6-23 for different volume constraints 0.3 and 0.32.

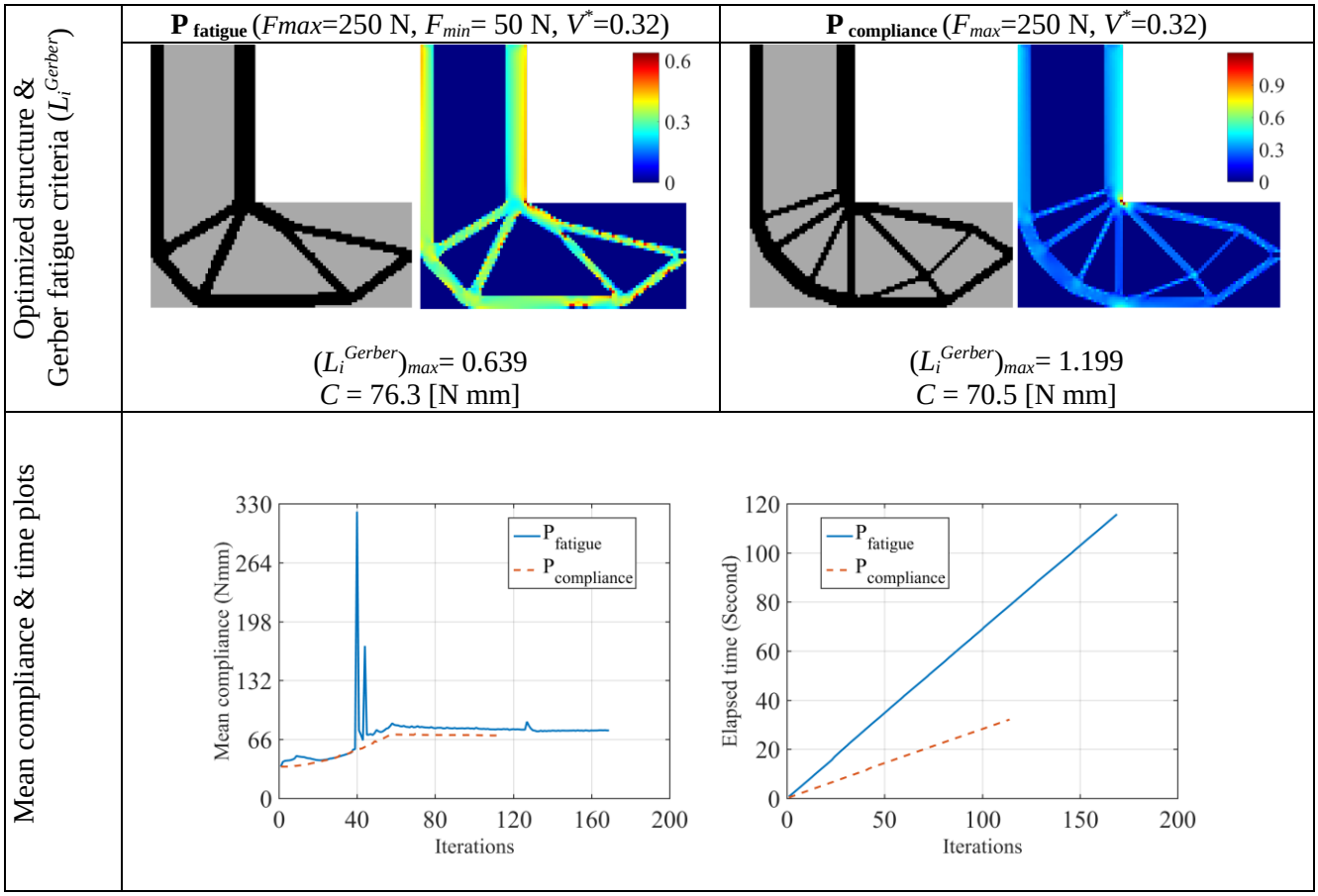

Fig. 6-25. Topology optimization results for L-bracket with Gerber fatigue (F_{max}=250 N, F_{min}=50 N, V^*=0.32)

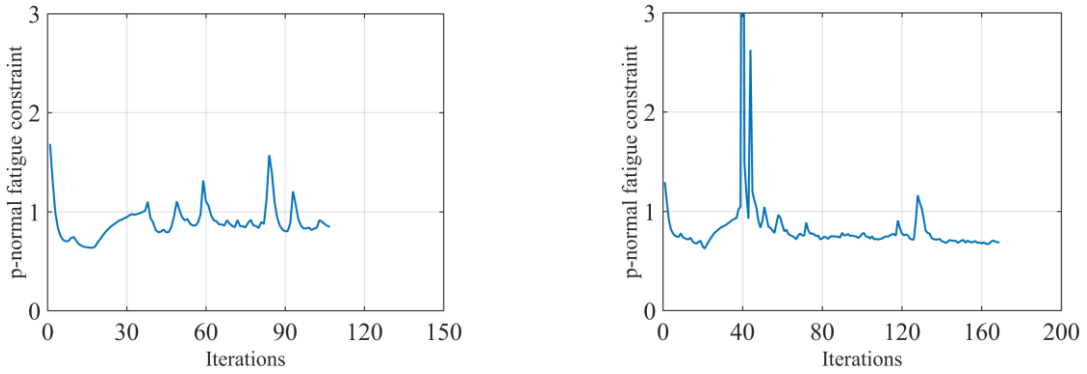

(a) (b)

Fig. 6-26. Convergence plots for L-bracket beam (**$P_{fatigue}$**) (a) (V^*=0.3), (b) (V^*=0.32)

6.8 Different BESO parameters effect

In this section, the effects of the different BESO parameters on the final optimal design are considered for the example of the cantilever beam, shown in Fig. 4-14 and solved in section 6.6.2. The different evolutionary rate and filter radius have been applied to reach the optimal designs for volume constraint 0.3, where the maximum load (F_{max}) is 250 N and the minimum load is -50 N. As discussed in Chapter 4, since the BESO method is a discrete design optimization solution, the Zig-Zag boundaries of the optimal designs are inevitable when compared with the continuous density approaches e.g. SIMP method.

r_{min}=1.5 mm	r_{min}=2 mm	r_{min}=2.5 mm
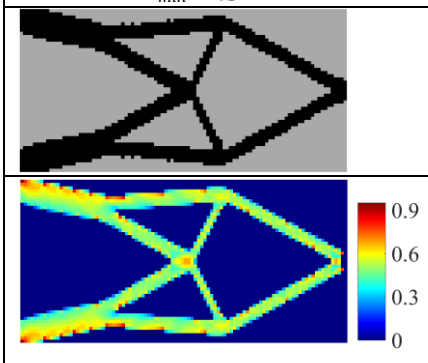	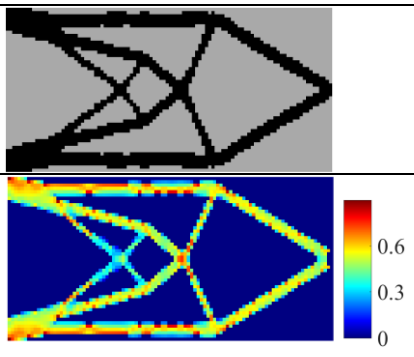	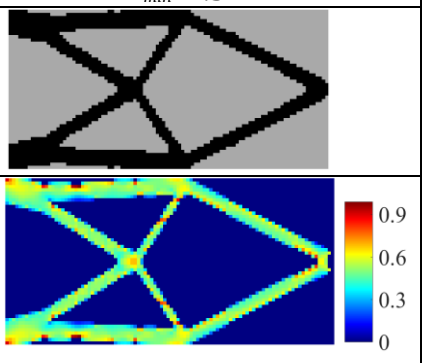
$(L_i^{GM})_{max}$= 0.950 C = 33.4 [N mm]	$(L_i^{GM})_{max}$= 0.895 C = 33.1 [N mm]	$(L_i^{GM})_{max}$= 0.989 C = 32.3 [N mm]

Fig. 6-27. Optimization layouts for cantilever beam with **ER=0.01** (for cantilever beam (F_{max}=250 N, F_{min}= -150 N, V^*=0.3)

r_{min}=1.5 mm	r_{min}=2 mm	r_{min}=2.5 mm
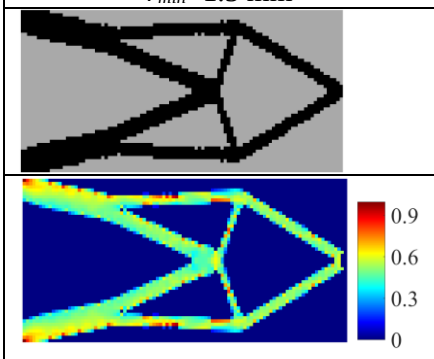	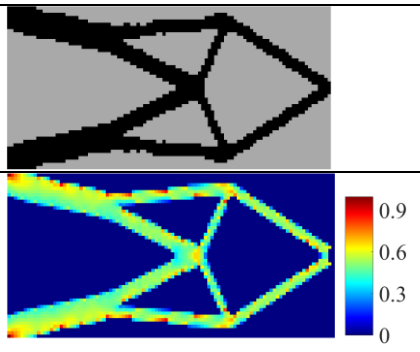	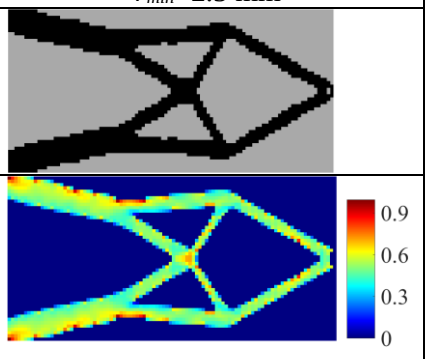
$(L_i^{GM})_{max}$= 0.998 C = 33.9 [N mm]	$(L_i^{GM})_{max}$= 0.996 C = 34.2 [N mm]	$(L_i^{GM})_{max}$= 0.995 C = 34.6 [N mm]

Fig. 6-28. Optimization layouts for cantilever beam with **ER=0.02** (for cantilever beam (F_{max}=250 N, F_{min}= -150 N, V^*=0.3)

According to the results, the larger filter radius may lead to reach a stiffer structure in some cases (e.g *ER*=0.01 and *ER*=0.025), but it cannot be guaranteed and in other cases it may not occur. The evolutionary rate (*ER*) does not lead to major changes to the final design but applying the smaller value of the *ER* leads to an increase in the computational cost due to the slow evolution of the volume fraction.

r_{min}=1.5 mm	r_{min}=2 mm	r_{min}=2.5 mm
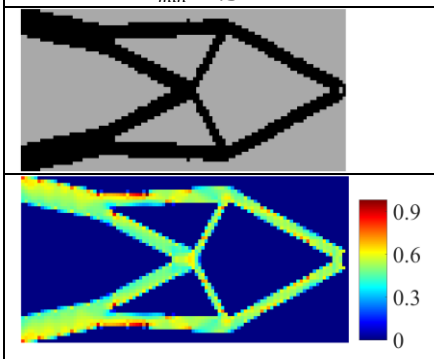	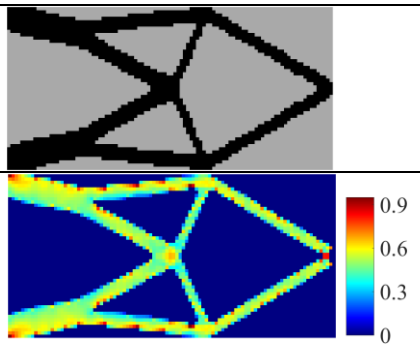	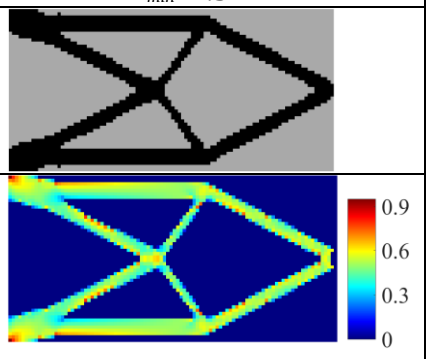
$(L_i^{GM})_{max}$= 0.983 C = 34.3 [N mm]	$(L_i^{GM})_{max}$= 0.949 C = 33.5 [N mm]	$(L_i^{GM})_{max}$= 0.949 C = 31.4 [N mm]

Fig. 6-29. Optimization layouts for cantilever beam with **ER=0.025** (for cantilever beam (F_{max}=250 N, F_{min}= -150 N, V^*=0.3)

The results show that the developed fatigue-based BESO problem can effectively fulfill the fatigue constraint and the maximum fatigue failure criteria, which in this section is based on the modified Goodman criterion, which is less than 1 in all the cases. Hence the final optimized structures in all cases with different BESO parameters are fatigue-resistant while satisfying the volume constraint as well.

6.9 Conclusion remarks

Since fatigue is one of the most important criteria for engineering problems, it should be considered during topology optimization. In this chapter, the fatigue-based BESO method has been proposed for minimizing the compliance, subject to the fatigue and volume constraints. The proportional loads with constant amplitude were used to evaluate the sensitivity numbers of the elements, based on the modified Goodman fatigue failure criterion which has been applied directly in the sensitivity analysis. Also, three combinations of mean and alternating stresses have been considered for controlling the fatigue failure of the final optimal design with the modified Goodman diagram. The proposed method was verified numerically, and the obtained results were appealing. Because of the adoption of the fatigue constraint in the proposed method, the compliance of the optimal fatigue-based design was slightly higher than that of the traditional compliance minimization. Also, the proposed approach has been modified for Gerber fatigue failure criterion and the optimization problem has been solved for different numerical examples. Although the proposed method can reach the preliminary fatigue-resistant optimized structure, but it is limited to the constant proportional loading condition with linear equivalent static analysis. The optimal design obtained from the proposed method was fatigue-resistant, as evidenced by the modified Goodman diagram, while the optimal design obtained from the traditional compliance minimization approach, violates the fatigue criterion applying the same loads used in our proposed approach.

Chapter 7

Final Remarks

7.1 Main achievements

This research is mainly focused on applying the stress and fatigue constraints in the BESO optimization approach to achieve an optimal design with no fatigue and stress failures. The key achievements are listed as follows:

Firstly, a novel approach for applying the stress constraint in the BESO method was proposed, where the global approach of the local stress constraint was used by applying the *p*-norm function to reduce the computational cost and overcome a large amount of the local constraints issue. Differing from (Xia et al. 2018) which simplified the sensitivity analysis due to the complexity of the stress-based topology optimization problems and overly damped the sensitivity numbers, in order to make the BESO procedure stable. In our proposed method, the stress vectors of the material have been fully considered in the sensitivity analysis. The linear static analysis was applied to evaluate the distribution of von-Mises stress and calculate the *p*-norm stress sensitivity of the elements. Then, the current BESO method was extended to find a design without large stress concentration and with local stress close to the stress limit. Three different optimization problems were solved for different numerical examples based on the proposed method.The first optimization problem (**P1** $_{\text{stress}}$) was formulated to minimize the compliance subject to the stress and volume constraints. The second problem (**P2** $_{\text{stress}}$) dealt with minimizing the *p*-norm stress subject to volume constraint. The third problem (**P3** $_{\text{stress}}$) was regarding the minimization of the structure's volume while satisfying the stress constraint. Compared with the traditional compliance minimization problem ($\mathbf{P}_{\text{complince}}$) where large stress concentration may occur, the numerical examples showed that considering stress minimization in the BESO method, the final optimal designs are closer to a practical engineering design where stress concentration has been reduced significantly.

The effect of different BESO parameters was considered on the proposed method as well, where the results demonstrated that a smaller filter radius (r_{min}) leads to the optimized design with a lower maximum stress but with more members, which may cause the extra cost in manufacturing, the considered evolutionary rates (*ER*) had no significant effect on the final optimized design. A smaller evolutionary rate causes the slow evolution of the topology to the specified volume fraction and increases the computational cost. The mesh-independence of the proposed method was also controlled by applying different mesh sizes for the optimization problems and checked the final optimized structures. The proposed stress-based approach is different from the traditional BESO mesh-independent approach (**$P_{complince}$**), as it is not mesh-independent. By changing the mesh sizes the same topology cannot be obtained due to the local optima. The same topology may be obtained for the proposed stress-based method by defining the larger filter values while using finer mesh sizes which are not based on the sizes of the mesh (as in the traditional BESO method) and is instead based on experience. Since stress is one of the most important criteria for engineering problems, it is not sufficient to use the BESO method to optimize the structure for the maximum stiffness. Therefore, the proposed method can be used as a tool to overcome the stress concentration issue of the final design, obtained from the original BESO method. In conclusion, this study solved the stress-based topology optimization in the framework of BESO with discrete design variables.

Secondly, since fatigue failure is another most important criterion for engineering problems and has never been developed in the BESO method, in this research, a method was developed for considering the critical fatigue stress as a constraint in the BESO method. The critical fatigue stress was calculated for a predefined number of cycles to failure for the structure as discussed previously and used as stress constraint in the topology optimization problem. The optimization problem, which is called **$P_{fatige\ stress}$** in this study, was formulated to minimize the mean compliance, while satisfying the volume and critical fatigue stress constraints. This was different from the proposed stress-based approach, discussed above. Since the fatigue failure generally does not occur for compressive stresses, the sensitivity analysis of the **$P_{fatige\ stress}$** problem was based on the highest tensile principal stress in each point of the elements. The aim was to reach an optimal design in which high cycle fatigue failure does

not occur for a specific lifetime. The critical fatigue stress is calculated based on modified Goodman criteria and used as a stress constraint in the topology optimization problem. The optimization results were also compared with the results from the compliance minimization problem ($\mathbf{P_{compliance}}$). The final optimized design, which was obtained from the proposed, method is fatigue-resistant for the prescribed life cycles, however, in the case of the original BESO method, the fatigue failure occurred. Since the proposed method is based on the maximum tensile principal stresses, it is purely fatigue-resistant while the combination of the mean and alternating stresses of the final design was checked by the tensile principal stress measurement. This means that in the case of the other stress measurements (von Mises, signed von Mises and Sine theory) as discussed in Chapter 5 the proposed fatigue-based method cannot fulfill the fatigue constraint, therefore the fatigue failure might occur. Hence the proposed fatigue-based method in which the critical fatigue stress has been used as the stress constraint, can be used as a tool to reach the fatigue-resistant optimal design which is limited to the maximum tensile principal stress application.

Finally, as the method with the critical fatigue stress considers the maximum tensile principal stress in the sensitivity numbers calculation and cannot be used in the other cases (e.g. von Mises, signed von Mises and Sine theory), a novel fatigue-based optimization approach was developed where the fatigue failure criterion was used directly in the sensitivity analysis. In the proposed fatigue-based BESO method the compliance was minimized, subject to the fatigue and volume constraints. The proportional loads with constant amplitude were used to evaluate the sensitivity numbers of the elements, based on the modified Goodman fatigue failure criterion which has been applied directly in the sensitivity analysis. Also, as was shown the proposed method could be used for the other fatigue failure criterion, for example, Gerber rather than modified Goodman where the sensitivity analysis should be modified based on the new criterion. The proposed method which is different from the fatigue optimization that was based on the critical fatigue stress (Chapter 5), can be used for the three combinations of mean and alternating stresses (von Mises, signed von Mises and Sine theory) where for the three combinations, all the interactions of the mean and alternating stresses of the final designs lay in the safe zone of the modified Goodman diagram. The proposed method was verified

numerically, and the results obtained were appealing. Because of the adoption of the fatigue constraint in the proposed method, the compliance of the optimal fatigue-based design was slightly higher than that of the traditional compliance minimization. The proposed method can reach the preliminary fatigue-resistant optimized structure, but it is limited to the constant proportional loading condition with linear equivalent static analysis. The optimal design obtained from the proposed method was fatigue-resistant, evidenced by the modified Goodman diagram. The optimal design obtained from the traditional compliance minimization approach violates the fatigue criterion under the same loads used in our proposed approach. Different topologies from the traditional compliance minimization were achieved when fatigue constraint was employed. It must be noted that the proposed fatigue-based approach is a simplified design tool that can enhance the traditional compliance BESO approach with respect to fatigue constraint and can be used as a preliminary optimal solution to help the designer to obtain fatigue-resistant optimal design.

Comparing with SIMP solution with intermediate elements, BESO is based on the discrete design variables and only allows remove elements as a whole and in some cases, we don't have smooth surface and zigzags are inherent in the final optimal layouts. In the fatigue-based optimization problems in chapter 5 and 6 of the thesis, the global function of the tensile stress and Goodman fatigue failure criteria has been used with the p-norm function, therefore this algorithm implemented an average effect on the local stress and local fatigue life of the element level. Thus, the zigzags on the edge of results do not affect this method significantly. The results in the thesis indicate that these zigzags have little effect on the fatigue life in the global approach. However, in the local approach which consider the local stress and fatigue life of each elements in the sensitivity analysis theses zigzags may affect the fatigue life and the final optimal design may not have theses zigzags. Since the local approach of the stress and fatigue-based topology optimization are very costly, they are out of scope of this thesis. Also, the original BESO method is mesh independent, however the new method in this thesis is mesh dependent and, in some cases, it might reach different topologies with a small negligible changing of the BESO parameters and mesh size. We adopted the following way to effectively compare the stress and fatigue results from different optimization problem: the same mesh

size and BESO parameters must be used in each problem. Based on our results presented in the thesis, it is acceptable to have the comparison with the same mesh size in all examples. In conclusion, this research investigated the stress-based and fatigue-based topology optimization in the framework of BESO with discrete design variables.

7.2 Future work

In this thesis, the BESO was developed to apply the stress and fatigue constraints in the topology optimization problem. The studies conducted in this thesis offer innovative solutions to reach the optimal design in which the stress concentrations were alleviated significantly in comparison to the original BESO method. In the fatigue-based approach, the optimal design was fatigue-resistant for the prescribed number of cycles. Since the proposed stress–based approach was not mesh-independent due to the nonlinear nature of the stress constraint, and the local optima issue, the proposed method should be developed further for obtaining a solution which is mesh dependent, and 3D examples can be used to extend the validity of the proposed stress-based BESO method. As mentioned previously, the fatigue-based approach was limited to the high cycle fatigue with a constant proportional loading condition, therefore the proposed fatigue-based method should be extended further to be applicable for the non-constant and non-proportional loading conditions as well. In addition, the short low cycle fatigue analysis, which is based on the strain, rather than stress, can be applied to future studies. Furthermore, since the current proposed fatigue-based approach is based on the high cycle fatigue analysis, which is based on the time domain fatigue analysis, the frequency domain fatigue optimization in the framework of the BESO method can also be considered for future studies. Furthermore, since the proposed stress-based and fatigue-based approaches are sensitive to mesh size, they are not applicable to be used for optimization of the complex structures directly. Due to the high sensitivity of theses proposed methods, their efficiency is not higher than the conventional methods. The future research should be done to resolve the mesh dependency of the theses methods which could be helpful in using them for the optimization of the complex structures.

References

Aliabadi, MH 1992, *Fundamentals of metal fatigue analysis: Julie A. Bannantine, Jess J. Comer & James L. Handrock, Prentice Hall Publishers, 1990. pp. 273. ISBN: 13 340191 X (Book Review)*, 0955-7997.

Allaire, G & Jouve, F 2008, 'Minimum stress optimal design with the level set method', *Engineering analysis with boundary elements*, vol. 32, no. 11, pp. 909-918.

Amstutz, S & Novotny, AA 2010, 'Topological optimization of structures subject to von Mises stress constraints', *Structural and Multidisciplinary Optimization*, vol. 41, no. 3, pp. 407-420.

Bendsøe, MP 2004, *Topology Optimization: Theory, Methods, and Applications*, Berlin/Heidelberg : Springer Berlin Heidelberg, Berlin/Heidelberg.

Bendsøe, MPa 1995, *Optimization of structural topology, shape, and material*, Springer, Berlin, [Germany] ; Heidelberg, [Germany].

Bruggi, M 2008, 'On an alternative approach to stress constraints relaxation in topology optimization', *Structural and Multidisciplinary Optimization*, vol. 36, no. 2, pp. 125-141.

Bruggi, M & Duysinx, P 2012, 'Topology optimization for minimum weight with compliance and stress constraints', *Struct Multidisc Optim*, vol. 46, no. 3, pp. 369-384.

Bruns, TE & Tortorelli, DA 2001, 'Topology optimization of non-linear elastic structures and compliant mechanisms', *Computer Methods in Applied Mechanics and Engineering*, vol. 190, no. 26, pp. 3443-3459.

Budynas, RG, Nisbett, JK & Shigley, JE 2011, *Shigley's mechanical engineering design*, 9th ed. edn, McGraw-Hill, New York.

Cheng, G & Guo, X 1997, 'ε-relaxed approach in structural topology optimization', *Structural optimization*, vol. 13, no. 4, pp. 258-266.

Cheng, G & Jiang, Z 1992, 'STUDY ON TOPOLOGY OPTIMIZATION WITH STRESS CONSTRAINTS', *Engineering Optimization*, vol. 20, no. 2, pp. 129-148.

Collet, M, Bruggi, M & Duysinx, P 2017, 'Topology optimization for minimum weight with compliance and simplified nominal stress constraints for fatigue resistance', *Structural and Multidisciplinary Optimization*, vol. 55, no. 3, pp. 839-855.

Duysinx, P & Bendsøe, MP 1998, 'Topology optimization of continuum structures with local stress constraints', *International Journal for Numerical Methods in Engineering*, vol. 43, no. 8, pp. 1453-1478.

Duysinx, P & Sigmund, O 1998, 'New developments in handling stress constraints in optimal material distribution', in *7th AIAA/USAF/NASA/ISSMO Symposium on Multidisciplinary Analysis and Optimization*, Multidisciplinary Analysis Optimization Conferences, American Institute of Aeronautics and Astronautics, viewed 2018/07/02, <https://doi.org/10.2514/6.1998-4906>.

Grunwald, J & Schnack, E 1998, 'Modeling fatigue for shape optimization of dynamically loaded parts', *Advances in Engineering Software*, vol. 29, no. 1, pp. 63-67.

Guo, X, Zhang, WS, Wang, MY & Wei, P 2011, 'Stress-related topology optimization via level set approach', *Computer Methods in Applied Mechanics and Engineering*, vol. 200, no. 47, pp. 3439-3452.

Hassani, Ba & Hinton, E 1999, *Homogenization and structural topology optimization : theory, practice, and software*, Softcover reprint of the hardcover 1st edition. edn, Springer, London.

Holmberg, E, Torstenfelt, B & Klarbring, A 2013, 'Stress constrained topology optimization', *Struct Multidisc Optim*, vol. 48, no. 1, pp. 33-47.

Holmberg, E, Torstenfelt, B & Klarbring, A 2014, 'Fatigue constrained topology optimization', *Structural and Multidisciplinary Optimization*, vol. 50, no. 2, pp. 207-219.

Huang, X & Xie, Y 2007, 'Convergent and mesh-independent solutions for the bi-directional evolutionary structural optimization method', vol.

Huang, X & Xie, Y 2010a, 'Evolutionary topology optimization of continuum structures with an additional displacement constraint', *Struct Multidisc Optim*, vol. 40, no. 1, pp. 409-416.

Huang, X & Xie, Y 2010b, 'Evolutionary topology optimization of geometrically and materially nonlinear structures under prescribed design load', *Structural Engineering and Mechanics*, vol. 34, no. 5, pp. 581-595.

Huang, X & Xie, YM 2007, 'Convergent and mesh-independent solutions for the bi-directional evolutionary structural optimization method', *Finite Elements in Analysis & Design*, vol. 43, no. 14, pp. 1039-1049.

Huang, X & Xie, YM 2010, *Evolutionary topology optimization of continuum structures : methods and applications*, Wiley, Chichester, West Sussex, U.K. ; Hoboken, N.J.

Jensen, KE 2016, 'Solving stress and compliance constrained volume minimization using anisotropic mesh adaptation, the method of moving asymptotes and a global p-norm', *Structural and Multidisciplinary Optimization*, vol. 54, no. 4, pp. 831-841.

Jeong, SH, Choi, D-H & Yoon, GH 2014, 'Separable stress interpolation scheme for stress-based topology optimization with multiple homogenous materials', *Finite Elements in Analysis & Design*, vol. 82, pp. 16-31.

Jeong, SH, Choi, D-H & Yoon, GH 2015, 'Fatigue and static failure considerations using a topology optimization method', *Applied Mathematical Modelling*, vol. 39, no. 3-4, pp. 1137-1162.

Jeong, SH, Park, SH, Choi, D-H & Yoon, GH 2012, 'Topology optimization considering static failure theories for ductile and brittle materials', *Computers and Structures*, vol. 110-111, pp. 116-132.

Kaya, N, Karen, İ & Öztürk, F 2010, 'Re-design of a failed clutch fork using topology and shape optimisation by the response surface method', *Materials and Design*, vol. 31, no. 6, pp. 3008-3014.

Kim, Y-I & Park, G-J 2010, 'Nonlinear dynamic response structural optimization using equivalent static loads', *Computer Methods in Applied Mechanics and Engineering*, vol. 199, no. 9, pp. 660-676.

Kirsch, U 1990, 'On singular topologies in optimum structural design', *Structural optimization*, vol. 2, no. 3, pp. 133-142.

Kreisselmeier, G & Steinhauser, R 1979, 'Systematic Control Design by Optimizing a Vector Performance Index', *IFAC Proceedings Volumes*, vol. 12, no. 7, pp. 113-117.

Le, C, Norato, J, Bruns, T, Ha, C & Tortorelli, D 2010, 'Stress- based topology optimization for continua', *Struct Multidisc Optim*, vol. 41, no. 4, pp. 605-620.

Lee, Y-L, Barkey, ME & Kang, H-T 2012, *Metal fatigue analysis handbook practical problem-solving techniques for computer-aided engineering*, Butterworth-Heinemann, Waltham, Mass.

Luo, Y & Kang, Z 2012, 'Topology optimization of continuum structures with Drucker–Prager yield stress constraints', *Computers & Structures*, vol. 90-91, pp. 65-75.

Mrzyglod, M & Zielinski, AP 2007, 'Multiaxial high-cycle fatigue constraints in structural optimization', *International Journal of Fatigue*, vol. 29, no. 9, pp. 1920-1926.

Norton, RL 2005, *Machine design : an integrated approach*, 3rd ed. edn, Prentice Hall, Upper Saddle River, NJ.

Oest, J & Lund, E 2017, 'Topology optimization with finite-life fatigue constraints', *Structural and Multidisciplinary Optimization*, vol. 56, no. 5, pp. 1045-1059.

Paris, J, Navarrina, F, Colominas, I & Casteleiro, M 2009, 'Topology optimization of continuum structures with local and global stress constraints', *Structural and Multidisciplinary Optimization*, vol. 39, no. 4, pp. 419-437.

París, J, Navarrina, F, Colominas, I & Casteleiro, M 2010a, 'Block aggregation of stress constraints in topology optimization of structures', *Advances in Engineering Software*, vol. 41, no. 3, pp. 433-441.

París, J, Navarrina, F, Colominas, I & Casteleiro, M 2010b, 'Stress constraints sensitivity analysis in structural topology optimization', *Computer Methods in Applied Mechanics and Engineering*, vol. 199, no. 33, pp. 2110-2122.

Park, GJ & Kang, BS 2003, 'Validation of a Structural Optimization Algorithm Transforming Dynamic Loads into Equivalent Static Loads', *Journal of Optimization Theory and Applications*, vol. 118, no. 1, pp. 191-200.

Querin, OM, Young, V, Steven, GP & Xie, YM 2000, 'Computational efficiency and validation of bi-directional evolutionary structural optimisation', *Computer Methods in Applied Mechanics and Engineering*, vol. 189, no. 2, pp. 559-573.

Rozvany, GIN 2001, 'On design-dependent constraints and singular topologies', *Struct Multidisc Optim*, vol. 21, no. 2, pp. 164-172.

Sherif, K, Witteveen, W, Puchner, K & Irschik, H 2010, 'Efficient Topology Optimization of Large Dynamic Finite Element Systems Using Fatigue', *AIAA Journal*, vol. 48, no. 7, pp. 1339-1347.

Suresh, S 1998, *Fatigue of materials*, 2nd ed. edn, Cambridge University Press, Cambridge ; New York.

Svanberg, K 1987, 'The method of moving asymptotes—a new method for structural optimization', *International Journal for Numerical Methods in Engineering*, vol. 24, no. 2, pp. 359-373.

Svanberg, K & Werme, M 2007, 'Sequential integer programming methods for stress constrained topology optimization', *Structural and Multidisciplinary Optimization*, vol. 34, no. 4, pp. 277-299.

Sved, G & Ginos, Z 1968, 'Structural optimization under multiple loading', *International Journal of Mechanical Sciences*, vol. 10, no. 10, pp. 803-805.

Xia, L, Zhang, L, Xia, Q & Shi, T 2018, 'Stress-based topology optimization using bi-directional evolutionary structural optimization method', *Computer Methods in Applied Mechanics and Engineering*, vol. 333, pp. 356-370.

Xie, YMa & Steven, 1997, *Evolutionary structural optimization*, Springer, London ; New York.

Yang, R & Chen, C 1996, 'Stress-based topology optimization', *Structural optimization*, vol. 12, no. 2, pp. 98-105.

Yi, J, Rong, J, Zeng, T & Huang, X 2013, 'A topology optimization method for multiple load cases and constraints based on element independent nodal density', *Structural Engineering and Mechanics*, vol. 6, no. 45, pp. 759-777.

Zuo, Z, Xie, Y & Huang, X 2011, 'Optimal topological design of periodic structures for natural frequencies', *Journal of Structural Engineering*

vol. 10.1061/(ASCE)ST.1943-541X.0000347